DEVELOPMENT OF CARBOHYDRATE BASED CONJUGATE VACCINES USING Qβ VIRUS LIKE PARTICLES WITH ANTI-BACTERIAL OR ANTI-CANCER PROPERTIES

By

Zahra Rashidijahanabad

A DISSERTATION

Submitted to
Michigan State University
in partial fulfillment of the requirements
for the degree of

Chemistry—Doctor of Philosophy

2021

ABSTRACT

DEVELOPMENT OF CARBOHYDRATE BASED CONJUGATE VACCINES USING Qβ VIRUS LIKE PARTICLES WITH ANTI-BACTERIAL OR ANTI-CANCER PROPERTIES

By

Zahra Rashidijahanabad

Chimeric antigen receptor (CAR) T cells and bispecific antibodies (BsAbs) are exciting directions to harness the power of the immune system to fight cancer. Chapter 1 is focused on GD2 ganglioside and the mucin-1 (MUC1) protein, two important tumor associated carbohydrate antigens, and latest advances in CAR T cells and bispecific antibodies targeting these two antigens are presented. The roles of co-stimulatory molecules, structures of the sequences for antigen binding, methods for CAR and antibody construction, as well as strategies to enhance solid tumor penetration and reduce T cell exhaustion and death are discussed. Furthermore, approaches to reduce "on target, off tumor" side effects are introduced.

Besides CAR T cells and bispecific antibodies, carbohydrate-based vaccines hold great promise for a number of diseases, which will be the focus of the rest of this dissertation. Several challenges are associated with carbohydrate antigens in regard to inducing specific and protective antibodies as they are poorly immunogenic and the resulting antibodies induced by immunizing with carbohydrates only, typically have low affinity. Currently, developing carbohydrate-based vaccines requires covalent conjugation of the carbohydrate antigen with a protein carrier for optimal antibody response. Thus, generated antibodies have higher affinity against glycan structures. In chapter 2, a potential conjugate vaccine was developed by linking *O*-specific polysaccharide (OSP) antigen purified from *Vibrio cholerae* Inaba with Qβ virus like particles (VLPs) efficiently *via* squarate chemistry as one of the first examples of polysaccharide conjugation to VLPs. The Qβ-OSP conjugate was characterized with mass photometry on the

whole particle level. Pertinent immunologic display of OSP was confirmed by immunoreactivity of the conjugate with convalescent phase samples from humans with cholera. Mouse immunization with the Qβ-OSP conjugate showed that the construct generated prominent and long-lasting IgG antibody responses against OSP, and the resulting antibodies could recognize the native lipopolysaccharide from *Vibrio cholerae* Inaba. This was the first time that Qβ was conjugated with a bacterial polysaccharide for vaccine development, broadening the scope of this powerful carrier.

Tumor associated carbohydrate antigens (TACAs) are another class of attractive carbohydrate antigens for the development of anti-cancer immunotherapy with respect to monoclonal antibodies and vaccines. Tetrasaccharide sialyl-Lewis^a is an attractive therapeutic target for cancer therapy since it is widely expressed on epithelial tumors of the gastrointestinal tract. The overexpression of sLe^a appears to be a key event in invasion and metastasis of many tumors and results in susceptibility to antibody-mediated lysis. In chapter 3, sialyl-Lewis^a conjugate vaccine with Qβ was developed. The resulting construct, Qβ-sLe^a, induced antibody production *in vivo* and the resulting antibodies showed high selectivity for sLe^a antigen in *in vitro* studies and effectively reduced tumor growth in mice.

To my beloved mother and father

ACKNOWLEDGEMENTS

These projects would not have been possible without the support of many people. I am extremely grateful to my supervisor, Prof. Xuefei Huang for his invaluable advice, continuous support, and patience during my PhD study. I have benefited greatly from his wealth of knowledge and meticulous editing. I am extremely grateful that he took me on as a student and continued to have faith in me over the years. I would also like to thank all my guidance committee members, Dr. Daniel Woldring, Dr. Jetze Tepe and Dr. Kevin Walker for reviewing my thesis, their assistance, good suggestions, and kindness. I am grateful to Dr. Babak Borhan, Dr. Gary Blanchard and other graduate research committee at chemistry department for giving me the opportunity to study at Michigan State University.

I would like to thank all instrumental specialists who assisted me to run all experiments involving sophisticated analytical instruments. My special thanks are to Dr. Daniel Holmes who kindly trained me to set up and run all kinds of NMR experiments; Tony Schilmiller, who trained me to run mass spectrometers and assisted me to process all data; Dr. Louis King, Dr. Daniel Vocelle and Dr. Matthew Bernard for the flow cytometry training and their support with data analysis.

I am indebted to all of my friends and colleagues from Huang group, especially Mehdi Hossaini Nasr and Suttipun Sungsuwan, who helped me to develop my research knowledge and skills. I appreciate Dr. Sherif Ramadan for our collaboration projects and his unlimited assistance during these years. Besides, I thank Dr. Herbert Kavunja for his invaluable assistance in my research. I also thank Xuanjun Wu, Tianlu Li, Shuyao Lang, Zibin Tan, Hunter McFall-Boegeman and Shivangi Chugh for their assistance in various aspect of my research. And all other members

in Huang lab: Weizhun Yang, Vincent Shaw, Jicheng Zhang, Changxin Huo, Peng Wang, Kedar Baryal, Mengxia Sun, Kunli Liu, Chia-wei Yang, Po-han Lin, Cameron Talbot, Setare Nick and Ida Shafieichaharberoud.

Finally, I would like to express my deepest gratitude to my parents and siblings- Ali, Yaser and Sima- for their love, support, and encouragement through this hard time of separation. I also wish to thank my grandfather, Haddad, for the love and support he gave to me. He will be missed forever.

TABLE OF CONTENTS

LIST OF TABLES

LIST OF FIGURES

LIST OF SCHEMES

KEY TO ABBREVIATIONS

ADCC	Antibody dependent cell-mediated cytotoxicity
APC	Antigen presenting cell
BCR	B-cell receptor
BMDC	Bone marrow dendritic cells
BSA	Bovine serum albumin
BsAbs	Bispecific antibodies
CAR	Chimeric antigen receptor
CDC	Complement-dependent cytotoxicity
CFA	Complete Freund's adjuvant
CTL	Cytotoxic T cell
DC	Dendritic cell
DMEM	Dulbecco’s modified Eagle’s medium
DMSO	Dimethyl sulfoxide
ELISA	Enzyme-linked immuno-sorbent assay
FACS	Fluorescence activated cell sorting
FBS	Fetal bovine serum
FDA	Food and Drug Administration
FITC	Fluorescein isothiocyanate
GD2	Disialoganglioside
HRP	Horseradish peroxidase
IFA	Incomplete Freund's adjuvant

IgG	Immunoglobulin G
IgM	Immunoglobulin M
KLH	Keyhole limpet hemocyanin
LCMS	Liquid chromatography–mass spectrometry
LPS	Lipopolysaccharide
mAb	Monoclonal antibody
MALDI-TOF	Matrix assisted laser desorption ionization-time of flight
MFI	Mean fluorescence intensities
MHC I	Major histocompatibility complex class I
MHC II	Major histocompatibility complex class II
MPLA	Monophosphoryl lipid A
mQβ	Mutant Qβ
MS	Mass spectrometry
MUC1	Glycoprotein Mucin 1
MW	Molecular weight
MWCO	Molecular weight cut-off
OD	Optical density
OSP	O-specific polysaccharide
PBS	Phosphate-buffered saline
PBST	Phosphate-buffered saline tween
PD-1	Programmed cell death protein 1
PD-L1	programmed death-ligand 1
PE	Phycoerythrin

Qβ	Bacteriophage Qbeta (Qubevirus durum)
SDS-PAGE	Sodium dodecyl sulfate polyacrylamide gel electrophoresis
SEC	Size-exclusion chromatography
SELDI-TOF	Surface-enhanced laser desorption/ionization time-of-flight mass spectrometry
sLe^a	sialyl $Lewis^a$
scFv	Single-chain variable fragment
ST	Sialylated Thomsen-Friedenreich antigen
STn	Sialylated Thomsen-nouveau antigen
T antigen	Thomsen-Friedenreich antigen
TACA	Tumor-associated carbohydrate antigen
TCR	T cell receptor
TEM	Transmission electron microscopy
TFA	Trifluoroacetic acid
Th	Helper T cell
TLR	Toll-like receptor
Tn antigen	Thomsen-nouveau antigen
TT	Tetanus toxoid
VLP	Virus-like particle
wtQβ	Wild-type Qβ

CHAPTER 1: Recent advances in tumor associated carbohydrate antigen based chimeric antigen receptor T cells and bispecific antibodies for anti-cancer immunotherapy

1.1 Introduction

Cancer is a leading cause of death worldwide. The global cancer burden, which has been estimated as 18.1 million new cases and 9.6 million deaths in 2018, is predicted to rise to 29.5 million new incidences in 2040 [1,2]. The alarming increase in cancer burden accentuates the urgent need to develop innovative approaches for more effective and less toxic cancer treatments complementing conventional therapeutics such as chemotherapy, radiotherapy, surgery and palliative care. Cancer immunotherapy holds great promises in cancer treatment, which was named as the Breakthrough of the Year in 2013 by *Science* [3].

Tumor associated carbohydrate antigens (TACAs) are a class of attractive antigens for anti-cancer immunotherapy development [4,5]. Multiple TACAs are over-expressed on the surface of cancer cells compared to those on normal cells [6]. In addition, TACAs can be found at high levels on many types of cancer, rendering them intriguing targets for potential broad spectrum anti-cancer immunotherapy [7]. Tremendous efforts have been devoted to the development of anti-cancer vaccines targeting TACAs with innovative designs of the antigen structures, the carrier moieties to deliver the antigens to the immune system, as well as the incorporation of immune activation elements including adjuvants and cytotoxic T cell epitopes into the vaccine constructs [8–11]. Besides vaccines, chimeric antigen receptor (CAR) T cells and bispecific antibodies (BsAbs) have emerged as appealing immunotherapeutic strategies to combat cancer, as evident from multiple products approved by the FDA [12]. Recently, great progresses have been achieved in the development of CAR T cells and BsAbs targeting two TACAs, i.e., gangliosides GD2 and glycoprotein mucin-1 (MUC1). In this review, we will discuss the advances and challenges in these areas to stimulate further development.

1.2 GD2 CAR T cells: going beyond the anti-GD2 monoclonal antibodies

Disialoganglioside GD2 is an *N*-acetyl neuraminic acid containing glycolipid antigen composed of five monosaccharides anchored to the lipid bilayer of plasma membrane through a ceramide lipid (**Figure 1.1**). Normal tissues have low expression levels of GD2 [13], but in various types of cancers such as neuroblastoma, small-cell lung cancer, melanoma, glioma, and sarcomas, the expression of this weakly immunogenic antigen can reach 10^7 molecules per cell [8,14,15]. Furthermore, GD2 has been discovered as a potential biomarker for the purported breast cancer stem cells [16]. GD2 can induce tyrosine phosphorylation leading to the activation of a variety of kinase pathways, resulting in increased proliferation, cell migration and invasion of cancer cells. Knockdown of GD2 levels abrogated tumor formation *in vivo* [16]. With its high expression on tumor cells and importance in tumor development, GD2 was ranked as one of the top antigenic targets for cancer [14,17].

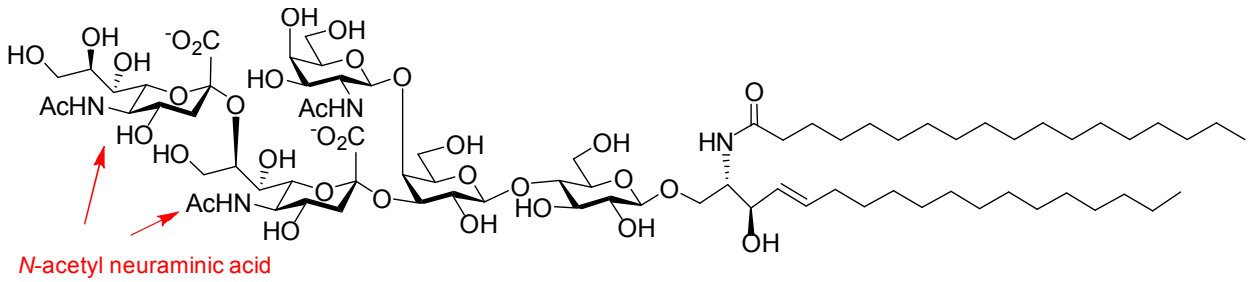

Figure 1. 1 Structure of the GD2 ganglioside.

Monoclonal antibodies against GD2 have achieved clinical success in cancer treatment. Early generation of anti-GD2 cancer immunotherapy utilized murine monoclonal antibodies, 14G2a and 3F8, in patients with melanoma, neuroblastoma, and osteosarcoma [14]. However, due to the mouse origin of these antibodies, human anti-mouse antibodies were induced, limiting the dose that can be administered and reducing their anti-tumor efficacy. In addition, administration of these antibodies has been associated with side effects such as pain, fever, hypertension and

urticarial reactions, which limit their wide applications. To overcome these challenges, human-mouse chimeric anti-GD2 monoclonal antibodies have been generated [14,18]. ch14.18 consisting of the variable regions of murine 14G2a mAb fused with the constant regions of human IgG1, has higher antibody-dependent cell-mediated cytotoxicity and longer half-life compared to 14G2a. Further development of humanized anti GD2 antibody, hu3F8 and hu14.18K322A with a K322A mutation of the Fc region to prevent complement fixation, improved their half-lives and tolerable dose. However, in clinical trials, similar side effects as m3F8, including pain and hypertension, were observed.

Adoptive transfer of CAR T cells is a promising immunotherapy strategy to treat cancer in an MHC-independent manner. CAR T cells are designed by linking the single-chain variable fragment (scFv) of a monoclonal antibody with the T cell receptor (TCR) ζ-chain transmembrane and cytoplasmic regions. Further development of CAR Ts by the addition of costimulatory signal (CD28) for full activation of these cells has led to 2nd generation of CAR Ts and the third generation includes additional signaling domain (CD27, 4-1BB or OX40) aimed at improving proliferation, survival and cytokine release from the cells. With the high anti-tumor efficacy in acute lymphoblastic leukemia, two anti-CD19 CAR T cell-based immunotherapies (KYMRIAH and CARTA) have been approved by FDA. However, applications of CAR T therapy in solid tumors have met with limited successes. Some of the main barriers of CAR T cell therapy include: limited ability of CAR T cells to proliferate, inefficient trafficking of CAR T cells to tumor tissues, limited T cell extravasation into solid tumor, and suppressive tumor microenvironment that dampens T cell proliferation and cytokine production[19]. With the importance and targetability of GD2 for solid tumors, anti GD2 CAR T cell immunotherapy has been investigated in various types of tumors.

1.2.1 Building co-stimulatory signals into GD2 CAR T cells

One of the first CAR T cells products tested in children was an anti-GD2 CAR containing only the CD3ζ endodomain but no costimulatory domain [20]. In preclinical models, Rossig et al. demonstrated that GD2 was a viable CAR T cell target for neuroblastoma. However, the culture of these first generation CAR T cells could not be maintained for longer than 8 weeks upon stimulation with $GD2^+$ tumor cells. In addition, these CAR T cells failed to proliferate when incubated with $GD2^+$ tumor cells presumably due to a lack of co-stimulatory signals upon antigen binding. Further investigations of GD2 CAR T focused on CAR constructs incorporating endodomain CD28 and OX40 together with the anti-GD2 scFv [21].

The importance of costimulatory signals has been studied in a clinical trial in eleven individuals with neuroblastoma, who had Epstein-Barr virus (EBV)-associated malignancies [22]. EBV-specific cytotoxic T lymphocytes (CTLs) or bulk T cells activated with anti-CD3 antibodies (ATCs) were transduced with a CAR specific for GD2 antigen. Equal numbers of GD2 CAR-CTLs and CAR-ATCs were injected into patients. Persistence of the EBV specific GD2 CAR-CTLs was detectable beyond 6 weeks, which were almost two times longer compared to the GD2 CAR-ATCs. These results highlight the importance of costimulation of native antigen receptor on CAR-CTLs, when these cells engaged EBV antigens on professional antigen-presenting cells through their native receptors. Four of the eight patients (50%) with evaluable tumors had shown tumor necrosis or regressions. A subsequent study with 19 patients including the original 11 patients for up to 4 years showed that although both CAR-CTLs and CAR-ATCs were low or undetectable beyond 6 weeks, the continued presence of even low levels of CAR T cells was associated with a significantly longer time to disease progression. Three patients achieved complete remission out of the 11 patients with active disease at the time of infusion. The proportion of $CD4^+$ helper cells

and central memory cells present in infused CAR T cells correlated with the long term persistence of CAR T cells [23].

To sustain the survival of GD2 CAR T cells, additional stimulatory molecule such as interleukin-15 (IL15) has been incorporated generating the GD2 CAR.15 T cells [24]. IL15 provided the survival signals to GD2 CAR.15 T cells while they were in circulation, and costimulation when the cells reached the tumor site. The GD2 CAR.15 T cells expressed lower amounts of programmed cell death protein-1 (PD-1), an immune checkpoint protein, and could proliferate and persist longer *in vitro* and *in vivo* even in the absence of exogenous cytokines or antigen support. GD2 CAR.15 T cells were more effective in controlling tumor growth with a lower number of total infused T cells, and in improving survival after rechallenging experiments. Further clinical trials (NCT03294954) for GD2 CAR.15 T cells are ongoing.

Besides IL15, another CAR T design incorporated the CD27 costimulatory domains [25], which can augment survival and tumor killing activities of T cells [26]. These CAR T cells showed long term persistence with 30% of infused CAR T cells lasting up to 180 days. Two patients had markedly tumor regression and the 1-year overall survival rate reached 74%.

1.2.2 Enhancing homing and penetration of solid tumor by GD2 CAR T cells

An important factor in dictating CAR T efficacy is the ability of these cells to reach solid tumor sites. To aid in trafficking and homing of CAR T cells, chemokine receptor can be incorporated [27]. While earlier finding confirmed the presence of C-C chemokine receptor type 2 (CCR2) on human activated T cells and T cell migration in response to C-C motif ligand 2 (CCL2) chemokine, CCR2 expression was deficient in CAR T cells due to culture conditions and the usage of anti-CD28 antibody, which reduced the levels of CCR2 following TCR activation. In this regard, modified GD2 CAR T cells expressing CCR2b was able to improve the homing and

expansion of T cells at tumor site *in vivo* by day 14. This increased the frequency of T cells at the tumor site correlated with reduced tumor growth. Hence, the CCL2 chemokine concentration at the tumor site can be exploited to attract effector cells to tumor environment.

In addition to the incorporation of the chemokine receptor, modification of the tumor microenvironment and vascularity with anti-angiogenic agents such as anti-vascular endothelial growth factor antibody (Bevacizumab, BEV) can improve the trafficking of CAR T cells to tumor [28]. In a mouse neuroblastoma (NB) model, administration of anti-GD2 CAR T cells alone failed to lead to any increases in survival compared to the control group receiving non-transduced T cells. To address this, the combination of BEV and anti-GD2 CAR T was tested. While injection of BEV at a relatively low dose (2 mg/kg) did not significantly affect the number of micro-blood vessels in tumor tissues, addition of BEV to the anti-GD2 CAR T cell treatment regime led to enhanced migration and infiltration to the inner tumor core by these T cells. This was confirmed by double CD31/CD3 immunostaining. The T cells produced interferon-γ and reprogrammed the tumor microenvironment, with the mice receiving the combination therapy showing modest improvements in survival. Interestingly, NB cells were found to upregulate the levels of PD-L1. As GD2-CAR T cells in tumors were found to express programmed cell death protein-1 (PD-1), this study suggested the interactions of PD-1 with its ligand PD-L1 may limit the anti-tumor efficacy.

Once reaching tumor tissues, the ability of CAR T cells to penetrate stroma-rich solid tumors is critical for antitumor effects. To facilitate tissue penetration, extracellular matrix (ECM), including the heparan sulfate proteoglycans (HSPGs) need to be degraded. The effect of *in vitro* culture of T lymphocytes on HSPG degrading heparanase enzyme (HPSE) has been investigated [29]. In a Matrigel - based cell invasion assay, briefly activated T cells showed 1.5 times higher

invasion of ECM compared to freshly isolated resting T cells. In contrast, long-term *ex vivo*–expanded T cells had 3 times lower invasion than the freshly isolated T cells. Mechanistic studies showed that the freshly isolated and briefly activated T cells retained the expression of active HPSE, while in long-term expanded T cells, the enzyme was not detected by either Western blotting or immunofluorescence. Building on this knowledge, CAR T cells were engineered to express HPSE, which exhibited improved capability of ECM degradation and deeper tumor penetration. While both HPSE modified and un-modified GD2-CAR T cells had similar efficiencies in lysing $GD2^+$ human cell lines *in vitro*, HPSE expressing GD2-CAR T cells provided significantly improved protection to mice from $GD2^+$ tumor cell induced death.

1.2.3 Combination of GD2 CAR T therapy with checkpoint blockade and chemotherapy

Improvement of GD2 CAR T cell therapy was investigated in combination with anti-PD-1 blockade to reduce T cell exhaustion and improve survival. *In vitro* study showed that repeated antigen stimulation reduced the percentage of viable GD2 CAR T cells [30]. This activation induced cell death (AICD) of CAR T cells is dependent on the level of antigen expression since CAR T cell survival was higher in cell lines with lower GD2 expression. The AICD process could be potentially reversed with anti-PD-1 blockade, as treatment with the anti-PD-1 mAb was able to restore CAR T-cell survival similar to the level observed for CAR T cells cultured with $GD2^-$ cell lines. Interestingly, while siRNA knockdown of PD-1 enhanced the CAR T-cell viability, PD-L1 was found to have a more complex role. PD-L1 signaling via PD-1 caused inhibition or deletion of activated $PD\text{-}1^+$ T cells [31,32], whereas signaling via CD80 stimulated naive T cells [33]. Furthermore, PD-L1 could mediate reverse signaling upon binding to PD-1 within $PD\text{-}L1^+$ T cells and promote their survival. SiRNA knockdown of PD-L1 significantly reduced cell survival. Following the detailed *in vitro* study, the GD2 CAR T construct was administrated to four

metastatic melanoma patients. The GD2-CAR population declined in all patients beyond day 28 post-infusion and failed to persist in two patients. These observations suggested that CAR T cells were also being depleted *in vivo*. Based on the *in vitro* data, combination of PD-1 blockade with CAR T therapy may help to augment the efficacy and persistence of CAR T cells.

GD2-CAR T cell treatment can be combined with chemotherapy to enhance efficacy. Heczey et. al [34] reported their clinical results in NB treatment, with three cohorts receiving GD2-CAR T, GD2-CAR T with cyclophosphamide and fludarabine (Cy/Flu) prior to cell infusions, and GD2-CAR T co-administered with Cy/Flu and PD-1 inhibitor respectively. GD2-CAR T and Cy/Flu treatment led to superior T cell expansion and higher levels of IL15 in the blood. Co-administering a PD-1 inhibitor did not make any differences in expansion, persistence of the cells, or circulating cytokine levels in this report. In contrast, other CAR T studies demonstrated beneficial clinical outcome when combined with PD-1 inhibitors [35–37], which may be due to variations in cancer types, antigen targets and timing/duration of PD-1 inhibitor treatment. Thus, careful optimization is necessary for each treatment protocol.

1.2.4 Reengineering of the GD2 CAR

As many anti-GD2 mAbs originated from mice, administration of CAR T cells based on these antibodies can potentially generate anti-idiotype or anti-mouse antibodies recognizing the CAR and causing immune rejections. Thomas et.al [38] modified GD2-CAR T to incorporate humanized scFv of anti-GD2 mAb. This humanized CAR T had the same efficiency in proliferation and cytokine release as its murine counterpart. In addition, the effect of spacer between the ScFv and CD28 on CAR function was investigated. The inclusion of IgG Fc domain (**Figure 1.2a**) showed optimal efficiency compared to CAR T comprising of the hinge alone (**Figure 1.2b**), the hinge attached to the stalk of CD8a (**Figure 1.2c**) or the CD8a stalk alone

(**Figure 1.2d**). These results showed the flexibility and binding ability to target antigen can play an important role in CAR T activation and cytokine release.

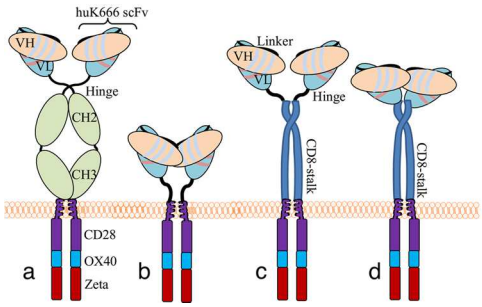

Figure 1. 2 Schematic demonstration of various GD2 CAR constructs. a) The CAR includes the hinge region as well as the Fc domain (CH2 and CH3); b) CAR without the Fc domain; c) CAR with the hinge attached to the stalk of CD8a; and d) CAR with CD8a stalk only without the hinge region. (Image adapted from [38])

Effective targeting of GD2 specific CAR T cells is a challenging task. Richman et.al.[39] showed by mutation of the aspartic acid residue 101 in the heavy chain of CAR scFv to lysine ($E101_HK$), the affinity of GD2-CAR T cells could be significantly improved towards various $GD2^+$ cell lines. In a mouse liver cancer model, histologic analysis of livers of mice treated with this construct showed less than 1% tumor cell foci compared to >95% in control and parent GD2 CAR T cell treated groups highlighting the efficacy of these engineered CAR T cells. However, all the mice treated developed severe neurotoxicity associated with T cell infiltration and proliferation into their brains presumably due to the expression of GD2 in brain tissues and the "on-target, off-tumor tissue" toxicity.

Enhancing the safety profile of CAR T cell therapy while achieving high anti-cancer efficacy of GD2 CAR T cells requires further cellular engineering. One potential cause for toxicity is the recognition of Fc on CAR-T by cells with Fcγ receptors. Since IgG Fc is the natural ligand for high affinity Fcγ receptors (CD64), mutation of the Fc domain, which is commonly used as the spacer between the antigen recognition domain and the intracellular signaling domain in CAR

structure (**Figure 1.2a**), significantly reduced the off target toxicity of GD2-CAR T cells by preventing the engagement of CD64 expressing myeloid cells with CAR T cells [38].

An alternative approach to avoid the "on-target, off-tumor" effect is to build in inducible suicide genes. The inducible Caspase 9 (iCasp9) suicide gene was incorporated into the CAR of GD2 CAR T cells [38,40]. The iCasp9 was not toxic at basal expression levels. Administration of the small molecule dimerizer drug to the cells induced the expression of iCasp9, resulting in rapid onset of apoptosis in transduced cells. Activated cells expressing the CAR were preferentially killed, providing a safety switch. Similarly, the iCasp9 suicide gene has been applied to another type of GD2 CAR T, i.e., GD2 CAR.15 T cells, enhancing the safety profile of the construct [24].

Mitwasi et al. [41] designed a new type CAR T, termed universal CAR T (UniCAR), whose activation is dependent on a target module (TM), and can be potentially turned on and off via dosing of TM. The scFv binding domain of UniCAR recognized a short peptide epitope of 10 amino acid derived from the human nuclear autoantigen (5B9). The UniCAR cells were inactive after infusion since the target epitope did not exist on the cell surface. A TM was synthesized by fusing the 5B9 antigen to GD2 binding scFv (**Figure 1.3**). In the presence of the TM, UniCARs were able to specifically target $GD2^{+}$ tumor in a TM-dependent manner. At effector to target cell ratio of 5:1, only less than 0.1 nM of GD2-TMs was needed for uniCAR T to mediate the lysis of tumor cells. No killings were observed in control cell lines or in the absence of TMs. In contrast to other safety switches such as modification with inducible suicide genes, the uniCAR T cells were unique that the activities could be modulated rapidly via dosing of a target module.

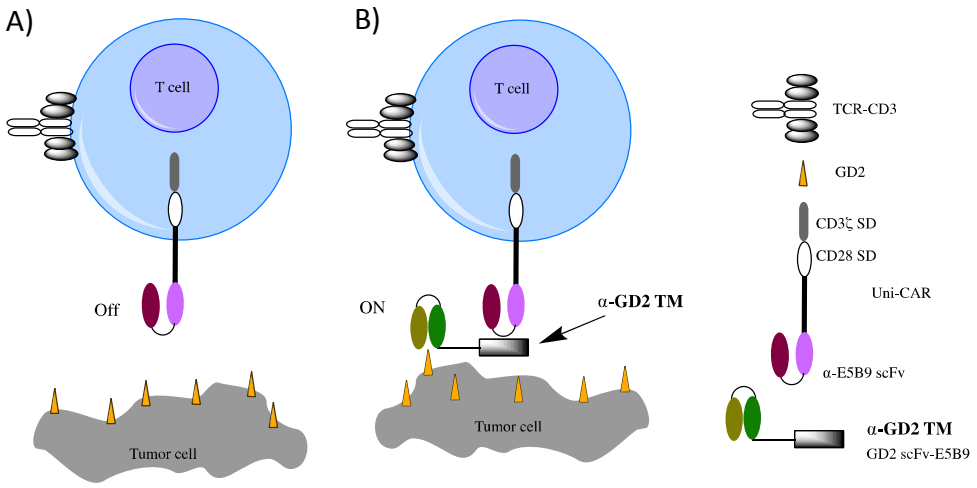

Figure 1. 3 Construction of UniCAR and TM. A) UniCAR cells do not recognize tumor cells in the absence of TM due to the lack of receptor on T cells towards tumor antigens. B) Upon addition of the TM comprised of the conjugate of anti-GD2 scFv and E5B9, the UniCAR can bind with the TM through E5B9, thus gaining the abilities to recognize $GD2^{+}$ tumor cells.

1.3 MUC1 CAR T cells

The human mucin 1 (MUC1) are high molecular weight glycoproteins expressed on the epithelial cell layers in the lung, breast, pancreas, kidney, ovary, colon, and other tissues to provide protection of these cells, which are exposed to external environments [42]. MUC1 consists of two subunits, MUC1-N and MUC1-C, which form a stable non-covalent complex at the cell surface. MUC1-N contains a variable number of 20 amino acid tandem repeats (VNTR) that are heavily glycosylated on serine or threonine residues of each VNTR in normal cells (**Figure 1.4**). However, on cancer cells, owing to altered glycosyltransferase expression, tumor-associated MUC1 is decorated by a preponderance of shorter glycans, including Thomsen-nouveau (Tn), sialyl Tn (STn), Thomsen-Friedenreich (Tf), and sialyl-T (STf) (**Figure 1.4**). Under-glycosylation of MUC1 unmasks cryptic epitopes within the extracellular domain, enabling tumor-selective binding by antibodies.

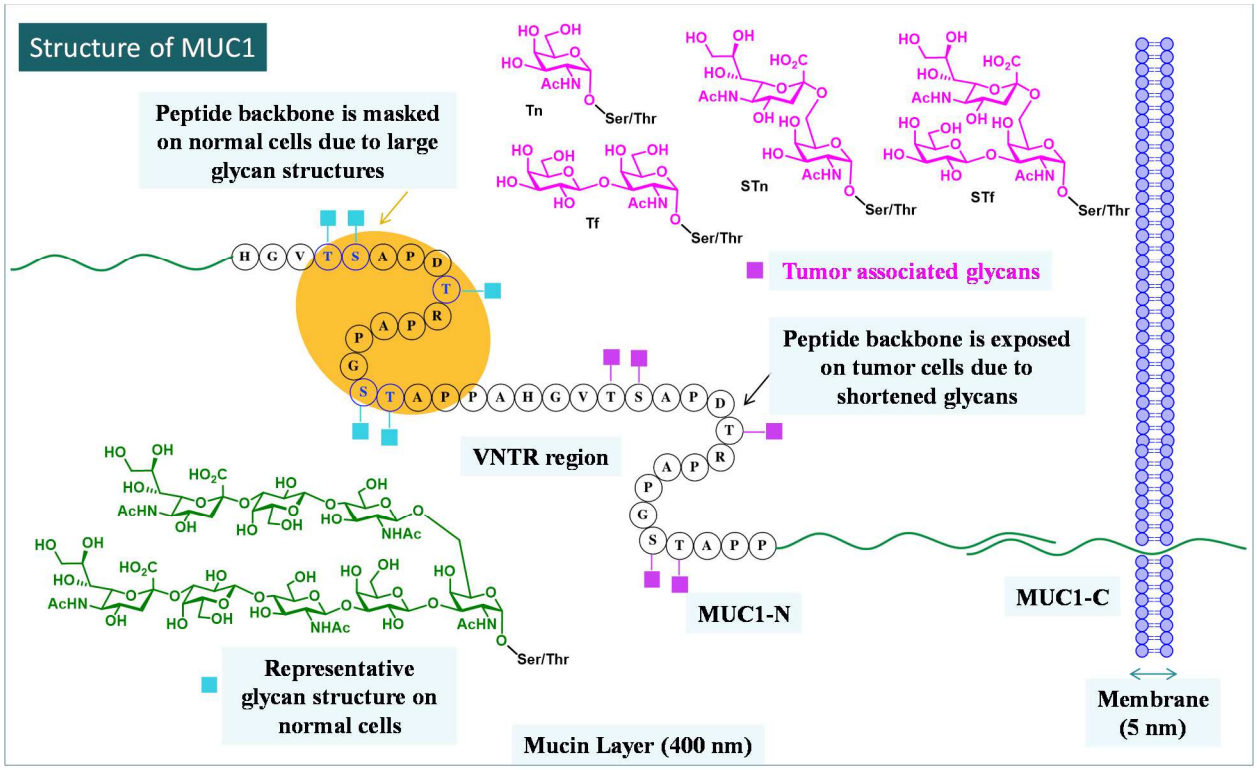

Figure 1. 4 Schematic demonstration of MUC1 glycoprotein structure. MUC1 is composed of a heterodimer of MUC1-N linked non-covalently with the transmembrane MUC1-C. MUC1-N contains a variable number of 20 amino acid VNTRs that are heavily glycosylated on serine or threonine residues of each VNTR in normal cells shielding the protein backbone for immune recognition. However, tumor associated MUC1 are hypoglycosylated exposing the protein backbone.

1.3.1 MUC1 epitope structures for CAR T cell targeting

Multiple mAbs are available against the MUC1-N domain. A representative example is AS1402, which has been evaluated in phase 1 clinical trial for breast cancer patients [43]. However, the result showed that the addition of AS1402 to chemotherapy had the same efficacy compared to chemotherapy treatment alone [44]. As MUC1-N is known to be shed from cancer cell surface into circulation, the extracellular pool of MUC1-N in plasma is considered a major barrier for antibody-dependent cellular toxicity against MUC1-N. In addition to passive immunity using anti-MUC1 mAbs, vaccines targeting tumor associated MUC1 have been evaluated,

including L-BLP25 and PANVAC-V, which have been tested in late-stage clinical trials for the treatment of breast cancer [43,45–47]. However, no successful anti-MUC1 vaccines are available yet. As an alternative to mAbs and vaccines, anti-MUC1 CAR T cells have been investigated.

One of the key considerations in designing anti-MUC1 CAR T cells is the epitope structure targeted by the CAR. As MUC1 is a large glycoprotein, there are many potential sequences with MUC1 that can be targeted. Early MUC1 CAR T design utilized scFvs derived from anti-MUC1 mAb SM3 [48]. While SM3 recognized well the unglycosylated PDTR peptide within the VNTR region of MUC1-N, it bound poorly with glycopeptides such as the STf antigen present on many types of cancer cells. As a result, the SM3 MUC1 CAR T cells did not respond strongly to MUC1 expressing tumor cells. Nevertheless, MUC1 CAR T cells expressing a mutated analog of SM3 to improve MUC1 binding, were evaluated in a first-in-human study by direct injection into tumor lesions [49]. Reduction of MUC1 expression due to apoptosis and necrosis of tumor cells were observed in solid tumors treated with these CAR T cells, providing new options for improved CAR T therapy.

To overcome the low MUC1 affinity of SM3 mAb, another anti-MUC1 mAb, HMFG2 was utilized to construct the CAR [48]. HMFG2 has higher affinities to MUC1 than SM3 and can bind STf bearing MUC1 glycopeptides. In order to reduce the steric hindrance posted by immobilized MUC1, an IgD hinge was inserted into the CAR yielding a potent receptor containing a fused CD28/OX40/CD3ζ endodomain, so that the Fab regions can engage antigen in virtually any orientations. These HMFG2-CD28-OX40-CD3ζ CAR T cells proliferated upon encountering the MUC1 antigen, mediated production of proinflammatory cytokines, and killed $MUC1^{+}$ tumor cells. When tested in a preclinical model, these CAR T cells led to a significant delay of tumor growth [48,50,51].

A potential drawback of the HMFG2 antibody is that besides the glycosylated form of MUC1, HMFG2 also recognizes unglycosylated MUC1 peptide, which raises concerns of possible auto-immunity due to the binding with unglycosylated MUC1 in normal tissues. Anti-MUC1 mAb 5E5 is an antibody that has been shown to have high affinities for the Tn glycosylated MUC1 (MUC1-Tn) with little cross-reactivity with the non-glycosylated MUC1-60-mer peptide or normal human tissues, supporting the more cancer specific expression of Tn-glycopeptide epitopes [52]. With the knowledge of high tumor selectivity by 5E5, Posey et. al. developed MUC1-Tn CAR T cells using 5E5, which recognized multiple tumor cell lines expressing MUC1-Tn [53]. Increasing the expression of enzymes in tumor cells that converts Tn to other glycans reduced the levels of MUC1-Tn on tumor cells. As a result, the 5E5 CAR T cell induced cytotoxicity to these cells were significantly suppressed, which may be concerning for cancer treatment due to the heterogeneity of MUC1 glycosylation patterns on cancer cells. Interestingly, when evaluated in xenograft model of human pancreatic cancer studies, 5E5 CAR T cells provided complete protection to tumor bearing mice, suggesting that 5E5 driven CAR T cells are able to detect low levels of antigen targets, and antigenic diversity does not preclude tumor eradication [53].

Another example of CAR-T design against the exposed peptide backbone of aberrantly glycosylated MUC1 is to use scFv derived from anti-MUC1 mAb (TAB004) for recognition of STAPPVHNV peptide sequence within the VNTR region. The scFv was fused to CD28 and CD3ζ T cell intracellular signaling molecule to generate the CAR T cells, which were evaluated in triple-negative breast cancer (TNBC) [54]. MUC1 CAR T cell mediated tumor cell lysis correlated with MUC1 expression levels *in vitro* without significant lysis of normal breast epithelial tissues, suggesting their high tumor selectivities. Treatment of HCC70 tumor-bearing mice with this construct dramatically reduced the tumor growth from as early as 4-days post T cell injection,

which lasted up to 57 days. However, the tumor started to progress faster after about 60 days post treatment compared to the control group. Histological analysis showed that MUC1 expression levels were similar in both treatment groups, suggesting MUC1 tumor antigen down-regulation to avoid immune clearance by MUC1 CAR T cells is likely not a major contributing factor to tumor escape. Instead, an approximate two-fold increase of PD-1 expression on tumor cells was observed after CAR T cell treatment, which may be a major reason causing the exhaustion of CAR T cells. Increased lysis potency by MUC1 CAR T cells with pretreatment of an anti-PD1 antibody suggested the potential beneficial combination of CAR T cells with an anti-PD1 antibody for future evaluations.

1.3.2 Building costimulatory signals into MUC1 based CAR T cells and dual targeting of tumor cells

To enhance the anti-tumor efficacy and reduce tumor escape from the immune pressure, an attractive strategy is to combine multiple types of CAR T cells. This combinational CAR T cell therapy has been investigated for the treatment of non-small-cell lung cancer [55]. Prostate stem cell antigen (PSCA) is frequently expressed in non-small-cell lung cancer along with MUC1 antigen. MUC1 and PSCA CAR T cells were constructed based on HMFG2 and humanized 1G8 antibodies respectively. When administered individually, MUC1 and PSCA CAR T cells significantly reduced tumor growth in a mouse non-small-cell lung cancer model compared to mock groups receiving non-tumor targeting CAR T cells. Combining the MUC1 and PSCA CAR T cells led to further reduction of tumor sizes, highlighting the power of this combinatorial approach.

Costimulatory signals such as CD28 and CD3ζ are critical to sustain CAR T cell proliferation, enhance cytotoxicity, and resist AICD. However, as the CAR T cells become more

powerful, toxicities have emerged [56,57], which are often attributed to "on target, off tumor" effects due to the presence of tumor – associated antigens in healthy tissues off tumor sites. CAR T cells are commonly designed with both CD28 and CD3ζ on the same gene (also known as cis arrangement). Upon CAR engagement, CD28 and CD3ζ are both activated with CD3ζ signaling eliciting cytotoxicity and interferon-γ production, and CD28 creating signal 2 to promote T-cell proliferation and interleukin (IL)-2 production.

One novel design to increase the specificity of CARs and improve their activity and safety is to physically separate the two stimulatory signals by incorporating them into 2 distinct CARs specific for 2 different antigens (*trans* signaling). In this regard, Wilkie and his coworkers engineered CAR T cells to simultaneously target ErbB2 and MUC1, two common breast cancer associated antigens [58]. The resulting CAR T, called ITH, coexpresses the ErbB2 specific CAR using scFv of anti ErbB2 mAb followed by CD3ζ signaling domain (Iz1) and MUC1 specific CARs based on scFv of anti MUC1 mAb, HMFG2, coupled to CD28 domain (HDF28). The two transgenes were co-expressed in equal amounts by separating the inserts with a Thosea asigna (T2A) peptide. The ITH construct could deliver complementary signals required for proliferation and lead to greater expansion of T cells compared to control CAR Ts with CD28 or CD3ζ alone. ITH CAR T cells showed similar cytolytic efficiency as anti-ErbB2 CAR T cells against multiple breast cancer cell lines with varying levels of ErbB2 and MUC1 expression.

Deeper analysis of ITH CAR T cells was performed. It was notable that the production of IL-2 by ITH CARs was much lower compared to the CARs with cis fused CD28 + CD3ζ endodomain. Possible reasons included the conformational changes of scFv induced after binding of the first antigen to its corresponding scFv, which may hinder the optimal binding of the second scFv with its respective antigen, posing steric challenge for simultaneous targeting of both target

antigens [59]. Alternatively, co-stimulatory signaling from the ITH CAR T cells may be either less efficient or distinct from that provided by CARs containing a fused CD28 + CD3ζ endodomain.

Besides the MUC1 and ErbB2 combination for ITH CAR T cells, other dual targeting CAR T cells with CAR pairs such as prostate antigens PSMA/PSCA and mesothelin/folate receptor have been evaluated *in vitro* and *in vivo* [60,61]. These studies showed that co-transduced trans-signaling CAR T cells could destroy tumors expressing both antigens, without affecting those with either antigen alone. Thus, a dual targeting, trans-signaling CAR approach can enhance the anti-cancer efficacy of CAR T cells while minimizing off tumor side effects against normal tissues bearing single antigen.

1.4 Bispecific antibodies targeting GD2 and MUC1

Bispecific antibodies (BsAbs) are engineered antibodies that can simultaneously engage two unique epitopes, such as ligands, receptors, and cytokines. While there are many different designs of BsAbs in development, they can be generally classified into two categories: immunoglobulin G (IgG)-like molecules and non-IgG-like molecules [62]. With two heavy and two light chains, the overall geometry of IgG like BsAbs resemble those of IgG (**Figure 1.5a**). However, unlike traditional IgGs, the two chains of BsAbs recognize two distinct epitopes. The IgG like BsAbs contain the Fc domain, which can mediate effector functions such as antibody-dependent cell-mediated cytotoxicity, complement-dependent cytotoxicity, and antibody-dependent cellular phagocytosis. In comparison, the non-IgG like BsAbs lack the entire Fc domain (**Figure 1.5b**). These BsAbs can include chemically linked Fabs, various types of bivalent and trivalent single-chain variable fragments (scFvs) with different epitope specificities.

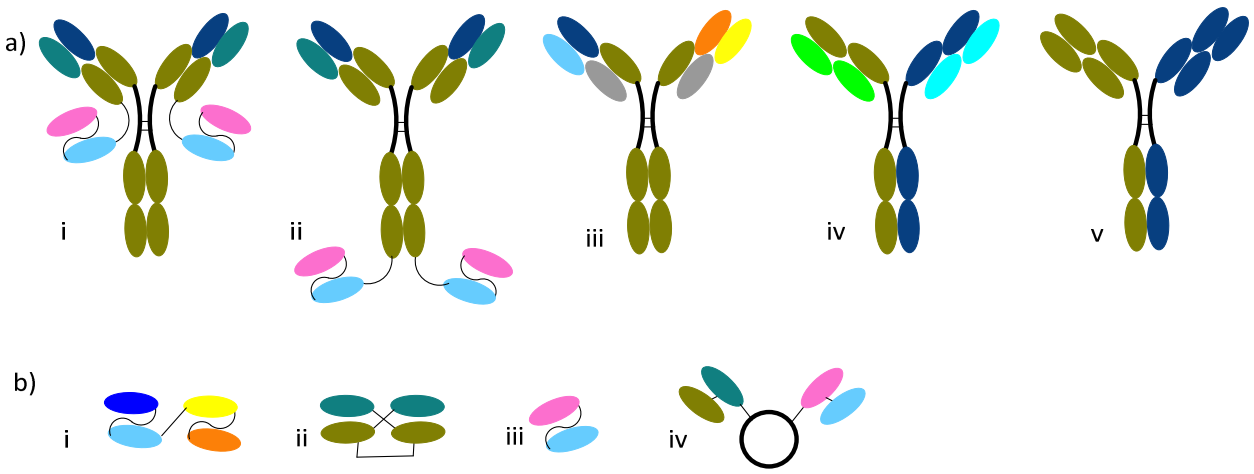

Figure 1. 5 Schematic representation of various BsAb formats. a) IgG-like BsAbs: i) and ii) IgG-scFv, iii) triomab, iv) quadroma, and v) half molecule exchange format. And b) non-IgG-like BsAb: i) tandem scFv, ii) dual-affinity re-targeting antibody, iii) bi-nanobody, iv) scFv-human serum albumin-scFv.

BsAbs may improve tumor targeting specificity by binding two tumor-associated antigens. Furthermore, BsAbs can be designed to engage immune system effector cells, usually through CD3 on cytotoxic T cells or CD16 on natural killer cells. This can bring the immune cells into close proximity with cancer cells and lead to the killing of cancer cells through perforin/granzyme-mediated non-MHC-restricted specific antitumor cytotoxicity [63–66].

1.4.1 GD2 targeting BsAbs

The most common TACA based BsAbs target GD2. One type of BsAbs was produced by chemically conjugating anti-CD3 (OKT3) and anti-GD2 (3F8) antibodies through a heterobifunctional linker [67]. This BsAb could coat expanded T cells *in vitro*, and help direct the activated T cells to neuroblastoma cells expressing GD2 antigens. The BsAb treatment could kill GD2 positive cells more effectively than T cells or 3F8 antibody treatment alone. Furthermore, it is highly promising that compared to intravenous injection of 3F8 mAb alone, the dose required for 3F8BsAb was 200 times lower for similar efficacy. This is a major advantage, as the lower

dose needed can potentially reduce the dose-limiting pain caused by 3F8 binding to peripheral nerve fibers.

A second type anti-GD2 BsAb, Ektomab, was built in a quadroma-based format. One binding arm of Ektomab is from mouse IgG2a ME361, which can recognize ganglioside GD2 albeit with a lower affinity compared to 3F8. The other binding arm is from rat IgG2b recognizing CD3 on human T cells. Significant lytic activity of Ektomab could be observed down to 40 ng/ml. However, both murine and rat components could induce neutralizing antibodies in humans, which diminish their effects rendering the need for higher doses.

To reduce anti-mouse/rat antibodies generated in humans, the first humanized IgG-scFv BsAb was developed for targeting GD2. In this work, the scFv of humanized mouse anti CD3 was attached to the carboxy end of anti GD2 light chain antibody (**Figure 1.6**) [68]. The BsAb has the same binding affinity for GD2 as parental IgG but CD3 binding was significantly reduced compared to parental anti-CD3 mAb. Using humanized anti GD2 and CD3 antibodies lowered the amounts of neutralizing antibodies generated when administered in humans. The Hu3f8-BsAb was highly potent against $GD2^+$ tumor with cytotoxicity at femtomolar concentrations and greater than 10^5 fold selectivity over normal tissues. In addition, asparagine 297 of the Fc was mutated to alanine to remove the Fc glycosylation, which was proposed to reduce the risk of cytokine storm syndrome by preventing Fc receptor mediated binding. The Hu3F8-BsAb effectively reduced tumor growth in humanized mouse model with a high safety profile. Mechanistic studies showed that besides T cells, monocytes also play critical roles in sustaining T-cell infiltration of tumor stroma, survival, or proliferation, and contributing significantly to the exceptional antitumor effect of Hu3f8-BsAb.

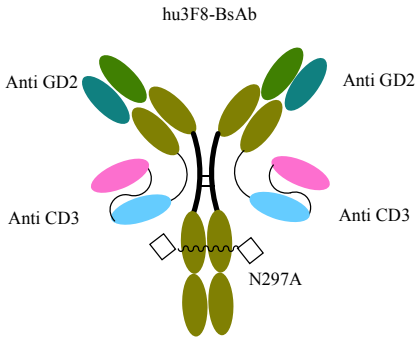

Figure 1. 6 Schematic demonstration of the Hu3F8-BsAb structure.

A non-IgG like anti-GD2 BsAb was designed by a tandem fusion of single chain variable fragment of Hu3F8 to anti-CD3 antibody HuOKT3-scFv with a 15-residue linker $(GGGGS)_3$ producing the hu3F8-scBA (**Figure 1.7)** [69]. This engineered BsAb contained the human anti GD2 (Hu3F8-scFv) rather than the murine anti-GD2 mAb 5F11 in earlier generation of the BsAb, resulting in a 13 fold higher affinity for GD2. This higher affinity led to stronger T cell activation and cytokine release *in vitro*. T cell cytotoxicity assays against GD2 expressing human cancer cells showed that Hu3F8-scFv was highly potent with EC50 values in the femtomolar range, which was up to 5,000-fold stronger than the 5F11 version of the BsAb. Hu3f8-scBA showed significant suppression of tumor growth in DKO mice with human neuroblastoma/melanoma xenografts. One drawback of Hu3F8-scFv is that this antibody has lower thermal stability, which needs to be improved for future clinical applications. Despite the decrease in thermal stability, this study highlighted that even relatively modest increases in antigen affinity could lead to substantial enhancement of the functional properties of the BsAb.

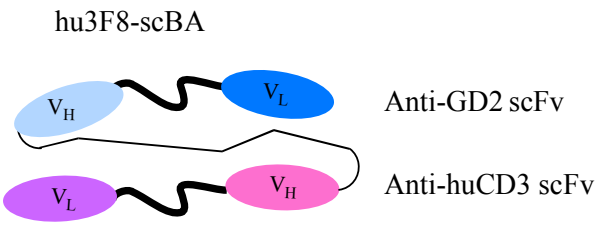

Figure 1. 7 scFv-based bispecific antibody format of Hu3F8-scBA (V_H is the heavy chain of the variable region, and the V_L is the light chain of the variable region).

BsAbs can be applied in combinatorial therapy to enhance the effectiveness of the therapy and address immune suppression encountered. Deppisch et. al. constructed a BsAb antibody termed Surek, which targets both GD2 and the CD3 receptor on murine T cells with the Fc region consisting of mouse IgG2a and rat IgG2b isotypes recognizable by Fc receptors [70]. The combination of mouse IgG2a and rat IgG2b isotypes can facilitate the purification of quadroma bispecific antibodies by affinity chromatography using protein A taking advantage of the differential affinities of various IgG isotypes with protein A. The Surek was able to successfully recruit T cells to tumor tissues. However, detailed analysis showed that cytotoxic T-lymphocyte-associated protein 4 (CTLA-4), another immune checkpoint protein, was upregulated in these redirected T cells, which led to the addition of an anti-CTLA-4 mAb for treatment. The combined Surek and anti-CTLA-4 mAb regime increased the overall survival of mice challenged with B78-D14 melanoma to 90% compared to the Surek alone (60%), while only 20% of the mice in the group receiving anti-CTLA-4 mAb alone survived the tumor. However, the survival advantage was more modest in another melanoma model B16-EpCAM.

Besides the direct effect of Surek on tumor cells, Surek could induce tumor-specific humoral immune responses [16], enhancing tumor protection *in vivo*. Combined administration of Surek with CTLA-4 blockade improved humoral immunity against cancer, which correlated with increased serum titers of melanoma-reactive IgG2a antibodies. The combinatorial vaccination markedly increased the number of memory $CD4^+$ T cells [70]. Survival rate of mice challenged with tumor three weeks after immunization receiving both Surek and anti-CTLA-4 antibodies was 40% better than the group immunized with Surek only.

1.4.2 MUC1 based BsAbs

Compared to GD2 based BsAbs, there are far fewer studies on MUC1 based BsAbs. Two BsAbs, i.e., MUC1 x CD3 and MUC1 x CD28 were constructed [71]. These two BsAbs reacted well with $MUC1^+$ tumor cells, and in the presence of interleukin-12 activated killer cells, were able to exhibit significant cytotoxicity to tumor cells. The cytotoxicity by MUC1 x CD3 BsAb alone was similar to those when the MUC1 x CD3 and MUC1 x CD28 BsAbs were combined. When evaluated in a mouse tumor model, MUC1 x CD3 BsAb was able to significantly slow down the growth of TFK-1, a type of human bile duct carcinoma.

In addition to T cells, natural killer cells (NK cells) are another type of effector cells capable of killing infected or malignant cells. NK cell mediated antibody-dependent cellular cytotoxicity plays a major role in antibody mediated targeted cancer therapy, including anti-MUC1 and anti-GD2 monoclonal antibody treatment [72–74]. As an alternative to T cell recruiting BsAbs, bispecific antibody capable of binding with NK cells has been investigated for TACAs. A new non-IgG like BsAb was designed by linking single domain anti-MUC1 and anti-CD16 antibodies through a short dipeptide linker. This BsAb could be efficiently expressed in *E. coli*, and recruit NK cells to bestow potent killing of MUC1 expressing tumor cells. In mouse xenograft tumor models, the BsAb provided significant protection from human colon cancer LS174 growth [75].

1.4.3 CAR T cells vs BsAbs

A direct comparison study of GD2 targeting BsAb (Hu3F8 x anti CD3) vs CAR T cells was reported by Cheung and coworkers [76]. When incubated with GD2 expressing tumor cells *in vitro*, a majority of CAR T cells with high density receptors were depleted while T cells stimulated with BsAb survived. Upregulations of PD1 and LAG3 marker expression were seen in both groups after stimulation with target cells suggesting that over-expression of PD1 was not the exhaustion

signal in this study and blocking of PD1 did not improve the CAR T cell survival. CAR T cell exhaustion was observed in all generated CAR T cells with different affinities, indicating that the density of CAR on the cell surface rather than the affinity of the CAR itself may be the important determinant of the GD2 CAR T cell depletion. BsAb in conjunction with untransduced T cells showed superior antitumor activity *in vivo* in human melanoma xenograft model. While both CAR T cells and BsAb recruited T cells penetrated into the tumor sites, the number of tumor infiltrating lymphocytes (TIL) was greater with untransduced T cells plus BsAb treatment compared to the CAR T cell group, which can be the result of higher proliferation of T cells in presence of BsAb. The TIL showed equal percentage of $CD4^+$ and $CD8^+$ T cell population for BsAb group *versus* CAR T group with almost all the CAR T cells expressing $CD8^+$. This absence of $CD4^+$ T cell may have compromised the therapeutic response of CAR T cells [76].

1.5 Conclusions and perspectives

With the overexpression on a wide range of cancer cells, TACAs are attractive targets for immunotherapy development. Anti-TACA CAR T cells and BsAbs are exciting directions for TACA based immunotherapy.

While the concept of CAR T cells can be relatively straightforward, multiple parameters need to be established for effective CAR T therapy. Early studies of GD2 CAR T cells demonstrated that it is important to build in costimulatory domains such as CD28 and OX40 into the T cells in order to maintain the abilities of cells to proliferate, as well as to reduce T cell exhaustion and AICD. Other stimulatory molecules including IL15 and CD27 have been incorporated into GD2 CAR T cells, which enabled long term persistence of the cells in human patients and led to improved clinical outcome. Co-administration of immune checkpoint blockade

through anti-PD-1 antibody may help further augment the efficacy and persistence of GD2 CAR T cells.

To overcome low penetration of CAR T cells into solid tumor tissues, GD2 CAR T therapy has been combined with anti-angiogenic agents as well as heparanase for digestion of extracellular matrix. This led to significantly improved protection of mice from $GD2^+$ tumor induced death.

As GD2 CAR T cells become more potent, the "on target, off tumor" binding of T cells to low level of GD2 expressed in normal tissues can cause serious side effects including neurotoxicity. To address this challenge, CAR engineering can be performed to reduce Fc receptor binding to CAR. Furthermore, innovative research has been established to introduce inducible suicide gene or design target modules to turn on and turn off the CAR T responses when necessary.

Similar to GD2 CAR T cells, the design of effective MUC1 CAR T cells required built-in co-stimulatory signals to sustain CAR T cell proliferation, enhance cytotoxicity, and resist AICD. Another major consideration for MUC1 CAR T cells is the MUC1 epitope to be targeted as MUC1 glycoprotein contains many potential antigenic sites. Early generations of the cells were based on antibodies recognizing the unglycosylated MUC1 peptides in the VNTR region of MUC1-N. While in preclinical models, these CAR T cells delayed tumor growth, there were concerns regarding potential auto-immunity. To address this issue, MUC1 CAR T cells were developed targeting the more tumor specific MUC1-Tn glycopeptides, which recognized multiple tumor cell lines. When evaluated in xenograft model of human pancreatic cancer studies, these CAR T cells provided complete protection to tumor bearing mice.

As an alternative to CAR T cells, bispecific antibodies have shown great promises in anti-cancer therapy. The most common type of TACA based BsAbs targets GD2 and CD3 on T cells. Engineering of the BsAbs include humanization of the non-human origin scFv to reduce the level

of neutralization antibodies, and Fc mutation to reduce the risk of cytokine storm syndrome. These BsAbs can direct activated T cells to GD2 expressing tumor tissues, leading to significant tumor lysis even with femtomolar concentrations of the BsAbs.

A direct comparison study has been performed to compare GD2 BsAbs and CAR T cells. Administration of BsAbs in conjunction with untransduced T cells were found to lead to longer survival of activated T cells. Furthermore, BsAbs-T cells provided more effective tumor protection in tumor models. The superiority of BsAbs-T cells could be partly attributed to the presence of $CD4^+$ helper T cells in BsAbs-T cells, while the infused CAR T cells were almost exclusively $CD8^+$ T cells.

Building on the results from the reported CAR T cell and BsAb studies, a promising direction to explore is to test novel combination therapies. As cancer cells may mutate to downregulate the levels of targeted antigen under immune pressure, constructs that can potentially bind with multiple types of antigens may help reduce the chances of tumor escape and enhance treatment efficacy. Other combinations can include the addition of checkpoint inhibition such as anti-PD1 and anti-CTLA4 mAbs, agents that can enhance the access and penetration of immune cells to solid tumor, as well as chemotherapeutic agents. In order to guide such studies, it is critical to gain a more thorough understanding of the tumor microenvironment and factors in suppressing the immune responses. These approaches may overcome the inhibitory signals in tumor microenvironment, high interstitial fluid pressure, compressed vasculature and dense fibrotic tissue surrounding solid tumors and increase the delivery of immunotherapeutic agents to solid tumors.

A critical factor in the success of immunotherapy is in minimizing potential toxicity and side effects, especially considering many tumor antigens can also be found in normal tissues, albeit

at low levels. To reduce the "on target, off tumor" side effects, further investigation for characterization of TACA structures in solid tumor tissues can lead to the discovery of unique TACA derivatives. For example, the expression of the 9-*O*-acetylated GD2 gangliosides has been reported to be restricted to tumor tissues, while they are not found in normal tissues [77]. Furthermore, compared to normal cells, tumors tend to contain more *N*-glycolyl neuraminic acid [78,79]. These rarer structures may provide more specific targets for anti-cancer immunotherapy to enhance the safety of the treatment.

REFERENCES

REFERENCES

[1] World Health Organisation, Latest global cancer data, Int. Agency Res. Cancer. (2018) 13–15. https://www.iarc.fr/wp-content/uploads/2018/09/pr263_E.pdf (accessed November 3, 2019).

[2] International Agency for Research on Cancer, Cancer Tomorrow, World Heal. Organ. (2019)1–2.

[3] J. Couzin-Frankel, Breakthrough of the year 2013. Cancer immunotherapy, Science. 342 (2013) 1432–3. doi:10.1126/science.342.6165.1432.

[4] S.I. Hakomori, Tumor-associated carbohydrate antigens defining tumor malignancy: Basis for development of anti-cancer vaccines, Adv. Exp. Med. Biol., 2001: pp. 369–402. doi:10.1007/978-1-4615-1267-7_24.

[5] T. Buskas, P. Thompson, G.J. Boons, Immunotherapy for cancer: Synthetic carbohydrate-based vaccines, Chem. Commun. (2009) 5335–5349. doi:10.1039/b908664c.

[6] X. Jing, H. Liang, C. Hao, X. Yang, X. Cui, Overexpression of MUC1 predicts poor prognosis in patients with breast cancer, Oncol. Rep. 41 (2019) 801–810. doi:10.3892/or.2018.6887.

[7] S. Danishefsky, J. Allen, From the laboratory to the clinic: A retrospective on fully synthetic carbohydrate-based anticancer vaccines frequently used abbreviations are listed in the appendix, Angew. Chem. Int. Ed. Engl. 39 (2000) 836–863. doi:10.1002/(sici)1521-3773(20000303)39:5<836::aid-anie836>3.0.co;2-i.

[8] Z. Yin, X. Huang, Recent development in carbohydrate based anticancer vaccines, J. Carbohydr. Chem. 31 (2012) 143–186. doi:10.1080/07328303.2012.659364.

[9] M.M. Wei, Y.S. Wang, X.S. Ye, Carbohydrate-based vaccines for oncotherapy, Med. Res. Rev. 38 (2018) 1003–1026. doi:10.1002/med.21493.

[10] D. Feng, A.S. Shaikh, F. Wang, Recent advance in tumor-associated carbohydrate antigens (TACAs)-based antitumor vaccines, ACS Chem. Biol. 11 (2016) 850–863. doi:10.1021/acschembio.6b00084.

[11] Z. Guo, Q. Wang, Recent development in carbohydrate-based cancer vaccines, Curr. Opin. Chem. Biol. 13 (2009) 608–617. doi:10.1016/j.cbpa.2009.08.010.

[12] R.S. Riley, C.H. June, R. Langer, M.J. Mitchell, Delivery technologies for cancer immunotherapy, Nat. Rev. Drug Discov. 18 (2019) 175–196. doi:10.1038/s41573-018-0006-z.

[13] K.O. Lloyd, L.J. Old, Human monoclonal antibodies to glycolipids and other carbohydrate antigens: dissection of the humoral immune response in cancer patients, Cancer Res. 49 (1989) 3445–3451. https://cancerres.aacrjournals.org/content/49/13/3445.full-text.pdf (accessed October 31, 2019).

[14] S. Sait, S. Modak, Anti-GD2 immunotherapy for neuroblastoma, Expert Rev. Anticancer Ther. 17 (2017) 889–904. doi:10.1080/14737140.2017.1364995.

[15] J.-T. Hung, A.L. Yu, GD2-Targeted Immunotherapy of Neuroblastoma, in: Neuroblastoma, Elsevier, 2019: pp. 63–78. doi:10.1016/b978-0-12-812005-7.00004-7.

[16] V.L. Battula, Y. Shi, K.W. Evans, R.Y. Wang, E.L. Spaeth, R.O. Jacamo, R. Guerra, A.A. Sahin, F.C. Marini, G. Hortobagyi, S.A. Mani, M. Andreeff, Ganglioside GD2 identifies breast cancer stem cells and promotes tumorigenesis, J. Clin. Invest. 122 (2012) 2066–2078. doi:10.1172/JCI59735.

[17] M.A. Cheever, J.P. Allison, A.S. Ferris, O.J. Finn, B.M. Hastings, T.T. Hecht, I. Mellman, S.A. Prindiville, J.L. Viner, L.M. Weiner, L.M. Matrisian, The prioritization of cancer antigens: A national cancer institute pilot project for the acceleration of translational research, Clin. Cancer Res. 15 (2009) 5323–5337. doi:10.1158/1078-0432.CCR-09-0737.

[18] S.D. Gillies, K.M. Lo, J. Wesolowski, High-level expression of chimeric antibodies using adapted cDNA variable region cassettes, J. Immunol. Methods. 125 (1989) 191–202. doi:10.1016/0022-1759(89)90093-8.

[19] M.M. D'Aloia, I.G. Zizzari, B. Sacchetti, L. Pierelli, M. Alimandi, CAR-T cells: The long and winding road to solid tumors review-article, Cell Death Dis. 9 (2018). doi:10.1038/s41419-018-0278-6.

[20] C. Rossig, C.M. Bollard, J.G. Nuchtern, D.A. Merchant, M.K. Brenner, Targeting of GD2-positive tumor cells by human T lymphocytes engineered to express chimeric T-cell receptor genes, Int. J. Cancer. 94 (2001) 228–236. doi:10.1002/ijc.1457.

[21] R.M. Richards, E. Sotillo, R.G. Majzner, CAR T cell therapy for neuroblastoma, Front. Immunol. 9 (2018) 2380. doi:10.3389/fimmu.2018.02380.

[22] M.A. Pule, B. Savoldo, G.D. Myers, C. Rossig, H. V. Russell, G. Dotti, M.H. Huls, E. Liu, A.P. Gee, Z. Mei, E. Yvon, H.L. Weiss, H. Liu, C.M. Rooney, H.E. Heslop, M.K. Brenner, Virus-specific T cells engineered to coexpress tumor-specific receptors: Persistence and antitumor activity in individuals with neuroblastoma, Nat. Med. 14 (2008) 1264–1270. doi:10.1038/nm.1882.

[23] C.U. Louis, B. Savoldo, G. Dotti, M. Pule, E. Yvon, G.D. Myers, C. Rossig, H. V. Russell, O. Diouf, E. Liu, H. Liu, M.F. Wu, A.P. Gee, Z. Mei, C.M. Rooney, H.E. Heslop, M.K. Brenner, Antitumor activity and long-term fate of chimeric antigen receptor-positive T cells in patients with neuroblastoma, Blood. 118 (2011) 6050–6056. doi:10.1182/blood-2011-05-354449.

[24] Y. Chen, C. Sun, E. Landoni, L. Metelitsa, G. Dotti, B. Savoldo, Eradication of neuroblastoma by T cells redirected with an optimized GD2-specific chimeric antigen receptor and interleukin-15, Clin. Cancer Res. 25 (2019) 2915–2924. doi:10.1158/1078-0432.CCR-18-1811.

[25] F. You, L. Jiang, B. Zhang, Q. Lu, Q. Zhou, X. Liao, H. Wu, K. Du, Y. Zhu, H. Meng, Z. Gong, Y. Zong, L. Huang, M. Lu, J. Tang, Y. Li, X. Zhai, X. Wang, S. Ye, D. Chen, L. Yuan, L. Qi, L. Yang, Phase 1 clinical trial demonstrated that MUC1 positive metastatic seminal vesicle cancer can be effectively eradicated by modified Anti-MUC1 chimeric antigen receptor transduced T cells, Sci. China Life Sci. 59 (2016) 386–397. doi:10.1007/s11427-016-5024-7.

[26] D.G. Song, Q. Ye, M. Poussin, G.M. Harms, M. Figini, D.J. Powell, CD27 costimulation augments the survival and antitumor activity of redirected human T cells in vivo, Blood. 119 (2012) 696–706. doi:10.1182/blood-2011-03-344275.

[27] J.A. Craddock, A. Lu, A. Bear, M. Pule, M.K. Brenner, C.M. Rooney, A.E. Foster, Enhanced tumor trafficking of GD2 chimeric antigen receptor T cells by expression of the chemokine receptor CCR2b, J. Immunother. 33 (2010) 780–788. doi:10.1097/CJI.0b013e3181ee6675.

[28] P. Bocca, E. Di Carlo, I. Caruana, L. Emionite, M. Cilli, B. De Angelis, C. Quintarelli, A. Pezzolo, L. Raffaghello, F. Morandi, F. Locatelli, V. Pistoia, I. Prigione, Bevacizumab-mediated tumor vasculature remodelling improves tumor infiltration and antitumor efficacy of GD2-CAR T cells in a human neuroblastoma preclinical model, Oncoimmunology. (2017). doi:10.1080/2162402X.2017.1378843.

[29] I. Caruana, B. Savoldo, V. Hoyos, G. Weber, H. Liu, E.S. Kim, M.M. Ittmann, D. Marchetti, G. Dotti, Heparanase promotes tumor infiltration and antitumor activity of CAR-redirected T lymphocytes, Nat. Med. 21 (2015) 524–529. doi:10.1038/nm.3833.

[30] T. Gargett, W. Yu, G. Dotti, E.S. Yvon, S.N. Christo, J.D. Hayball, I.D. Lewis, M.K. Brenner, M.P. Brown, GD2-specific CAR T cells undergo potent activation and deletion following antigen encounter but can be protected from activation-induced cell death by PD-1 blockade, Mol. Ther. 24 (2016) 1135–1149. doi:10.1038/mt.2016.63.

[31] R.M. Gibbons, X. Liu, V. Pulko, S.M. Harrington, C.J. Krco, E.D. Kwon, H. Dong, B7-H1 limits the entry of effector CD8+ T cells to the memory pool by upregulating bim, Oncoimmunology. 1 (2012) 1061–1073. doi:10.4161/onci.20850.

[32] Y.E. Latchman, S.C. Liang, Y. Wu, T. Chernova, R.A. Sobel, M. Klemm, V.K. Kuchroo, G.J. Freman, A.H. Sharpe, PD-L1-deficient mice show that PD-L1 on T cells, antigen-presenting cells, and host tissues negatively regulates T cells, Proc. Natl. Acad. Sci. U. S. A. 101 (2004) 10691–10696. doi:10.1073/pnas.0307252101.

[33] J.H. Rowe, T.M. Johanns, J.M. Ertelt, S.S. Way, PDL-1 blockade impedes T Cell expansion and protective immunity primed by attenuated listeria monocytogenes, J. Immunol. 180 (2008) 7553–7557. doi:10.4049/jimmunol.180.11.7553.

[34] A. Heczey, C.U. Louis, B. Savoldo, O. Dakhova, A. Durett, B. Grilley, H. Liu, M.F. Wu, Z. Mei, A. Gee, B. Mehta, H. Zhang, N. Mahmood, H. Tashiro, H.E. Heslop, G. Dotti, C.M. Rooney, M.K. Brenner, CAR T cells administered in combination with lymphodepletion and PD-1 Inhibition to patients with neuroblastoma, Mol. Ther. 25 (2017) 2214–2224. doi:10.1016/j.ymthe.2017.05.012.

[35] L.B. John, M.H. Kershaw, P.K. Darcy, Blockade of PD-1 immunosuppression boosts CAR T-cell therapy, Oncoimmunology. 2 (2013) e26286. doi:10.4161/onci.26286.

[36] L. Cherkassky, A. Morello, J. Villena-Vargas, Y. Feng, D.S. Dimitrov, D.R. Jones, M. Sadelain, P.S. Adusumilli, Human CAR T cells with cell-intrinsic PD-1 checkpoint blockade resist tumor-mediated inhibition, J. Clin. Invest. 126 (2016) 3130–3144. doi:10.1172/JCI83092.

[37] E.A. Chong, J.J. Melenhorst, S.F. Lacey, D.E. Ambrose, V. Gonzalez, B.L. Levine, C.H. June, S.J. Schuster, PD-1 blockade modulates chimeric antigen receptor (CAR)-modified T cells: Refueling the CAR, Blood. 129 (2017) 1039–1041. doi:10.1182/blood-2016-09-738245.

[38] S. Thomas, K. Straathof, N. Himoudi, J. Anderson, M. Pule, An optimized GD2-targeting retroviral cassette for more potent and safer cellular therapy of neuroblastoma and other cancers, PLoS One. 11 (2016). doi:10.1371/journal.pone.0152196.

[39] S.A. Richman, S. Nunez-Cruz, B. Moghimi, L.Z. Li, Z.T. Gershenson, Z. Mourelatos, D.M. Barrett, S.A. Grupp, M.C. Milone, High-Affinity GD2-specific CAR T cells induce fatal encephalitis in a preclinical neuroblastoma model, Cancer Immunol. Res. 6 (2018) 36–46. doi:10.1158/2326-6066.CIR-17-0211.

[40] T. Gargett, M.P. Brown, The inducible caspase-9 suicide gene system as a “safety switch” to limit on-target, off-tumor toxicities of chimeric antigen receptor T-cells, Front. Pharmacol. 5 (2014) 235. doi:10.3389/fphar.2014.00235.

[41] N. Mitwasi, A. Feldmann, R. Bergmann, N. Berndt, C. Arndt, S. Koristka, A. Kegler, J. Jureczek, A. Hoffmann, A. Ehninger, M. Cartellieri, S. Albert, C. Rossig, G. Ehninger, J. Pietzsch, J. Steinbach, M. Bachmann, Development of novel target modules for retargeting of UniCAR T cells to GD2 positive tumor cells, Oncotarget. 8 (2017) 108584–108603. doi:10.18632/oncotarget.21017.

[42] P.X.X. Apostolopoulos Vasso, Hu Xiu Fen, Pouniotis Dodie Stephanie, MUC1: a molecule of many talents, Curr. Trends Immunol. 6 (2004) 39–55.

[43] D.W. Kufe, MUC1-C oncoprotein as a target in breast cancer: Activation of signaling pathways and therapeutic approaches, Oncogene. 32 (2013) 1073–1081. doi:10.1038/onc.2012.158.

[44] N.K. Ibrahim, K.O. Yariz, I. Bondarenko, A. Manikhas, V. Semiglazov, A. Alyasova, V. Komisarenko, Y. Shparyk, J.L. Murray, D. Jones, S. Senderovich, A. Chau, F. Erlandsson, G. Acton, M. Pegram, Randomized phase II trial of letrozole plus Anti-MUC1 antibody

AS1402 in hormone receptor-positive locally advanced or metastatic breast cancer, Clin. Cancer Res. 17 (2011) 6822–6830. doi:10.1158/1078-0432.CCR-11-1151.

[45] C. Steentoft, D. Migliorini, T.R. King, U. Mandel, C.H. June, A.D. Posey, Glycan-directed CAR-T cells, Glycobiology. 28 (2018) 656–669. doi:10.1093/glycob/cwy008.

[46] M.K. Hossain, K.A. Wall, Immunological evaluation of recent MUC1 glycopeptide cancer vaccines, Vaccines. 4 (2016) 25. doi:10.3390/vaccines4030025.

[47] J. Taylor-Papadimitriou, J.M. Burchell, R. Graham, R. Beatson, Latest developments in MUC1 immunotherapy, Biochem. Soc. Trans. 46 (2018) 659–668. doi:10.1042/BST20170400.

[48] S. Wilkie, G. Picco, J. Foster, D.M. Davies, S. Julien, L. Cooper, S. Arif, S.J. Mather, J. Taylor-Papadimitriou, J.M. Burchell, J. Maher, Retargeting of human T cells to tumor-associated MUC1: the evolution of a chimeric antigen receptor, J. Immunol. 180 (2008) 4901–4909. doi:10.4049/jimmunol.180.7.4901.

[49] F. You, L. Jiang, B. Zhang, Q. Lu, Q. Zhou, X. Liao, H. Wu, K. Du, Y. Zhu, H. Meng, Z. Gong, Y. Zong, L. Huang, M. Lu, J. Tang, Y. Li, X. Zhai, X. Wang, S. Ye, D. Chen, L. Yuan, L. Qi, L. Yang, Phase 1 clinical trial demonstrated that MUC1 positive metastatic seminal vesicle cancer can be effectively eradicated by modified Anti-MUC1 chimeric antigen receptor transduced T cells, Sci. China Life Sci. 59 (2016) 386–397. doi:10.1007/s11427-016-5024-7.

[50] J. Maher, S. Wilkie, CAR mechanics: Driving T cells into the MUC of cancer, Cancer Res. 69 (2009) 4559–4562. doi:10.1158/0008-5472.CAN-09-0564.

[51] E. Gheybi, J. Amani, A.H. Salmanian, F. Mashayekhi, S. Khodi, Designing a recombinant chimeric construct contain MUC1 and HER2 extracellular domain for prediagnostic breast cancer, Tumor Biol. 35 (2014) 11489–11497. doi:10.1007/s13277-014-2483-y.

[52] A.L. Sørensen, C.A. Reis, M.A. Tarp, U. Mandel, K. Ramachandran, V. Sankaranarayanan, T. Schwientek, R. Graham, J. Taylor-Papadimitriou, M.A. Hollingsworth, J. Burchell, H. Clausen, Chemoenzymatically synthesized multimeric Tn/STn MUC1 glycopeptides elicit cancer-specific anti-MUC1 antibody responses and override tolerance, Glycobiology. 16 (2006) 96–107. doi:10.1093/glycob/cwj044.

[53] A.D. Posey, R.D. Schwab, A.C. Boesteanu, C. Steentoft, U. Mandel, B. Engels, J.D. Stone, T.D. Madsen, K. Schreiber, K.M. Haines, A.P. Cogdill, T.J. Chen, D. Song, J. Scholler, D.M. Kranz, M.D. Feldman, R. Young, B. Keith, H. Schreiber, H. Clausen, L.A. Johnson, C.H. June, Engineered CAR T cells targeting the cancer-associated Tn-glycoform of the membrane mucin MUC1 control adenocarcinoma, Immunity. 44 (2016) 1444–1454. doi:10.1016/j.immuni.2016.05.014.

[54] R. Zhou, M. Yazdanifar, L. Das Roy, L.M. Whilding, A. Gavrill, J. Maher, P. Mukherjee, CAR T cells targeting the tumor MUC1 glycoprotein reduce triple-negative breast cancer growth, Front. Immunol. 10 (2019) 1–12. doi:10.3389/fimmu.2019.01149.

[55] X. Wei, Y. Lai, J. Li, L. Qin, Y. Xu, R. Zhao, B. Li, S. Lin, S. Wang, Q. Wu, Q. Liang, M. Peng, F. Yu, Y. Li, X. Zhang, Y. Wu, P. Liu, D. Pei, Y. Yao, P. Li, PSCA and MUC1 in non-small-cell lung cancer as targets of chimeric antigen receptor T cells, Oncoimmunology 6 (2017) e1284722. doi:10.1080/2162402X.2017.1284722.

[56] G. Dotti, B. Savoldo, M. Brenner, Fifteen years of gene therapy based on chimeric antigen receptors: Are we nearly there yet?, Hum. Gene Ther. 20 (2009) 1229–1239. doi:10.1089/hum.2009.142.

[57] H. Büning, W. Uckert, K. Cichutek, R.E. Hawkins, H. Abken, Do CARs need a driver's license? Adoptive cell therapy with chimeric antigen receptor-redirected T cells has caused serious adverse events, Hum. Gene Ther. 21 (2010) 1039–1042. doi:10.1089/hum.2010.131.

[58] A.L. Szymczak, C.J. Workman, Y. Wang, K.M. Vignali, S. Dilioglou, E.F. Vanin, D.A.A. Vignali, Correction of multi-gene deficiency in vivo using a single "self-cleaving" 2A peptide-based retroviral vector, Nat. Biotechnol. 22 (2004) 589–594. doi:10.1038/nbt957.

[59] S. Wilkie, M.C.I. Van Schalkwyk, S. Hobbs, D.M. Davies, S.J.C. Van Der Stegen, A.C.P. Pereira, S.E. Burbridge, C. Box, S.A. Eccles, J. Maher, Dual targeting of ErbB2 and MUC1 in breast cancer using chimeric antigen receptors engineered to provide complementary signaling, J. Clin. Immunol. 32 (2012) 1059–1070. doi:10.1007/s10875-012-9689-9.

[60] C.C. Kloss, M. Condomines, M. Cartellieri, M. Bachmann, M. Sadelain, Combinatorial antigen recognition with balanced signaling promotes selective tumor eradication by engineered T cells, Nat. Biotechnol. 31 (2013) 71–75. doi:10.1038/nbt.2459.

[61] E. Lanitis, M. Poussin, A.W. Klattenhoff, D. Song, R. Sandaltzopoulos, C.H. June, D.J. Powell, Chimeric antigen receptor T Cells with dissociated signaling domains exhibit focused antitumor activity with reduced potential for toxicity in vivo, Cancer Immunol. Res. 1 (2013) 43–53. doi:10.1158/2326-6066.CIR-13-0008.

[62] G. Fan, Z. Wang, M. Hao, J. Li, Bispecific antibodies and their applications, J. Hematol. Oncol. 8 (2015) 130. doi:10.1186/s13045-015-0227-0.

[63] R.E. Kontermann, U. Brinkmann, Bispecific antibodies; different formats, Drug Discov. Today. 20 (2015) 838–847. doi:10.1016/j.drudis.2015.02.008.

[64] D. Bhutani, L.G. Lum, Activated T cells armed with bispecific antibodies kill tumor targets, Curr. Opin. Hematol. 22 (2015) 476–483. doi:10.1097/MOH.0000000000000176.

[65] B. Husain, D. Ellerman, Expanding the Boundaries of Biotherapeutics with Bispecific Antibodies, BioDrugs. 32 (2018) 441–464. doi:10.1007/s40259-018-0299-9.

[66] D. Holmes, Buy buy bispecific antibodies, Nat. Rev. Drug Discov. 10 (2011) 798–800. doi:10.1038/nrd3581.

[67] M. Yankelevich, S.V. Kondadasula, A. Thakur, S. Buck, N.K. V. Cheung, L.G. Lum, Anti-CD3×anti-GD2 bispecific antibody redirects T-cell cytolytic activity to neuroblastoma targets, Pediatr. Blood Cancer. 59 (2012) 1198–1205. doi:10.1002/pbc.24237.

[68] H. Xu, M. Cheng, H. Guo, Y. Chen, M. Huse, N.K. V. Cheung, Retargeting T cells to GD2 pentasaccharide on human tumors using bispecific humanized antibody, Cancer Immunol. Res. 3 (2015) 266–277. doi:10.1158/2326-6066.CIR-14-0230-T.

[69] M. Cheng, B.H. Santich, H. Xu, M. Ahmed, M. Huse, N.K. V. Cheung, Successful engineering of a highly potent single-chain variable-fragment (scFv) bispecific antibody to target disialoganglioside (GD2) positive tumors, Oncoimmunology 5 (2016) 1–9. doi:10.1080/2162402X.2016.1168557.

[70] N. Deppisch, P. Ruf, N. Eißler, H. Lindhofer, R. Mocikat, Potent CD4+ T cell-associated antitumor memory responses induced by trifunctional bispecific antibodies in combination with immune checkpoint inhibition, Oncotarget. 8 (2017) 4520–4529. doi:10.18632/oncotarget.13888.

[71] Y. Katayose, T. Kudo, M. Suzuki, M. Shinoda, S. Saijyo, N. Sakurai, H. Saeki, K. Fukuhara, K. Imai, S. Matsuno, MUC1-specific targeting immunotherapy with bispecific antibodies: Inhibition of xenografted human bile duct carcinoma growth, Cancer Res. 56 (1996) 4205–4212. http://www.ncbi.nlm.nih.gov/pubmed/8797593 (accessed October 31, 2019).

[72] S. Modak, J.B. Le Luduec, I.Y. Cheung, D.A. Goldman, I. Ostrovnaya, E. Doubrovina, E. Basu, B.H. Kushner, K. Kramer, S.S. Roberts, R.J. O'Reilly, N.K. V. Cheung, K.C. Hsu, Adoptive immunotherapy with haploidentical natural killer cells and Anti-GD2 monoclonal antibody m3F8 for resistant neuroblastoma: Results of a phase I study, Oncoimmunology 7 (2018) e1461305. doi:10.1080/2162402X.2018.1461305.

[73] N. Tarek, J.B. Le Luduec, M.M. Gallagher, J. Zheng, J.M. Venstrom, E. Chamberlain, S. Modak, G. Heller, B. Dupont, N.K. V. Cheung, K.C. Hsu, Unlicensed NK cells target neuroblastoma following anti-GD2 antibody treatment, J. Clin. Invest. 122 (2012) 3260–3270. doi:10.1172/JCI62749.

[74] J. Schettini, A. Kidiyoor, D.M. Besmer, T.L. Tinder, L. Das Roy, J. Lustgarten, S.J. Gendler, P. Mukherjee, Intratumoral delivery of CpG-conjugated anti-MUC1 antibody enhances NK cell anti-tumor activity, Cancer Immunol. Immunother. 61 (2012) 2055–2065. doi:10.1007/s00262-012-1264-y.

[75] Y. Li, C. Zhou, J. Li, J. Liu, L. Lin, L. Li, D. Cao, Q. Li, Z. Wang, Single domain based bispecific antibody, Muc1-Bi-1, and its humanized form, Muc1-Bi-2, induce potent cancer cell killing in muc1 positive tumor cells, PLoS One 13 (2018) 1–14. doi:10.1371/journal.pone.0191024.

[76] S.S. Hoseini, K. Dobrenkov, D. Pankov, X.L. Xu, N.K. V. Cheung, Bispecific antibody does not induce T-cell death mediated by chimeric antigen receptor against disialoganglioside GD2, Oncoimmunology 6 (2017) e1320625. doi:10.1080/2162402X.2017.1320625.

[77] N. Alvarez-Rueda, A. Desselle, D. Cochonneau, T. Chaumette, B. Clemenceau, S. Leprieur, G. Bougras, S. Supiot, J.M. Mussini, J. Barbet, J. Saba, F. Paris, J. Aubry, S. Birklé, A monoclonal antibody to O-Acetyl-GD2 ganglioside and not to GD2 shows potent anti-tumor activity without peripheral nervous system cross-reactivity, PLoS One 6 (2011) e25220. doi:10.1371/journal.pone.0025220.

[78] A.N. Samraj, H. Läubli, N. Varki, A. Varki, Involvement of a non-human sialic acid in human cancer, Front. Oncol. 4 MAR (2014) 33. doi:10.3389/fonc.2014.00033.

[79] S. Inoue, C. Sato, K. Kitajima, Extensive enrichment of N-glycolylneuraminic acid in extracellular sialoglycoproteins abundantly synthesized and secreted by human cancer cells, Glycobiology 20 (2010) 752–762. doi:10.1093/glycob/cwq030.

CHAPTER 2: Virus like particle display of *Vibrio cholerae O*-specific polysaccharide as a potential vaccine against cholera

2.1 Introduction

Cholera is an acute, secretory diarrheal disease caused by the highly transmissible bacterium *Vibrio cholerae. V* (*V. cholerae*)*. cholerae* are gram-negative and highly motile bacteria with a single polar flagellum. There are more than 200 serogroups of *V. cholerae* based on the O antigen of surface lipopolysaccharide (LPS) structures, but only serogroups O1 and O139 are capable of causing epidemic cholera. *V. cholerae* O1 has two serotypes, i.e., Ogawa and Inaba, based on the presence or absence of a methyl group on the non-reducing terminal perosamine moiety of the surface O-specific polysaccharide (OSP, O-antigen) [1]. There are 2-3 million cases of cholera each year, resulting in tens of thousands of deaths annually [2]. Current cholera vaccines include oral killed whole cell vaccine with or without cholera toxin B subunit (CtxB), and attenuated oral cholera vaccine [3]. Inclusion of the cholera vaccine into global cholera control strategies has been transformative, but current oral vaccines have the lowest level and duration of protection in young children [4–8], who bear a large share of global cholera burden, especially in cholera-endemic countries [2,3,9–11]. As such, there is a need to develop new cholera vaccines that can provide high level and long-term immunity.

Immunity protective against cholera infection targets the OSP of *V. cholerae* [12,13]. However, as O-antigens are T cell independent B cells antigens, direct administration of the O-antigens often only leads to low titers of low□affinity IgM antibodies with limited duration of antibody responses and a lack of induction of immunological memory, rendering O-antigen-based vaccination suboptimal [14–16]. Covalent linkage of carbohydrate to a carrier protein provides a T cell-dependent immune response by activating $CD4^+$ T cells and enables memory B cell proliferation for long lasting antibody protection. Recently, we have demonstrated that self□

assembled virus□like particles (VLPs) such as bacteriophage Qβ could be used to conjugate with carbohydrate antigens such as the Thomsen-Nouveau (Tn) antigen and ganglioside GM2 and GD2 as potential vaccines [17,18]. The resulting glycoconjugates were able to induce strong glycan specific IgG antibody responses. However, to date, only low molecular weight (MW generally below 2,000 Da) glycans have been investigated for Qβ based anti-carbohydrate vaccine studies. It is not known whether bacterial polysaccharide antigens could be conjugated with Qβ and whether such conjugates could induce strong IgG antibody responses to such polysaccharides.

Herein, we report that the native *O*-specific polysaccharide (OSP) **1** of *Vibrio cholerae* O1, Inaba serotype was successfully conjugated with Qβ through squarate chemistry, which is the first time that a bacterial polysaccharide antigen is covalently linked with Qβ as a potential vaccine. This approach provides direct conjugation without prior introduction of a linker to the protein carrier. High levels of anti-polysaccharide IgG antibodies were induced by the conjugate in mice, and the antibodies were effective in killing the bacteria.

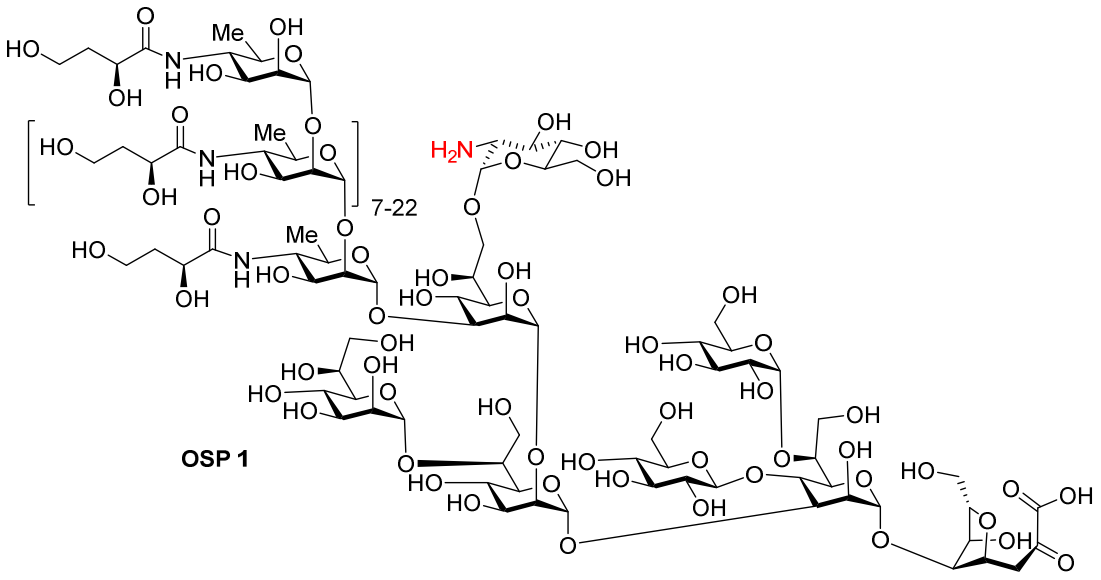

Figure 2. 1 Structure of *O*-specific polysaccharide (OSP) **1** of *Vibrio cholerae* O1

2.2 Results

2.2.1 Conjugation of the OSP core antigen to Qβ

To efficiently link the OSP antigen to Qβ, we built upon previous work using squarate based conjugation of polysaccharide (the conjugation and characterization part of the work were performed by Dr. Peng Xu) [19–21]. 3,4-Dimethoxy-3-cyclobutene-1,2-dione (dimethyl squarate) **2** is a unique bifunctional linker, both of whose methoxy groups are reactive with amines but under different pH conditions. The first methoxy group can be substituted by a primary amine in neutral pH and the second one is active toward amines in a basic solution. The squaramide moiety itself is stable to hydrolysis under the aqueous reaction conditions [22]. To optimize the conjugation reaction with the squarate ester chemistry, Qβ was conjugated with a squarate functionalized lactose **3**[23] as a model reaction. Lactoside **3** was prepared by derivatizing lactose **4**[23] with dimethyl squarate **2** in 76% yield (**Scheme 2.1a**). In parallel, the coat protein of Qβ triple mutant A38K/A40C/D102C was expressed in *E. coli*, which self-assembled into nanoparticles with average diameters of 28 nm consisting of 180 copies of the monomer [24]. The lactoside **3** was then incubated with Qβ (14eq per monomer) at 22°C for 20 hours leading to the Qβ-lactose conjugate **5** (**Scheme 2.1b).** In order to quantify the degree of modification, surface-enhanced laser desorption/ionization time-of-flight (SELDI-TOF) mass spectrometry analysis was performed (**Figure 2.1**). Based on the intensities of the mass spectrometry (MS) peaks for Qβ coat protein monomer conjugated with lactosides, it was estimated there was an average loading of 4.5 haptens per Qβ monomer, corresponding to 810 copies per Qβ capsid. Increasing the amount of **3** to 28 eq led to an average of 8 lactosides conjugated per Qβ monomer unit (1,440 copies per Qβ capsid). As each monomer of the Qβ triple mutant A38K/A40C/D102C has 9 total free amines (8 lysines plus the free *N*-terminus), the ability to nearly fully functionalize Qβ suggests the squarate

chemistry is highly efficient in promoting glycan conjugation with Qβ. To further characterize the conjugate, gel electrophoresis analysis was carried out **(Figure 2.2)**. In the presence of reducing agents, the Qβ capsid disassembled to its subunits showing bands at 14KDa and 28KDa corresponding to the monomer and dimer of the coat protein respectively (**Figure 2.2,** lane 11). After conjugation, the monomer band of the Qβ coat protein shifted to about 19 KDa, correlating well with the addition of ~8 lactose units per Qβ monomer on average (lane 10).

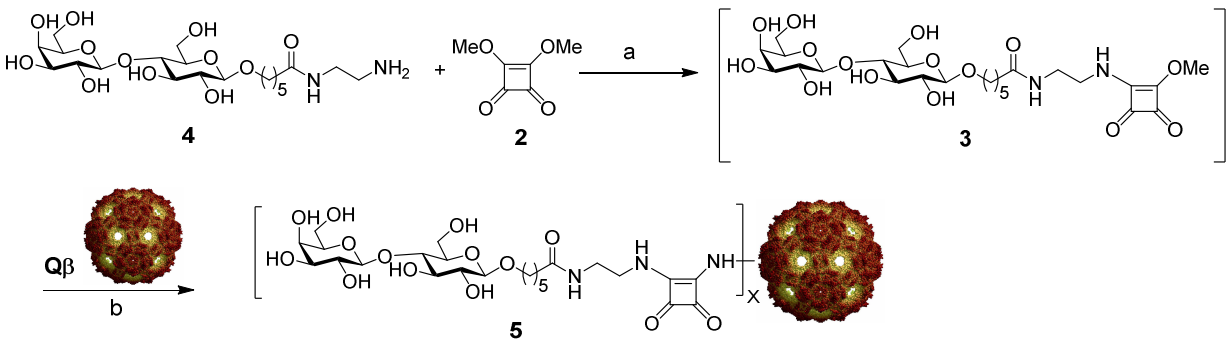

Scheme 2. 1 Qβ conjugation to lactose squarate **3**. a) 0.5M pH 7.0 phosphate buffer, r.t., 3h, 76%; b) 0.5M borate buffer, pH 9.0, r.t., 90h.

We next explored the conjugation of *Vibrio cholerae* O1 Inaba OSP from PIC018[21] with Qβ using the squarate chemistry. *V. cholerae* O1 Inaba OSP **1** was treated with dimethyl squarate **2** first, which was then incubated with Qβ. To preserve the valuable material, the amount of OSP-squarate was reduced to 8 equivalents per Qβ monomer (**Scheme 2.2**). After 120 h, the conjugation reaction was analyzed by SELDI-TOF, which only showed the peak for Qβ monomer at 14.1 KDa with very weak signals from the potential OSP adduct (Appendix, **Figure 2.12**). The SDS-PAGE of the Qβ-OSP conjugate (**Figure 2.2**, lane 9) showed a very faint band close to the Qβ monomer MW under the reducing condition with the majority of the protein sample appearing smeared at the high MW region of the gel. The incomplete disassembly of Qβ-OSP under the reducing

condition as compared to Qβ-lactose may be due to the large size of the OSP (~6 kDa), which may sterically hinder the reduction of disulfides thus holding multiple coat protein monomers together. As there was little Qβ monomer observed on the gel, the low signal from the OSP conjugate observed in SELDI-TOF (Appendix, **Figure 2.12**) was most likely due to the difficulty in ionizing the Qβ-OSP conjugate by MS. Thus, we needed to employ additional techniques beyond SELDI-TOF and SDS-PAGE to provide more quantitative information on the degree of OSP functionalization on Qβ.

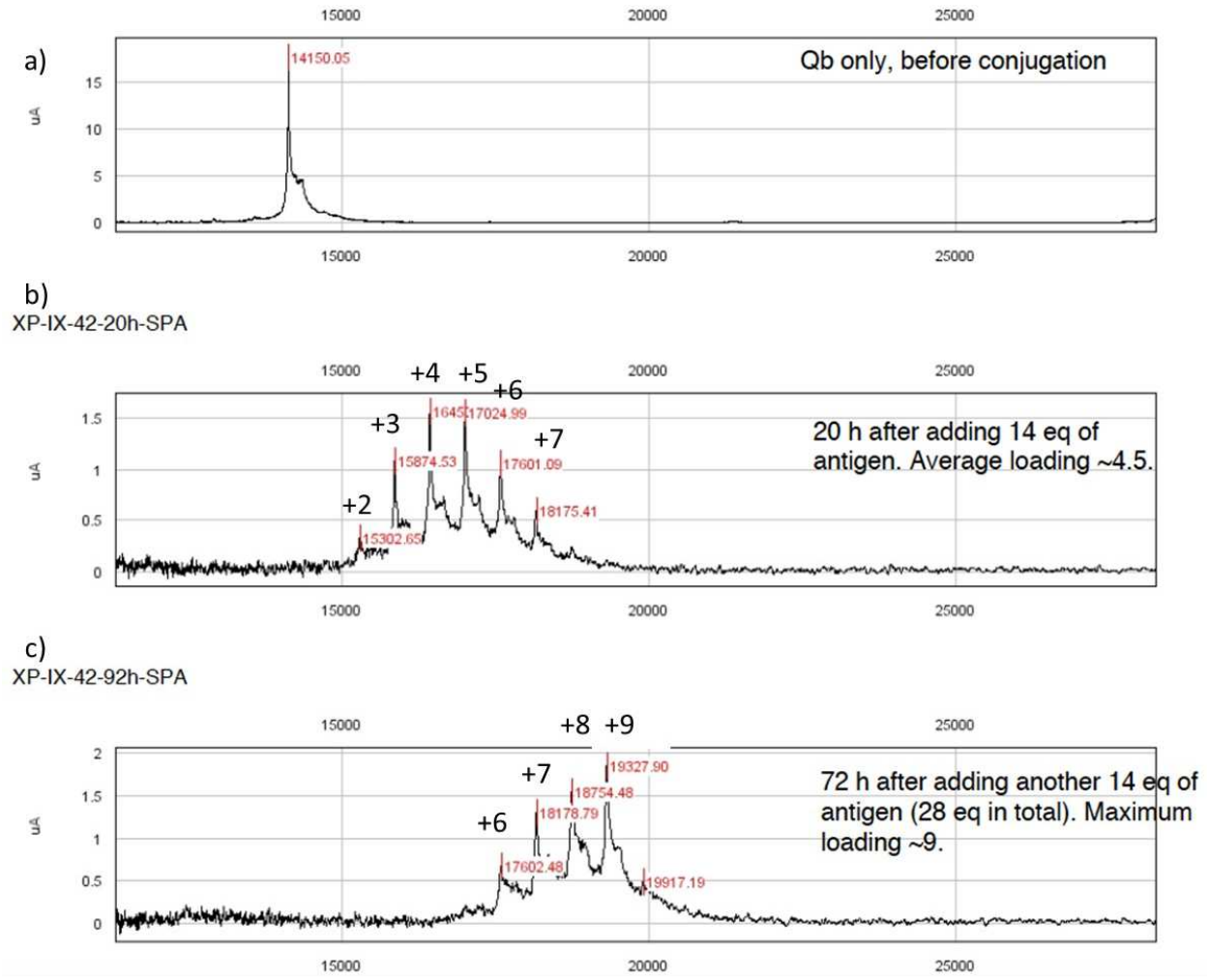

Figure 2. 2 SELDI-TOF MS result of the conjugation of Qβ triple mutant A38K/A40C/D102C and lactose squarate **3**. a) Qβ before conjugation, b) 14 eq of **3** was added to Qβ and the reaction mixture was incubated for 20h, c) An additional 14eq of **3** was added to reaction and incubated for 72h. The mass difference between the peaks corresponds to the addition of a lactose squarate with MW of 577 Da. The average loading was calculated based on the ratio of the sum of respective antigen number of each peak multiplied by their intensity to the total intensity of all peaks.

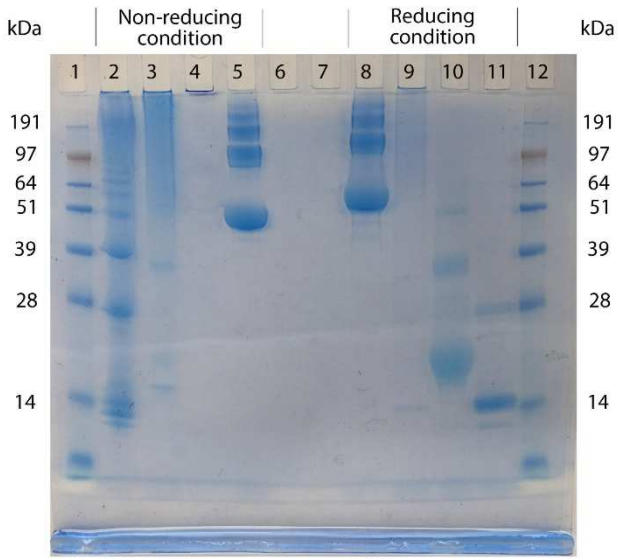

Figure 2. 3 The SDS-PAGE of different samples at non-reducing (Lanes 1-5) and reducing (Lanes 8-12) conditions. Lanes 1, 12: Molecular weight ladder; lanes 2, 11: unconjugated Qβ; lanes 3, 10: Qβ-lactose conjugate; lanes 4, 9: Qβ-OSP conjugate; lanes 5, 8: BSA. The Qβ monomer and dimer appeared at 14KDa and 28KDa under the reducing condition. The band corresponding to the Qβ-lactose **5** monomer shifted to about 19 kDa after conjugation, corresponding to the addition of about 8 lactoses per monomer. Qβ-OSP conjugate showed up as a smear at higher MW on the gel.

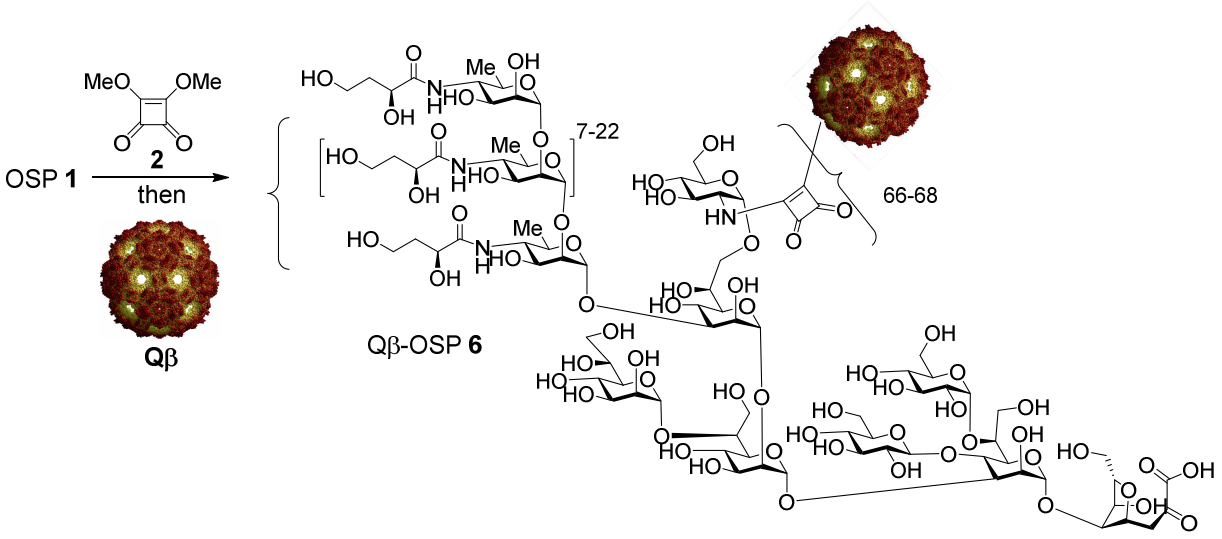

Scheme 2. 2 Conjugation of OSP **1** to Qβ VLP. OSP **1** was activated with dimethyl squarate **2**, and subsequently added to a Qβ solution in 0.5M borate buffer, pH=9.0. After 120h, the reaction was worked up by ultrafiltration against pH 7.2 (1x) PBS buffer.

We next tested Mass Photometry (MP)[25] to quantify OSP functionalization of Qβ. While the aforementioned SELDI-TOF and SDS-PAGE methods for VLP analysis rely on disassembly of the particles and assessing the conjugation at the individual monomeric coat protein levels, MP measures light scattering from the intact particle, which is proportional to the mass of the scattering particles. By analyzing hundreds to thousands of particles, the mass distribution of the sample is generated. To the best of our knowledge, MP has only been applied twice to study VLPs to date [26,27]. When we measured the Qβ sample, there were two populations and the MW was decreasing over time (**Figure 2.3**). This could be resulting from the instability and degradation of RNA encapsulated inside the Qβ. To test this possibility, we prepared a Qβ sample without RNA by cleaving the RNA chemically with Lead acetate and measured the empty particles with MP. Although we still observed two populations in the sample, the MW remained stable in two different measurements of the same sample over a 3-month interval (**Figure 2.4**). This supported that the result is reproducible and that MW reduction over time observed with full Qβ was likely due to RNA degradation. The population of Qβ particles with smaller molecular weight that was observed in the MP spectrum may be the result of partially disassembled VLPs.

In order to calibrate the mass shifts in MP, we conjugated the Qβ capsid without RNA with lacoside **3** as a control sample. Based on the MW of this conjugate obtained from MP, the lactose loading was about 7 per monomer (**Figure 2.5**), which was close to the average loading of 6 obtained from the same sample on QTOF-ESI (Appendix, **Figure 2.14**) and SELDI-TOF (Appendix, **Figure 2.15**). With this result, we confirmed that the mass shift in Qβ sample after conjugation is due to the loading of the carbohydrate and hence the difference in mass can be used to calculate the loading.

We analyzed the Qβ-OSP conjugate with MP next. Upon OSP conjugation, the mean mass shifted about 400 kDa based on the MW of intact particles (**Figure 2.6**). With the average MW of OSP at ~6,000 Da, it was calculated that on average there were 68 OSP molecules per Qβ capsid. The OSP conjugation and MP protocols were reproducible, giving 66-68 OSP units per Qβ on two independent batches of Qβ-OSP conjugates.

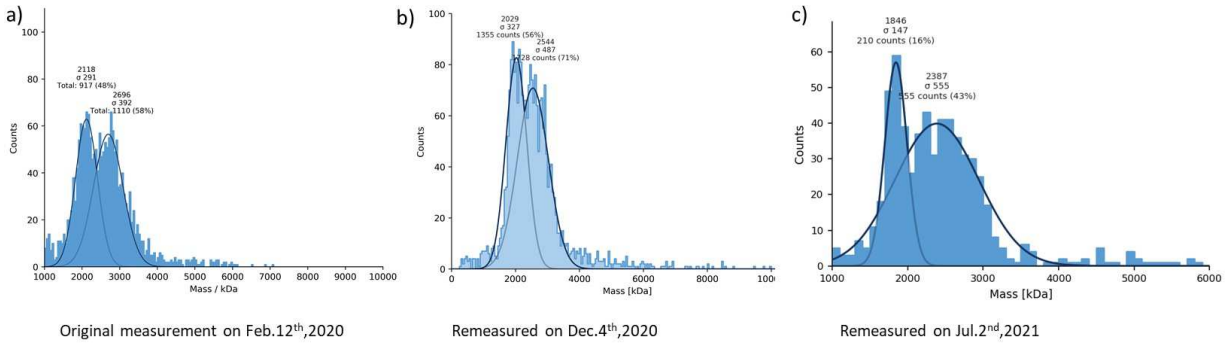

Figure 2. 4 The MP result of Qβ triple mutant A38K/A40C/D102C. The same Qβ sample which was measured several times over time of this study showed a decrease of the MW. The right peak shifted from 2696 KDa in (a) to 2544KDa (b) and 2387KDa in (c).

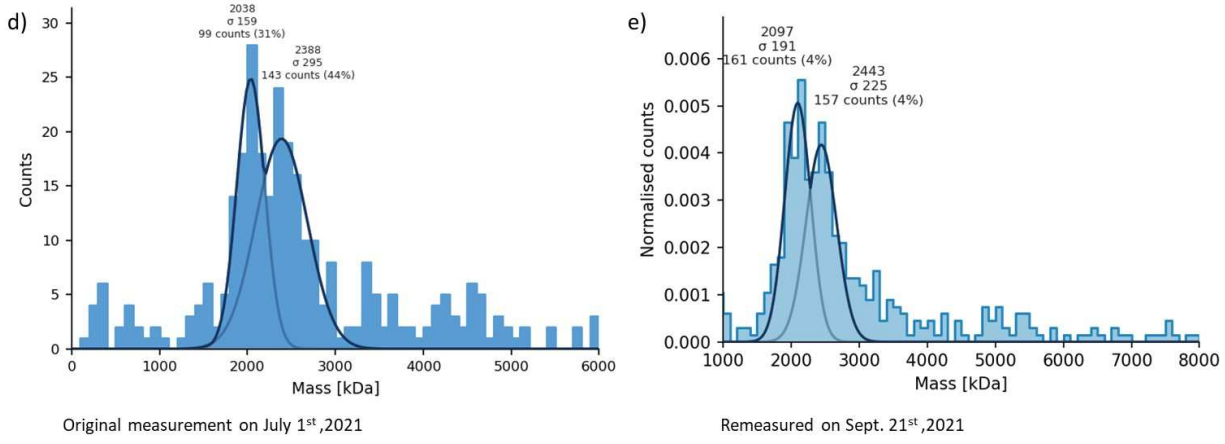

Figure 2. 5 The MP result of Qβ without RNA. The measurement of Qβ sample without RNA was repeated after three months. The MW of right peak was 2388 KDa in (d) and 2443 KDa in (e) respectively.

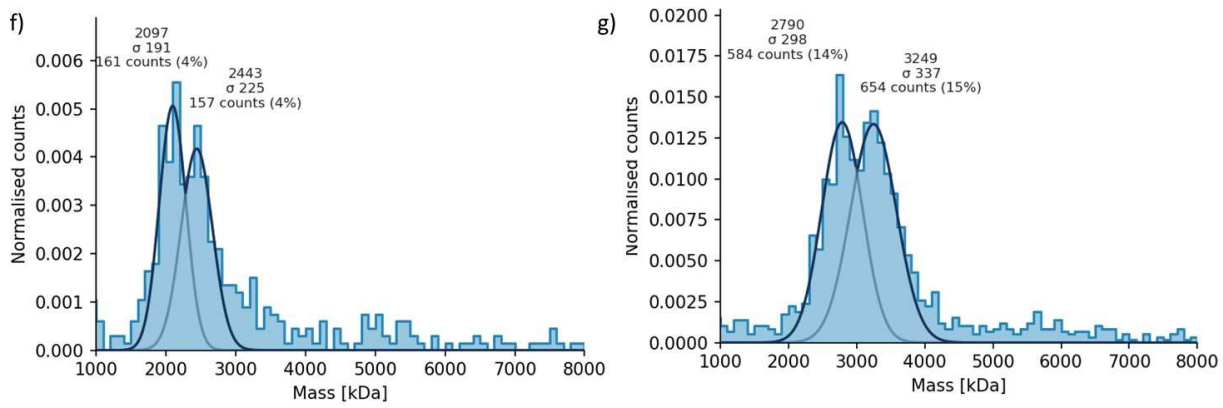

Figure 2. 6 The MP result of wild-type Qβ without RNA f) before and g) after conjugation with lactoside **3**. The right peak shifted from 2,443 KDa to 3,249 KDa, which suggests the conjugation of about 7 lactosides per Qβ monomer on average.

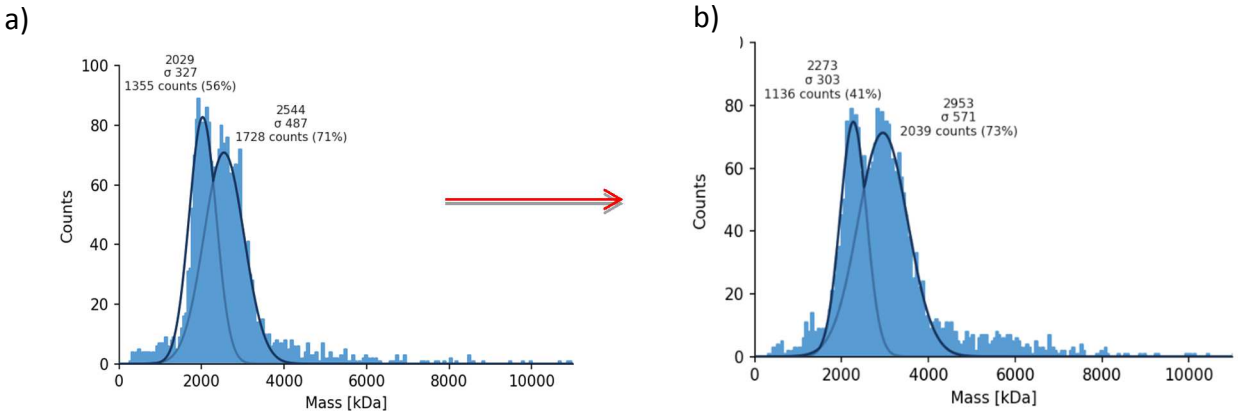

Figure 2. 7 MP results of a) Qβ and b) Qβ-OSP conjugate. The right peak shifted from 2,544 KDa to 2,953 KDa, which suggests the conjugation of an average 68 OSP per full Qβ capsid calculated based on the mass of the intact particle.

2.2.2 Immunogenicity of the Qβ-OSP conjugate

With the Qβ-OSP conjugate in hand, to analyze whether the Qβ-OSP was displaying OSP in an immunologically relevant manner, we assessed the ability of convalescent plasma from humans recovering from cholera to recognize Qβ-OSP. Plasma was collected and analyzed as previously described [21]. As shown in figure **2.7**, Qβ-OSP was recognized by convalescent phase

plasma of humans recovering from cholera (day 7 sample), but not by acute phase plasma (day 2 sample). This is most likely due to the production of protective antibodies in patients recovering from the infection. In comparison to Qβ-OSP, there was little binding of convalescent sera to Qβ by itself. Furthermore, there was no increased immune-recognition of Qβ-OSP by plasma from S. Typhi infected patients suggesting the binding of Qβ-OSP was a result from cholera infection.

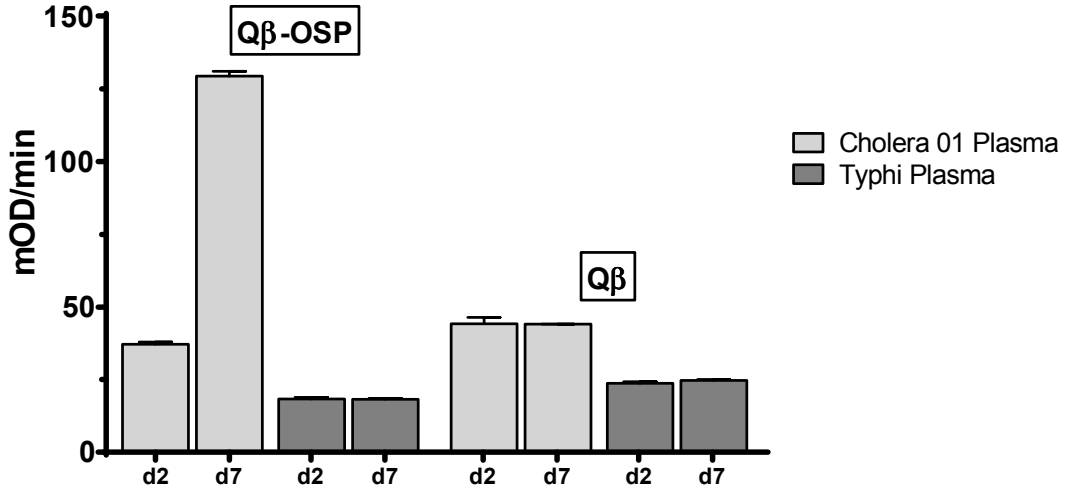

Figure 2. 8 Immunoreactivities of human plasma toward Qβ and Qβ-OSP were measured by acute phase plasma (day 2 sample) versus convalescent phase plasma (day 7 sample) of patients with cholera versus typhoid fever in Dhaka, Bangladesh.

Next, we evaluated the ability of Qβ-OSP to generate anti-OSP antibodies in animals. A group of five female Swiss-Webster (3–5 week old) mice was injected intramuscularly on days 0, 21 and 42 with the Qβ-OSP construct (10 μg OSP per mouse) in the absence of any exogenous adjuvants (**Figure 2.8a**). Blood was collected from the immunized mice on days 0, 7, 28, 49, 56 and during the study as shown in figure **2.8a**. A control group of Swiss-Webster mice received Qβ only following the same protocol. To analyze the levels of anti-OSP antibodies in the sera by enzyme-linked immunosorbent assay (ELISA), a bovine serum albumin (BSA) conjugate of OSP was prepared to avoid the interference of anti-Qβ antibodies. The anti-OSP IgG titer, the highest

dilution above background that gives optical density (OD) = 0.1, was determined in pooled sera at different time points by ELISA. While there were weak IgG responses one week after the first immunization, after the second immunization, significantly higher levels of IgG were observed on day 28, 49 and 56 (**Figures 2.8b** and **2.9**). The average IgG titers reached the maximum value of 226,504 on day 56 (**Figure 2.8c**). The IgG titer from the Qβ-OSP group remained at high levels over time with IgG titers still detectable at day 265. In contrast, there was no detectable anti-OSP IgG responses in the control group at any time point suggesting Qβ-OSP potently induced antibody responses against OSP. No anti-OSP IgM antibodies were detected. The high anti-OSP IgG levels suggested that the Qβ-OSP constructs successfully induced the activation of helper T cells, which could promote the isotype switching to IgG.

In order to assess whether memory responses were generated, on day 265 post initial immunization, mice received an additional vaccination. One week (day 272) after the booster, the average anti-OSP IgG antibody levels of the mice increased over 35 times compared to those on day 265 and reached the similar level of IgG titer as day 56. These results suggest that Qβ-OSP vaccination induced memory B cell responses and the anti-OSP humoral immunity could be boosted (**Figure 2.8b**).

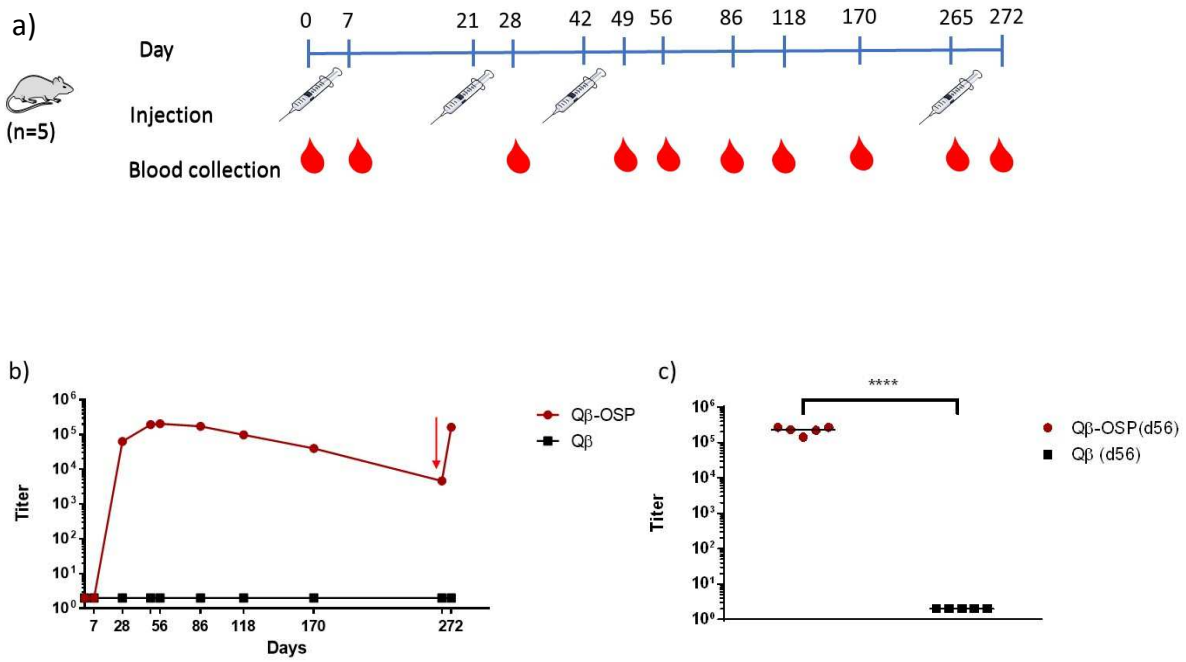

Figure 2. 9 Evaluation of Qβ-OSP immunogenicity. a) Immunization and blood collection schedule. Each group received 3 immunization three weeks apart with blood collected at day 0 and on days 56, 86, 118, 170, 265 and 272 respectively. b) OSP-specific IgG titer of pooled sera from Qβ and Qβ-OSP groups up to day 272 post-immunization. The red arrow indicates a booster injection at day 265. c) individual mouse serum OSP-specific IgG titer of Qβ and Qβ-OSP groups at day 56. The statistical significance was determined through a two tailed t-test using GraphPad Prism. ** $p < 0.0001$.

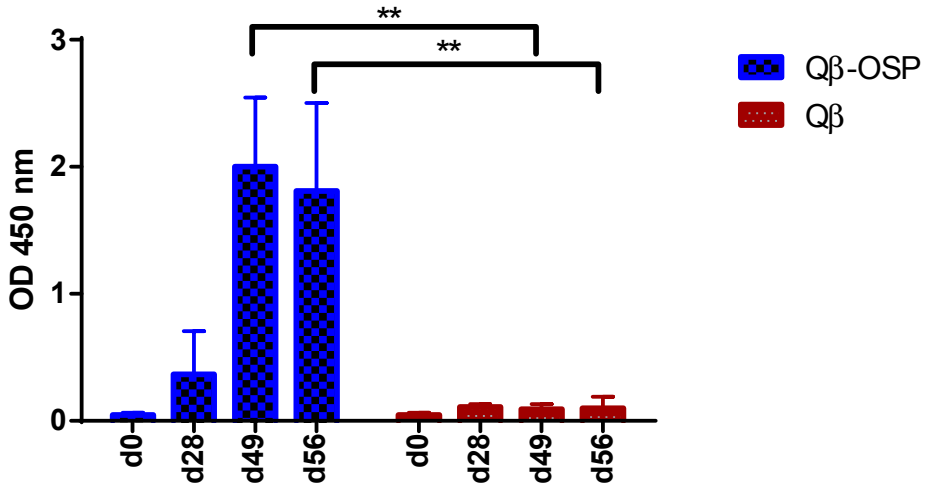

Figure 2. 10 ELISA analysis showed significant IgG binding to BSA–OSP by post-immune sera at d49 and d56 (p=0.0014 and 0.0065 respectively), compared to the control sera from mice immunized with Qβ only. Each bar represents data for 5 mice at 20,000 fold of serum dilution.

In order to determine whether immunization with Qβ-OSP would elicit antibodies recognizing the native LPS containing OSP from *V. cholerae*, ELISA analysis was also performed using *V. cholerae* O1 Inaba LPS PIC018 as the coating antigen. Sera from mice immunized with Qβ-OSP had significantly higher levels of anti-LPS IgG antibodies as compared to those from mice receiving Qβ alone (**Figure 2.10**). Furthermore, serum binding to Inaba LPS was significantly higher compared to binding to LPS from *E. coli* suggesting the antibodies induced by Qβ-OSP were selective toward Inaba (**Figure 2.10**).

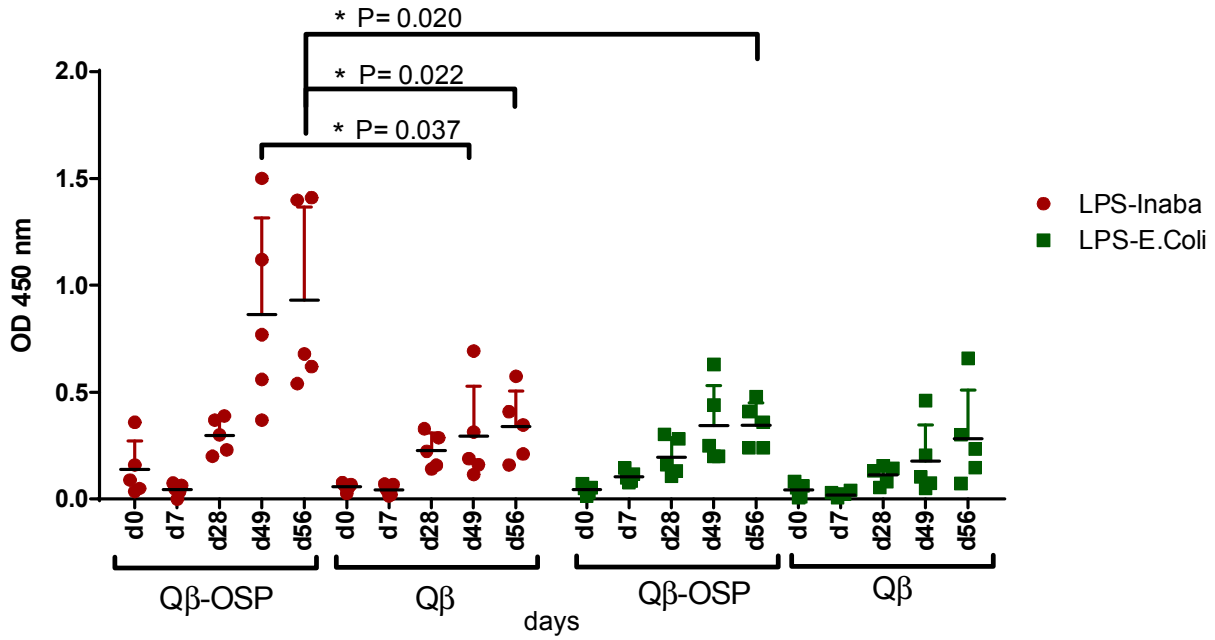

Figure 2. 11 Binding of mouse serum immunized with Qβ-OSP and Qβ to LPS from Inaba vs *E. coli*. Serum binding against Inaba LPS was observed in the Qβ-OSP immunized group while sera from the Qβ group had lower binding. The binding to *E. coli* LPS was lower by sera from both Qβ-OSP and Qβ immunized mice. The statistical significance was determined through an unpaired two tailed t-test using GraphPad Prism. * $p < 0.05$.

With the ability to selectively bind native *V. cholerae* O1 Inaba LPS and OSP by the Qβ-OSP induced antibodies established, we next measured the vibriocidal activities of the post-immune sera [21]. In the presence of an exogenous source of complement, *V. cholerae* cells are

incubated with serial serum dilutions. Anti-*V. cholerae* antibodies present in the serum sample(s) in combination with complement can lyse the live bacteria. While none of the mice from the Qβ immunized group showed any vibriocidal activities, sera from 2 of the 5 Qβ-OSP immunized mice were able to kill the bacteria at dilutions higher than those in mice immunized with Qβ alone (**Figure 2.11**).

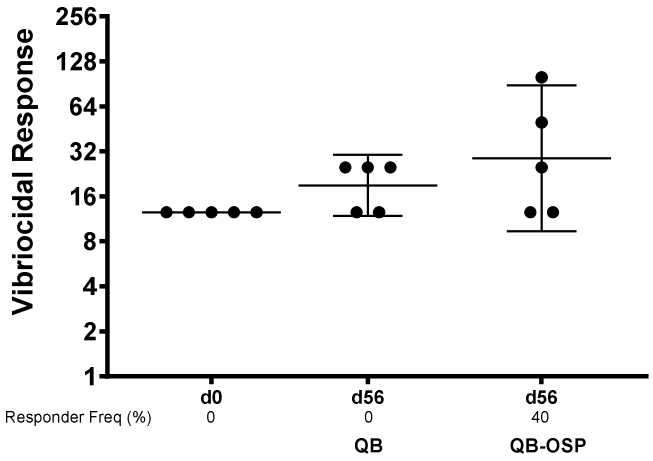

Figure 2. 12 Vibriocidal responses in vaccine cohorts. We defined responders as having an increase in vibriocidal titer by 4-fold at day 56 than day 0.

2.3 Discussion

OSP of *V. cholerae* has been used as an antigen in conjugation with BSA and recombinant heavy chain of tetanus toxin, and synthetic hexasaccharide and synthetic hexasaccharide cluster conjugates have also been evaluated as vaccine antigens against *V. cholera* [21,28–30]. A virus like particle (VLP) based approach has a number of attractive features for vaccine applications since the highly ordered organization of the protein(s) in the VLPs is well recognized via pathogen-associated molecular patterns (PAMPs) [31]. VLPs can present antigens in an organized and polyvalent manner to crosslink B-cell receptors to induce intense cellular signaling for strong

immune activation. Bacteriophage Qβ VLP is a promising platform for organized display to induce antibody responses against a target antigen.

For polysaccharide based conjugate vaccines, there are several coupling methods such as periodate activation for reductive amination, cyanylation and carbodiimide-mediated coupling. These approaches can suffer from incompatibility with some proteins and substrates and low selectivity. Squaric acid esters are favorable linker molecules in glyco-conjugate formation between amino-saccharides and proteins due to the amine-selectivity, high reactivity at room temperature, possibility of stoichiometric modification, and recovery of high-value unreacted (oligo)saccharid [32]. In the current study, we have prepared the squaric acid monoester derivative of *V. cholerae* O1 OSP core antigen utilizing the core amine group of the OSP and conjugated the monoester with VLP (carrier protein). While bacteriophage Qβ has been conjugated with glycan antigens [33–35], this is the first example of using a squarate linker for glycan conjugation with Qβ VLP. The squarate chemistry was highly efficient, leading to close to full derivatization of all free amines of Qβ coat proteins with a small glycan such as lactose **4**.

With squarate chemistry, the polysaccharide of *V. cholerae* O1 OSP was conjugated to the Qβ carrier protein via single point attachment due to the presence of single amino group per OSP molecule. The final construct may mimic native bacteria by presenting multiple OSP polysaccharide on the surface. OSP display on Qβ was in an immunologically relevant manner, which was recognized by convalescent sera of cholera infected humans but not of typhoid fever patients. The Qβ-OSP vaccine was immunogenic in mice, inducing persistent IgG responses against OSP. Such long term IgG production may assist with the long term protective goal of anti-cholera vaccination [36].

The vaccine was administrated in the absence of an exogenous adjuvant. This in part may be due to inherent adjuvant properties of Qβ VLP, which can encapsulate *E. coli* RNA molecules, thus stimulating internal cellular signals via TLR7/8 in the antigen presenting cells [37]. The induced IgG antibodies recognized native *V. cholerae* LPS and had vibriocidal activities. Induction of vibriocidal antibodies correlate with protection against cholera [38], and these responses largely target V. cholerae OSP [38,39]. The mechanism of protection against *V. cholerae* in the intestinal lumen is currently unclear, but may involve inhibition of *V. cholerae* motility through the binding of OSP-specific antibodies [40,41]. The induction of low levels *E. coli* LPS-specific IgG antibody responses (**Figure 2.10**) may be due to the presence of trace amounts of residual *E. coli* LPS in Qβ VLP preps. Studies are ongoing to express Qβ VLPs in LPS deficient *E. coli* strains.

Our study has several limitations. We focused on developing suitable coupling chemistry and analytical tools to synthesize and characterize the Qβ-OSP conjugate. We evaluated the immunogenicity of the conjugate, and future assessments could evaluate protective efficacy in a wild type *V. cholerae* challenge assay. We did not investigate the effect of adjuvant administration on anti-OSP IgG production, or the mechanism by which induced antibodies can provide protection. In addition to protective studies, the future work will analyze the effect of antibodies in inhibition of *V. cholerae* colonization in *in vitro* model using HT-29 cells, human colon carcinoma cell line, which have been widely used for interaction between host and enteric pathogens due to the similarity of structure and their function to human intestinal epithelial cells [42].

2.4 Conclusions

In this work, we have conjugated the *V. cholerae* O1 OSP polysaccharide to Qβ carrier for the first time. The MP technique yielded critical info on the level of OSP loading on Qβ. The Qβ-

OSP conjugate was recognized by sera from humans with cholera and was able to induce long lasting antibody production in the absence of adjuvant in a mice immunization study. The resulting antibodies exhibited vibriocidal activities. VLP-based display of bacterial OSP can be an attractive lead as a next generation anti-cholera vaccine.

2.5 Materials and methods

2.5.1 General experimental procedures and methods for synthesis

All chemicals were reagent grade and were used as received from the manufacturer, unless otherwise noted. Protein concentration was measured using the Coomassie Plus Protein Reagent (Bradford Assay, Pierce) with BSA as the standard. OSP and BSA-OSP was produced as previously described [21].

2.5.2 Qβ conjugation to lactoside 3 and purification

A stock solution of 4.8 mg/mL Qβ in 0.1 M (pH 7.0) KPB buffer (208 mL) was placed in a Millipore Amicon Ultra-0.5 (10 kDa cut-off) ultrafiltration device and the content was ultrafiltered against 0.5 M pH 9.0 borate buffer for three times at 10°C to exchange the buffer to 0.5 M pH 9.0 borate buffer. The filtrates were discarded and the final retentate was transferred into a 0.5 mL V-shaped reaction vessel and the same buffer was added to adjust the overall volume to 200 mL. Lactose squarate **3** (0.6 mg, 0.986 mmol) was carefully added into the reaction mixture and the content of the vessel was stirred at r.t. for 20 h. SELDI-TOF-MS analysis showed that an average loading (lactose/Qβ monomer ratio) of ~4.5 was achieved (**Figure 2.1b**). Another 0.6 mg (0.986 mmol) of compound **3** was added and the reaction mixture was further stirred for 72 h. SELDI-TOF-MS showed that the average loading reached ~8.0. The reaction was worked up by ultrafiltering the reaction mixture in a Millipore Amicon Ultra-0.5 (30k Da cut-off) tube against pH 7.2 PBS (1x) buffer for 6 times to remove the unconjugated lactose derivatives. The final retentate was transferred into a conical tube for storage.

1 mL of the above reaction mixture was diluted with 10 mL of 0.5 M pH 7.0 phosphate buffer and then mixed with 11 mL of dithiothreitol (DTT) solution (0.1 M in water). The mixture

was incubated at 37°C for 30 min. 1 mL of the above solution was withdrawn from the mixture for SELDI analysis [19] using sinapinic acid (SPA) as matrix.

2.5.3 Qβ conjugation to OSP and purification

V.cholerae O1 Inaba OSP **1** (5.4 mg, 0.0009 mmol) was converted to its squarate derivative by reacting with 3,4-dimethoxy-3-cyclobutene-1,2-dione (**2**, 2.56 mg, 0.018 mmol) in 0.5 M pH 7.0 phosphate buffer as described previously [20]. A white fluffy solid (5.4 mg, 0.00088 mmol, 98%) was obtained after work up. A stock solution of 6.7 mg/mL Qβ in 0.1 M (pH 7.0) KPB buffer (240 mL) was placed in a Millipore Amicon Ultra-0.5 (10k Da cut-off) ultrafiltration device and the content was ultrafiltered against 0.5 M pH 9.0 borate buffer for three times (at 10°C, for speed/rpm, time and volume of the concentrate, manufacturer's suggestions were followed) to exchange the buffer to 0.5 M pH 9.0 borate buffer. The filtrates were discarded and the final retentate was transferred into a 1 mL V-shaped reaction vessel and the same buffer was added to adjust the overall volume to 225 mL. The squarate derivative obtained above (5.4 mg, 0.00088mmol) was added into the vessel and the clear solution formed was stirred at r.t. After 120 h, the reaction was worked up by ultrafiltering the reaction mixture in a Millipore Amicon Ultra-4 (30k Da cut-off) tube against pH 7.2 PBS (1x) buffer for 6 times to remove the unconjugated antigen. The final retentate was transferred into a conical tube for storage.

2.5.4 MP procedure

The 24x50 mm microscope coverslips (Fisher Scientific, Waltham, MA) and precut 2x2 silicon gasket wells (GBL103250, Sigma, MO) are cleaned and assembled as described in reference [44]. Measurements were performed on OneMP instrument (Refeyn, Oxford, UK) at room temperature. PBS (1x, pH 7.2) buffer was filtered through 0.22 μM filters before use. Ten microliters of buffer was loaded in gasket well to focus the objective on the coverslip surface. Qβ

conjugates stock were diluted 100 times in PBS (1x, pH 7.2) buffer and added to buffer in the well. The MP video was immediately recorded after the sample loading using the AcquireMP software (Refeyn, Oxford, UK). A one-minute video was recorded for each sample, and each sample was repeated twice. Data were processed using DiscoverMP software (Refeyn, Oxford, UK) with the threshold filter values of 5. The mass distribution was plotted as histograms with bin width of 50kD and fit with Gaussian peaks to obtain the average mass of different species. The contrast-to-mass calibration is performed using an unstained protein ladder (LC0725, Thermofisher, Wattham, MA) and empty AAV5 sample (Virovek, Hayward, CA).

2.5.5 Immunization

All animal experiments were approved by and performed in accordance with the guidelines of the Institutional Animal Care and Use Committee (IACUC) of Michigan State University. The animal usage protocol number is PROTO201900423. Female Swiss-Webster (3–5 week old) mice were used for studies, 5 for each group. Mice were injected intramuscularly on day 0, 21 and 42 with 0.06 mL Qβ-OSP construct (10 μg OSP, 65 μg Qβ per mouse) without an exogenous adjuvant. The control group was injected with the same amount of Qβ carrier (65 μg Qβ per mouse) as the experimental group. The final boost was given at day 265. Serum samples were collected on days 0 (before immunization), 7, 28, 49, 56, 86, 118, 170, 265, and 272.

2.5.6 Evaluation of antibody titers by ELISA

The Nunc MaxiSorp® flat-bottom 96-well microtiter plates were coated with 1 μg mL^{-1} of the BSA-OSP conjugate (100 μL/well) [21] in $NaHCO_3/Na_2CO_3$ buffer (0.05 M, pH 9.6) containing 0.02 % NaN_3 by incubation at 4°C overnight. For ELISA study against LPS, plates were coated with 10 μg mL^{-1} of LPS, Inaba or E. coli, in PBS buffer overnight at room temperature. The coated plates were washed with PBS/0.5% Tween-20 (PBST) (4 × 200 μL) and blocked with

1 % BSA in PBS (200μL/well) at rt for 1 h. The plates were washed again with PBST (4 × 200 μL) and incubated with serial dilutions of mouse sera in 0.1 % BSA/PBS (100 μL/well, 2 wells for each dilution). The plates were incubated for 2 h at 37 °C and then washed with PBST (4 × 200 μL). A 1:2000 dilution of HRP-conjugated goat anti-mouse IgG or IgM (Jackson ImmunoResearch Laboratory, 115-035-003) in 0.1% BSA/PBS (100 μL) was added to the wells respectively to determine the titers of antibodies generated. The plates were incubated for 1 h at 37 °C and then washed with PBST (4 × 200 μL). A solution of enzymatic substrate 3,3',5,5'- tetramethylbenzidine (TMB, 200 μL) was added to the plates (for one plate: 5 mg of TMB was dissolved in 2 mL of DMSO plus 18 mL of citric acid buffer containing 20 μL of H_2O_2). Color was allowed to develop for 15 min and then quenched by adding 50 μL of 0.5 M H_2SO_4. The readout was measured at 450 nm using a microplate reader. The titer was determined by regression analysis with log10 dilution plotted with optical density and reported as the highest fold of dilution giving the optical absorbance value of 0.1 over those of the pre-immune control sera. 1:5000 serum dilution was used for LPS binding study as showed in figure **2.10**.

2.5.7 Evaluation of Qβ-OSP conjugates using human serum

To assess immunoreactivity of the OSP display on the Qβ conjugates, antigen specific ELISAs using sera collected from humans with cholera in Bangladesh were performed. The responses to human sera with cholera were compared to the response detected in humans with typhoid fever in Bangladesh. The plates coated with 100ng of Qβ or Qβ-OSP (based on protein mass) per well. After blocking and washing of plates, acute and convalescent phase sera from humans with cholera or typhoid (diluted 1:250 in 0.1% BSA in phosphate buffered saline-Tween) were added and incubated for 90 min at 37°C. HRP-conjugate anti-human IgG antibody at 1:5000 dilution in 0.1% BSA in phosphate buffered saline-Tween was used to detect antigen-specific

antibodies. After 90 min incubation at 37°C, 0.55 mg/ml solution of 2,2'-azinobis (3-ethylbenzothiazoline-6-sulfonic acid) (ABTS; Sigma) with 0.03% H_2O_2 (Sigma) were added to the plates and optical density was read at 405 nm for 5min at 30 s intervals. The maximum slope for an optical density change of 0.2 U was reported as millioptical density units per minute (mOD/min).

2.5.8 Serum vibriocidal responses

The vibriocidal antibody titers against V. cholerae O1 El Tor Inaba strain PIC018 were assessed in a micro-assay as previously reported [21]. The endogenous complement activity of mouse serum was inactivated by heating it for 30 min at 56°C. 50 µl aliquots of serial dilution of heat-inactivated sera in 0.15 M saline were added to wells of sterile 96-well tissue culture plates containing 25 µl/well of V. cholerae O1 El Tor Inaba strain PIC018 (OD 0.3) in 0.15 M saline and 22% guinea pig complement. After 1 hr incubation at 37°C, 150 µl of brain heart infusion broth was added to each well, and plates were incubated for an additional 2h at 37°C. The optical density of plates was then measured at 595nm. A responder was defined as having a 4-fold increase of vibriocidal titer at day 56 compared with baseline day 0 titer.

APPENDIX

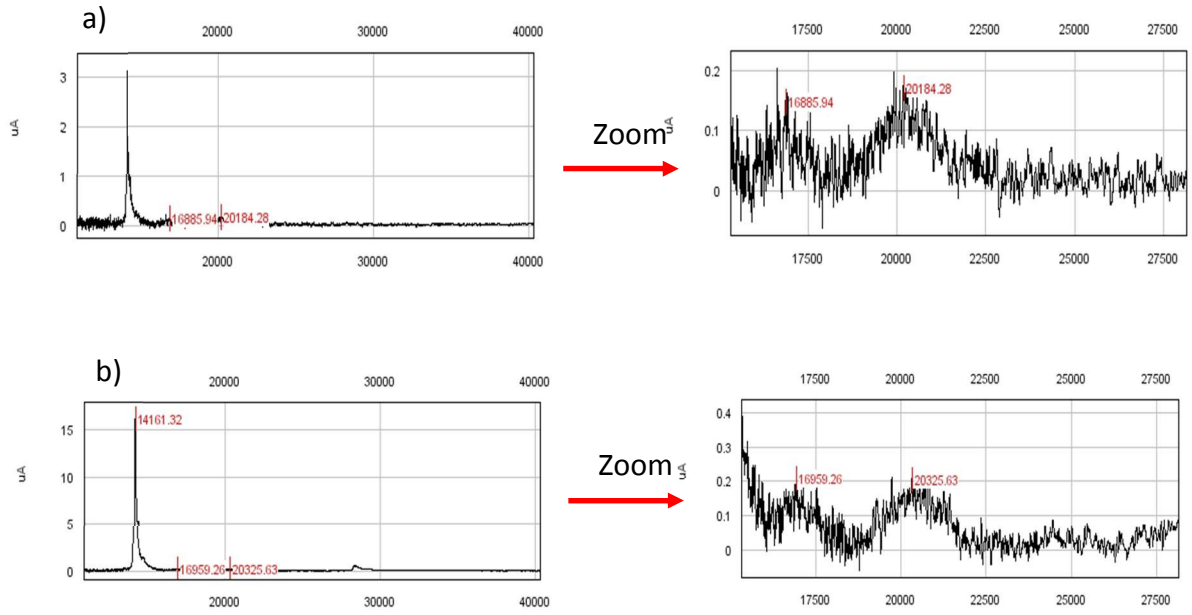

Figure 2. 13 SELDI-TOF MS result of conjugation of a) wild type Qβ or b) mutant Qβ to squarate-OSP. The broad weak peak could be observed at ~20 KDa which correlates to conjugate **6** with loading 1 OSP.

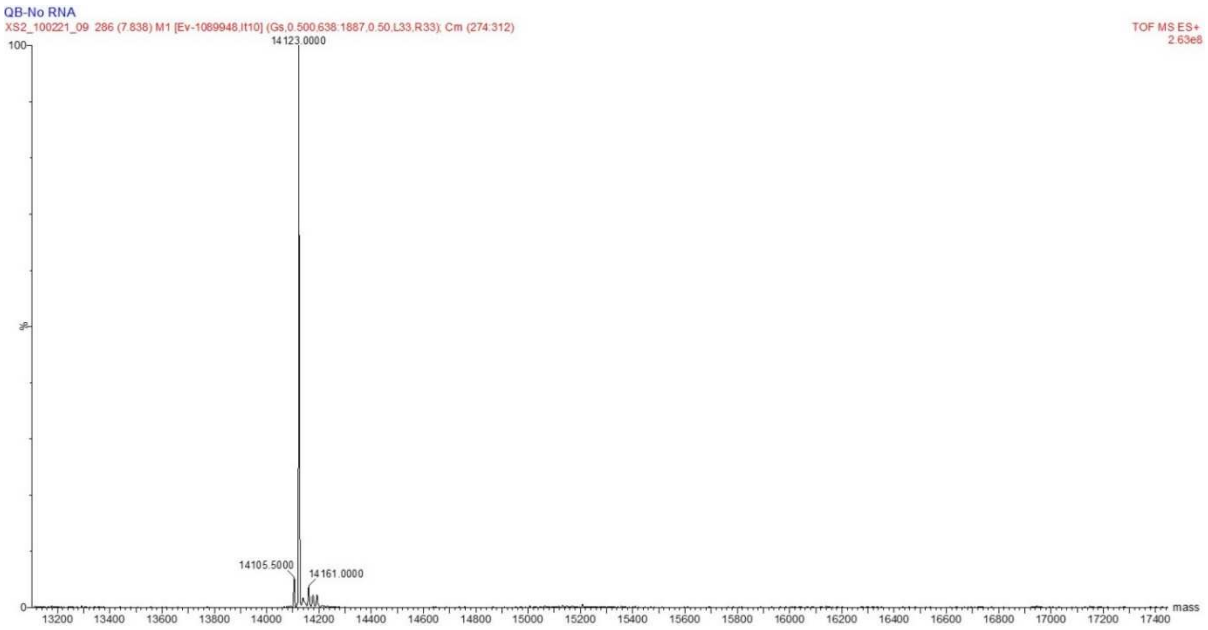

Figure 2. 14 Mass spectrum of wild-type Qβ without RNA.

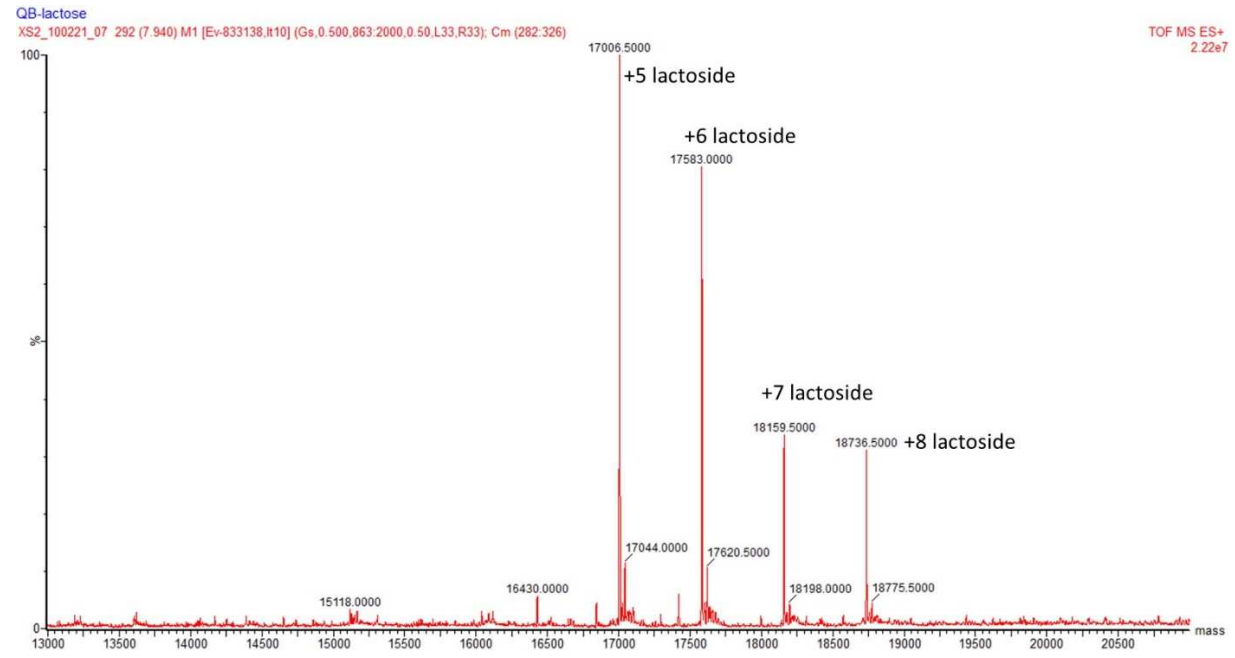

Figure 2. 15 Mass spectrum of wild-type Qβ without RNA after conjugation to lactoside. The average loading of lactoside is 6 per Qβ monomer.

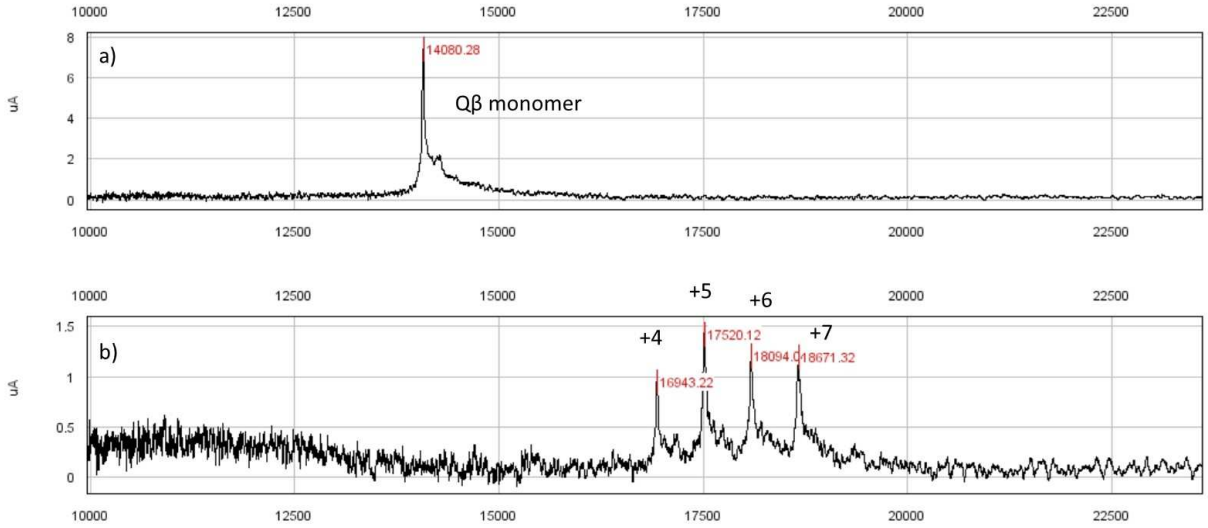

Figure 2. 16 SELDI-TOF MS result of a) wild type Qβ without RNA or b) wild type Qβ without RNA conjugated to compound **3**. The average loading of lactoside is about 6 per Qβ monomer.

REFERENCES

REFERENCES

[1] J.J. Du, C.W. Wang, W.B. Xu, L. Zhang, Y.K. Tang, S.H. Zhou, X.F. Gao, G.F. Yang, J. Guo, Multifunctional Protein Conjugates with Built-in Adjuvant (Adjuvant-Protein-Antigen) as Cancer Vaccines Boost Potent Immune Responses, IScience. 23 (2020) 100935. https://doi.org/10.1016/j.isci.2020.100935.

[2] L. Pezzoli, Global oral cholera vaccine use, 2013–2018, Vaccine. 38 (2020) A132–A140. https://doi.org/10.1016/j.vaccine.2019.08.086.

[3] J.B. Harris, Cholera: Immunity and prospects in vaccine development, J. Infect. Dis. 218 (2018) S141–S146. https://doi.org/10.1093/infdis/jiy414.

[4] S. Kanungo, A. Paisley, A.L. Lopez, M. Bhattacharya, B. Manna, D.R. Kim, S.H. Han, S. Attridge, R. Carbis, R. Rao, J. Holmgren, J.D. Clemens, D. Sur, Immune responses following one and two doses of the reformulated, bivalent, killed, whole-cell, oral cholera vaccine among adults and children in Kolkata, India: A randomized, placebo-controlled trial, Vaccine. 27 (2009) 6887–6893. https://doi.org/10.1016/j.vaccine.2009.09.008.

[5] A. Saha, M.I. Chowdhury, F. Khanam, M.S. Bhuiyan, F. Chowdhury, A.I. Khan, I.A. Khan, J. Clemens, M. Ali, A. Cravioto, F. Qadri, Safety and immunogenicity study of a killed bivalent (O1 and O139) whole-cell oral cholera vaccine Shanchol, in Bangladeshi adults and children as young as 1 year of age, Vaccine. 29 (2011) 8285–8292. https://doi.org/10.1016/j.vaccine.2011.08.108.

[6] D.T. Leung, M.A. Rahman, M. Mohasin, S.M. Patel, A. Aktar, F. Khanam, T. Uddin, M.A. Riyadh, A. Saha, M.M. Alam, F. Chowdhury, A.I. Khan, R. Charles, R. LaRocque, J.B. Harris, S.B. Calderwood, F. Qadri, E.T. Ryan, Memory B cell and other immune responses in children receiving two doses of an oral killed cholera vaccine compared to responses following natural cholera infection in Bangladesh, Clin. Vaccine Immunol. 19 (2012) 690–698. https://doi.org/10.1128/CVI.05615-11.

[7] D. Sinclair, K. Abba, K. Zaman, F. Qadri, P.M. Graves, Oral vaccines for preventing cholera, Cochrane Database Syst. Rev. (2011). https://doi.org/10.1002/14651858.cd008603.pub2.

[8] D. Sur, S. Kanungo, B. Sah, B. Manna, M. Ali, A.M. Paisley, S.K. Niyogi, J.K. Park, B. Sarkar, M.K. Puri, D.R. Kim, J.L. Deen, J. Holmgren, R. Carbis, R. Rao, N. van Thu, S.H. Han, S. Attridge, A. Donner, N.K. Ganguly, S.K. Bhattacharya, G.B. Nair, J.D. Clemens, A.L. Lopez, Efficacy of a Low-Cost, inactivated Whole-Cell oral cholera vaccine: Results from 3 years of Follow-Up of a randomized, controlled trial, PLoS Negl. Trop. Dis. 5 (2011). https://doi.org/10.1371/journal.pntd.0001289.

[9] H. Shaikh, J. Lynch, J. Kim, J.L. Excler, Current and future cholera vaccines, Vaccine. 38 (2020) A118–A126. https://doi.org/10.1016/j.vaccine.2019.12.011.

[10] G. Gabutti, A. Rossanese, A. Tomasi, S. Giuffrida, V. Nicosia, J. Barriga, C. Florescu, F.

Sandri, A. Stefanati, Cholera, the current status of cholera vaccines and recommendations for travellers, Vaccines. 8 (2020) 1–17. https://doi.org/10.3390/vaccines8040606.

[11] M. Ali, A.L. Lopez, Y.A. You, Y.E. Kim, B. Sah, B. Maskery, J. Clemens, The global burden of cholera, Bull World Heal. Organ. 90 (2012) 209–218. https://doi.org/10.2471/BLT.11.093427.

[12] K. Islam, M. Hossain, M. Kelly, L.M. Mayo Smith, R.C. Charles, T.R. Bhuiyan, P. Kováč, P. Xu, R.C. LaRocque, S.B. Calderwood, J.K. Simon, W.H. Chen, D. Haney, M. Lock, C.E. Lyon, B.D. Kirkpatrick, M. Cohen, M.M. Levine, M. Gurwith, J.B. Harris, F. Qadri, E.T. Ryan, Anti-O-specific polysaccharide (OSP) immune responses following vaccination with oral cholera vaccine CVD 103-HgR correlate with protection against cholera after infection with wild-type Vibrio cholerae O1 El Tor Inaba in North American volunteers, PLoS Negl. Trop. Dis. 12 (2018). https://doi.org/10.1371/journal.pntd.0006376.

[13] A. Aktar, M.A. Rahman, S. Afrin, A. Akter, T. Uddin, T. Yasmin, M.I.N. Sami, P. Dash, S.R. Jahan, F. Chowdhury, A.I. Khan, R.C. LaRocque, R.C. Charles, T.R. Bhuiyan, A. Mandlik, M. Kelly, P. Kováč, P. Xu, S.B. Calderwood, J.B. Harris, F. Qadri, E.T. Ryan, Plasma and memory B cell responses targeting O-specific polysaccharide (OSP) are associated with protection against Vibrio cholerae O1 infection among household contacts of cholera patients in Bangladesh, PLoS Negl. Trop. Dis. 12 (2018) e0006399. https://doi.org/10.1371/journal.pntd.0006399.

[14] X. Sun, G. Stefanetti, F. Berti, D.L. Kasper, Polysaccharide structure dictates mechanism of adaptive immune response to glycoconjugate vaccines, Proc. Natl. Acad. Sci. U. S. A. 116 (2019) 193–198. https://doi.org/10.1073/pnas.1816401115.

[15] F. Micoli, S.P. Bjarnarson, M. Arcuri, A.A.A. Pind, G.J. Magnusdottir, F. Necchi, R. Di Benedetto, M. Carducci, F. Schiavo, C. Giannelli, I. Pisoni, L.B. Martin, G. Del Giudice, C.A. MacLennan, R. Rappuoli, I. Jonsdottir, A. Saul, Short Vi-polysaccharide abrogates T-independent immune response and hyporesponsiveness elicited by long Vi-CRM197 conjugate vaccine, Proc. Natl. Acad. Sci. U. S. A. 117 (2020) 24443–24449. https://doi.org/10.1073/pnas.2005857117.

[16] J. Enotarpi, M. Tontini, C. Balocchi, D. van der Es, L. Auberger, E. Balducci, F. Carboni, D. Proietti, D. Casini, D. V Filippov, H.S. Overkleeft, G.A. van der Marel, C. Colombo, M.R. Romano, F. Berti, P. Costantino, J.D.C. Codeé, L. Lay, R. Adamo, A stabilized glycomimetic conjugate vaccine inducing protective antibodies against Neisseria meningitidis serogroup A, Nat. Commun. 11 (2020). https://doi.org/10.1038/s41467-020-18279-x.

[17] Z. Yin, S. Chowdhury, C. McKay, C. Baniel, W.S. Wright, P. Bentley, K. Kaczanowska, J.C. Gildersleeve, M.G. Finn, L. BenMohamed, X. Huang, Significant Impact of Immunogen Design on the Diversity of Antibodies Generated by Carbohydrate-Based Anticancer Vaccine, ACS Chem. Biol. 10 (2015) 2364–2372. https://doi.org/10.1021/acschembio.5b00406.

[18] Z. Yin, S. Dulaney, C.S. McKay, C. Baniel, K. Kaczanowska, S. Ramadan, M.G. Finn, X.

Huang, Chemical Synthesis of GM2 Glycans, Bioconjugation with Bacteriophage Qβ, and the Induction of Anticancer Antibodies, ChemBioChem. 17 (2016) 174–180. https://doi.org/10.1002/cbic.201500499.

[19] P. Xu, P. Kováč, Direct conjugation of bacterial polysaccharides to proteins by squaric acid chemistry, in: Methods Mol. Biol., 2019: pp. 89–98. https://doi.org/10.1007/978-1-4939-9154-9_8.

[20] P. Xu, M. Kelly, W.F. Vann, F. Qadri, E.T. Ryan, P. Kováč, Conjugate Vaccines from Bacterial Antigens by Squaric Acid Chemistry: A Closer Look, ChemBioChem. 18 (2017) 799–815. https://doi.org/https://doi.org/10.1002/cbic.201600699.

[21] M.A. Sayeed, M.K. Bufano, P. Xu, G. Eckhoff, R.C. Charles, M.M. Alam, T. Sultana, M.R. Rashu, A. Berger, G.G. Escobedo, A. Mandlik, T.R. Bhuiyan, D.T. Leung, R.C. LaRocque, J.B. Harris, S.B. Calderwood, F. Qadri, W.F. Vann, P. Kováč, E.T. Ryan, A cholera conjugate vaccine containing ospecific polysaccharide (OSP) of V. cholera o1 inaba and recombinant fragment of tetanus toxin heavy chain (OSP:rTTHC) induces serum, memory and lamina proprial responses against OSP and is protective in mice, PLoS Negl. Trop. Dis. 9 (2015). https://doi.org/10.1371/journal.pntd.0003881.

[22] R.I. Storer, C. Aciro, L.H. Jones, Squaramides: Physical properties, synthesis and applications, Chem. Soc. Rev. 40 (2011) 2330–2346. https://doi.org/10.1039/c0cs00200c.

[23] S.-J. Hou, R. Saksena, P. Kovác, Preparation of glycoconjugates by dialkyl squarate chemistry revisited., Carbohydr. Res. 343 (2008) 196–210. https://doi.org/10.1016/j.carres.2007.10.015.

[24] S. Sungsuwan, X. Wu, V. Shaw, H. Kavunja, H. McFall-Boegeman, Z. Rashidijahanabad, Z. Tan, S. Lang, Z. Tahmasebi Nick, Setare Yin, S. Ramadan, X. Jin, X. Huang, Structure Guided Design of Bacteriophage Qβ Mutants as Next Generation Carriers for Conjugate Vaccines, Submitted. (2021).

[25] G. Young, N. Hundt, D. Cole, A. Fineberg, J. Andrecka, A. Tyler, A. Olerinyova, A. Ansari, E.G. Marklund, M.P. Collier, S.A. Chandler, O. Tkachenko, J. Allen, M. Crispin, N. Billington, Y. Takagi, J.R. Sellers, C. Eichmann, P. Selenko, L. Frey, R. Riek, M.R. Galpin, W.B. Struwe, J.L.P. Benesch, P. Kukura, Quantitative mass imaging of single biological macromolecules, Science (80-.). 360 (2018) 423 LP – 427. https://doi.org/10.1126/science.aar5839.

[26] R.F. Garmann, A.M. Goldfain, V.N. Manoharan, Measurements of the self-assembly kinetics of individual viral capsids around their RNA genome, Proc. Natl. Acad. Sci. U. S. A. 116 (2019) 22485–22490. https://doi.org/10.1073/pnas.1909223116.

[27] D. Wu, P. Hwang, T. Li, G. Piszczek, Rapid Characterization of AAV gene therapy vectors by Mass Photometry, BioRxiv. (2021) 2021.02.18.431916. https://doi.org/10.1101/2021.02.18.431916.

[28] P. Xu, M.M. Alam, A. Kalsy, R.C. Charles, S.B. Calderwood, F. Qadri, E.T. Ryan, P. Kováĉ,

Simple, direct conjugation of bacterial O-SP-core antigens to proteins: Development of cholera conjugate vaccines, Bioconjug. Chem. 22 (2011) 2179–2185. https://doi.org/10.1021/bc2001984.

[29] J.E. Rollenhagen, A. Kalsy, R. Saksena, A. Sheikh, M.M. Alam, F. Qadri, S.B. Calderwood, P. Kovác, E.T. Ryan, Transcutaneous immunization with a synthetic hexasaccharide-protein conjugate induces anti-Vibrio cholerae lipopolysaccharide responses in mice., Vaccine. 27 (2009) 4917–4922. https://doi.org/10.1016/j.vaccine.2009.06.040.

[30] H.B. Pfister, M. Kelly, F. Qadri, E.T. Ryan, P. Kováč, Synthesis of glycocluster-containing conjugates for a vaccine against cholera, Org. Biomol. Chem. 17 (2019) 4049–4060. https://doi.org/10.1039/C9OB00368A.

[31] M.F. Bachmann, R.M. Zinkernagel, Neutralizing antiviral B cell responses, Annu. Rev. Immunol. 15 (1997) 235–270. https://doi.org/10.1146/annurev.immunol.15.1.235.

[32] F.R. Wurm, H.A. Klok, Be squared: Expanding the horizon of squaric acid-mediated conjugations, Chem. Soc. Rev. 42 (2013) 8220–8236. https://doi.org/10.1039/c3cs60153f.

[33] D. Dhara, S.M. Baliban, C.X. Huo, Z. Rashidijahanabad, K.T. Sears, S.T. Nick, A.K. Misra, S.M. Tennant, X. Huang, Syntheses of Salmonella Paratyphi A Associated Oligosaccharide Antigens and Development towards Anti-Paratyphoid Fever Vaccines, Chem. - A Eur. J. 26 (2020) 15953–15968. https://doi.org/10.1002/chem.202002401.

[34] X. Wu, Z. Yin, C. McKay, C. Pett, J. Yu, M. Schorlemer, T. Gohl, S. Sungsuwan, S. Ramadan, C. Baniel, A. Allmon, R. Das, U. Westerlind, M.G. Finn, X. Huang, Protective Epitope Discovery and Design of MUC1-based Vaccine for Effective Tumor Protections in Immunotolerant Mice, J. Am. Chem. Soc. 140 (2018) 16596–16609. https://doi.org/10.1021/jacs.8b08473.

[35] L.H. Jones, Recent advances in the molecular design of synthetic vaccines, Nat. Chem. 7 (2015) 952–960. https://doi.org/10.1038/nchem.2396.

[36] S.M. Patel, M.A. Rahman, M. Mohasin, M.A. Riyadh, D.T. Leung, M.M. Alam, F. Chowdhury, A.I. Khan, A.A. Weil, A. Aktar, M. Nazim, R.C. LaRocque, E.T. Ryan, S.B. Calderwood, F. Qadri, J.B. Harris, Memory B cell responses to Vibrio cholerae O1 lipopolysaccharide are associated with protection against infection from household contacts of patients with cholera in Bangladesh, Clin. Vaccine Immunol. 19 (2012) 842–848. https://doi.org/10.1128/CVI.00037-12.

[37] B. Akache, R.D. Weeratna, A. Deora, J.M. Thorn, B. Champion, J.R. Merson, H.L. Davis, M.J. McCluskie, Anti-ige Qb-VLP conjugate vaccine self-adjuvants through activation of TLR7, Vaccines. 4 (2016). https://doi.org/10.3390/vaccines4010003.

[38] R.A. Johnson, T. Uddin, A. Aktar, M. Mohasin, M.M. Alam, F. Chowdhury, J.B. Harris, R.C. LaRocque, M.K. Bufano, Y. Yu, Y. Wu-Freeman, D.T. Leung, D. Sarracino, B. Krastins, R.C. Charles, P. Xu, P. Kováč, S.B. Calderwood, F. Qadri, E.T. Ryan, Comparison of immune responses to the O-specific polysaccharide and lipopolysaccharide of Vibrio

cholerae O1 in Bangladeshi adult patients with cholera, Clin. Vaccine Immunol. 19 (2012) 1712–1721. https://doi.org/10.1128/CVI.00321-12.

[39] D. Saha, R.C. LaRocque, A.I. Khan, J.B. Harris, Y.A. Begum, S.M. Akramuzzaman, A.S.G. Faruque, E.T. Ryan, F. Qadri, S.B. Calderwood, Incomplete correlation of serum vibriocidal antibody titer with protection from Vibrio cholerae infection in urban Bangladesh, J. Infect. Dis. 189 (2004) 2318–2322. https://doi.org/10.1086/421275.

[40] K.R. C., A. Oluwaseyi, Y. Hanyi, C. Alice, N.L. E., K. Meagan, H.J. B., B.T. Rahman, Q. Firdausi, C.S. B., C.R. C., R.E. T., K. Jun, W. Jens, M.N. J., M.L. S., Impact of Immunoglobulin Isotype and Epitope on the Functional Properties of Vibrio cholerae O-Specific Polysaccharide-Specific Monoclonal Antibodies, MBio. 12 (2021) e03679-20. https://doi.org/10.1128/mBio.03679-20.

[41] R.C. Charles, M. Kelly, J.M. Tam, A. Akter, M. Hossain, K. Islam, R. Biswas, M. Kamruzzaman, F. Chowdhury, A.I. Khan, D.T. Leung, A. Weil, R.C. Larocque, T.R. Bhuiyan, A. Rahman, L.M. Mayo-Smith, R.L. Becker, J.M. Vyas, C.S. Faherty, K.P. Nickerson, S. Giffen, A.S. Ritter, M.K. Waldor, P. Xu, P. Kováč, S.B. Calderwood, R.C. Kauffman, J. Wrammert, F. Qadri, J.B. Harris, E.T. Ryan, Humans surviving cholera develop antibodies against vibrio cholerae o-specific polysaccharide that inhibit pathogen motility, MBio. 11 (2020) 1–13. https://doi.org/10.1128/mBio.02847-20.

[42] J.S. Yang, S.J. An, M.S. Jang, M. Song, S.H. Han, IgM specific to lipopolysaccharide of Vibrio cholerae is a surrogate antibody isotype responsible for serum vibriocidal activity, PLoS One. 14 (2019). https://doi.org/10.1371/journal.pone.0213507.

[43] D. Wu, G. Piszczek, Standard protocol for mass photometry experiments, Eur. Biophys. J. 50 (2021) 403–409. https://doi.org/10.1007/s00249-021-01513-9.

CHAPTER 3: Development of Sialyl-Lewis a conjugate vaccine for targeted cancer immunotherapy.

3.1 Introduction

Pancreatic cancer is one of the most common and aggressive cancer types and the average five-year survival rate is less than 10% [1,2]. Pancreatic cancer incidence and mortality has been predicted to take over other cancer types by 2030, due to the complexity of screening and early detection of disease along with the absence of efficacious and less toxic therapeutic agents[3].

The glycan carbohydrate antigen 19-9 (CA19-9), also called sialyl Lewis^a (sLe^a), is an important and widely used biomarker for pancreatic cancer diagnosis [4]. CA 19-9 was first described as a tumor antigen in 1979 by its recognition with monoclonal antibody NS19-9, which was developed by using human colorectal cancer cell line SW1116 as an immunizing antigen [5]. 10 to 30% of pancreatitis patients and 75% of pancreatic cancer patients have shown elevated serum levels of CA19-9. CA19-9 elevation is also detected in other gastrointestinal diseases like pancreatic intraepithelial neoplasms (PanINs), which are precursors to pancreatic ductal adenocarcinoma (PDAC) [6]. CA19-9 has been investigated as a biomarker, predictor, and promoter in pancreatic cancer [7]. Although CA19-9 has approximately 80% sensitivity for diagnosis, its application for mass screening is limited due to the false positive results in benign diseases such as pancreatitis and nonpancreatic cancer conditions and false negative result in Lewis-negative individuals which counts for 5–10% of population [8–10]. CA19-9 as a predictor correlates strongly with tumor stage, following patients with known disease, treatment response, recurrence and overall survival [7,11]. The role of CA19-9 in promoting pancreatic cancer was recently demonstrated, suggesting a glycosylation linkage between pancreatitis and pancreatic cancer via CA19-9 biosynthesis [6]. Importantly, antibodies against CA19-9 were able to reverse pancreatitis in the Kras G12D mouse model [6]. The over expression of sLe^a correlates with

metastasis and poor survival, promotes cancer development and progression by facilitating tumor cell adhesion, angiogenesis, tumor vascularization and mediating adhesion of circulating cancer cells to endothelial cells resulting in extravasation and metastasis formation [8,12–14].

sLe^a is a tetrasaccharide (NeuAcα2,3Galβ1,3[Fucα1,4]GlcNAc-R) [15] and is a type of Lewis blood group on the cell membrane surface in which a sialic acid is added to the Lewis a sugar chain (Lea) [16–18]. sLe^a is predominantly expressed in pancreatic ducts and islet cells, while the natural counterpart, disialyl-Lewis a, is found in nonmalignant epithelial cells [14]. sLe^a is a structural isomer of sLe^x, another common tumor antigen overexpressed in carcinoma cells [19], with alternated attachment of L-fucose and D-galactose to the glucosamine moiety.

Although many tumor-associated carbohydrate antigens (TACAs) have been identified and routinely used in the clinic to monitor tumor progression and response to treatment, the development of an effective carbohydrate-targeting antitumor vaccine or antibody is extremely challenging [20,21]. To date, only one TACA-targeting antibody, anti-GD2 monoclonal antibody dinutuximab [22], has been FDA approved. A major obstacle is due to the T-cell independency of glycans, which makes them unable to induce the production of long-lived protective antibodies and does not establish immunological memory if immunized with the glycan antigen alone. Glycans can be recognized by B cells and trigger the secretion of low-avidity IgM antibodies. To overcome this challenge, glycan epitopes have been conjugated to an immunogenic carrier ranging from proteins, to peptides, oligonucleotides, lipids, zwitterionic polysaccharides, and nanoparticles to boost the anti-glycan antibody responses [23].

While the sLe^a as an attractive therapeutic target for cancer therapy [18,24,25], only one study investigated the sLe^a based vaccine with KLH as the carrier [26]. The 5B1 monoclonal antibody obtained from patients immunized with KLH-sLe^a conjugate had good affinity and

specificity for sLe^a [27] and was under investigation for cancer imaging in clinical trials [28]. Building on our previous studies which we showed the superiority of bacteriophage Qβ over KLH in ease of preparation, characterization and the ability to elicit high levels of antibodies [29,30], we became interested in testing whether the virus-like particle (VLP) platform could potently induce antibody response against sLe^a. We have also developed an efficient approach for chemical synthesis of sLe^a. Our data suggests that anti-sLe^a vaccination has the potential for treatment of vulnerable population at risk of pancreatic cancer.

3.2 Results

3.2.1 Synthesis of Qβ-sLe^a conjugate vaccine and mouse immunization

sLe^a tetrasaccharide **1** with the isothiocyanate moiety at the reducing end was chemically synthesized by Dr. Sherif Ramadan. Isothiocyanate can provide an efficient conjugation method between the sLe^a tetrasaccharide and Qβ protein. Moreover, the valuable unconjugated sugar can be recovered as the free amine form from the reaction mixture and the isothiocyanate group can be regenerated, which adds to the practical advantage of this chemistry. The Qβ-sLe^a conjugation was readily performed by mixing the isothiocyanate functionalized sLe^a **1** (**Scheme 3.1a**) and Qβ in buffered solution overnight at 37°C. The sLe^a / Qβ epitope ratio of the sLe^a conjugate was determined using mass spectrometry. There were on average 300 sugar moieties per Qβ capsid (Appendix, **Figure 3.12**). KLH-sLe^a conjugate was also prepared for comparison studies and the total loading was 400 sLe^a per KLH molecule (**Scheme 3.1b**). BSA-sLe^a conjugate was prepared by a similar method and was characterized by MALDI-TOF MS, which showed conjugation of four sLe^a per BSA molecule (Appendix, **Figure 3.13**). The BSA-sLe^a conjugated was used in Enzyme Linked Immunosorbent Assay (ELISA) to analyze the anti-sLe^a antibodies generated in

post-immune sera without the interference of anti-Qβ antibodies. Qβ-sLe^a conjugate and physical mixture of sLe^a and Qβ were used for mouse immunization. Groups of five C57BL/6 female mice were injected subcutaneously under the scruff on days 0, 14 and 28 with 0.2 mL Qβ constructs (containing 4 µg carbohydrate) mixed with 20 µg MPLA as the adjuvant. Mice were bled at day35 and different time points throughout the study (**Figure 3.2**).

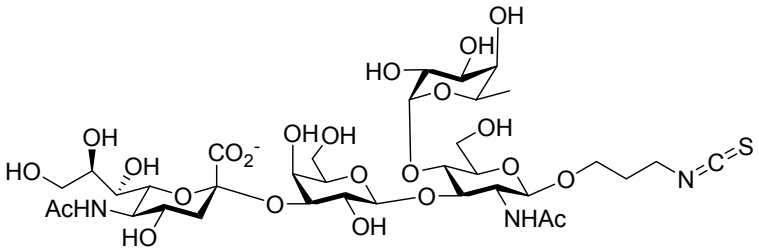

sLe^a-isothiocyanate **1**

Figure 3. 1 Structure of sLe^a-isothiocyanate (sLe^a-NCS)

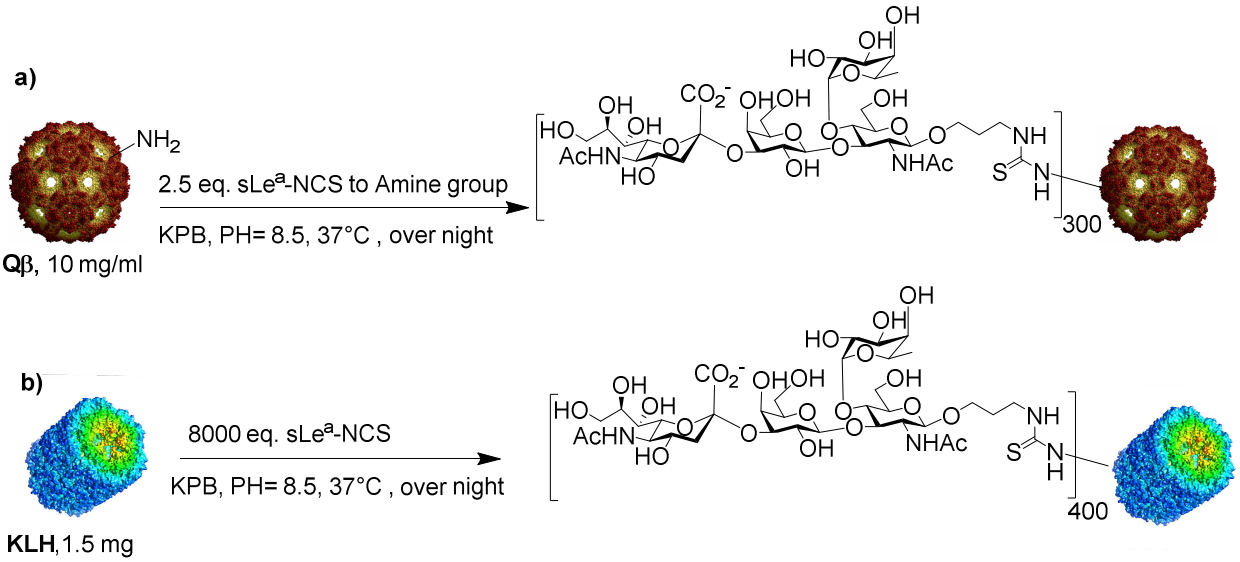

Scheme 3. 1 synthesis of a) Qβ-sLe^a conjugate. To a solution of Qβ (1 mg, 10 mg/ml concentration, 0.4 nmol subunit, 0.36 µmol reactive amine) in 0.1 M potassium phosphate (KPB) buffer pH 8.5, was added sLe^a-NCS (2.5 equivalent to reactive amine) and the reaction was incubated at 37 □ overnight and worked up by ultrafiltering the reaction mixture against 0.1 M KPB buffer (pH 7.0, 0.1 M). b) KLH-sLe^a conjugate was synthesized under a similar condition.

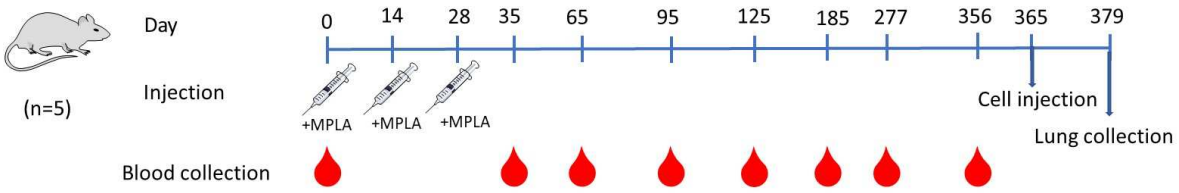

Figure 3. 2 Immunization and blood collection schedule. Groups of five C57BL/6 female mice received 3 immunizations of Qβ-sLe^a conjugate or sLe^a and Qβ mixture two weeks apart with blood collected at days 0, 35, 65, 95, 125, 185, 277, and 356. At day 365, both groups were inoculated i.v. with 5×10^5 B16-FUT3 tumor cells and lungs were collected 14 days later.

3.2.2 Qβ-sLe^a conjugate elicited high titers of IgG antibodies titers and longer lasting anti-sLe^a IgG antibodies in mice compared with the KLH-sLe^a conjugate as well as the admixture of Qβ and sLe^a

The peak anti-sLe^a ELISA titers were observed on day 35 after 1st vaccination with Qβ-sLe^a conjugate, which reached 2,137,962 ELISA units (**Figure 3.3a**). No evidence of significant antibody induction above background was observed after immunization with the sLe^a and Qβ mixture. The antibody level induced by Qβ-sLe^a conjugate remained significantly elevated up to 277 days. The average level of KLH-sLe^a conjugate induced antibodies was significantly lower than that by Qβ-sLe^a conjugate and was not detectable at any time points following immunization (**Figure 3.3b**). The IgM antibody was not detected for day 35 sera at 1:100,000 dilution.

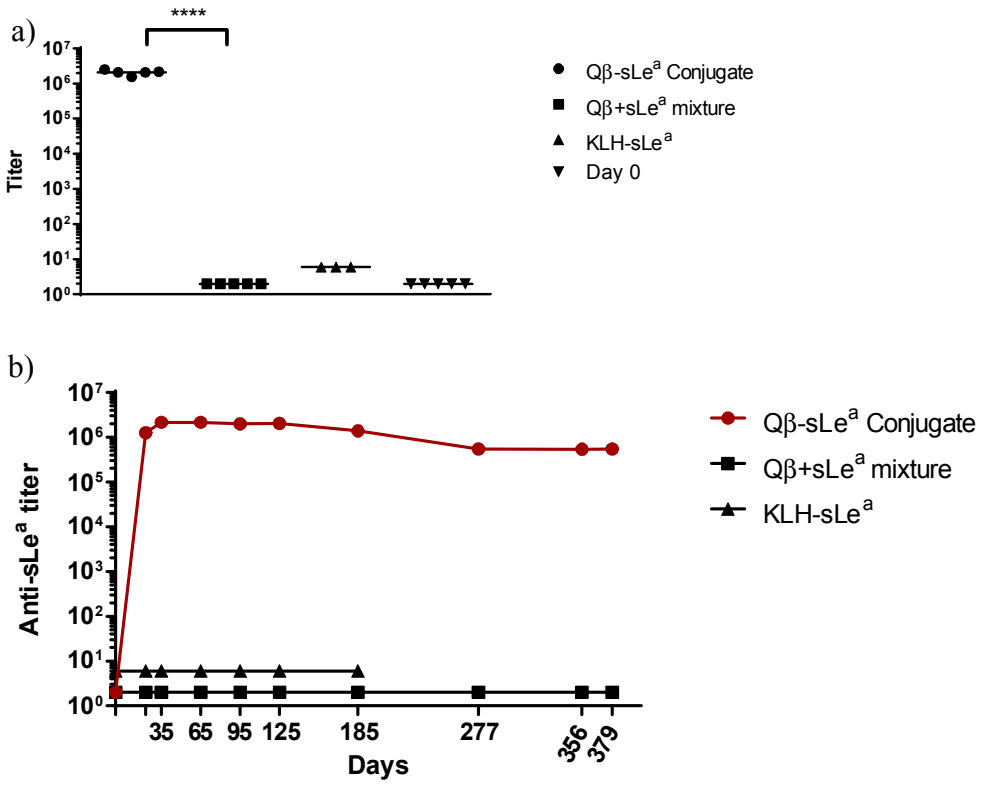

Figure 3. 3 a) Titers of anti-sLe^a IgG antibodies from mice immunized with the Qβ-sLe^a conjugate against BSA-sLe^a (each symbol represents one mouse, n=5 mice for Qβ-sLe^a or sLe^a and Qβ mixture group and n=3 for KLH-sLe^a group). Pooled sera from 5 mice were used for Qβ and day 0. The statistical significance was determined through an unpaired two tailed t-test using GraphPad Prism. **** p<0.0001. b) Changes of the titers of anti-sLe^a IgG antibodies from Qβ-sLe^a immunized mice over time. The IgG titers were determined with pooled sera.

3.2.3 Qβ-sLe^a conjugate elicited antibodies capable of binding with sLe^a expressing tumor cells

To assess whether the induced antibodies after vaccination could bind to natural sLe^a, three mouse cell lines were investigated. The mouse pancreatic cancer cells are represented by neo FC1199, FC1242, and FC1245. As mouse cells do not endogenously express sLe^a due to the lack of fucosyl transferase, transfection of these pancreatic cancer cells with the genes encoding both *Fucosyltransferase 3* (FUT3) and *1,3-galactosyltransferase 5* (b3GALT5) led to cell surface production of CA19-9 on FC1199, FC1242, and FC1245 FB cells at levels equivalent to those

observed in human cancer cell lines. The results of flow cytometry testing on these cancer cell lines are demonstrated in figure 3.4a

Striking increases in IgG reactivity against FC1245FB cells were seen for all mice immunized with Qβ-sLe^a conjugate while no reactivity above the background was detected in the sera from mice receiving the mixture of Qβ and sLe^a. Mouse anti-sLe^a antibody was used as the positive control (clone 121SLE) in the flow cytometry testing. All 5 sera from Qβ-sLe^a vaccinated group showed stronger binding to sLe^a expressing cells compared to monoclonal antibody 121SLE. The cell surface binding was not observed in neo cell lines, which did not express sLe^a, neither with monoclonal antibody or post-immune sera, confirming that serum binding to FB cells was specific to sLe^a expression (**Figure 3.4a**).

Cell surface reactivity against fucosyl transferase reprogrammed 1199 FB cells was also demonstrated by complement dependent cytotoxicity (CDC) assays using rabbit complement and mouse sera from different groups (**Figure 3.4b**). Both 121SLE antibody and sera from sLe^a-Qβ immunized group showed close to 80% killing activities, while sera from group receiving the mixture had little killing activities, similar to pre-immunization sera. The 121SLE mAb showed similar CDC potency to sera of Qβ-sLe^a immunized group although its binding was weaker in FACS study. Since 121SLE is an IgM isotype, its higher cytotoxicity could be related to the higher efficiency of IgM in complement activation.

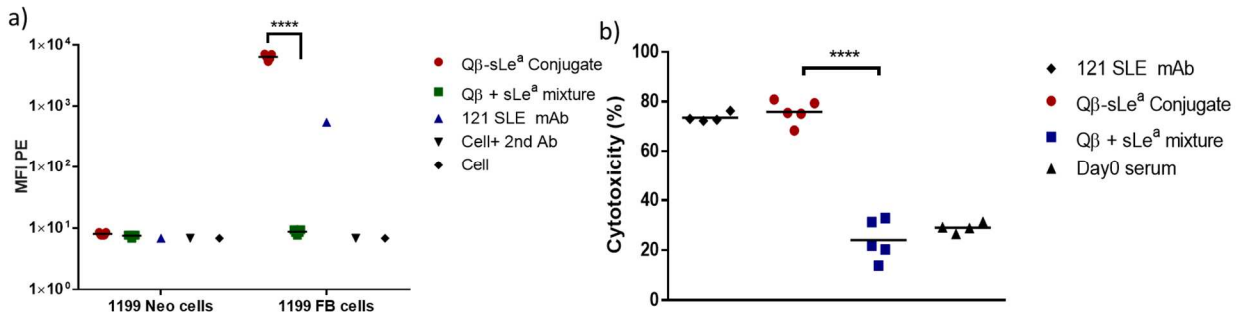

Figure 3. 4 Recognition of cell surface expression of sLe^a with FACS (a) and CDC (b) of 1199FB cells in presence of Qβ-sLe^a antisera. a) 3x10^5 cells were incubated with mouse sera dilution (1:20), or 10 µg/ml of anti-sLe^a 121SLE mAb for 0.5h at 4°C and washed with FACS buffer. The sera binding to cells were assessed using PE conjugated anti-mouse IgG or IgM (121SLE) secondary Antibodies. b) 3x10^4 1199FB cells were incubated with mouse sera dilution (1:20), or 10 µg/ml of anti-sLe^a 121SLE mAb for 1h at 4°C. Then cells were washed, and rabbit sera complement at 1:10 dilution was added and further incubated at 37°C for 3h. The cell viability was tested with MTS assay. **** $p<0.0001$. The p values were determined through a two-tailed unpaired t test using GraphPad Prism.

3.2.4 Antibodies induced by the Qβ-sLe^a conjugate were highly selective toward human pancreatic ductal adenocarcinoma tissues

To test the translational potential of Qβ-sLe^a conjugate vaccine to human patients, we obtained pancreatic ductal adenocarcinoma and pancreatic cancer tissue microarray containing cancer tissues from different patients. Pooled sera from Qβ-sLe^a conjugate vs mixture immunized mice were used to stain the tissue microarrays at 1:1000 dilution. In the pancreatic ductal adenocarcinoma array, 16 cores out of 24 different core samples (67% positive staining) showed strong binding with sera from Qβ-sLe^a group while there was not any staining for sera from mice immunized with the mixture of Qβ and sLe^a (**Figure 3.5a, 3.5b**, Appendix **Figure 3.15** and **Figure 3.16**). In a separate experiment, pancreatic cancer tissue microarray contains normal and metastatic cancer tissue from 48 different patients was stained with pooled sera from Qβ-sLe^a group. In this array, 26 cores out of 31 pancreatic adenocarcinoma were stained in remarkable contrast to normal tissues. The staining was also observed for squamous cell and adenosquamous carcinoma but not for metastatic or neuroendocrine tumor (**Figure 3.6**, Appendix **Figure 3.17**).

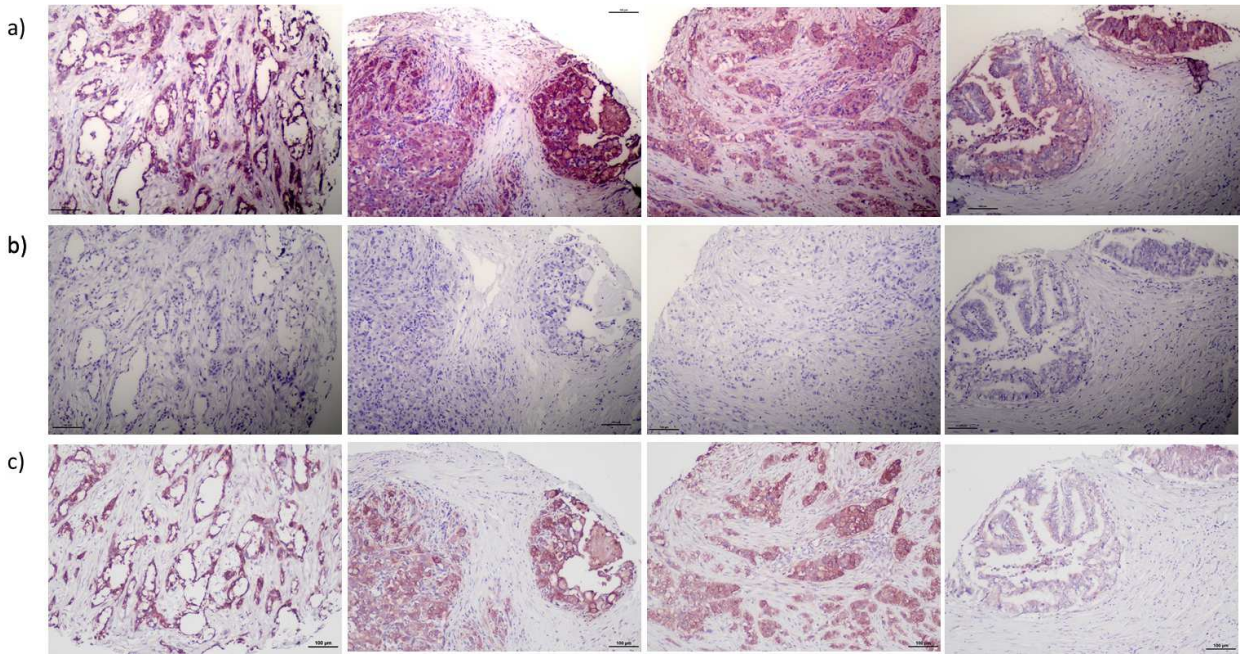

Figure 3. 5 Individual XPAN024 microarray slides stained with pooled serum of 5 mice immunized with Qβ-sLe^a conjugate(a), sLe^a and Qβ mixture (b) at day 35 at 1:1000 serum dilution or with 5B1 recombinant antibody at 1.08 µg/ml final concentration (c). Similar cores have been shown here to compare the intensity of staining. Characterization of each core has been provided in appendix, table **3.1** based on their map ID and the pictures of all the cores in appendix, figure **3.15** and **3.16**. The brown/red color was due to antibody binding to tissues. The lack of brown/red staining indicates little binding of antibodies to the tissues. Scale bar is 100µm.

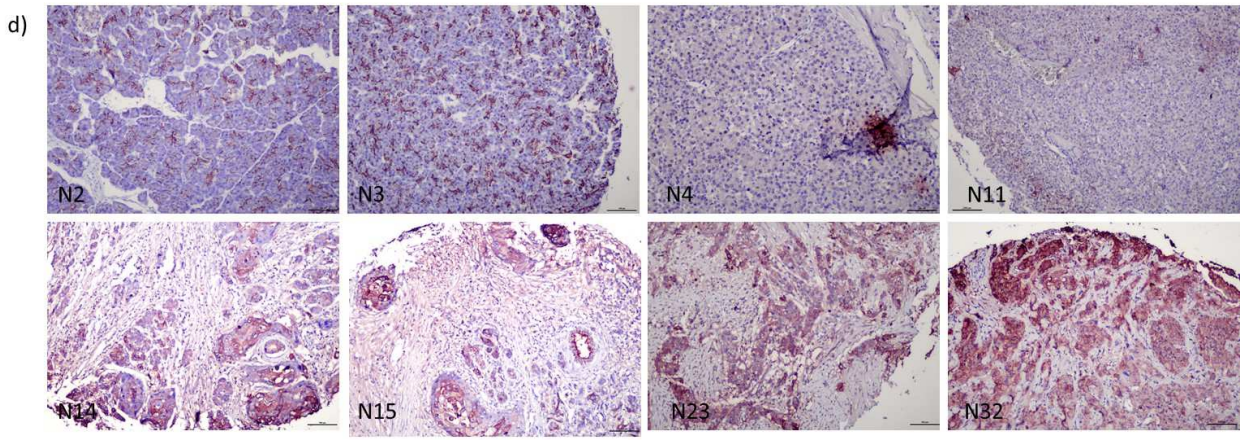

Figure 3. 6 XPAN048 microarray stained with pooled serum of 5 mice immunized with Qβ-sLe^a conjugate at day 35 at 1:1000 serum dilution. Selected cores: N2 and N3 are normal pancreatic tissue, N4 metastatic pancreatic malignant islet cell tumor, N11 Neuroendocrine tumor, N14 Squamous cell carcinoma, N15 Adenosquamous carcinoma, N23 and N32 Adenocarcinoma. Characterization of each core has been provided in appendix, table **3.2** based on their core number and the pictures of all the cores in appendix, figure **3.17.** The brown/red color was due to antibody

binding to tissues. The lack of brown/red staining indicates little binding of antibodies to the tissues. Scale bar is 100μm.

3.2.5 Antibodies induced by the Qβ-sLe^a conjugate were highly selective toward sLe^a binding based on glycan microarray analysis

The carbohydrate specificity of induced antibodies at day 35 was probed in glycan array analysis against 815 glycans. The sera were tested individually at 1:100 dilution. The results confirmed the high specificity of sera from mice group immunized with Qβ-sLe^a conjugate with selective recognition of the sLe^a tetrasaccharide. There was no binding to closely related antigens that were present in the array, including sLe^x, Le^a, Le^x, Le^y or GD2, GD3, GM2 and GM3 gangliosides. We observed some binding to sLe^c antigens, but the result was not consistent in all sera samples (Appendix, **Table 3.3**).

3.2.6 Vaccine activity in animal model for metastasis

In order to study the vaccine efficacy against sLe^a in an immunocompetent environment, two murine cell lines (i.e., B16 melanoma and EL4 lymphoma murine tumor cell lines) that stably express sLe^a were obtained [31]. These two cell lines are well-established model systems for studying the antitumor activities of antibodies, which are transduced to express human fucosyltransferase III (FUT3). FUT3 is responsible for sLe^a synthesis in cells. To set up a positive control for our *in vivo* study, we used the well-studied sLe^a monoclonal antibody, 5B1, which was generated from patients immunized with KLH-sLe^a. 5B1 has shown high specificity for sLe^a antigen and low cross reactivity with similar carbohydrates. The variable regions of human 5B1 mAb, were expressed as murine IgG2a to generate chimeric recombinant antibody with murine Fc portion. In ELISA experiment, 5B1-IgG2a gave titer of 331,131 comparing to the sera from Qβ-sLe^a conjugate at day35 which gave average IgG titer of 2,137,962 ELISA units. Tissue staining with 5B1-IgG2a gave comparable staining to the pooled sera from Qβ-sLe^a conjugate.

The expression of sLe^a was confirmed in both EL4-FUT3 and B16-FUT3 cell lines (**Figure 3.7a** and **Figure 3.7b**) with mouse anti-Sialyl Lewis^a antibody (121SLE). While 5B1 has comparable binding to EL4-FUT3 cell line with 121SLE antibody at 10 µg/ml concentration, its binding was lower than the binding by serum of mice immunized with Qβ-sLe^a conjugate at 1:20 serum dilution (**Figure 3.7a**). Moreover, monoclonal antibodies and sera from immunized group showed binding to the EL4-FUT3 cell line and there was not any binding against EL4 parent cell line.

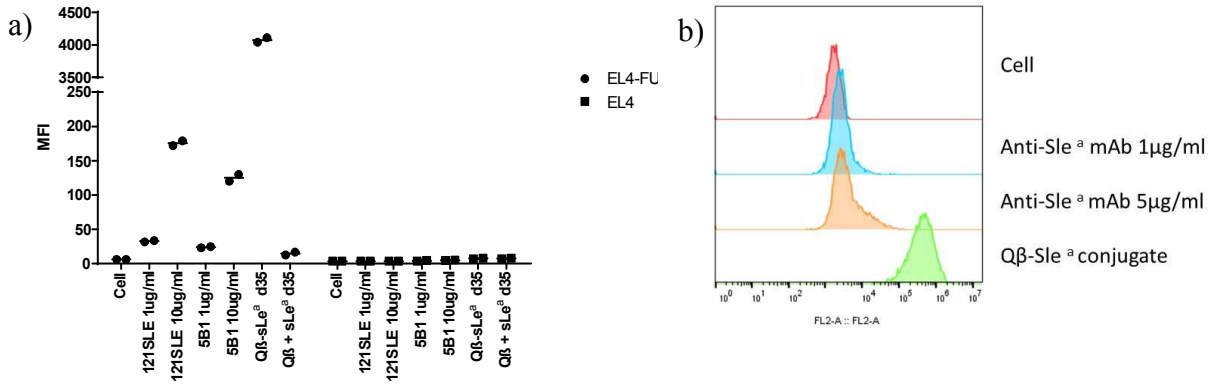

Figure 3. 7 Expression of sLe^a confirmed through FACS experiment by using a) 121SLE mAb and chimeric recombinant antibody 5B1 at 10ug/ml concentration in EL4-FUT3 cells. Pooled serum from group immunized with Qβ-sLe^a conjugate showed significantly higher binding toward EL4-FUT3 cell line. The absence of non-specific binding was confirmed by using EL4 parent cell line. b) 121SLE mAb at different concentration and pooled sera from Qβ-sLe^a conjugate in B16-FUT3 cells which showed binding to sLe^a expressed on cell surface. PE-anti mouse IgG or IgM was used as secondary antibody.

To mimic clinical conditions for cancer treatment, we evaluated the vaccine efficacy in a therapeutic setting in two different models I) immunization of mice followed by challenge by tumor cell injection. This model will provide information if active immunization can protect mice from tumor metastasis; and II) the effect of anti- sLe^a generated antibodies in preventing tumor metastasis in a passive protection model.

We validated the progress of tumor models with both EL4-FUT3 and B16-FUT3 cells in naïve mice. WT C57BL/6 immunocompetent mice were inoculated i.v. either with B16-FUT3 or EL4-FUT3 tumor cells (which express sLe^a) (**Figure 3.8a**) and treated with 5B1-mIgG2a. Treatment with anti-sLe^a antibody increased the overall survival of mice inoculated with EL4-FUT3 cells (**Figure 3.8b**) or dramatically reduced metastatic colonization of B16-FUT3 cells in lung (**Figure 3.8c**).

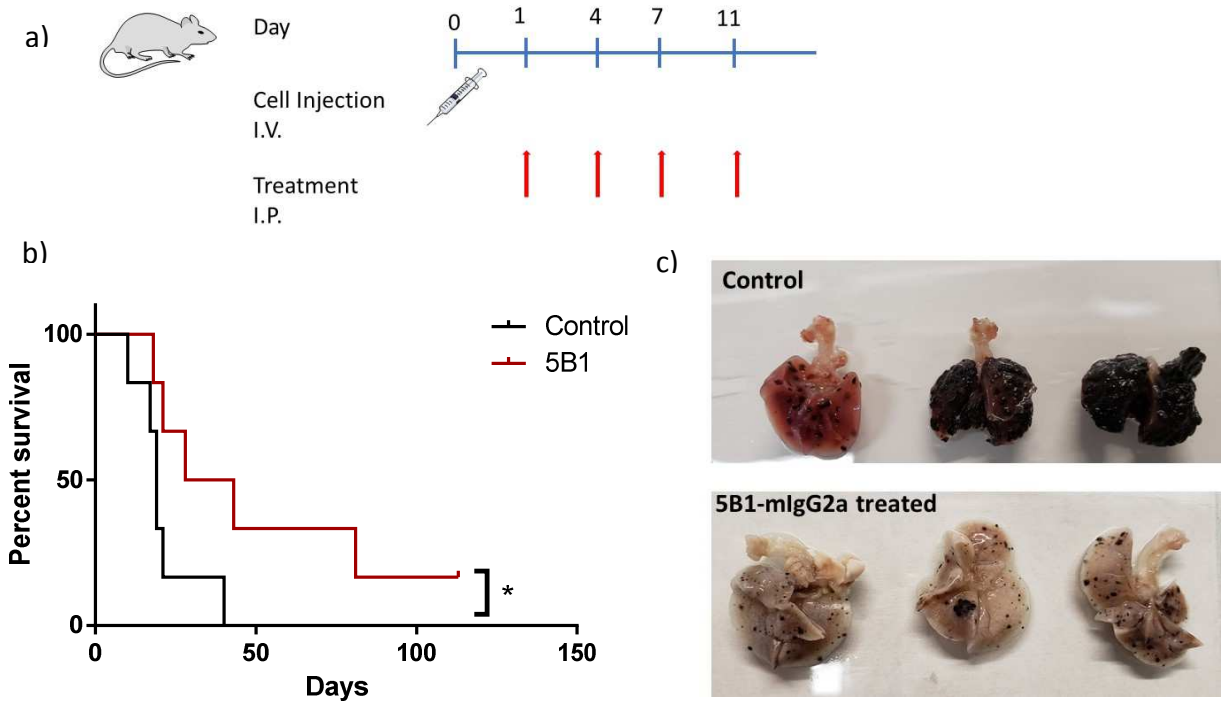

Figure 3. 8 a) WT C57BL/6 mice were inoculated i.v. with 5×10^5 B16-FUT3 (n=3) or EL4-FUT3 (n=6) tumor cells. 100µg of anti-sLe^a 5B1 Ab was administered i.p. on days 1, 4, 7, and 11 and survival was assessed daily for EL4-FUT3 group (b), p= 0.0448 and for B16-FUT3 group, mice were euthanized, lungs were excised and fixed fourteen days after cell inoculation (c).

To examine the potency of vaccine in preventing pancreatic cancer in the therapeutic model I, the mice immunized with Qβ-sLe^a conjugate were challenged with B16-FUT3 cell line at day 365 post immunization. The serum obtained at day 356 post immunization was still able to recognize the sLe^a expression on B16-FUT3 cells (**Figure 3.9**). Mice immunized with Qβ-sLe^a

conjugate or sLe^a and Qβ mixture were inoculated i.v. with 5 × 10^5 B16-FUT3 tumor cells. Fourteen days after inoculation, mice were euthanized, lungs were excised and fixed, and metastatic foci were counted. There were 3 mice in Qβ-sLe^a conjugate vaccinated group which showed lower tumor development trend and tumor burden remained below 10% of total lung area (**Figure 3.9**, Appendix **Figure 3.20**).

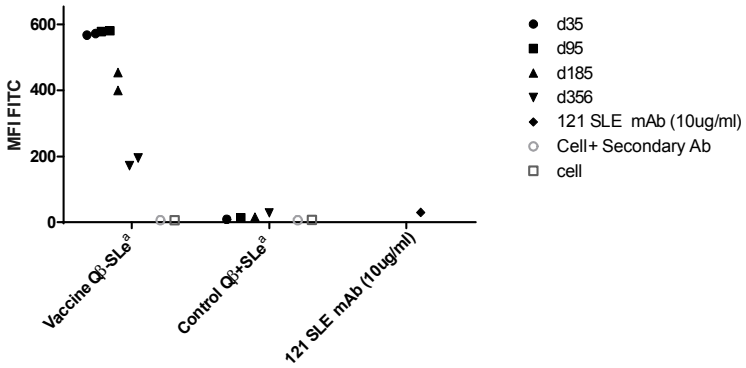

Figure 3. 9 The binding of pooled mice sera from day 35, 95, 185 and 356 against sLe^a antigen at 1:10 dilution with B16-FUT3 cell line were analyzed with flow cytometry with two biological replicates. 356 days after immunization the sera from Qβ-sLe^a conjugate vaccinated group showed binding toward cell surface expression of sLe^a antigen.

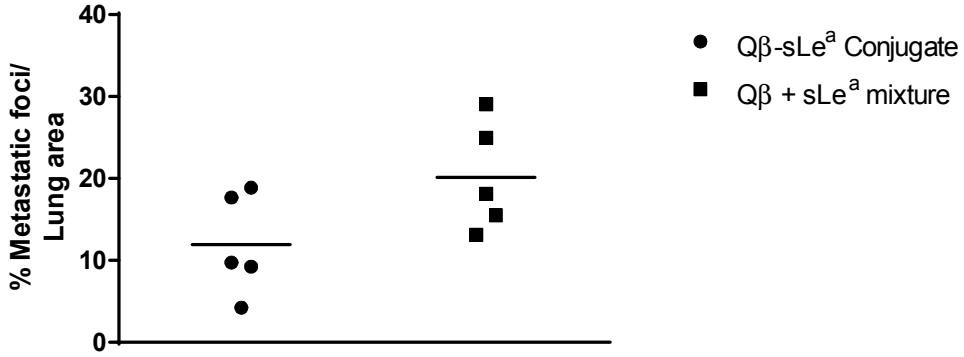

Figure 3. 10 Total tumor area ratio to lung tissue after analyzing the pictures with ImageJ. The tumor area in Qβ-sLe^a conjugate vaccinated group had lower trending compared with group vaccinated with sLe^a and Qβ mixture.

3.2.7 Ongoing experiments

Building on the results we obtained in previous mice protection study, an expanded experiment is undergoing. In this study, 2 group of C57BL/6 mice (WT, n=10) are immunized with Qβ-sLe^a conjugate or sLe^a and Qβ mixture biweekly at days 0, 14, 28 (containing 4 µg carbohydrate) mixed with 20 µg MPLA as adjuvant. Mice will be bled at day35 and will be challenged at day 42 with B16-FUT3 cells. Lung tumor metastasis will be analyzed fourteen days after tumor cell inoculation. Two groups of 5 mice (n=5) are considered as controls which will be treated as vehicle or 5B1-mIgG2a following the protocol discussed previously (**Figure 3.9a**).

We are also interested in developing the therapeutic model II to address the question whether induced anti-sLe^a antibodies can prevent tumor progression, which can have clinical application in terms of passive immunization and monoclonal antibody development. Two rabbits are being immunized with (containing 8 µg for the first dose and 4 µg carbohydrate for subsequent immunizations) mixed with CFA or IFA adjuvant (Figure 3.11). The sera collected at day 63 will be used to prevent tumor development in mice challenged with B16-FUT3 or EL4-FUT3 in the set up discussed in figure **3.9a**.

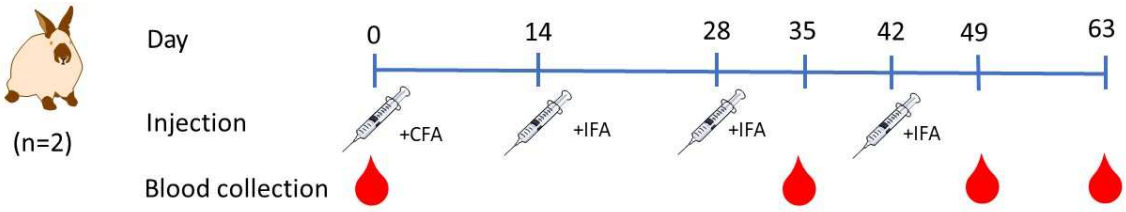

Figure 3. 11 Two New Zealand rabbits were injected subcutaneously on day 0 with 0.1 mL Qβ-sLe^a constructs (at 8µg glycan) as emulsions in Complete Freund's Adjuvant according to manufacturer's instructions. Boosters were given subcutaneously on days 14, 28 and 42 (at 4µg glycan) mixed with Incomplete Freund's Adjuvant. Serum samples were collected on days 0 (before immunization), 35, 49 and 63.

3.3 Discussion

Changes in carbohydrate expression is often associated with tumor development. These changes are in the carbohydrate core structure and/or terminal carbohydrate structure such as incomplete synthesis and modification of normal cell surface carbohydrates [27]. The incomplete synthesis of the cell surface carbohydrates results in an increased expression of the precursor structures such as sLe^a, one of the blood group-related antigens [13]. sLe^a is a well-stablished biomarker for pancreatic cancer and other malignant stomach, lung, colon, breast, ovary, and uterus tumor cells [10]. Targeting carbohydrate antigens has been hampered due to the complexity of carbohydrate chemistry and biology. sLe^a is a well-recognized and the most extensively studied biomarker in diagnosis of pancreatic cancer in symptomatic patients, and can be monitored for information regarding prognosis, overall survival and prediction of recurrence inpatients with established disease [9]. Although the proteins carrying sLe^a are secreted into blood, the significant higher concentration of antigen in the tumor microenvironment than in serum lead to accumulation of antibodies in the tumor tissue [28,32]. The result from KLH-sLe^a conjugate vaccine in human was promising for developing monoclonal antibody targeting sLe^a [27]. The KLH-sLe^a conjugate vaccine was not effective in our study and this could be due to the lower loading, which reported the loading of 874 sLe^a per KLH molecule and different adjuvant that we have used [26].

Here we showed that sLe^a antigen was conjugated with a powerful protein carrier, bacteriophage Qβ, and this conjugate was superior in eliciting antibody response corresponding to the KLH conjugate. Considering the differences in antibodies produced by Qβ-sLe^a versus KLH-sLe^a in ELISA experiment, Qβ-sLe^a conjugate was selected for further *in vitro* and *in vivo* studies. Mice immunized with Qβ-sLe^a were able to generate significantly higher levels of IgG antibodies as compared to those immunized with sLe^a and Qβ mixture and the induced antibody responses

were long lasting up to 277 days. Furthermore, Qβ-sLe^a induced antibodies showed selective binding in glycan microarray analysis and sLe^a specific tissue staining. The generated anti-sLe^a antibodies were able to lyse 80% of sLe^a expressing cells in CDC assay and had strong binding to multiple sLe^a expressing cells. This result suggested that the induced antibodies can recognize the sLe^a antigen either as synthetic conjugated form (in ELISA and glycan micro array) or as natural antigen on cancer cell surface. Building on the encouraging *in vitro* result obtained, further *in vivo* studies have been designed to confirm the efficacy of Qβ-sLe^a conjugate vaccine which include the mouse protection model study after mice have been challenged with sLe^a expressing tumor cells either in active immunization or passive antibody treatment.

3.4 Materials and methods

3.4.1 General experimental procedures and methods for synthesis

All chemicals were reagent grade and used as received from the manufacturer unless otherwise noted. Centrifugal filter units of 10,000 and 100,000 molecular weight cut-off (MWCO) were purchased from EMD Millipore. For characterization of Qβ-sLe^a conjugates, liquid chromatography-mass spectrometry (LCMS) analysis was performed. The samples for LCMS were prepared as follows: 1:1 v/v of 40 μg mL^{-1} of Qβ-sLe^a stock solution and an aqueous solution of 100 mM DTT was mixed and incubated in a water bath at 37 □ for 30 min. One drop of 50% formic acid was added to the mixture. LCMS was performed on Waters Xevo G2-XS quadrupole/time-of-flight UPLC/MS/MS. The liquid chromatography was done on Hypersil GOLD™ Cyano HPLC Column, 1mm x 10mm (3um particle size) with 1 mm I.D. Uniguard™ direct-connection guard cartridge holder using gradient eluent from 95% 0.1% formic acid in water to 95% 0.1% formic acid in CH_3CN (0.3 mL min^{-1} flowrate). The multiple charge mass spectra were transformed to a single charge by using the algorithm MaxEnd148a. The average number of sLe^a on each Qβ subunit was analyzed by the signal intensities of the respective peaks in mass spectrum. For characterization of BSA-sLe^a conjugates, MALDI-TOF MS analysis was performed. The samples for MALDI-TOF were prepared as follows: 1:1 v/v of 2 mg mL^{-1} of BSA-sLe^a conjugates and 100 mM DTT was mixed and incubated in a water bath at 37 □ for 30 min. After desalting using Cleanup C18 Pipette Tips (Agilent Technologies), the sample (5 μL) and matrix solution (5 μL, 10 mg mL^{-1} sinapic acid in 50/50/0.1 CH_3CN/H_2O/TFA) was mixed and spotted on a MALDI plate, air-dried (3 rounds) and then analyzed by MALDI-TOF mass spectrometry (Applied Biosystems Voyager DE STR). Protein concentration was measured using

the Coomassie Plus Protein Reagent (Bradford Assay, Pierce) with bovine serum albumin (BSA) as the standard.

For cell studies, EL4 lymphoma cells were from ATCC and grown in Dulbecco's Modified Eagle's Medium (DMEM) supplemented with 10% horse serum, 100 U mL^{-1} penicillin/100 μg mL^{-1} streptomycin, 2 mM L-glutamine, and 1 mM sodium pyruvate. 1199, 1242, 1245 FB and Neo cell lines were generously provided by Dr. Dannielle D. Engle's laboratory and cultured in DMEM with 10% FBS and 1%PS. B16-FUT3 and EL4-FUT3 cells were kindly provided by Dr. Jeffrey V. Ravetch's laboratory and maintained in DMEM with 10% FBS and 1%PS.

Monoclonal anti-sLe^a antibody produced in mouse, clone 121SLE, was obtained from sigma (SAB4700773). Low-Tox®-M Rabbit Complement (CL3051) was obtained from Cedarlane. Peroxidase-conjugate AffiniPure Goat Anti-Mouse IgG (H+L) (115-035-003) was obtained from Jackson ImmunoResearch. 5B1 recombinant antibody was constructed at Sino Biological through HEK293 expression using mouse IgG2a heavy chain and mouse kappa light chain backbone.

The gene sequence for 5B1 rAb:

Heavy chain

MEFGLSWLFLVAILKGVQVQLVESGGGSVQPGRSLRLSCEASGFTFEAYAMHW
VRQPPGKGLEWVSSINWNSGRIAYADSVKGRFTISRDNARNSLYLQMNSLRLEDTAFYY
CAKDIRRFSTGGAEFEYWGQGTLVTVSSSAKTTAPSVYPLAPVCGDTTGSSVTLGCLVK
GYFPEPVTLTWNSGSLSSGVHTFPAVLQSDLYTLSSSVTVTSSTWPSQSITCNVAHPASST
KVDKKIEPRGPTIKPCPPCKCPAPNLLGGPSVFIFPPKIKDVLMISLSPIVTCVVVDVSEDD
PDVQISWFVNNVEVHTAQTQTHREDYNSTLRVVSALPIQHQDWMSGKEFKCKVNNKD
LPAPIERTISKPKGSVRAPQVYVLPPPEEEMTKKQVTLTCMVTDFMPEDIYVEWTNNGK

TELNYKNTEPVLDSDGSYFMYSKLRVEKKNWVERNSYSCSVVHEGLHNHHTTKSFSRT
PGK

Light chain

MAGFPLLLTLLTHCAGSWAQSVLTQPPSASGTPGQRVTISCSGSSSNIGSNFVYW
YQQLPGTAPKLLIYRNNQRPSGVPDRFSGSRSGTSASLAISGLRSEDEADYYCAAWDDS
LGGHYVFGTGTKVTVFSGSRSGTSASLAISGLRSEDEADYYCAAWDDSLGGHYVFGTG
TKVTVRADAAPTVSIFPPSSEQLTSGGASVVCFLNNFYPKDINVKWKIDGSERQNGVLNS
WTDQDSKDSTYSMSSTLTLTKDEYERHNSYTCEATHKTSTSPIVKSFNRNEC

3.4.2 Synthesis of Qβ-sLe^a conjugate

To a solution of Qβ (1 mg, 5 mg/ml concentration, 0.4 nmol subunit, 0.36 μmol reactive amine) in 0.1 M K-Phos buffer pH 8.5, was added 3.28 mg of sLe^a-NCS (2.5 equivalent to reactive amine, 3.6 μmol). The reaction was incubated at 37 □ overnight and was gently inverted several times to ensure that the reactants were mixed. The unreactive tetrasaccharides were separated from the conjugate by centrifugal filtration against 0.1 M KPB buffer (pH 7.0, 0.1 M). The extent of particle modification was determined by ESI-TOF LC-MS and electrophoretic analysis. The total protein concentration was determined by Bradford assay against BSA standards. Percent protein recovery was 50–70 %.

3.4.3 KLH-sLe^a conjugation

1.5 mg of KLH was washed with 0.1 M KPB buffer, pH=8.6 for several rounds and the final concentration was determined with Bradford assay. 8000 equivalents of sLe^a-NCS sugar was added to KLH solution and the mixture was incubated at 37°C overnight. The reaction was purified by ultracentrifugation using 100 KDa cut off filter. The protein content was determined with the

Bradford assay and the sugar loading was quantified using anthrone assay[10]. Total carbohydrate content was 69 ug/ml, which corresponds to 400 copy of sLe^a per KLH molecule. A group of three C57BL/6 female mice was injected subcutaneously under the scruff on day 0, 14 and 28 with KLH-sLe^a constructs mixed with 20 ug MPLA as the adjuvant.

3.4.4 Synthesis of BSA-sLe^a conjugate

For the synthesis of BSA-sLe^a conjugate, a solution of BSA (0.5 mg, 25 mg/ml) in 0.1 M KPB buffer pH 8.5, and sLe^a-NCS (20 equivalent, 0.137 mg, in 0.1 M KPB buffer pH 8.5) were added to the BSA solution (1.5 mg). The reaction was inverted and incubated at 37°C overnight. The product was purified by an Amicon Ultra 10 kDa MW cut-off against 0.1 M KPB. Total protein content was quantified by the Bradford assay against BSA standards. The extent of modification was determined by MALDI-TOF MS.

3.4.5 Mouse immunization

Pathogen-free C57BL/6 female mice aged 6–10 weeks were maintained in the University Laboratory Animal Resources facility of Michigan State University. All animal experiments were performed in accordance with the guidelines of the Institutional Animal Care and Use Committee (IACUC) of Michigan State University (approved protocol #: PROTO201900423). For evaluation of Qβ-sLe^a and KLH-sLe^a, C57BL/6 mice were subcutaneously injected under the scruff on day 0 with 0.2 mL of various Qβ-sLe^a / sLe^a + Qβ mixture / KLH-sLe^a vaccines in PBS containing MPLA (20 μL, 1 mg mL^{-1} in DMSO) for each mouse. For the Qβ-sLe^a conjugate or sLe^a + Qβ mixture, 5 mice immunized in each group and for KLH-sLe^a, 3 mice immunized. Boosters were given subcutaneously with the same amounts of vaccines with MPLA under the scruff on days 14 and 28. All Qβ-sLe^a /sLe^a + Qβ mixture / KLH-sLe^a conjugates administered have the same

amounts of sLe^a (4μg). Sera samples were collected on days 0 (before immunization), 35, 65, 95, 125, 185 and 277.

3.4.6 Rabbit immunization

Rabbit immunization was performed by ProSci Incorporated (Poway, CA) with 2 New Zealand rabbits. Each rabbit was immunized subcutaneously on day 0 with Qβ-sLe^a (100 μl, 8 μg of sLe^a) as emulsions in Complete Freund's Adjuvant according to the manufacturer's instructions. Boosters were given subcutaneously under the scruff on days 14, 28 and 42 mixed with Incomplete Freund's Adjuvant and 4 μg of sLe^a. Serum samples were collected on days 0 (before immunization), 49 and day 63 for the final bleed.

3.4.7 Tumor challenge and antibody treatments

B16-FUT3 and EL4-FUT3 (5×10^5 cells/mouse) cells were inoculated i.v. into the lateral tail vein in 200 μL PBS. Mice were given intraperitoneal injections of 100 μg of 5B1 sLe^a recombinant antibody, rabbit sera (the amount for rabbit sera will be determined based on ELISA result) or PBS serving as control, on days 1, 4, 7, and 11 after inoculation. For the B16-FUT3 lung colonization model, the lungs were harvested on day 14 and analyzed for the presence of surface metastatic foci. For EL4-FUT3 tumor model, survival was assessed daily.

3.4.8 Evaluation of antibody titers by ELISA

The Nunc MaxiSorp® flat-bottom 96-well microtiter plates were coated with 1 μg mL^{-1} of the BSA-sLe^a conjugate (100 μL/well) in $NaHCO_3/Na_2CO_3$ buffer (0.05 M, pH 9.6) containing 0.02 % NaN_3 by incubation at 4 ^oC overnight. The coated plates were washed with PBS/0.5% Tween-20 (PBST) (4 × 200 μL) and blocked with 1 % BSA in PBS (200 μL/well) at rt for 1 h. The plates were washed again with PBST (4 × 200 μL) and incubated with serial dilutions of 5B1

recombinant antibody mice or rabbit sera in 0.1 % BSA/PBS (100 μL/well, 3 wells for each dilution). The plates were incubated for 2 h at 37 □ and then washed with PBST (4 × 200 μL). A 1:2000 dilution of HRP-conjugated goat anti-mouse IgG (Jackson ImmunoResearch Laboratory) in 0.1% BSA/PBS (100 μL) or peroxidase conjugated rabbit anti-rabbit IgG (SigmaAldrich, A6792) in 0.1% BSA/PBS (100 μL) was added to the wells respectively to determine the titers of antibodies generated. The plates were incubated for 1 h at 37 □ and then washed with PBST (4 × 200 μL). A solution of enzymatic substrate 3,3',5,5'-tetramethylbenzidine (TMB, 200 μL) was added to the plates (for one plate: 5 mg of TMB was dissolved in 2 mL of DMSO plus 18 mL of citric acid buffer containing 20 μL of H_2O_2). Color was developed for 15 min and quenched by adding 50 μL of 0.5 M H_2SO_4. The readout was measured at 450 nm using a microplate reader. The titer was determined by regression analysis with log10 dilution plotted with optical density and reported as the highest fold of dilution giving the optical absorbance value of 0.1 over those of the pre-immune control sera (OD ~ 0.1). All samples were performed in three replicates.

3.4.9 Detection of antibody binding to cells by FACS

1199, 1242, 1245 FB and Neo cell lines, B16-FUT3, EL4-FUT3 and EL4 cells were respectively cultured at 37 °C under 5% CO_2 in cell growth medium (DMEM with 10% FBS and 1% P.S.). The number of cells was determined using a hemocytometer. Suspensions of 3.0×10^5 cells were added to each FACS tube, then centrifuged at 300X g for 5 min to remove the supernatant. The cell pellets were washed with FACS buffer (1% BSA in PBS with 0.1 % NaN_3) and incubated with 1:20 dilution of mouse sera or different concentration of 5B1 or 121 SLE anti-sLe^a mAb in FACS buffer (100 μL) for 30 min on ice. The incubated cells were washed twice with FACS buffer, followed by incubation with PE conjugated goat anti-mouse IgG (minimal x-reactivity) antibody (Biolegend, 1 μL, 0.2 mg mL^{-1}) for 30 min on ice. The cells were washed

twice, re-suspended in FACS buffer, and analyzed by LSR II (BD Biosciences). Data was processed by FlowJo software.

3.4.10 Complement dependent cytotoxicity

1199 FB cells (30,000 cells/well) were added in 96 well plate in DMEM. The culture medium was centrifuged at 1,600 rpm for 5 min and then removed carefully. Various dilutions of mouse sera (starting dilution is 20 fold) from different groups of immunized mice in 50 μL of DMEM were respectively added to the plate and incubated for 1h at 4°C. After 1h, the cells were washed twice with 1% BSA in PBS and supernatant discarded. Then rabbit serum complement at a dilution (1:10 dilution) in 100 μL of DMEM was added and incubated at 37 °C for 3 h. MTS (CellTiter 96® AQueous One Solution Cell Proliferation Assay; Promega, 20 μL) was added into each well and further incubated at 37 °C for 3 h. The optical absorption of the MTS assay was measured at 490 nm. Cells treated alone complement only were used as a positive control (maximum OD), and 5% Triton X-100 treated cells were used as a negative control (minimum OD). All data were performed in three replicates. Cytotoxicity was calculated as follows: Cytotoxicity (%) = (OD positive control – OD experimental) / (OD positive control – OD negative control) × 100.

3.4.11 Immunochemistry staining of cancer tissue microarrays

Tissue arrays were purchased from US Biolab (XPan024 and XPan048) and stained at investigative Histopathology laboratory at Michigan State University using IP FLX background punisher (IP974), MACH3 mouse probe (MP530H), MACH3 mouse HPR-Poly (MH530H), Romulin AEC (RAEC810), and Cat Hematoxylin (CATHE) from BioCare Medical. Pooled sera from 5 mice (1:1000 dilution) from each group of Qβ-sLe^a or sLe^a + Qβ mixture at day 35 and

5B1 recombinant antibody at 1.08 μg/ml final concentration were used to stain the tissue arrays. Images were obtained with Nikon upright microscope, ECLIPSE Ci-L, with 10x magnitude.

3.4.12. Active tumor protection model

C57BL/6 mice were subcutaneously injected under the scruff on day 0 with 0.2 mL of various Qβ-sLe^a / sLe^a + Qβ mixture vaccines in PBS containing MPLA (20 μL, 1 mg mL^{-1} in DMSO) for each mouse. For the Qβ-sLe^a conjugate or sLe^a + Qβ mixture, 10 mice immunized in each group. Boosters were given subcutaneously with the same amounts of vaccines with MPLA under the scruff on days 14 and 28. All Qβ-sLe^a /sLe^a + Qβ mixture administered have the same amounts of sLe^a (4μg). Serum samples were collected on days 0 (before immunization), 23, 35. At day 35, B16-FUT3 (5×10^5 cells/mouse) cells were inoculated i.v. into the lateral tail vein in 200 μL PBS. Two control groups (5 mice per group) will receive PBS or 100 μg of 5B1 IgG2a on days 1, 4, 7, and 11 after inoculation. The lung will be harvested on day 14 and analyzed for the presence of surface metastatic foci.

3.4.13 Passive tumor protection model

B16-FUT3 and EL4-FUT3 (5×10^5 cells/mouse) cells will be inoculated i.v. into the lateral tail vein in 200 μL PBS. Mice will be given intraperitoneal injections of 100 μg of 5B1 recombinant antibody, rabbit sera (the amount for rabbit sera will be determined based on ELISA result) or PBS serving as control, on days 1, 4, 7, and 11 after inoculation. For the B16-FUT3 lung colonization model, the lungs will be harvested on day 14 and analyzed for the presence of surface metastatic foci. For EL4-FUT3 tumor model, survival will be assessed daily.

APPENDIX

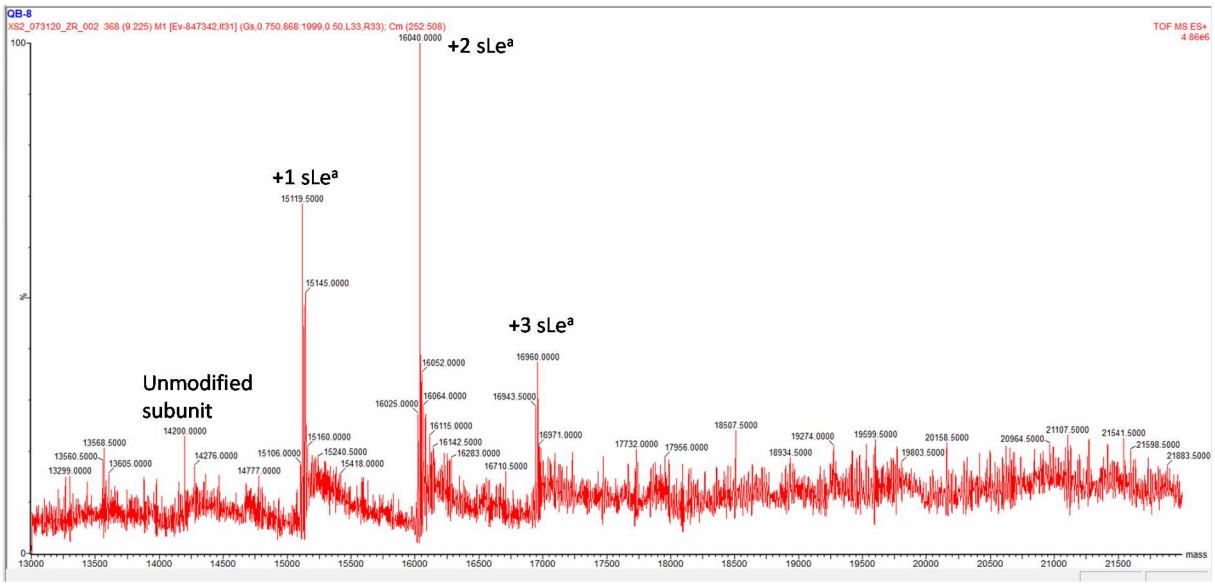

Figure 3. 12 ESI-TOF HRMS spectrum for Qβ-sLe^a conjugate. Mass spectrometry analysis of the Qβ-sLe^a conjugate showed average loading of 300 tetrasaccharides on viral capsid. Each peaks shows the addition of sLe^a with MW of 918 Da. The average loading was calculated based on ratio of sum of peaks loading multiplied by their intensity to total intensity of all peaks.

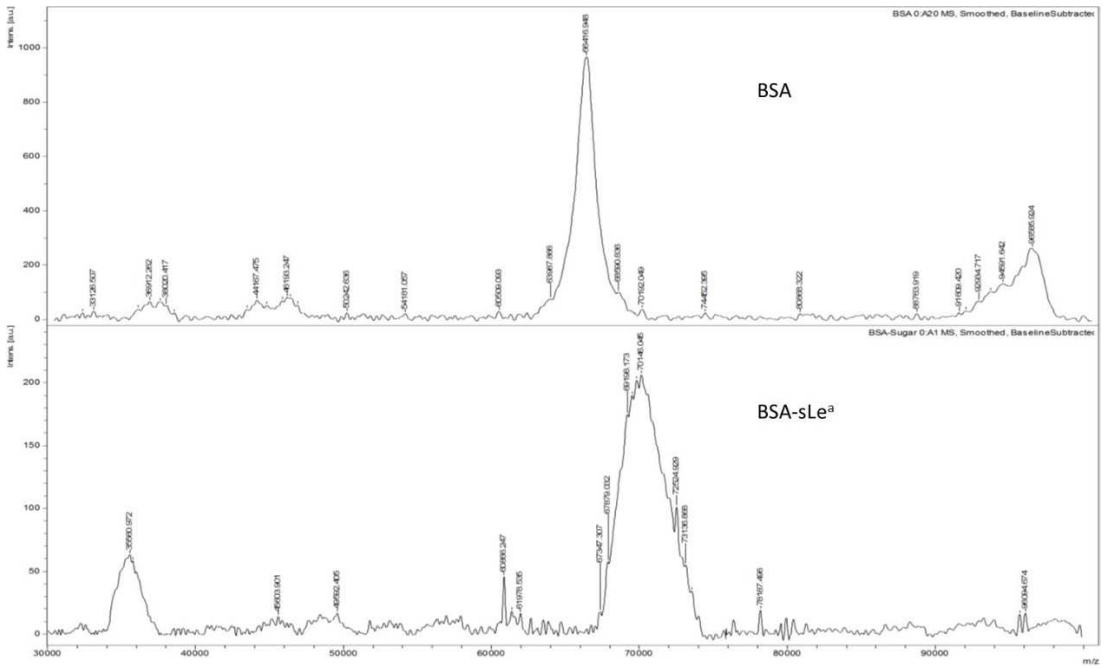

Figure 3. 13 MALDI-TOF characterization of BSA-sLe^a. The molecular weight of BSA shifted from 66,417 Da to 70,146 Da after conjugation. The difference of MW before and after conjugation is divided to the sLe^a MW (918) to obtain the average loading of four sLe^a sugar per BSA molecule.

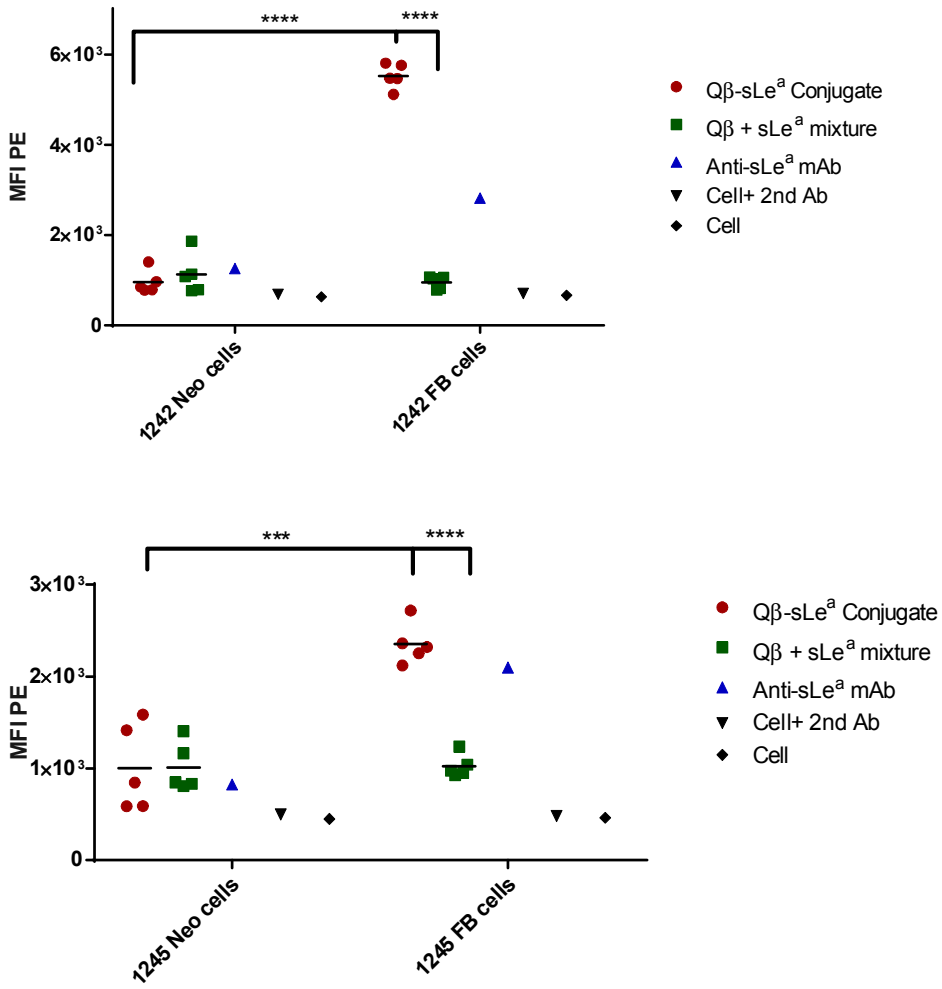

Figure 3. 14 Sialyl Lewis a expression in 1242 and 1245 FB cell line versus neo cells was analyzed with flow cytometry. Sera from mice immunized with Qβ-sLe^a conjugate bind to FB cells very strongly, while binding to Neo cells was similar to the cells without addition of serum in presence or absence of secondary Ab which served as negative control cells. The sLe^a and Qβ mixture did not show binding to FB or neo cell lines. Anti-Sialyl Lewis a mAb, 121 SLE, served as positive control. ***P = 0.0004, ****P < 0.0001 (unpaired two tailed t test). (The experiments for 1242 and 1245 were done separately with different instrument setting which resulted in different background level)

No.	Map ID	Sex	Age	Organ	Pathology Diagnosis	Grade	Stage	TNM
1	A1	M	50	Pancreas	Ductal adenocarcinoma	3	IIB	T3N1M0
2	A2	F	62	Pancreas	Ductal adenocarcinoma	3	IIA	T3N0M0
3	A3	F	23	Pancreas	Ductal adenocarcinoma	3	IIA	T3N0M0
4	A4	F	46	Pancreas	Ductal adenocarcinoma	3	III	T4N0M0
5	A5	F	47	Pancreas	Ductal adenocarcinoma	3	IIB	T3N1M0
6	B1	F	61	Pancreas	Ductal adenocarcinoma	1--2	IB	T2N0M0
7	B2	M	49	Pancreas	Ductal adenocarcinoma	3	IIB	T3N1M0
8	B3	M	64	Pancreas	Ductal adenocarcinoma	3	IIA	T3N0M0
9	B4	F	55	Pancreas	Ductal adenocarcinoma	3	IB	T2N0M0
10	B5	F	76	Pancreas	Ductal adenocarcinoma	2--3	IIA	T3N0M0
11	C1	F	51	Pancreas	Ductal adenocarcinoma	2	IB	T2N0M0
12	C2	M	44	Pancreas	Ductal adenocarcinoma	2	IIA	T3N0M0
13	C3	M	44	Pancreas	Ductal adenocarcinoma	3	IIA	T3N0M0
14	C4	M	74	Pancreas	Ductal adenocarcinoma	2	IIA	T3N0M0
15	C5	M	54	Pancreas	Ductal adenocarcinoma	2--3	IIA	T3N0M0
16	D1	M	49	Pancreas	Ductal adenocarcinoma	2	IB	T2N0M0
17	D2	M	41	Pancreas	Ductal adenocarcinoma	2	III	T4N1M0
18	D3	F	58	Pancreas	Ductal adenocarcinoma	2	IIB	T3N1M0
19	D4	F	64	Pancreas	Ductal adenocarcinoma	2	IIA	T3N0M0
20	D5	M	54	Pancreas	Ductal adenocarcinoma	2	IB	T2N0M0
21	E1	M	55	Pancreas	Ductal adenocarcinoma	2	IIA	T3N0M0
22	E2	M	65	Pancreas	Ductal adenocarcinoma	2	IIB	T3N1M0
23	E3	M	42	Pancreas	Ductal adenocarcinoma	2	IIA	T3N0M0
24	E4	F	42	Pancreas	Ductal adenocarcinoma	2	IIA	T3N0M0

Table 3. 1 Human pancreatic ductal adenocarcinoma tissue microarray (XPAN024-01) specification which contains 24 cores and 24 cases. 1 core per case. Each core has 1.5 mm diameter with 5μm thickness and fixed with formalin.

No.	Map ID	Sex	Age	Organ	Pathology Diagnosis	Grade	Stage	TNM
1	A1	M	40	Pancreas	Pancreatic tissue			
2	A2	M	45	Pancreas	Pancreatic tissue			
3	A3	F	42	Pancreas	Pancreatic tissue			
4	A4	M	48	Pancreas	Metastatic pancreatic malignant islet cell tumor			
5	A5	M	54	Pancreas	Metastatic pancreatic papillary adenocarcinoma			
6	A6	F	45	Pancreas	Neuroendocrine tumor		IIA	T3N0M0
7	A7	M	29	Pancreas	Neuroendocrine tumor (myeloid) G3		IIB	T3N1M0
8	A8	F	37	Pancreas	Neuroendocrine tumor	2	IB	T2N0M0
9	B1	M	28	Pancreas	Neuroendocrine tumor	1	IIB	T2N1M0
10	B2	F	30	Pancreas	Mixed acinar-endocrine tumor	-	IB	T2N0M0
11	B3	M	62	Pancreas	Neuroendocrine tumor	-	IIA	T3N0M0
12	B4	F	47	Pancreas	Neuroendocrine tumor	-	IIA	T3N0M0
13	B5	M	62	Pancreas	Squamous cell carcinoma	2--3	IIA	T3N0M0
14	B6	F	49	Pancreas	Squamous cell carcinoma	2	IIB	T3N1M0
15	B7	M	52	Pancreas	Adenosquamous carcinoma	-	IIA	T3N0M0
16	B8	M	64	Pancreas	Adenosquamous carcinoma	-	IIA	T3N0M0
17	C1	F	62	Pancreas	Adenosquamous carcinoma	-	IIA	T3N0M0
18	C2	M	50	Pancreas	Adenocarcinoma	3	IIA	T3N0M0
19	C3	M	60	Pancreas	Adenocarcinoma	3	IIA	T3N0M0
20	C4	M	52	Pancreas	Adenocarcinoma	3	IB	T2N0M0
21	C5	M	62	Pancreas	Adenocarcinoma	3	IIA	T3N0M0
22	C6	F	66	Pancreas	Adenocarcinoma	3	IIB	T2N1M0
23	C7	M	50	Pancreas	Adenocarcinoma	3	IIB	T3N1M0
24	C8	M	45	Pancreas	Adenocarcinoma	3	IIA	T3N0M0
25	D1	F	46	Pancreas	Adenocarcinoma	3	III	T4N0M0
26	D2	F	23	Pancreas	Adenocarcinoma	3	IIA	T3N0M0
27	D3	F	62	Pancreas	Adenocarcinoma	3	IIA	T3N0M0
28	D4	F	47	Pancreas	Adenocarcinoma	3	IIB	T3N1M0
29	D5	F	61	Pancreas	Adenocarcinoma	2--3	IB	T2N0M0
30	D6	M	49	Pancreas	Adenocarcinoma	2--3	IIB	T3N1M0
31	D7	F	55	Pancreas	Adenocarcinoma	2--3	IIA	T3N0M0
32	D8	M	64	Pancreas	Adenocarcinoma	2--3	IIA	T3N0M0
33	E1	M	55	Pancreas	Adenocarcinoma	2--3	IIA	T3N0M0
34	E2	F	76	Pancreas	Adenocarcinoma	2	IIA	T3N0M0
35	E3	F	51	Pancreas	Adenocarcinoma	2	IB	T2N0M0
36	E4	M	44	Pancreas	Adenocarcinoma	2	IIA	T3N0M0
37	E5	M	74	Pancreas	Adenocarcinoma	2	IIA	T3N0M0
38	E6	M	54	Pancreas	Adenocarcinoma	2	IIA	T3N0M0
39	E7	M	44	Pancreas	Adenocarcinoma	2	IIA	T3N0M0
40	E8	M	49	Pancreas	Adenocarcinoma	2	IB	T2N0M0
41	F1	M	41	Pancreas	Adenocarcinoma	2	III	T4N1M0
42	F2	F	58	Pancreas	Adenocarcinoma	2	IIB	T3N1M0
43	F3	M	55	Pancreas	Adenocarcinoma	2	IIA	T3N0M0
44	F4	F	64	Pancreas	Adenocarcinoma	2	IIA	T3N0M0
45	F5	M	54	Pancreas	Adenocarcinoma	1--2	IIA	T3N0M0
46	F6	M	65	Pancreas	Adenocarcinoma	1	IIB	T3N1M0
47	F7	M	42	Pancreas	Adenocarcinoma	1	IIA	T3N0M0
48	F8	F	42	Pancreas	Adenocarcinoma	1	IIA	T3N0M0

Table. 2 Human pancreatic cancer tissue microarray (XPAN048-01) specification which contains 48 cores and 48 cases. 1 core per case. It contains 3 cases of normal tissue, 2 cases of metastatic cancer, 2 cases of squamous cell carcinoma, 2 cases of adenosquamous carcinoma, and 31 cases of pancreatic adenocarcinoma.

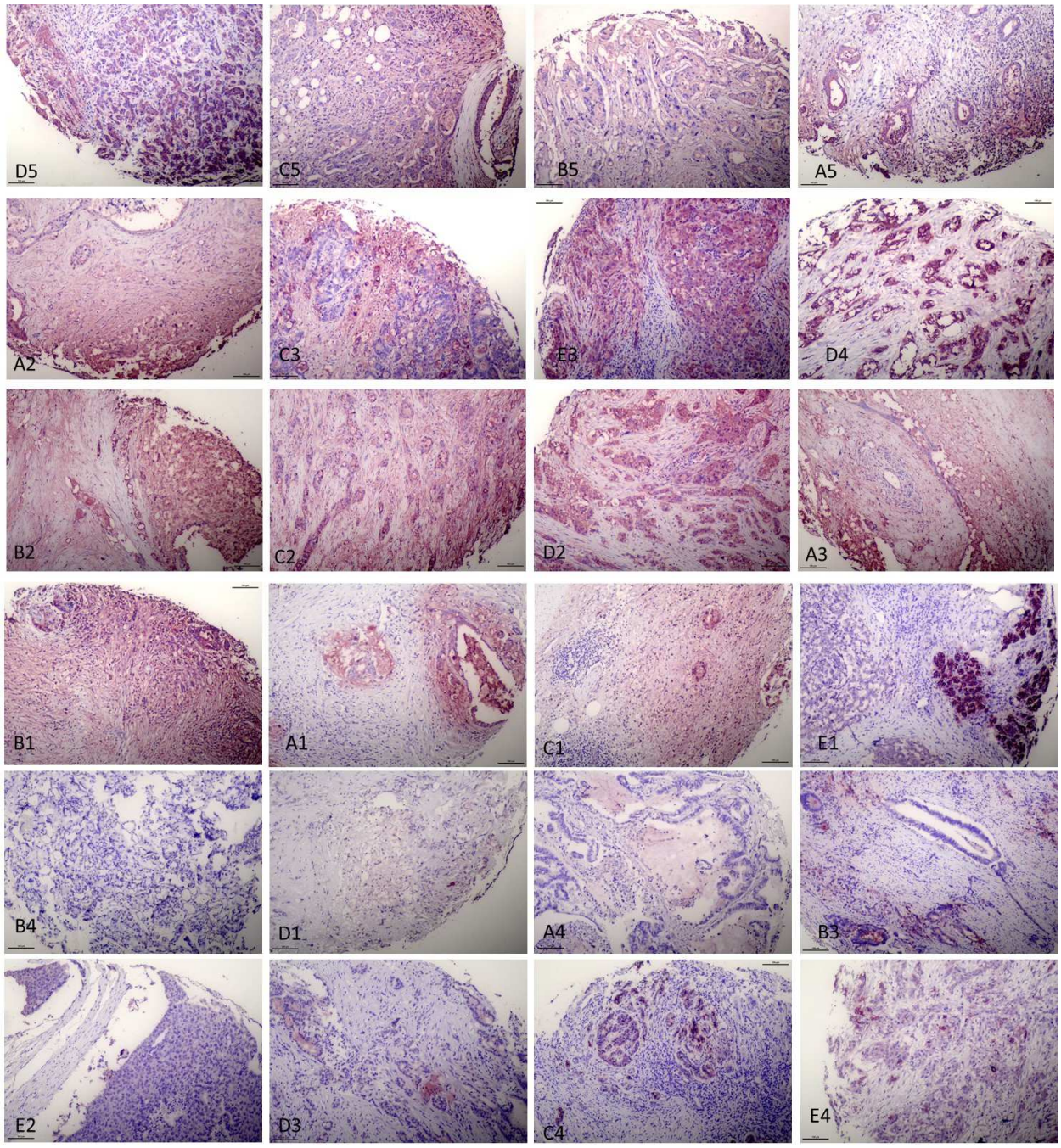

Figure 3. 15 XPAN024 microarray stained with pooled serum of 5 mice immunized with Qβ-sLe^a conjugate at day 35 at 1:1000 serum dilution. Characterization of each core has been provided in table 1 based on their map ID. The brown/red color was due to antibody binding to tissues. The lack of brown/red staining indicates little binding of antibodies to the tissues. Scale bar is 100μm.

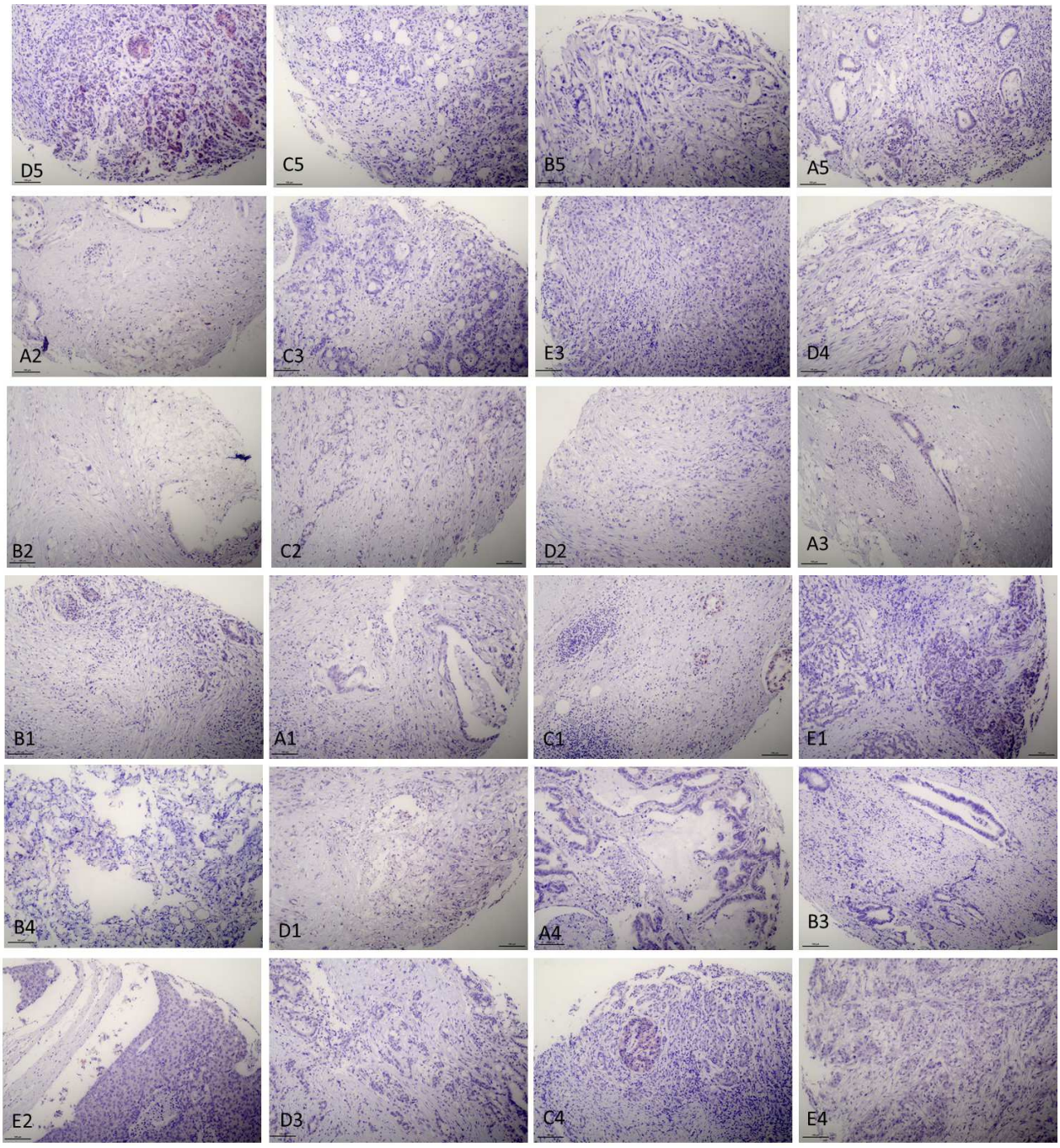

Figure 3. 16 XPAN024 microarray stained with pooled serum of 5 mice immunized with sLe^a and Qβ mixture at day35 at 1:1000 serum dilution. Characterization of each core has been provided in table 1 based on their map ID. The brown/red color was due to antibody binding to tissues. The lack of brown/red staining indicates little binding of antibodies to the tissues. Scale bar is 100μm.

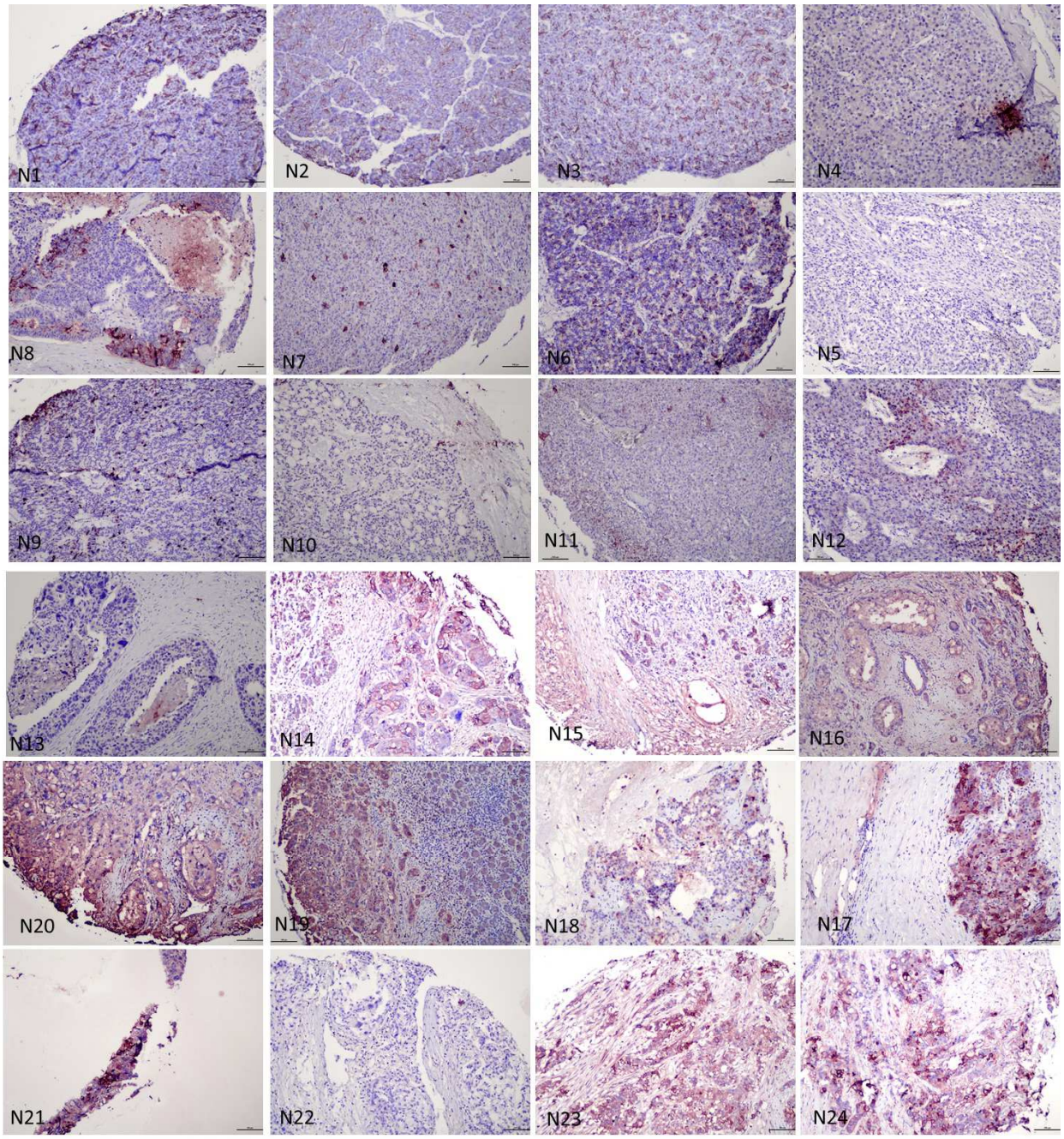

Figure 3. 17 XPAN048 microarray stained with pooled serum of 5 mice immunized with Qβ-sLe^a conjugate at day 35 at 1:1000 serum dilution. Characterization of each core has been provided in table 2 based on their number. The brown/red color was due to antibody binding to tissues. The lack of brown/red staining indicates little binding of antibodies to the tissues. Scale bar is 100μm.

Figure 3.17 (cont'd)

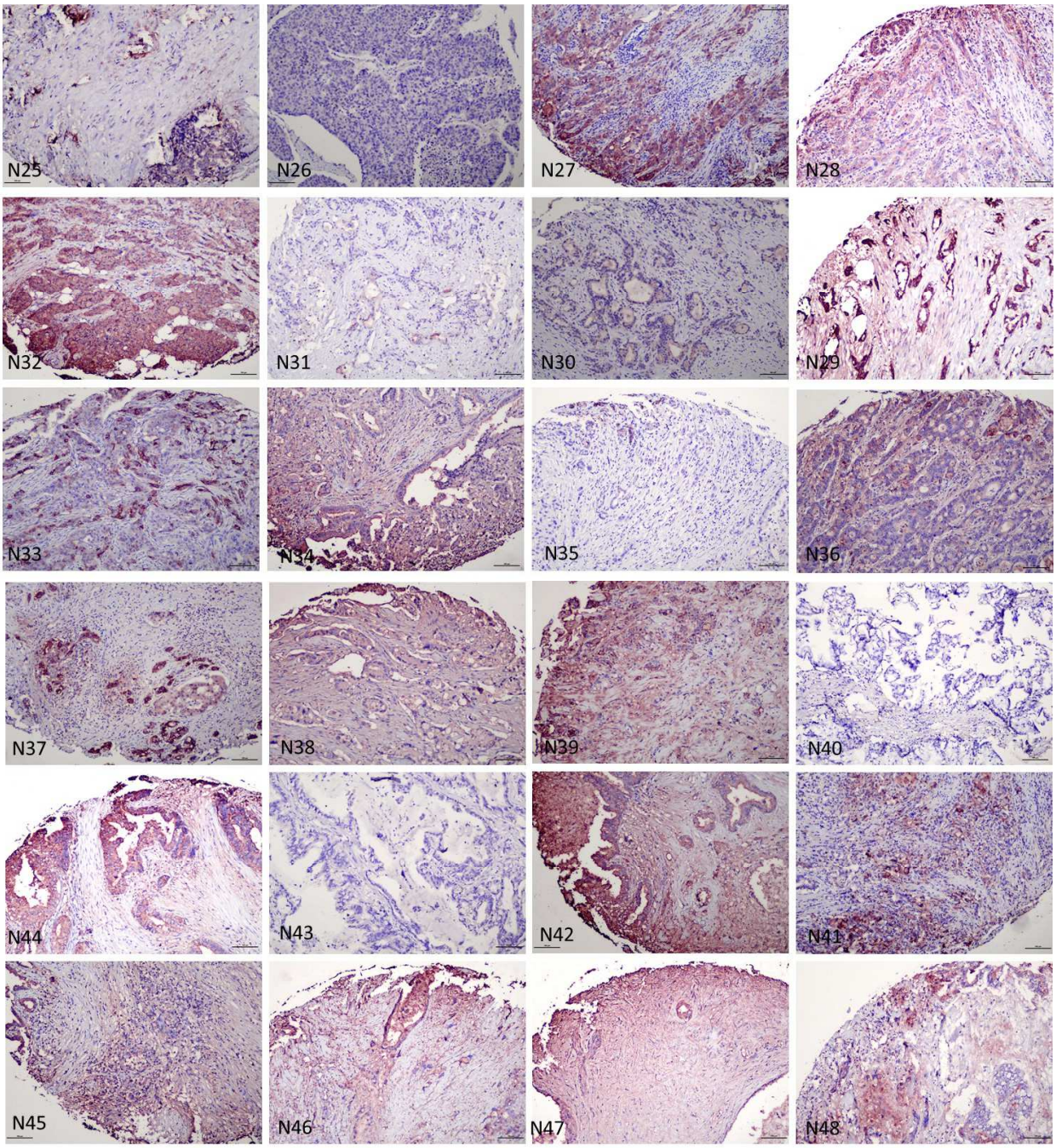

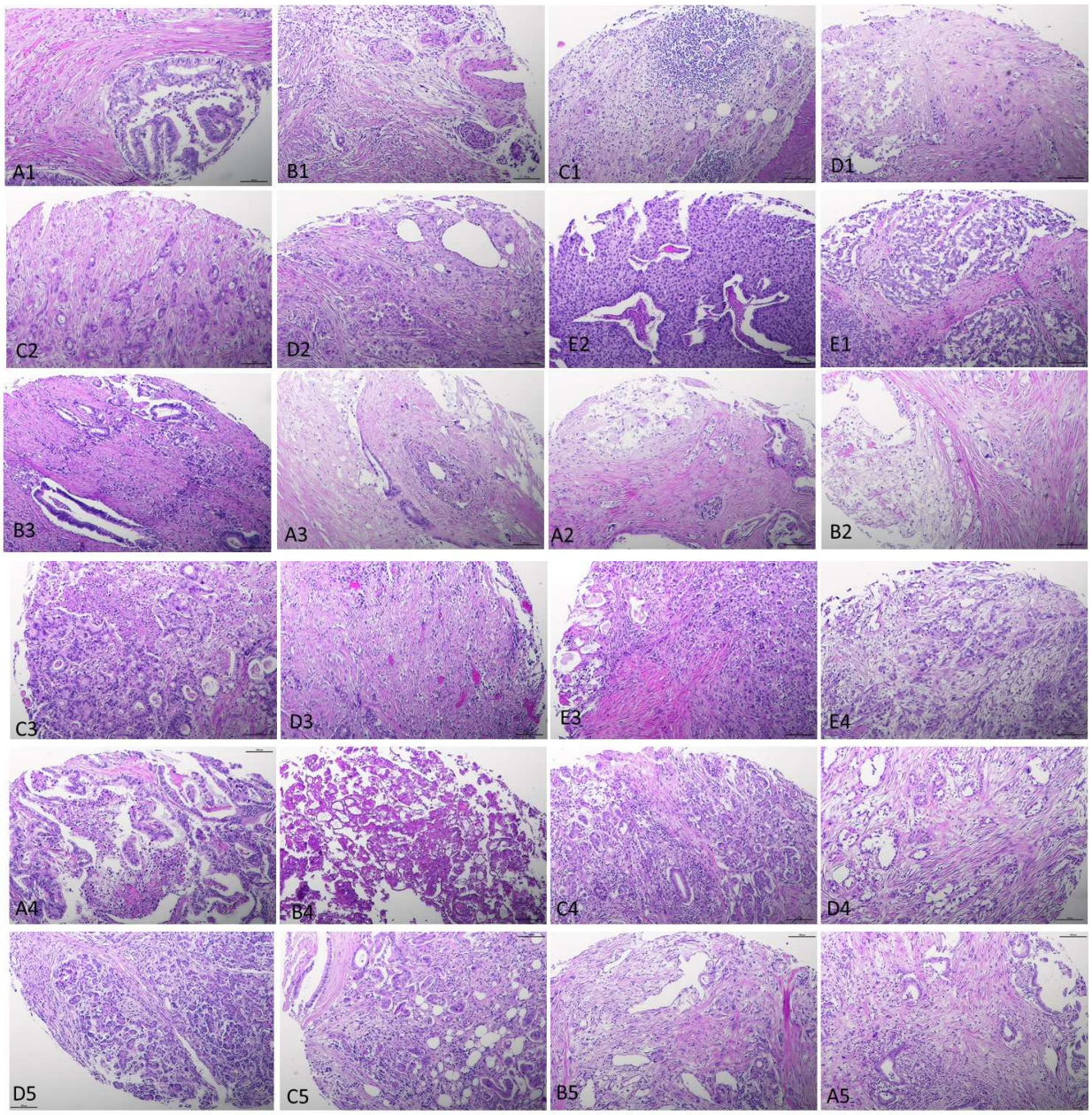

Figure 3. 18 XPAN024 microarray hematoxylin and eosin (H&E) staining. Pictures were obtained to determine the inflammatory stage of tissues. Areas with dense nucleus population (dark blue spots) suggests the presence of macrophages. Characterization of each core has been provided in table 1 based on their map ID. Scale bar is 100µm.

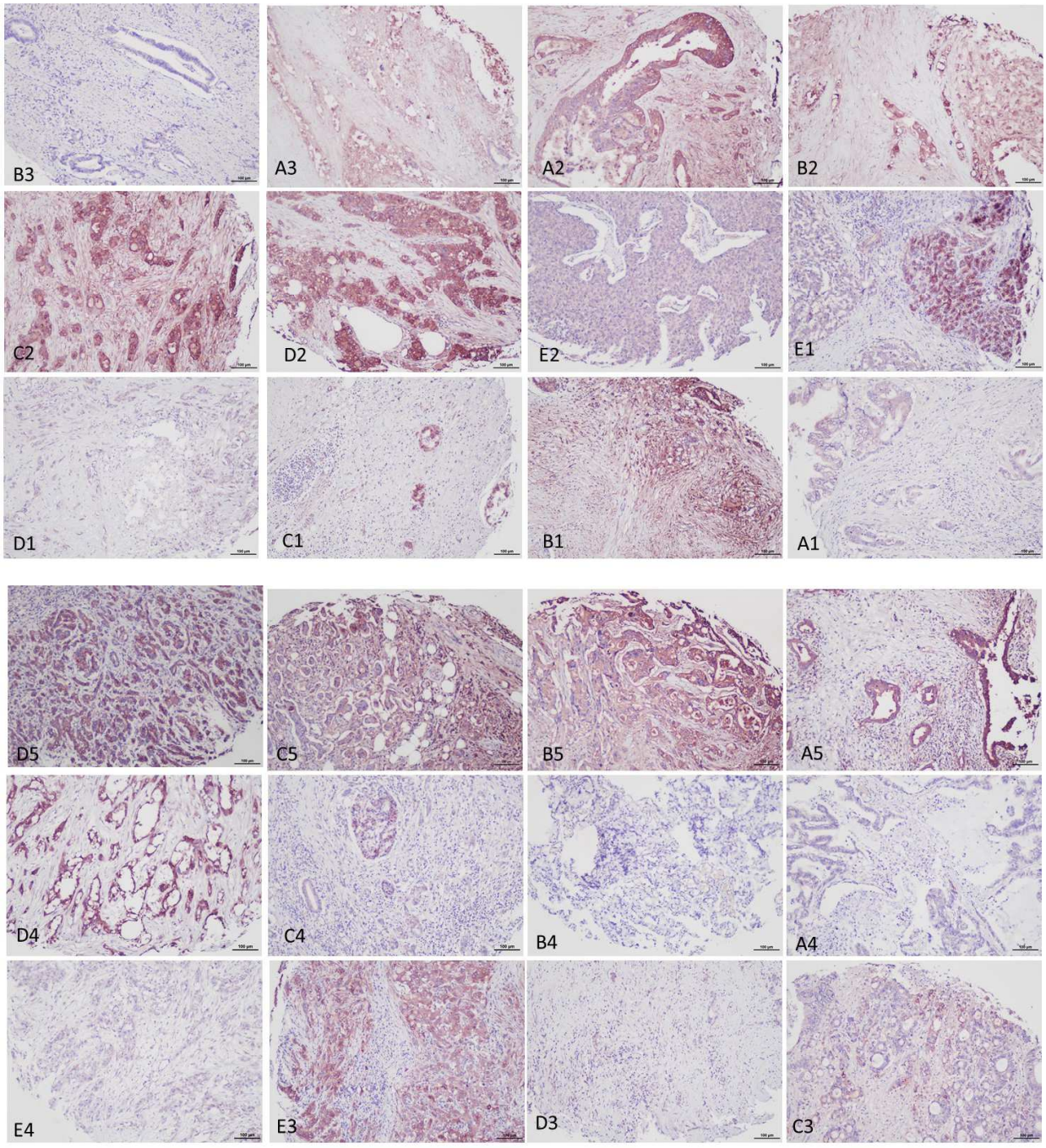

Figure 3. 19 XPAN024 microarray stained with 5B1 recombinant antibody at 1.08 µg/ml final concentration. Characterization of each core has been provided in table 1 based on their map ID. The brown/red color was due to antibody binding to tissues. The lack of brown/red staining indicates little binding of antibodies to the tissues. Scale bar is 100µm.

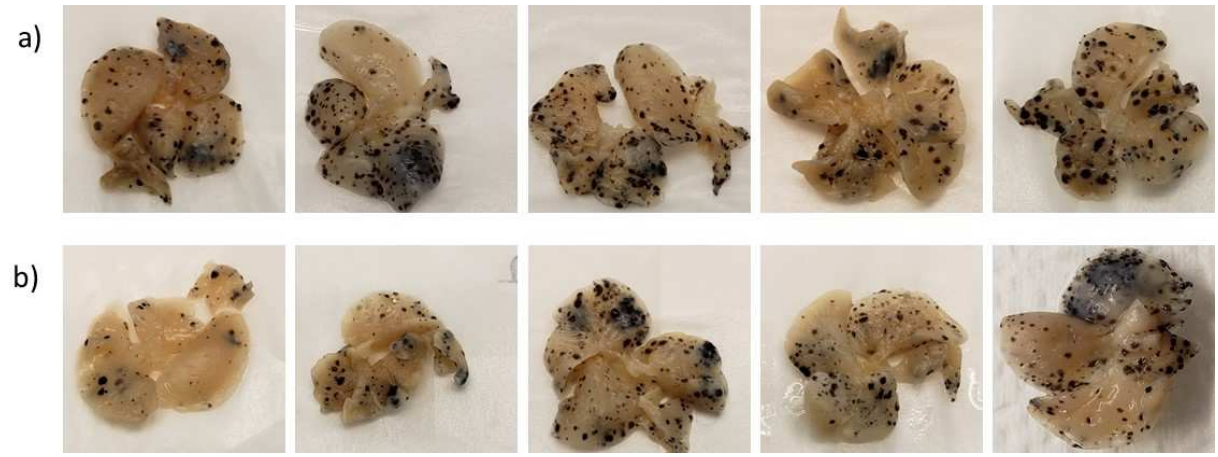

Figure 3. 20 Images of lung tissues obtained from the mice immunized with a) sLea and Qβ mixture, and b) Qβ-sLe^a conjugate which challenged with B16-FUT3 cell line 356 days post immunization.

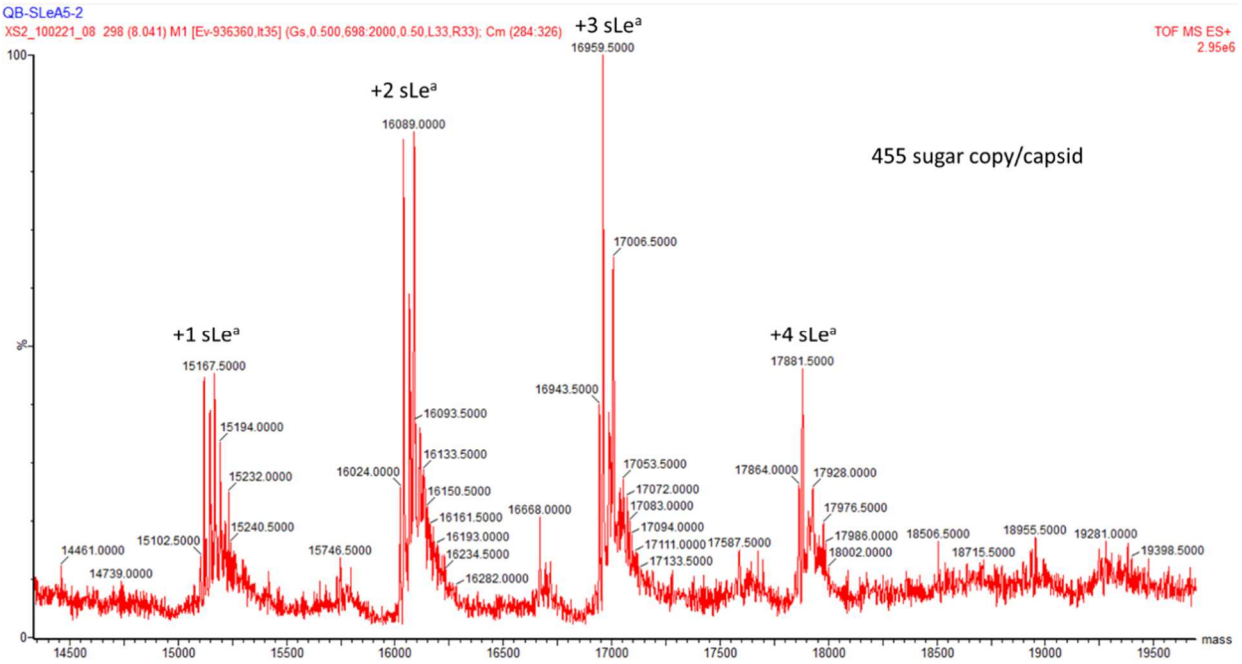

Figure 3. 21 ESI-TOF HRMS spectrum for the 2nd batch of Qβ-sLe^a conjugate that used for rabbit study. Mass spectrometry analysis of the Qβ-sLe^a conjugate showed that the number of tetrasaccharides on viral capsid were 455 on average.

						Qβ-sLe^a conjugate						Qβ + sLe^a mixture				
						IgG								IgG		
Family	a815	Abbreviation	Description	S-LR	S-N	S-L	S-R	S-2L	average		C-R	C-2L	C-LR	C-N	C-L
Lewis	48	3'Neu5Ac-LeA -12	Neu5Aca2-3Galb1-3[Fuca1-4)GlcNAcb1-3Galb1-APD-HAS; Sialyl Lewis A; SLeA	5447	32545	32206	26581	25451	24446		213	6	9	0	6
Lewis	281	3'Neu5Ac-LeC-Sp -12	Neu5Aca2-3Galb1-3GlcNAcb-Sp-BSA	65479	65357	286	105	159	26277		-54	8	0	-30	0
Lewis	284	3'Neu5Ac-LeC-Sp -05	Neu5Aca2-3Galb1-3GlcNAcb-Sp-BSA	65476	65360	122	50	79	26217		-57	11	12	-32	3
Lewis	303	3'Neu5Gc-LeC-Sp -12	Neu5Gca2-3Galb1-3GlcNAcb-Sp-BSA	54451	55663	124	6	39	22057		-24	7	19	-20	5
Lewis	233	3'Neu5Ac(9Ac)-LeC-Sp - 12	Neu5Ac(9Ac)a2-3Galb1-3GlcNAcb-Sp-BSA	17534	15768	266	2	150	6744		-54	8	0	-16	0
Lewis	310	3'Neu5Ac(9Ac)-LeC-Sp - 05	Neu5Ac(9Ac)a2-3Galb1-3GlcNAcb-Sp-BSA	14805	16309	126	-43	93	6258		-82	0	0	-40	0
Lewis	268	3'KDN-LeC-Sp - 12	KDNa2-3Galb1-3GlcNAcb-Sp-BSA	61039	46803	0	-34	0	21561		-63	5	6	-29	0
Lewis	316	3'Neu5Gc-LeC-Sp -05	Neu5Gca2-3Galb1-3GlcNAcb-Sp-BSA	43014	48599	34	-20	11	18328		-60	5	6	-34	0
Lewis	263	3'KDN-LeC-Sp - 04	KDNa2-3Galb1-3GlcNAcb-Sp-BSA	31708	23708	5	-31	0	11078		-45	5	6	-25	0
glycolipid	659	GD2 tetra (Kdn, Gc)	Kdna2-8Neu5Gca2-3(GlcNAcb1-4)Galb1-	1309	-3	57	-40	0	265		-40	32	0	-20	3
glycolipid	644	3'Neu5Ac-LNnT	Neu5Aca2-3Galb1-4GlcNAcb1-3Galb1-4	887	-20	42	-57	0	170		-65	20	3	-40	0
glycolipid	647	GD3 tri (Ac-Kdn)	Neu5Aca2-8Kdna2-3Galb1-	710	-10	34	-32	0	141		-37	12	0	-23	0
non-human	671	laminarihexaose - 05	Glcb1-3Glcb1-3Glcb1-3Glcb1-3Glcb1-3Glcb1-	771	179	42	-59	130	212		-12	17	91	-42	3
non-human	547	Glcb1-3Glcb- 26	Glcb1-3Glcb-	0	332	11	535	1132	402		2712	3	74	-31	0
Blood Group A	294	Globo A - 09	GalNAca1-3(Fuca1-2)Galb1-3GalNAcb1-3Gala1-4Galb1-BSA	28156	3809	31608	5882	19376	17766		10741	45	21254	32	1791
Blood Group A	63	BG-A4-14	GalNAca1-3(Fuca1-2)Galb1-3GalNAcb1-linker-BSA	21755	1428	19453	388	18890	12383		5244	22	7843	-65	221
Blood Group A	58	BG-A3-14	GalNAca1-3(Fuca1-2)Galb1-3GalNAcα1-linker-BSA	17664	574	8961	310	12985	8099		564	28	16648	-54	279
Blood Group A	94	Globo A - 03	GalNAca1-3(Fuca1-2)Galb1-3GalNAcb1-3Gala1-4Galb1-BSA	5375	133	4452	85	5158	3040		351	20	2140	-66	204
y-glycoprotein	363	PSM A pos	porcine submaxillary mucin (A+)	1831	14	206	-9	93			9	20	247	-45	125
glycolipid-neutral	31	Gala1-4Galb - 11	Gala1-4Galb-CETE-BSA	574	45	105	3	2			11	168	70	25	102
Blood Group A	62	BG-A4-05	GalNAca1-3(Fuca1-2)Galb1-3GalNAcb1-linker-BSA	164	117	1630	-34	1128			68	3	1484	-49	11
non-human	13	Rha-b - 21	Rha-b - BSA	34	39	139	0	5			-23	40	108	-3	68
Blood Group B	71	BG-B3-17	Gala1-3(Fuca1-2)Galb1-3GalNAcα1-linker-BSA	6	-34	102	-9	5			-119	11	159	-51	136
Blood Group B	112	Globo B - 12	Gala1-3(Fuca1-2)Galb1-3GalNAcb1-3Gala1-4Galb1-BSA	6	-31	140	-33	17			-91	3	105	-57	42
non-human	619	Rha-a-23	Rha-a – BSA	572	6	551	0	177			-12	322	788	15	506
non-human	12	Rha-a - 18	Rha-a – BSA	402	-3	538	-14	430			-33	278		-3	707
y-other	481	DNP-BSA	dinitrophenylated lysines on BSA	19	110	226	314	262			646	5134	26	159	25
y-other	401	dsDNA	double stranded calf thymus DNA	6	-3	746	0	11			-3	3	40	-3	5
peptide-Tn	173	Ac-P-Tn(Thr)-T-G - 22	Ac-Pro-(GalNAca)Thr-Thr-Gly-Hex-BSA (muc2)	6	-25	143	-51	0			-31	5	103	-32	6
non-human	692	Xylb5 - 05	Xylb1-4Xylb1-4Xylb1-4Xylb1-4Xylb1-BSA	420	-18	28	-40	0			950	12	6	-51	0
carb-GlcNAc	266	3'GN type1-Sp - 16	GlcNAcb1-3Galb1-3GlcNAcb-Sp-BSA	133	-6	200	-11	0			-39	0	-3	-27	62
carb-GlcNAc	286	3'GN-LacNAc (dimeric)-Sp - 14	GlcNAcb1-3(Galb1-4GlcNAcb1-3)2b-Sp-BSA	43	-26	113	-57	0			-93	0	3	-59	79
carb-GalNAc	719	GalNAca-phenyl amide- high	GalNAca-O-phenyl-amide linked	43	-12	7	-28	0			-25	0	0	-17	3
carb-GlcNAc	320	3'GN-LacNAc (dimeric)-Sp - 06	GlcNAcb1-3(Galb1-4GlcNAcb1-3)2b-Sp-BSA	17	-9	171	-37	0			-46	-3	6	-31	94
carb-GalNAc	5	GalNAc-a - 22	GalNAc-a - BSA	6	-9	8	-31	8			-40	3	9	-26	0
peptide-core 3	338	Ac-S-Thr(core 3)-S-G - 21	Ac-Ser-(GlcNAcb1-3GalNAca)Thr-Ser-Gly-Hex-BSA	3	-40	197	-40	0			-66	5	6	-35	20
peptide-GalNAc Tyr	518	AzHex-G-Y(GalNAc-a	BSA-AzHex-G-Y(GalNAc-a)-A-amide	3	-42	0	-22	0			-32	2	0	-17	0
Blood Group H	350	BG-H6-21	Fuca1-2Galb1-4Glcb1-linker-BSA	3	-10	191	-51	0			-54	0	6	-49	3
carb-GlcNAc	255	GNLacNAc-Sp - 16	GlcNAcb1-3Galb1-4GlcNAcb-Sp-BSA	3	-26	221	-48	0			-95	8	29	-63	193
glycolipid-neutral	80	P1 - 09	Gala1-4Galb1-4GlcNAc-BSA	3	-29	3	-45	0			-80	-1	0	-43	0
non-human	45	X3Glc3 - 15	Xyla1-6Glcb1-4(Xyla1-6)Glcb1-4(Xyla1-6)Glcb1-BSA	3	-26	3	-43	4			-63	0	2	-46	0
glycolipid-neutral	124	GA2di - 37	GalNAcb1-4Galb - BSA (aka: asialo-GM2)	2	-27	11	-31	3			-54	3	196	-43	0
glycolipid-neutral	164	GA2di (accurate) - 28	GalNAcb1-4Galb - BSA (aka: asialo-GM2)	0	-32	3	-40	0			-57	5	168	-37	0

Table. 3 Glycopeptide microarray screening results of antisera induced by Qβ-sLe^a or Qβ and sLe^a mixture.

Table 3.3 (cont'd)

non-human	512	AX3 - 04	Xylβ1-4(Arafα1-2)Xylβ1-4Xylβ-]; 3^3-α-L-Arabinofuranosyl-xylotriose	0	-22	5	-22	0		1750	-4	0	-49	0
non-human	801	Xylb2 - 26	Xylb1-4Xylb1-BSA	0	-3	11	6	0			-3	6	-15	9
non-human	769	Xylb3 - 05	Xylb1-4Xylb1-4Xylb1-BSA	0	-20	5	-17	0			0	6	-29	0
carb-Sia	274	6'Neu5Ac-LDN-Sp - 13	Neu5Aca2-6GalNAcb1-4GlcNAcb-Sp-BSA	19	-8	0	-31	0		-47	0	6	-29	0
Carb-Glc	736	Glca1-6Glca -15	Glca1-6Glca -BSA	0	-22	2	-46	0		-71	-3	3	-40	-3
Blood Group B	61	BG-B4-06	Gala1-3(Fuca1-2)Galb1-3GalNAcb1-linker-BSA	8	-29	28	-56	8		-108	0	27	-57	0
non-human	674	chitotriose - 04	GlcNAcb1-4GlcNAcb1-4GlcNAcb1-	911	-14	45	-41	0		-55	20	0	-42	0
carb-Glc	686	Isomaltotriose - 05	Glca1-6Glca1-6Glca1-	895	-20	59	-78	0		-102	20	0	-59	3
carb-GlcNAc	287	LNT-2-Sp - 06	GlcNAcb1-3Galb1-4Glcb-Sp-BSA	684	105	98	-37	0		-57	3	3	-37	9
glycolipid	650	GD3 tri (Kdn-Kdn)	Kdna2-8Kdna2-3Galb1-	655	-3	34	-23	0		-20	17	0	-14	-6
glycolipid	653	GD3 tri (Ac-Gc)	Neu5Aca2-8Neu5Gca2-3Galb1-	649	-3	31	-28	0		-29	20	3	-17	-3
carb-Man	641	Mana1-6Man-a - 14	Mana1-6Man-a - HSA	622	-3	28	-20	0		-23	23	0	-8	-3
glycolipid	662	GD2 tetra (Gc, Kdn)	Neu5Gca2-8Kdna2-3(GlcNAcb1-4)Galb1-	618	-5	28	-9	0		-11	15	0	-12	0
non-human-aGal	290	alpha-Gal tetra - 17	Gala1-3Galb1-4GlcNAcb1-3Galb1-BSA	567	54	0	-29	0		-48	3	9	-29	3
glycolipid	665	GD1a (Gc, Gc)	Neu5Gca2-8Neu5Gca2-3(Galb1-3GlcNAcb1-4)Galb1-	544	-8	28	-22	0		-26	23	0	-18	3
glycolipid	656	GD2 tetra (Kdn, Kdn	Kdna2-8Kdna2-3(GlcNAcb1-4)Galb1-	513	-8	27	-23	0		-26	26	0	-14	0
Lewis	668	LeY tetra-10	Fuca1-2Galb1-4[Fuca1-3)GlcNAcb1-	500	-11	31	-17	0		-27	15	0	-23	6
carb-Gal	683	Galb1-6Galb1 - 05	Galb1-6Galb1-	394	6	39	-43	0		-63	12	0	-40	14
glycolipid	695	GD2-NHAc (Xuefei)	Neu5Ac9NHAca2-8Neu5Aca2-3(GlcNAcb1-4)Galb1-Glc-	371	12	34	0	14		-26	15	3	-14	11
glycolipid	280	GQ2-Sp - 06	Neu5Aca2-8Neu5Aca2-8Neu5Aca2-8Neu5Aca2-3[GalNAcb1-4]Galb1-4Glcb-Sp-BSA	366	145	0	-17	0		-48	3	0	-26	3
peptide-GlcNAcb	306	Ac-S-Ser(GlcNAc-b)-S-G - 07	Ac-Ser-(GlcNAcβ)Ser-Ser-Gly-Hex-BSA	346	15	17	-29	5		-46	-3	14	-27	0
carb-Glc	680	maltotriose - 21	Glca1-4Glca1-4Glca1-	298	-10	22	-26	0		-29	5	3	-20	5
carb-Glc	677	maltoheptaose - 21	Glca1-4Glca1-4Glca1-4Glca1-4Glca1-4Glca1-4Glca1-	238	-9	8	-21	0		-20	6	3	-17	6
carb-Sia	319	6'Neu5Ac-LacNAc-Sp - 11	Neu5Aca2-6Galb1-4GlcNAcb-Sp-BSA	199	54	0	-17	0		-23	0	0	-10	3
Blood Group H	293	Globo H - 10	Fuca1-2Galb1-3GalNAcb1-3Gala1-4Galb1-BSA	193	35	3	-40	0		-51	3	6	-31	0
carb-Glc	701	Glcb1-4Glcb1-4Glc - 04	Glcb1-4Glcb1-4Glcb1-	190	-8	17	-37	0		-40	9	2	-23	3
carb-Sia	297	3'Neu5Ac-LacNAc (dimeric)-Sp - 13	Neu5Aca2-3(Galb1-4GlcNAcb1-3)2b-Sp-BSA	171	-9	142	-37	110		-40	0	79	-35	17
non-human-aGal	309	alpha-Gal tetra - 04	Gala1-3Galb1-4GlcNAcb1-3Galb1-BSA	167	9	26	-26	5		-40	0	11	-17	3
Blood Group H	300	TFiLNO(1-2,1-2,1-4) - 06	Fuca1-2Galb1-3GlcNAcb1-3Galb1-4GlcNAcb1-6[Fuca1-2Galb1-3(Fuca1-4)GlcNAcb1-3]Galb-BSA	164	-11	74	-34	28		-57	0	34	-39	14
carb-Glc	698	maltopentaose - 17	Glca1-4Glca1-4Glca1-4Glca1-4Glca1-	153	-8	20	-22	0		-34	6	9	-23	0
carb-Gal	707	Galb1-3Galb1 - 24	Galb1-3Galb1-	133	-20	11	-57	0		-65	6	0	-43	3
carb-Glc	710	maltohexaose - 20	Glca1-4Glca1-4Glca1-4Glca1-4Glca1-4Glca1-	131	-5	14	-20	0		-22	6	6	-23	3
carb-type 1	313	MFiLNO(1-3) - 09	Galb1-3GlcNAcb1-3Galb1-4(Fuca1-3)GlcNAcb1-6(Galb1-3GlcNAcb1-3)Galb1-BSA	105	-12	5	-59	0		-82	0	0	-45	0
glycolipid	288	GT2-Sp - 08	Neu5Aca2-8Neu5Aca2-8Neu5Aca2-3[GalNAcb1-4]Galb1-4Glcb-Sp-BSA	102	-3	3	-17	0		-23	0	3	-14	0
carb-Glc	716	maltotetraose - 05	Glca1-4Glca1-4Glca1-4Glca1-	80	-14	6	-32	0		-31	0	6	-21	3
carb-GalNAc	713	GalNAcb-phenyl Dz-high	GalNAcb-O-phenyl-diazirine linker	79	-5	5	-20	0		-34	3	0	-11	3
glycolipid	271	GD3-Sp - 04	Neu5Aca2-8Neu5Aca2-3Galb1-4Glcb-Sp-BSA	71	0	3	-20	0		-29	0	0	-12	0
Carb-Glc	794	Glcb1-4Manb1 - 15	Glcb1-4Manb1 - BSA	68	-20	17	-59	0		-68	6	0	-34	-3
Carb-Glc	809	Glca1-6Glca1-6Glca	Glca1-6Glca1-6Glca1-6Glca1-6Glca1-6Glca -BSA	54	0	8	-7	0		-40	3	0	-20	0
non-human PNAG	737	PNAG 16 (10000)	GlcNAcb1-6GlcNb1-6GlcNb1-6GlcNb1-6GlcNb1-	54	3	5	-8	0		-23	0	0	-15	3
glycolipid	236	GD1a-Sp - 10	Neu5Aca2-3[Neu5Aca2-3Galb1-3GalNAcb1-4]Galb1-4Glcb-Sp-BSA	51	3	0	-11	0		-8	0	3	3	0
glycolipid	312	GM2-Sp - 07	Neu5Aca2-3[GalNAcb1-4]Galb1-4Glcb-Sp-BSA	51	-11	11	-28	5		-63	3	11	-43	5
Blood Group B	269	B tetra type 2-Sp - 20	Gala1-3[Fuca1-2]Galb1-4GlcNAcb-Sp-BSA	48	-3	74	-34	0		-42	0	-3	-29	-3
Blood Group A	99	BG-A1- 05	GalNAca1-3(Fuca1-2)Galb1-3GlcNAcb1-3Galb1-4(Glc)-APD-HSA	47	156	141	105	113		-77	-3	3	-34	0
non-human PNAG	746	PNAG 25 (11001)	GlcNAcb1-6GlcNAcb1-6GlcNb1-6GlcNb1-6GlcNAcb1-	46	-9	3	-17	0		-20	3	3	-3	3
non-human	743	Ara3 - 06	Araa1-5Araa1-5Ara-BSA	45	-12	0	-31	79		-88	0	23	-60	8
glycolipid	322	GM3(Gc)-Sp - 05	Neu5Gca2-3Galb1-4Glcb-Sp-BSA	45	-7	0	-42	0		-70	0	0	-45	0
non-human PNAG	740	PNAG 19 (10011)	GlcNAcb1-6GlcNb1-6GlcNb1-6GlcNAcb1-6GlcNAcb1-	40	-3	3	-20	0		-31	3	0	-19	-3
non-human PNAG	779	PNAG 27 (11011)	GlcNAcb1-6GlcNAcb1-6GlcNb1-6GlcNAcb1-6GlcNAcb1-	40	0	8	-8	8		-9	0	6	-6	6
carb-Sia	296	3'Neu5Gc-LacNAc-Sp - 10	Neu5Gca2-3Galb1-4GlcNAcb-Sp-BSA	39	3	5	-31	0		-54	0	6	-31	0

Table 3.3 (cont'd)

non-human	791	4-Me-GlcAa1-2Xylb	4-Me-GlcAa1-2Xylb1-4Xylb- BSA	37	-9	5	-23	0		-23	0	-3	-9	-6
carb-Sia	315	6'Neu5Ac-LacNAc (dimeric)-Sp - 05	Neu5Aca2-6[Galb1-4GlcNAcb1-3)2b-Sp-BSA	37	-17	11	-42	5		-83	0	6	-48	3
carb-GalNAc	728	GalNAca-phenyl Dz-low	GalNAca-O-phenyl-diazirine linker	37	-3	3	-12	0		-20	2	0	-8	3
non-human PNAG	770	PNAG 20 (10100)	GlcNAcb1-6GlcNb1-6GlcNAcb1-6GlcNb1-6GlcNb1-	36	-5	5	-17	22		-26	0	9	-16	5
non-human PNAG	785	PNAG 31 (11111)	GlcNAcb1-6GlcNAcb1-6GlcNAcb1-6GlcNAcb1-6GlcNAcb	34	0	5	-11	34		-13	0	6	-6	0
Blood Group B	66	BG-B1-05	Gala1-3(Fuca1-2)Galb1-3GlcNAcb1-linker-BSA	34	-6	32	-23	61		-37	3	23	-20	3
non-human PNAG	788	PNAG 1 (00001)	GlcNb1-6GlcNb1-6GlcNb1-6GlcNb1-6GlcNAcb1-	31	-6	5	-11	39		-1	6	11	-3	0
carb-GalNAc	731	GalNAcb-phenyl amide- low	GalNAcb-O-phenyl-amide linked	28	0	5	-8	0		-12	6	3	-14	-2
glycolipid	676	GD2 (Xuefei)	Neu5Aca2-8Neu5Aca2-3(GlcNAcb1-4)Galb1-Glc-	28	19	22	15	14		-25	3	6	-12	20
non-human PNAG	782	PNAG 7 (00111)	GlcNb1-6GlcNb1-6GlcNAcb1-6GlcNAcb1-6GlcNAcb1-	27	-8	5	-15	0		-18	5	3	-14	0
carb-Sia	308	3'Neu5Ac-LacNAc (dimeric)-Sp - 06	Neu5Aca2-3(Galb1-4GlcNAcb1-3)2b-Sp-BSA	26	-5	5	-42	0		-37	0	0	-28	0
y-glycoprotein	359	CEA	carcinoembryonic antigen isolated from human metastatic liver	26	40	54	45	28		37	20	39	32	25
non-human	539	KDOa2-8KDOa2-4KI	KDOa2-8KDOa2-4KDOa-APTE-BSA	26	28	25	46	11		66	26	6	29	14
non-human	800	Manb2 - 18	Manb1-4Man	26	-6	14	-39	0		128	6	0	-46	0
non-human PNAG	749	PNAG 4 (00100)	GlcNb1-6GlcNb1-6GlcNAcb1-6GlcNb1-6GlcNb1-	26	-5	5	-21	0		-11	3	0	-12	3
non-human PNAG	734	PNAG 0 (00000)	GlcNb1-6GlcNb1-6GlcNb1-6GlcNb1-6GlcNb1-	25	-3	7	-8	0		-3	3	5	-6	0
glycolipid	651	GM2 tri (8MeAc)	Neu5Ac8Mea2-3(GlcNAcb1-4)Galb1-	25	-16	22	-49	0		-85	23	37	-29	31
non-human	803	Arafa1-3(Arafa1-2)X	Arafa1-3(Arafa1-2)Xylb1-4Xylb -BSA	23	0	5	-8	0		-11	0	3	-9	-3
Blood Group A	351	BG-A5-16	GalNAca1-3(Fuca1-2)Galb1-3Galb1-linker-BSA	23	-17	16	-40	20		-54	0	12	-40	0
non-human	97	Cellotriose - 13	Glcb1-4Glcb1-4Glcb-BSA	23	-14	21	-34	0		-31	6	40	-34	5
non-human	289	Forssman Tetra-BSA - 13	GalNAca1-3GalNAcb1-3Gala1-4Galb-BSA	23	-17	0	-45	0		-85	0	6	-45	0
non-human	51	G2M4 - 07	Manb1-4(Gala1-6)Manb1-4(Gala1-6)Manb1-4Manb1-BSA	23	-3	125	-20	184		66	3	0	-34	3
glycolipid	325	GT3-Sp - 07	Neu5Aca2-8Neu5Aca2-8Neu5Aca2-3Galb1-4Glcb-Sp-BSA	23	3	3	-6	0		-12	3	3	-9	3
glycolipid-neutral	305	Gb5/SSEA3 - 12	Galb1-3GalNAcb1-3Gala1-4Galb1-BSA	20	6	3	-32	0		-34	0	0	-14	12
glycolipid	285	GM3-Sp - 04	Neu5Aca2-3Galb1-4Glcb-Sp-BSA	20	-13	3	-43	0		-51	0	0	-32	3
carb-type 1	302	LNT-Sp - 15	Galb1-3GlcNAcb1-3Galb1-4GlcNAcb-Sp-BSA	20	3	5	-29	0		-37	3	6	-9	3
Peptide	722	TSSASTGH-BSA	N-terminus Muc4 – TSSASTGH-BSA	20	-3	0	-22	0		-28	0	0	-20	-3
carb-GlcNAc	328	3'GN type1-Sp - 04	GlcNAcb1-3Galb1-3GlcNAcb-Sp-BSA	17	-9	71	-40	0		-57	3	6	-37	11
Lewis	812	3'Neu5Ac-LeX (Sialyl LeX) - HSA	Neu5Aca2-3Galb1-4[Fuca1-3)GlcNAc – HSA	17	-8	5	-12	0		-9	3	0	-6	0
carb-Sia	324	6'Neu5Ac-LDN-Sp - 05	Neu5Aca2-6GalNAcb1-4GlcNAcb-Sp-BSA	17	-10	5	-34	0		-40	3	3	-23	0
glycolipid-neutral	291	Gb5/SSEA3 - 04	Galb1-3GalNAcb1-3Gala1-4Galb1-BSA	17	-8	5	-34	0		-43	3	0	-22	0
glycolipid	318	GD1b - 05	Neu5Aca2-8Siaa2-3(Galb1-3GalNAcb1-4)Galb1-4-BSA	17	-17	5	-32	3		-57	2	6	-40	0
N-linked	321	Man1 - 12	Manβ1-4GlcNAcβ1-4GlcNAcβ1-BSA	17	-12	17	-26	0		-31	3	0	-28	0
non-human PNAG	752	PNAG 18 (10010)	GlcNAcb1-6GlcNb1-6GlcNb1-6GlcNAcb1-6GlcNb1-	17	3	0	-11	3		-3	3	6	-9	-3
non-human	755	Xylb2 - 05	Xylb1-4Xylb1-BSA	17	-14	5	-42	0		261	0	0	-37	0
Blood Group H	193	6'Neu5Ac-LNF V - 12	Fuca1-2Galb1-3(Neu5Aca2-6)GlcNAcb1-3Galb1-APD-HSA	14	85	54	5	39		-77	0	0	-45	-2
glycolipid	522	GM2 tri (Ac) - 06	Neu5Aca2-3(GalNAcb1-4)Galb-	14	-14	3	-45	0		-128	12	11	-43	14
glycolipid	304	GQ2-Sp - 03	Neu5Aca2-8Neu5Aca2-8Neu5Aca2-8Neu5Aca2-3[GalNAcb1-4]Galb1-4Glcb-Sp-BSA	14	-14	3	-37	0		-59	0	6	-40	0
carb-type 2	311	LacNAc (dimeric)-Sp - 06	(Galb1-4GlcNAcb1-3)2b-Sp-BSA	14	-17	237	-45	0		-57	-3	0	-37	-3
Blood Group B	92	2'F-B type 2-Sp - 07	Gala1-3[Fuca1-2]Galb1-4[Fuca1-3]GlcNAcb-Sp-BSA	11	-11	5	-34	0		-43	0	3	-31	5
Blood Group B	267	2'F-B type 2-Sp - 15	Gala1-3[Fuca1-2]Galb1-4[Fuca1-3]GlcNAcb-Sp-BSA	11	-11	0	-23	0		-54	0	3	-28	0
carb-Sia	292	3'Neu5Ac-LacNAc-Sp - 10	Neu5Aca2-3Galb1-4GlcNAcb-Sp-BSA	11	-6	3	-28	0		-54	0	3	-29	0
peptide-Gal	410	Ac-S-S(Gala)-S-G - 16	Ac-S-S$^{(Gal\ a)}$-S-G-Hex-OH	11	-9	25	-14	31		-9	6	46	0	22
non-human	638	Forssman Di - 05-HS	GalNAca1-3GalNAcb1-HSA	11	-9	0	-17	0		-8	0	0	-14	-3
glycolipid	295	GT2-Sp - 03	Neu5Aca2-8Neu5Aca2-8Neu5Aca2-3[GalNAcb1-4]Galb1-4Glcb-Sp-BSA	11	-16	5	-48	0		-80	3	6	-54	0
y-glycoprotein	368	hsp90	Heat Shock Protein 90	11	33	20	51	5		62	6	8	43	17
carb-type 2	307	LacNAc (dimeric)-Sp - 16	(Galb1-4GlcNAcb1-3)2b-Sp-BSA	11	-12	0	-39	0		-67	-3	3	-34	-3
carb-GalNAc	323	LDN-Sp - 05	GalNAcb1-4GlcNAcb-Sp-BSA	11	-3	5	-42	0		-51	0	6	-20	3
Lewis	239	LeC (dimeric)-Sp - 06	Galb1-3GlcNAcb1-3Galb1-3GlcNAcb-Sp-BSA	11	-9	3	-28	0		-43	3	2	-23	3
carb-Man	275	Man-a - 05	Man-a - BSA	11	0	0	-32	0		-33	3	0	-20	0

Table 3.3 (cont'd)

non-human PNAG	764	PNAG 14 (01110)	GlcNb1-6GlcNAcb1-6GlcNAcb1-6GlcNAcb1-6GlcNb1-	11	-5	5	-17	0			-26	0	3	-13	-3
non-human PNAG	767	PNAG 3 (00011)	GlcNb1-6GlcNb1-6GlcNb1-6GlcNAcb1-6GlcNAcb1-	11	-3	4	-11	17			-14	0	9	-12	3
non-human PNAG	758	PNAG 5 (00101)	GlcNb1-6GlcNb1-6GlcNAcb1-6GlcNb1-6GlcNAcb1-	11	-3	0	-6	0			-17	-3	3	-6	0
peptide-TF	725	TSSA(S-TF)TGHA(T-TF)PLPVTD-BSA	TF-5,10-MUC4- TSSA(S-TF)TGHA(T-TF)PLPVTD-BSA	11	-3	0	-20	0			-46	-3	0	96	-5
carb-Sia	327	3'Neu5Ac-LDN-Sp - 11	Neu5Aca2-3GalNAcb1-4GlcNAcb-Sp-BSA	9	-10	5	-26	0			-48	0	0	-20	0
peptide-Glc	393	Ac-A-S(Glcb)-S-G-Hex-18	Ac-A-S(Glcb)-S-G-Hex-BSA	9	-6	82	-23	0			-54	42	60	-20	0
peptide-TF	616	APF (asialo)		9	14	30	45	14			25	14	14	22	14
Blood Group B	64	BG-B2-03	Gala1-3(Fuca1-2)Galb1-4GlcNAcb1-linker-BSA	9	-17	14	-65	11			-78	3	14	-43	3
carb-Sia	298	CT/Sda-Sp - 05	Neu5Aca2-3[GalNAcb1-4]Galb1-4GlcNAcb-Sp-BSA; like GM2 but on glycoproteins	9	-23	5	-43	0			-71	0	3	-37	2
GAG-Hep	570	Hep-Octa-GT24-02	Glc(6S, Nac)a1-4GlcAb1-4Glc(6S, 3S, NS)a1-4IdoA(2S)a1-4Glc(6S, NS)a1-4IdoA(2S)a1-4Glc(6S, NS)a1-4GlcAb-Benzamide-	9	15	20	-15	0			-20	11	6	48	9
carb-type 1	278	LNT-Sp - 06	Galb1-3GlcNAcb1-3Galb1-4GlcNAcb-Sp-BSA	9	-20	0	-43	0			-50	5	0	-34	0
non-human	761	Manb1-4Glcb1 - 06	Manb1-4Glcb1 -BSA	9	-17	8	-32	0			28	3	3	-40	-3
non-human	10	Fuc-b - 22	Fuc-b - BSA	8	-12	60	-23	5			-46	3	15	-20	5
Blood Group B	333	2'F-B type 2-Sp - 03	Gala1-3[Fuca1-2]Galb1-4[Fuca1-3]GlcNAcb-Sp-BSA	6	-20	5	-37	0			-52	0	0	-37	5
carb-Sia	273	3'Neu5Ac-LacNAc-Sp - 05	Neu5Aca2-3Galb1-4GlcNAcb-Sp-BSA	6	-20	2	-26	0			-78	0	0	-31	0
carb-Sia	331	3'Neu5Ac-LDN-Sp - 05	Neu5Aca2-3GalNAcb1-4GlcNAcb-Sp-BSA	6	-14	3	-34	0			-57	-3	0	-34	-3
Blood Group A	334	A tetra type 2-Sp - 05	GalNAca1-3[Fuca1-2]Galb1-4GlcNAcb-Sp-BSA	6	-14	2	-43	0			-54	3	3	-37	-6
peptide-Core4	433	Ac-S-Core4(Thr)-S-G-07	Ac-Ser-Core4(Thr)-Ser-Gly-Hex-BSA	6	-17	22	-37	0			-71	3	0	-34	3
peptide-TF	464	Ac-S-TFa(Ser)-TFa(Ser)-G-03	Ac-Ser-Ser(Galb1-3GalNAca-)-Ser(Galb1-3GalNAca-)-Gly-Hex	6	-14	0	-31	0			-74	-1	3	-37	0
peptide-core 3	326	Ac-S-Thr(core 3)-S-G - 05	Ac-Ser-(GlcNAcb1-3GalNAca)Thr-Ser-Gly-Hex-BSA	6	-6	5	-51	0			-48	0	0	-23	0
peptide-F1a	341	Ac-S-Thr(F1a)-S-G - 18	AcSer-(Galb1-4GlcNAcb1-6GalNAca)Thr-Ser-Gly-Hex-BSA	6	-14	0	-32	0			-43	-3	0	-29	0
y-glycoprotein	354	Alpha-fetoprotein	alpha fetoprotein (AFP)-human, from cell culture	6	-3	5	-15	0			-31	-3	3	-8	0
peptide	449	AzHex-D-T-R-NH2-07	BSA--hexyl-D-T-R-amide	6	-6	0	-26	0			-48	0	6	-30	0
peptide-GalNAc Tyr	531	AzHex-G-Y(GalNAc-l	BSA-AzHex-G-Y(GalNAc-b)-A-amide	6	-9	5	-17	0			-45	3	3	-29	2
peptide	516	AzHex-G-Y-A-NH2 - 11	BSA-AzHex-G-Y-A-amide	6	0	0	-9	0			-1	0	0	3	6
peptide-GalNAc Tyr	527	AzHex-L-Y(GalNAc-a	BSA-AzHex-L-Y(GalNAc-a)-W-amide	6	-7	3	-10	0			-27	0	0	-11	8
peptide-GalNAc Tyr	520	AzHex-L-Y(GalNAc-a	BSA-AzHex-L-Y(GalNAc-a)-W-amide	6	-12	34	247	3			37	5	3	17	17
peptide-GalNAc Tyr	557	AzHex-L-Y(GalNAc-b	BSA-AzHex-L-Y(GalNAc-b)-W-amide	6	12	7	26	0			0	0	0	3	25
peptide-GalNAc Tyr	535	AzHex-L-Y(GalNAc-b	BSA-AzHex-L-Y(GalNAc-b)-W-amide	6	12	3	52	0			8	5	6	12	5
peptide-Tn	440	AzHex-PD-Tn(Thr)-RP-NH2-07	BSA--hexyl-PD-T(GalNAc-a)-RP-amide	6	-17	13	-40	0			-65	0	6	-45	0
peptide-Tn-Ser	425	AzHex-S-Tn(Ser)-V-G-HexOH-15	BSA-AzHex-S-Tn(Ser)-V-G-HexOH	6	6	3	-3	0			3	3	0	3	0
peptide	452	AzHex-V-T-S-A-P-D-T-R-P-A-P-G-S-NH2-07	BSA--hexyl-VTSAPDTRPAPGS-amide	6	-6	0	-13	0			-37	-3	6	-20	0
Blood Group B	276	B tetra type 1-Sp - 04	Gala1-3[Fuca1-2]Galb1-3GlcNAcb-Sp-BSA	6	-11	0	-29	0			-55	0	0	-34	-3
Blood Group B	335	B tetra type 2-Sp - 05	Gala1-3[Fuca1-2]Galb1-4GlcNAcb-Sp-BSA	6	-8	19	-33	0			-54	0	5	-29	0
non-human-aGal	20	Bdi -23	Gala1-3Gal– BSA	6	-6	8	-34	5			-51	3	9	-28	3
non-human-aGal	242	Bdi-g - 16	Gala1-3Galb– BSA	6	-5	3	-23	0			-34	0	0	-17	0
Blood Group A	67	BG-A1-04	GalNAca1-3(Fuca1-2)Galb1-3GlcNAcb1-linker-BSA	6	-9	8	-29	3			-46	0	12	-22	0
Blood Group A	69	BG-A2-04	GalNAca1-3(Fuca1-2)Galb1-4GlcNAcb1-linker-BSA	6	-20	8	-42	14			-71	-3	9	-43	0
Blood Group B	101	BG-B (Dextra) - 13	Gala1-3(Fuca1-2)Galb-BSA [BG-B] from Dextra	6	-6	5	-26	0			-47	3	6	-28	6
Blood Group B	339	BG-B5-04	Gala1-3(Fuca1-2)Galb1-3Galb1-linker-BSA	6	-17	3	-26	0			-40	0	0	-24	-3

Table 3.3 (cont'd)

Blood Group H	342	BG-H1-10	Fuca1-2Galb1-3GlcNAcb1-linker-BSA	6	-17	5	-37	0		-62	0	0	-43	-3
y-glycoprotein	357	BSM (deacetylated)	Deacetylated-Bovine submaxillary mucin	6	3	3	12	0		3	3	0	0	0
y-glycoprotein	356	BSM (ox)	periodate oxidized bovine submaxillary mucin	6	9	0	-13	0		-1	0	3	6	0
non-human	28	Cellobiose -13	Glcb1-4Glcb-BSA	6	-12	11	-45	4		-62	20	74	-39	3
non-human	618	Chitotriose - 07	GlcNAcb1-4GlcNAcb1-4GlcNAcb-	6	-37	0	-88	0		-134	3	6	-80	3
non-human	75	Chitotriose - 08	GlcNAcb1-4GlcNAcb1-4GlcNAcb-BSA	6	-8	0	-26	5		-48	0	6	-31	3
Lewis	329	DFLNHc, LacNAc/LeB - 08	Galb1-4GlcNAcb1-6[Fuca1-2Galb1-3(Fuca1-4)GlcNAcb1-3]Galb1-BSA	6	-3	4	-37	0		-41	-3	6	-17	0
Lewis	317	DFLNnH, LeX/LeX - 10	Galb1-4(Fuca1-3)GlcNAcb1-6[Galb1-4(Fuca1-3)GlcNAcb1-3]Galb1-BSA	6	-20	78	-40	0		-51	3	3	-23	12
glycolipid	90	DSLNT - 06	Neu5Aca2-3Galb1-3(Neu5Aca2-6)GlcNAcb1-3Galb1-BSA	6	-17	3	-43	0		-54	0	6	-40	0
y-glycoprotein	360	FABP	Fatty Acid Binding Protein	6	9	3	-3	0		20	3	0	23	0
y-glycoprotein	362	fetuin (asialo)	asialofetuin from calf serum- type I (Sigma A4781; Galb1-4GlcNAc, Galb1-3GlcNAc, Galb1-3GalNAc; mostly NA2 and NA3)	6	8	0	23	0		20	0	6	9	0
y-glycoprotein	365	Fetuin (ox)	periodate oxidized fetuin	6	9	0	0	0		11	-1	0	3	0
glycolipid-neutral	57	GA1 tri- 20	Galb1-3GalNAcb1-4Galb1-BSA (GA1tri or asialo-GM1)	6	-14	21	-34	17		-60	-3	0	-34	-3
glycolipid-neutral	22	GA1di -11	Galb1-3GalNAcb – HSA	6	-15	5	-40	3		-62	0	6	-31	3
carb-Gal	14	Gal-a- 24	Gal-a - BSA	6	-5	54	-31	3		-39	5	14	-28	3
carb-GalNAc	17	GalNAca1-6Galb - 22	GalNAca1-6Galb-BSA	6	0	5	-20	11		-29	5	12		0
carb-GalNAc	9	GalNAc-b - 21	GalNAc-b - BSA	6	-34	25	-36	5		-65	3	43	-46	8
glycolipid-neutral	81	Gb4 - 09	GalNAcb1-3Gala1-4Galb1-BSA (aka: P antigen)	6	-20	0	-34	5		-37	0	6	-22	3
glycolipid-neutral	620	Gb4 - 10-HSA	GalNAcβ1-3Galα1-4Galβ1-HSA (Gb4)	6	-3	3	-17	0		-26	0	0	-14	0
glycolipid	314	GD2-Sp - 04	Neu5Aca2-8Neu5Aca2-3[GalNAcb1-4]Galb1-4Glcb-Sp-BSA	6	-29	0	-51	0		-60	0	2	-34	0
y-glycoprotein	366	glycophorin (asialo)	asialo-glycophorin A (aGn)	6	-22	5	-36	5		-62	0	3	-46	0
glycolipid	507	GM2 tri (Gc) - 04	Neu5Gca2-3(GalNAcb1-4)Galb-	6	-26	0	-57	0		-139	5	6	-62	6
GAG-Hep	587	Hep-Hexa-GT23-04	Glc(6S, NS)a1-4GlcAb1-4Glc(6S, 3S, NS)a1-4IdoA(2S)a1-4Glc(6S, NS)a1-4GlcAb-Benzamide-	6	3	8	-11	5		-23	6	6	9	0
GAG-Hep	581	Hep-NAc-Hexa-05	GlcNAca1-4GlcAb1-4GlcNAca1-4GlcAb1-4GlcNAca1-4GlcAb-Benzamide- (Heparosan)	6	-28	0	-85	0		-116	3	-2	-82	3
GAG-Hep	585	Hep-Nona-GT14-02	GlcAb1-4GlcNSa1-4GlcAb1-4GlcNSa1-4GlcAb1-4Glc(6S, NS)a1-4GlcAb1-4Glc(6S, NS)a1-4GlcAb-Benzamide-	6	-20	0	-54	0		-85	5	0	-46	0
GAG-Hep	536	Hep-Octa-GT21-03	Glc(6S, NS)a1-4GlcAb1-4Glc(6S, NS)a1-4IdoA(2S)a1-4Glc(6S, NS)a1-4IdoA(2S)a1-4Glc(6S, NS)a1-4GlcAb-Benzamide-	6	0	11	-17	0		-12	0	3	20	8
carb-type 2	21	LacNAc - 22	Galb1-4GlcNAc – BSA	6	-14	5	-37	2		-48	-1	3	-31	3
carb-GalNAc	234	LDN-Sp - 14	GalNAcb1-4GlcNAcb-Sp-BSA	6	-15	3	-20	0		-57	0	6	-25	3
Lewis	37	LeA-Lac -18 (LNFP II)	Galb1-3[Fuca1-4)GlcNAcb1-3Galb1-4Glcb- BSA	6	-17	7	-43	0		-65	0	9	-43	3
Lewis	279	LeC-Sp - 07	Galb1-3GlcNAcb-Sp-BSA	6	-14	3	-26	0		-22	0	0		0
glycolipid-neutral	623	LNT - 17-HSA	Galβ1-3GlcNAcβ1-3Galβ-HSA (LNT)	6	-6	0	-26	0		-36	0	0	-17	0
carb-Man	439	Ma2Ma2Ma3(Ma3N	aMan(1-2)aMan(1-2)aMan(1-3)[aMan(1-3)aMan(1-6)]	6		181		11		-190	5	9		3
carb-Man	431	Ma2Ma3(Ma6)-08	aMan(1-2)aMan(1-3)[aMan(1-6)]	6	-31	11	-68	0		-122	-3	3	-68	6
carb-Man	469	Ma2Ma6(Ma2Ma3)I	aMan(1-2)aMan(1-6)[aMan(1-2)aMan(1-3)]aMan(1-6)	6	-32	3	-74	0		-142	0	0	-79	-3
carb-Man	494	Ma6(Ma3)Ma6-04	aMan(1-6)[aMan(1-3)]aMan(1-6)	6	-11	5	-49	0		-44	0	3	-17	0
N-linked	84	Man7D3 - 08	Mana1-2Mana1-6(Mana1-3)Mana1-6(Mana1-2Mana1-3)Manb1-4GlcNAc-BSA	6	-20	17	-42	2		-51	-3	6	-34	0
N-linked	167	NGA4 - 06	GlcNAcb1-2(GlcNAcb1-6)Mana1-6[GlcNAcb1-2(GlcNAcb1-4)Mana1-3]Manb1-4GlcNAc -BSA	6	-20	0	-46	0		-82	3	5	-46	-3
y-glycoprotein	374	ovalbumin	ovalbumin (Sigma A5503; 56% Man5+Man6)	6	3	5	19	5		20	0	0	11	4
y-glycoprotein	375	Ovalbumin (ox)	periodate oxidized ovalbumin	6	17	8	26	2		76	3	6	20	3
y-glycoprotein	376	PSA	Prostate Specific Antigen (PSA); human seminal fluid	6	6	3	9	37		10	0	3	14	0

Table 3.3 (cont'd)

y-glycoprotein	364	PSM A neg	porcine submaxillary mucin (A-)	6	0	0	-6	0		6	3	-3	4	0
glycolipid	614	SSEA-4-penta-05	Neu5Aca2-3Galb1-3GlcNAcb1-3Gala1-4Galb1-	6	-14	5	-83	0		-105	-3	0	-67	2
glycolipid	617	SSEA-4-penta-11	Neu5Aca2-3Galb1-3GlcNAcb1-3Gala1-4Galb1-	6	-12	0	-40	0		-73	-3	0	-51	-3
glycolipid	231	SSEA-4-Sp - 05	Neu5Aca2-3Galb1-3GalNAcb1-3Gala1-4Galb1-4Glcb-Sp-BSA	6	-17	5	-37	5		-77	-3	3	-51	3
y-glycoprotein	377	Tgl	Thyroglobulin -human	6	0	0	26	5		17	6	6	3	5
glycolipid	559	3'Kdn-Gb5 - 04	Kdna2-3Galb1-3GalNAcb1-3Gala1-4Galb-	6	-28	0	-85	0		-142	0	3	-74	0
carb-Sia	272	3'KDN-LacNAc-Sp - 12	KDNa2-3Galb1-4GlcNAcb-Sp-BSA	6	-5	3	-17	0		-29	0	0	-14	6
Blood Group A	277	A tetra type 2-Sp - 07	GalNAca1-3[Fuca1-2]Galb1-4GlcNAcb-Sp-BSA	6	-34	0	-59	0		-94	0	6	-48	0
y-glycoprotein	353	Alpha-1-acid glycoprotein	alpha1 Acid Glycoprotein-purified from human serum (Sigma G9985)	6	3	0	-11	0		-9	3	3	6	0
glycolipid	330	GD2-Sp - 10	Neu5Aca2-8Neu5Aca2-3[GalNAcb1-4]Galb1-4Glcb-Sp-BSA	6	-8	3	-14	0		-23	0	0	-14	0
Lewis	532	3'Neu5Ac-LeX-Gal - 04	Neu5Aca2-3Galb1-4(Fuca1-3)GlcNAcb1-3Galb-	5	-26	0	-57	0		-92	-3	0	-43	0
glycolipid-neutral	612	Gb5 tetra - 07	Galb1-3GalNAcb1-3Gala1-4Galb-	5	-31	0	-71	0		-102	-5	0	-68	3
GAG-Hep	594	Hep-Octa-GT19-03	GlcNAca1-4GlcAb1-4GlcNSa1-4IdoA(2S)a1-4GlcNSa1-4IdoA(2S)a1-4GlcNSa1-4GlcAb-Benzamide-	5	-9	0	-28	3		18	0	3	-12	6
glycolipid-neutral	578	iGb4 tri - 05	GalNAcb1-3Gala1-3Galb-	5	-20	0	-57	0		-85	3	0	-46	0
Blood Group A	253	2'F-A type 2-Sp - 05	GalNAca1-3[Fuca1-2]Galb1-4[Fuca1-3]GlcNAcb-Sp-BSA	3	-9	3	-29	0		-60	0	6	-25	0
glycolipid	528	3'Kdn-LNT - 04	Kdna2-3Galb1-3GlcNAcb1-3Galb-	3	-11	0	-37	0		-89	0	2	-25	6
carb-Sia	232	3'Neu5Ac(9Ac)-LacNAc-Sp - 10	Neu5Ac(9Ac)a2-3Galb1-4GlcNAcb-Sp-BSA	3	-11	0	-34	0		-46	0	3	-28	0
carb-Sia	562	3'Neu5Ac8Me-Galb- 04	Neu5Ac8Mea2-3Galb-	3	-43	0	-99	0		-153	-3	3	-94	0
glycolipid	493	3'-Neu5Ac-Gb3 - 04	Siaa2-3Gala1-4Galb1-	3	-6	0	-34	0		-54	3	0	-29	3
glycolipid	472	3'-Neu5Ac-Gb3-08	Siaa2-3Gala1-4Galb-	3	-34	0	-85	0		-142	0	-3	-65	0
glycolipid	654	3'Neu5Ac-Gb5	Neu5Aca2-3Galb1-3GlcNAcb1-3Gala1-4Galb1-	3	-8	0	-23	0		-45	2	0	-26	6
glycolipid	657	3'Neu5Gc-Gb5	Neu5Gca2-3Galb1-3GlcNAcb1-3Gala1-4Galb1-	3	-17	0	-22	0		-75	6	0	-28	0
carb-Sia	256	3'Neu5Gc-LacNAc-Sp - 06	Neu5Gca2-3Galb1-4GlcNAcb-Sp-BSA	3	-16	3	-34	0		-52	0	6	-31	0
glycolipid	540	3'Neu5Gc-LNT - 06	Neu5Gca2-3Galb1-3GlcNAcb1-3Galb-	3	-6	0	-25	0		-83	0	0	-37	0
carb-Sia	47	6'Neu5Ac-Lac	Neu5Aca2-6Galb1-4Glc-APD-HSA	3	-12	5	-48	167		-68	0	9	-37	2
Lewis	211	6'-sulpho-LeA - 16	6-SO3-Galb1-3[Fuca1-4)GlcNAc-BSA	3	-17	3	-34	0		-45	0	0	-31	0
Blood Group A	265	A tetra type 1-Sp - 05	GalNAca1-3[Fuca1-2]Galb1-3GlcNAcb-Sp-BSA	3	-17	0	-31	0		-57	5	3	-26	0
Blood Group A	243	A tetra type 1-Sp - 15	GalNAca1-3[Fuca1-2]Galb1-3GlcNAcb-Sp-BSA	3	0	3	0	0		-9	0	6	6	-3
N-linked	588	A2 (a2-3) - 01.4	Neu5Aca2-3Galb1-4GlcNAcb1-2Mana1-6(Neu5Aca2-3Galb1-4GlcNAcb1-2Mana1-3)Manb1-4GlcNAcb1-	3	-9	0	-27	0		-46	0	0	-9	0
peptide-Fuc	386	Ac-G-S(Fuca)-S-G-Hex-05	Ac-G-S(Fuca)-S-G-Hex-BSA	3	-9	0	-20	0		-25	0	3	-12	0
peptide-Xyl	389	Ac-G-S(Xylb)-G-G-Hex-21	Ac-Gly-Ser(Xylb)-Gly-Gly-Hex-BSA	3	-5	3	-23	0		-25	3	3	-12	0
peptide	417	Ac-GSTAP-G-05	Ac-G-S-T-A-P-G-	3	-17	0	-28	0		-51	0	3	-26	0
peptide-Man	408	Ac-P-T(Mana)-A-G - 07	Ac-Pro-Thr$^{(Man\ a)}$-Ala-Gly-Hex-BSA	3	-6	0	-15	0		-35	0	3	-11	0
Peptide-core-5	383	Ac-Ser(core 5)-S-G-05	Ac-(GalNAca1-3GalNAca)Ser-Ser-Gly-Hex-BSA	3	-15	0	-28	0		-34	2	0	-23	0
peptide-Gal	626	Ac-S-S(Gala)-S-G - 06	Ac-S-S$^{(Gal\ a)}$-S-G-Hex-OH	3	-9	0	-41	0		-44	0	0	-34	0
peptide-TF	123	Ac-S-TF(Ser)-S-G - 04	Ac-Ser-(Galb1-3GalNAca)Ser-Ser-Gly-Hex-BSA	3	-6	0	-31	0		-49	0	6	-20	3
peptide-core 2	379	Ac-S-Thr(core 2)-S-G - 12	Ac-Ser-(Galb1-3(GlcNAcb1-6)GalNAca)Thr-Ser-Gly-Hex-BSA	3	-17	5	-35	0		-68	0	-6	-39	0
peptide-Tn-Ser	120	Ac-S-Tn(Ser)-S-G - 04	AcSer-(GalNAca)Ser-Ser-Gly-Hex-BSA	3	-11	3	-28	0		-60	0	6	-29	0
peptide-Tn-Ser	126	Ac-S-Tn(Ser)-S-G - 33	Ac-Ser-(GalNAca)Ser-Ser-Gly-Hex-BSA	3	-15	11	-23	5		-40	0	12	-26	0
peptide-Tn	163	Ac-S-Tn(Thr)-A-G - 04	Ac-Ser-(GalNAca)Thr-Ala-Gly-Hex-BSA (muc1)	3	-14	5	-40	2		-59	3	3	-31	6
peptide-Tn	152	Ac-S-Tn(Thr)-G-G - 19	Ac-Ser-(GalNAca)Thr-Gly-Gly-Hex-BSA (muc4)	3	-6	5	-19	0		-28	0	6	-17	0
peptide-Tn	122	Ac-S-Tn(Thr)-S-G - 04	Ac-Ser-(GalNAca)Thr-Ser-Gly-Hex-BSA	3	-3	3	-31	3		-40	-3	21	-20	3
peptide-Tn	16	Ac-Tn(Thr)-G - 21	Ac(GalNAca)Thr-Gly-Hex-BSA	3	-29	17	-42	5		-68	3	34	-47	3
peptide-Tn	160	Ac-T-Tn(Thr)-P-G - 04	Ac-Thr-(GalNAca)Thr-Pro-Gly-Hex-BSA (muc2,6,7)	3	-11	5	-26	0		-34	5	0	-14	3
Blood Group A	18	Adi - 17	GalNAca1-3Galb-BSA	3	-17	8	-34	5		-40	0	6	-26	0
y-glycoprotein	589	alpha 1 acid glycopr	Alpha-1-Acid Glycoprotein, Oroscomucoid, from Humar	3	-3	0	-9	0		-9	0	0	-6	0
non-human	750	Arafa1-3(Arafa1-2)X	Arafa1-3(Arafa1-2)Xylb1 - BSA	3		23		0		-102	6	0		9
peptide	513	AzHex-L-Y-W-NH2 -	BSA-AzHex-L-Y-W-amide	3	-6	0	-22	0		-40	5	3	-20	6
peptide-Tn-Ser	427	AzHex-S-Tn(Ser)-V-G-HexNH2-16	BSA-AzHex-S-Tn(Ser)-V-G-HexNH2	3	-6	0	-11	0		-23	0	0	-12	0
Blood Group A	70	BG-A2-16	GalNAca1-3(Fuca1-2)Galb1-4GlcNAcb1-linker-BSA	3	-20	5	-51	0		-71	0	6	-48	0

Table 3.3 (cont'd)

Blood Group B	72	BG-B1-15	Gala1-3(Fuca1-2)Galb1-3GlcNAcb1-linker-BSA	3	-34	5	-54	5		-97	0	3	-79	0
Blood Group B	347	BG-B6- 03	Gala1-3(Fuca1-2)Galb1-4Glcb1-linker-BSA	3	-14	0	-40	0		-51	0	-3	-17	0
Blood group H	586	BG-H di	Fuca1-2Galb-BSA	3	-9	0	-29	0		-40	0	6	-20	0
Blood Group H	100	BG-H3- 04	Fuca1-2Galb1-3GalNAcα1-linker-BSA	3	-17	5	-37	0		-48	0	6	-28	0
Blood Group H	140	BG-H3- 14	Fuca1-2Galb1-3GalNAcα1-linker-BSA	3	-12	3	-34	0		-56	0	10	-25	0
Blood Group H	345	BG-H5-04	Fuca1-2Galb1-3Galb1-linker-BSA	3	-11	3	-25	0		-34	3	0	-20	0
Blood Group H	346	BG-H5-19	Fuca1-2Galb1-3Galb1-linker-BSA	3	-17	5	-40	0		-51	0	6	-25	-6
non-human	669	cellotetraose - 05	Glcb1-4Glcb1-4Glcb1-4Glcb1-	3	-17	5	-51	0		-60	5	3	-29	8
non-human	577	Chitotriose - 04	GlcNAcb1-4GlcNAcb1-4GlcNAcb-	3	-28	0	-76	0		-148	-3	0	-78	3
carb-Sia	247	CT/Sda-Sp - 13	Neu5Aca2-3[GalNAcb1-4]Galb1-4GlcNAcb-Sp-BSA; like GM2 but on glycoproteins	3	-17	0	-37	0		-59	0	3	-29	0
glycolipid	496	di-sialyl type 1 - 04	NeuAcα2-8Neu5Acα2-3Galβ1-3GlcNAcβ1-3Galb-	3	-11	0	-37	0		-65	0	-3	-32	-3
y-glycoprotein	378	FABP-3	Fatty Acid Binding Protein (Heart type)	3	2	0	0	0		22	3	0	12	0
non-human	119	Forssman Di - 04	GalNAca1-3GalNAcb1-BSA	3	-9	3	-52	0		-77	0	6	-44	3
non-human	108	Forssman Di - 21	GalNAca1-3GalNAcb1-BSA	3	-14	0	-34	0		-54	0	3	-29	-3
non-human	639	Forssman Di - 22-HS	GalNAca1-3GalNAcb1-HSA	3	-6	0	-9	0		-22	3	0	-5	0
carb-Fuc	11	Fuc-a - 22	Fuc-a - BSA	3	-6	11	-31	5		-45	0	9	-26	0
non-human-aGal	76	Gal3- 07	Gala1-3Galb1-4Gala-BSA	3	-3	6	-23	0		-36	5	0	-7	0
non-human	208	Gala1-2Gal - 13	Gala1-2Gal-BSA	3	-17	6	-31	0		-46	5	9	-31	0
glycolipid-neutral	510	Gala1-4Galb-	Gala1-4Galb-	3	-23	0	-43	0		-88	5	-3	-31	0
non-human	25	Galb1-6Man-a - 13	Galb1-6Man-a - BSA	3	0	8	-12	0		-30	0	9	3	3
non-human-aGal	605	Galili Hexa-13	Gala1-3(Galb1-4GlcNAcb1-3)$_2$Galb-	3	-15	0	-32	0		-51	0	0	-40	-6
non-human-aGal	192	Galilli - 21	Gala1-3Galb1-4Glc-BSA	3	-10	5	-34	3		-43	5	6	-15	0
glycolipid-neutral	42	Gb3- 13	Gala1-4Galb1-4Glc-HSA [aka: Pk or CD77]	3	-17	5	-43	0		-49	0	3	-23	0
glycolipid-neutral	87	Gb4 tetra (P1 tetra)-Sp - 06	GalNAcb1-3Gala1-4Galb1-4GlcNAcb-Sp-BSA	3	-20	5	-40	3		-54	0	6	-37	3
glycolipid related	600	Gb5 analogue type 2-04	Galb1-4GlcNAcb1-3Gala1-4Galb-	3	-6	0	-11	0		-12	0	0	-3	0
glycolipid	229	GD1a-Sp - 05	Neu5Aca2-3[Neu5Aca2-3Galb1-3GalNAcb1-4]Galb1-4Glcb-Sp-BSA	3	-14	3	-46	0		-74	0	3	-40	0
glycolipid	537	GD2 tetra (Kdn/Ac) - 03	Kdna2-8Neu5Aca2-3(GalNAcb1-4)Galb-	3	-5	0	-23	0		-37	0	0	-14	0
glycolipid	455	GD$_3$(9-OAc)-b-propy	Neu5Ac(9-OAc)a2-8Neu5Aca2-3Galb1-4Glcb-propyl-BSA	3	-14	0	-22	0		-63	0	3	-31	0
glycolipid	457	GD$_3$(Gc-Ac)-b-propy	Neu5Gca2-8Neu5Aca2-3Galb1-4Glcb-propyl-BSA	3	-3	0	-37	0		-57	0	0	-31	0
carb-GlcNAc	132	GlcNAca1-4Galb - 03	GlcNAca1-4Galb-BSA	3	-8	3	-35	0		-43	0	6	-23	0
N-linked	197	GlcNAc-Man3 - 02	Mana1-6(GlcNAcb1-2Mana1-3)Manb1-4GlcNAcb-BSA	3	-3	9	-31	0		-51	5	6	-22	5
N-linked	199	GlcNAc-Man5 - 03	Mana1-6(Mana1-3)Mana1-6(GlcNAcb1-2Mana1-3)Manb1-4GlcNAcb-BSA	3	-12	4	-34	0		-37	5	3	-17	3
Blood Group H	110	Globo H - 03	Fuca1-2Galb1-3GalNAcb1-3Gala1-4Galb1-BSA	3	-9	3	-29	0		-48	0	3	-20	0
Blood Group H related	611	Globo H analogue type 2-10	Fuca1-2Galb1-4GlcNAcb1-3Gala1-4Galb-	3	-12	85	-57	0		-65	-3	0	-40	0
y-glycoprotein	367	Glycophorin A	Glycophorin A (Gn; Sigma G6017)	3	0	0	-8	0		-26	0	0	-9	0
glycolipid	467	GM1b-13	Siaa2-3Galb1-3GalNAcb1-4Galb-	3	-17	0	-37	0		-63	0	5	-43	0
glycolipid	46	GM3 - 12	Neu5Aca2-3Galb1-4Glc-APD-HSA	3	-17	9	-47	0		-78	0	8	-45	3
glycolipid	250	GM3(Gc)-Sp - 14	Neu5Gca2-3Galb1-4Glcb-Sp-BSA	3	-17	0	-49	0		-63	0	3	-27	0
glycolipid	434	GT1a - 04	Neu5Aca2-8Neu5Aca2-3Galb1-3GalNAcb1-4(Neu5Aca2-3)Galb-	3	-20	0	-35	0		-65	-1	0	-45	6
peptide-TF	188	GTSSASTGHA-TF(Thr)-PLPVTD	BSA-PEG7-Gly-Thr-Ser-Ser-Ala-Ser-Thr-Gly-His-Ala-(Galb1-3GalNAca)Thr-Pro-Leu-Pro-Val-Thr-Asp	3	-6	5	-34	0		-35	3	-3	-17	0

Table 3.3 (cont'd)

GAG-Hep	565	Hep-NAc-Nona-04	GlcAb1-4GlcNAca1-4GlcAb1-4GlcNAca1-4GlcAb1-4GlcNAca1-4GlcAb1-4GlcNAca1-4GlcAb-Benzamide-(Heparosan)	3	-23	0	-56	0		-65	0	0	-40	0
GAG-Hep	584	Hep-NS-Hepta-03	GlcAb1-4GlcNSa1-4GlcAb1-4GlcNSa1-4GlcAb1-4GlcNSa1-4GlcAb-Benzamide-	3	-14	0	-37	0		-43	0	0	-32	-3
GAG-Hep	574	Hep-NS-Penta-05	GlcAb1-4GlcNSa1-4GlcAb1-4GlcNSa1-4GlcAb-Benzamide-	3	-17	0	-43	0		-55	-3	0	-28	2
GAG-Hep	582	Hep-Octa-GT17-02	GlcNSa1-4GlcAb1-4GlcNSa1-4GlcAb1-4GlcNSa1-4IdoA(2S)a1-4GlcNSa1-4GlcAb-Benzamide-	3	-11	0	-32	0		-40	0	0	-19	0
GAG-Hep	590	Hep-Octa-GT18-02	GlcNSa1-4GlcAb1-4GlcNSa1-4IdoA(2S)a1-4GlcNSa1-4IdoA(2S)a1-4GlcNSa1-4GlcAb-Benzamide-	3	-8	0	-27	0		-31	0	0	-21	3
Carb-HNK-1	598	HNK 1 precursor-05	GlcAcb1-3Galb-	3	-12	0	-26	0		-37	0	0	-26	0
Carb-HNK-1	606	HNK 1 precursor-18	GlcAcb1-3Galb-	3	-14	0	-31	0		-40	0	0	-26	6
N-linked	214	Hybrid-M5N4B - 03	GlcNAcb1-2Mana1-3[Mana1-3(Mana1-6)Mana1-6](GlcNAcb1-4)Manb1-4GlcNAcb1-BSA	3	-17	0	-43	0		-57	3	3	-29	-3
glycolipid-neutral	420	iGb5-06	Galb1-3GalNAcb1-3Gala1-3Galb-	3	-20	0	-37	3		-71	0	3	-43	0
glycolipid-neutral	23	Lac - 33	Galb1-4Glcb – BSA	3	-14	8	-43	0		-57	-3	6	-37	0
glycolipid-neutral	240	Lac-C5 - 05	Galb1-4Glcb – BSA	3	-6	0	-20	0		-49	5	3	-23	0
carb-type 2	238	LacNAc-Sp - 15	Galb1-4GlcNAcb-Sp-BSA	3	-3	5	-28	0		-43	4	5	-17	0
Lewis	40	LeX-Lac (monomeric, LNFIII)	Galb1-4[Fuca1-3)GlcNAcb1-3Galb1-4Glc-APD-HSA ; SSEA-1; CD-15; Glycotech	3	-15	5	-37	0		-17	0	5	-14	3
Lewis	621	LeY -08 (repeat)	Fuca1-2Galb1-4[Fuca1-3)GlcNAc –HSA	3	-20	5	-45	0		-74	0	0	-31	0
glycolipid-neutral	579	LNT tri - 10	Galb1-3GlcNAcb1-3Galb-	3	-11	0	-34	0		-54	3	0	-31	0
glycolipid	54	LSTa - 10	Neu5Aca2-3Galb1-3GlcNAcb1-3Galb1-BSA	3	6	11	-8	19		-35	0	0	-19	0
carb-Man	484	Ma2Ma2-06	aMan(1-2)aMan(1-2)	3	-9	3	-23	0		-26	5	0	-15	6
carb-Man	491	Ma2Ma2-11	aMan(1-2)aMan(1-2)	3	-17	0	-53	0		-88	0	5	-48	0
carb-Man	454	Ma2Ma2Ma3(Ma6M	aMan(1-2)aMan(1-2)aMan(1-3)[aMan(1-6)aMan(1-6)]	3	-34	3	-85	0		-142	0	0	-77	0
carb-Man	443	Ma2Ma3(Ma6)-04	aMan(1-2)aMan(1-3)[aMan(1-6)]	3	-12	0	-37	0		-71	0	6	-34	3
carb-Man	478	Ma2Ma3-04	aMan(1-2)aMan(1-3)	3	-11	0	-25	0		-60	-3	-3	-29	6
carb-Man	441	Ma2Ma3Ma6(Ma3)-	aMan(1-2)aMan(1-3)aMan(1-6)[aMan(1-3)]	3	-14	0	-29	0		-51	0	-3	-27	3
carb-Man	500	Ma2Ma3Ma6-03	aMan(1-2)aMan(1-3)aMan(1-6)	3	-20	0	-54	0		-68	0	0	-45	0
carb-Man	460	Ma2Ma6(Ma3)Ma6-	aMan(1-2)aMan(1-6)[aMan(1-3)]aMan(1-6)	3	-22	0	-71	0		-116	3	-3	-65	0
carb-Man	446	Ma2Ma6-16	aMan(1-2)aMan(1-6)	3	-28	3	-82	0		-94	5	6	-57	3
carb-Man	463	Ma2Ma6Ma6-06	aMan(1-2)aMan(1-6)aMan(1-6)	3	-22	0	-54	0		-96	0	-3	-54	6
carb-Man	495	Ma3(Ma6)-07	aMan(1-3)[aMan(1-6)]	3	-20	0	-54	0		-153	0	3	-74	3
carb-Man	492	Ma3Ma6(Ma3)-04	aMan(1-3)aMan(1-6)[aMan(1-3)]	3	-15	6	-34	0		-60	0	-3	-29	3
carb-Man	497	Ma3Ma6(Ma3)-11	aMan(1-3)aMan(1-6)[aMan(1-3)]	3	-12	0	-15	0		-29	0	0	-17	0
carb-Glc	687	maltohexaose - 04	Glca1-4Glca1-4Glca1-4Glca1-4Glca1-4Glca1-	3	-8	0	-20	0		-26	0		-17	
carb-Glc	104	Maltopentaose - 11	Glca1-4Glca1-4Glca1-4Glca1-4Glca-BSA	3	-6	16	-29	0		-57	8	3	-26	6
N-linked	78	Man3 - 06	Mana1-6(Mana1-3)Manb1-4GlcNAc -BSA	3	-17	0	-45	3		-73	-5	6	-34	5
N-linked	508	Man3a - 07	Mana1-2Mana1-3Manb1-4GlcNAcb-	3	-22	5	-54	0		-130	0	0	-56	-6
N-linked	86	Man5 - 06	Mana1-6(Mana1-3)Mana1-6(Mana1-3)Manb1-4GlcNAcb-	3	-6	8	-68	0		-77	0	3	-34	3
N-linked	88	Man6 - II - 05	Mana1-2Mana1-3Mana1-6(Mana1-2Mana1-3)Manb1-BSA	3	-23	5	-68	0		-79	3	3	-32	0
N-linked	95	Man7D1 - 10	Mana1-6(Mana1-3)Mana1-6(Mana1-2Mana1-2Mana1-3)Manb1-4GlcNAc-BSA	3	3	3	-26	0		-40	0	3	-20	5
N-linked	506	Man7D2 - 05	Mana1-6(Mana1-2Mana1-3)Mana1-6(Mana1-2Mana1-3)Manb1-4GlcNAcb-	3	-17	0	-40	0		-43	-3	0	-31	-3
N-linked	615	Man7D3 - 06	Mana1-2Mana1-6(Mana1-3)Mana1-6(Mana1-2Mana1-3)Manb1-4GlcNAcb-	3	-26	0	-52	0		-94	0	3	-57	-3
carb-Man	26	Mana1-6Man-a - 15	Mana1-6Man-a - BSA	3	9	4	-15	3		-14	0	3	-3	0
peptide-Tn	396	Muc1-Tn8	BSA--hexyl-G-V-T-S-A-P-D-T(GalNAc-a)-R-P-A-P-G-S-T-A-P-P-A-amide	3	0	3	-23	0		-43	5	3	-20	0

Table 3.3 (cont'd)

N-linked	170	NA4 - 05	Galb1-4GlcNAcb1-2(Galb1-4GlcNAcb1-6)Mana1-6[Galb1-4GlcNAcb1-2(Galb1-4GlcNAcb1-4)Mana1-3]Manb1-4GlcNAc -BSA	3	-19	3	-54	0		-61	3	-3	-37	0
N-linked	168	NGA4(B)2 - 04	GlcNAcb1-2(GlcNAcb1-4)(GlcNAcb1-6)Mana1-6[GlcNAcb1-2Mana1-3](GlcNAcb1-4)Manb1-4GlcNAc -BSA	3	-22	5	-39	5		-60	3	6	-34	14
N-linked	169	NGA5B - 02	GlcNAcb1-2(GlcNAcb1-4)(GlcNAcb1-6)Mana1-6[GlcNAcb1-2(GlcNAcb1-4)Mana1-3](GlcNAcb1-4)Manb1-4GlcNAc -BSA	3	-15	5	-28	0		-34	3	6	-23	0
non-human PNAG	744	PNAG 22 (10110)	GlcNAcb1-6GlcNb1-6GlcNAcb1-6GlcNAcb1-6GlcNb1-	3	-14	3	-40	0		-80	3	3	-51	5
glycolipid	241	SSEA-4-Sp - 12	Neu5Aca2-3Galb1-3GalNAcb1-3Gala1-4Galb1-4Glcb-Sp-BSA	3	0	0	-14	5		-33	0	6	-17	0
glycolipid	301	GD3-Sp - 08	Neu5Aca2-8Neu5Aca2-3Galb1-4Glcb-Sp-BSA	3	-25	3	-31	0		-49	0	0	-26	0
GAG-Hep	526	Hep-NS-Hexa-04	GlcNSa1-4GlcAb1-4GlcNSa1-4GlcAb1-4GlcNSa1-4GlcAb-Benzamide-	3	-11	0	-39	0		-62	3	6	-32	3
Lewis	552	3'Neu5Ac8Me-LeX-Gal - 04	Neu5Ac8Mea2-3Galb1-4(Fuca1-3)GlcNAcb1-3Galb-	2	-25	0	-66	0		-99	-1	0	-62	-3
glycolipid	564	3'Neu5Ac8Me-LNT - 04	Neu5Ac8Mea2-3Galb1-3GlcNAcb1-3Galb-	2	-28	0	-57	0		-82	0	0	-63	0
carb-Sia	249	6'Neu5Ac-LacNAc (dimeric)-Sp - 13	Neu5Aca2-6[Galb1-4GlcNAcb1-3)2b-Sp-BSA	2	-14	0	-29	0		-48	0	6	-22	-3
peptide-Glc	392	Ac-A-S(Glcb)-S-G-Hex-05	Ac-A-S(Glcb)-S-G-Hex-BSA	2	-6	3	-15	0		-29	5	6	-11	0
peptide-Tn-Ser	79	Ac-S-Tn(Ser)-S-G - 22	Ac-Ser-(GalNAca)Ser-Ser-Gly-Hex-BSA	2	-20	17	-40	5		-57	3	23	-37	0
peptide-Tn	161	Ac-S-Tn(Thr)-G-G - 03	Ac-Ser-(GalNAca)Thr-Gly-Gly-Hex-BSA (muc4)	2	-9	3	-29	0		-17	3	6	-8	0
Blood Group B	348	BG-B6-15	Gala1-3(Fuca1-2)Galb1-4Glcb1-linker-BSA	2	-23	14	-37	0		-71	0	3	-31	0
Blood Group H	98	BG-H4- 04	Fuca1-2Galb1-3GalNAcb1-linker-BSA	2	-6	0	-37	0		-37	-1	3	-17	3
glycolipid related	597	Gb5 analogue type 1-06	Galb1-3GlcNAcb1-3Gala1-4Galb-	2	-3	0	-10	0		-15	0	0	-9	0
glycolipid	459	GD_3(Gc-Gc)-b-propyl	Neu5Gca2-8Neu5Gca2-3Galb1-4Glcb-propyl-BSA	2	-15	0	-37	0		-62	3	0	-26	0
carb-Glc	6	Glc-a - 22	Glc-a - BSA	2	-20	4	-33	0			0	0	-38	0
glycolipid	461	GM1b-05	Siaa2-3Galb1-3GalNAcb1-4Galb-	2	-17	0	-63	0		-85	0	0	-57	3
GAG-Hep	530	Hep-Nona-GT15-04	GlcAb1-4GlcNSa1-4GlcAb1-4Glc(6S, NS)a1-4GlcAb1-4Glc(6S, NS)a1-4GlcAb1-4Glc(6S, NS)a1-4GlcAb-Benzamide-	2	-12	5	-23	0		-54	3	0	-12	3
carb-type 2	227	LacNAc-Sp - 06	Galb1-4GlcNAcb-Sp-BSA	2	-11	5	-28	0		-44	0	-2	-28	3
N-linked	166	NGA3 - 01	GlcNAcb1-2Mana1-6[GlcNAcb1-2(GlcNAcb1-4)Mana1-3]Manb1-4GlcNAc -BSA	2	-17	5	-37	0		-45	5	6	-34	0
y-glycoprotein	371	OSM (ox)	periodate oxidized ovine submaxillary mucin	2	0	0	-11	0		-11	-3	0	-6	6
non-human	810	Xylb5 - 17	Xylb1-4Xylb1-4Xylb1-4Xylb1-4Xylb1-BSA	2	-3	22	-3	0		621	0	3	-12	6
non-human	538	KDOa2-4KDOa - 09	KDOa2-4KDOa-APTE-BSA	0	-14	0	-25	0		-51	-3	0	-24	0
carb-Sia	517	3'Kdn-Galb- 03	Kdna2-3Galb-	0	-12	3	-34	0		-65	0	-3	-30	6
glycolipid	555	3'Kdn-iGb5 - 04	Kdna2-3Galb1-3GalNAcb1-3Gala1-3Galb-	0	-20	0	-47	0		-68	0	0	-34	0
carb-Sia	251	3'KDN-LacNAc-Sp - 05	KDNa2-3Galb1-4GlcNAcb-Sp-BSA	0	-20	5	-23	0		-27	5	6	-23	6
Lewis	533	3'Kdn-LeX-Gal - 03	Kdna2-3Galb1-4(Fuca1-3)GlcNAcb1-3Galb-	0	-34	0	-85	0		-88	0	0	-51	0
glycolipid	551	3'Kdn-LNnT - 05	Kdna2-3Galb1-4GlcNAcb1-3Galb-	0	-20	0	-56	0		-74	0	0	-49	0
carb-Sia	222	3'Neu5Ac(9Ac)-LacNAc-Sp - 04	Neu5Ac(9Ac)a2-3Galb1-4GlcNAcb-Sp-BSA	0	-23	5	-40	0		-51	-3	3	-34	0
carb-Sia	195	3'Neu5Ac-3-FL - 07	Neu5Aca2-3Galb1-4(Fuca1-3)Glc -BSA	0	-17	5	-32	0		-48	0	-2	-29	-2
glycolipid	660	3'Neu5Ac-iGb5	Neu5Aca2-3Galb1-3GlcNAcb1-3Gala1-3Galb1-	0	-6	2	-14	0		-30	0	0	-15	0
carb-Sia	33	3'Neu5Ac-LacNAc - 19	Neu5Aca2-3Galb1-4GlcNAc – BSA	0	-17	5	-43	3		-51	-3	6	-37	0
Lewis	127	3'Neu5Ac-LeX (Sialyl LeX) - ??	Neu5Aca2-3Galb1-4[Fuca1-3)GlcNAc – BSA	0	-23	4	-54	0		-88	0	0	-49	0
Lewis	41	3'Neu5Ac-LeX (Sialyl LeX) - 09	Neu5Aca2-3Galb1-4[Fuca1-3)GlcNAc – BSA	0	-9	4	-37	0		-39	0	6	-11	-3
Lewis	643	3'Neu5Ac-LeX (Sialyl LeX) -APD-HAS	Neu5Aca2-3Galb1-4[Fuca1-3)GlcNAc –APD-HSA	0	-8	2	-20	0		-51	0	0	-26	3
carb-Sia	201	3'Neu5Ac-LNnT - 09	Neu5Aca2-3Galb1-4GlcNAcb1-3Galb1-APD-HSA	0	-15	3	-43	0		-46	0	0	-32	3
glycolipid	561	3'Neu5Ac-LNT - 08	Neu5Aca2-3Galb1-3GlcNAcb1-3Galb-	0	-26	3	-71	0		-128	0	-2	-74	0
carb-Sia	563	3'Neu5Gc-Galb- 06	Neu5Gca2-3Galb-	0	-34	0	-60	0		-119	0	0	-74	-3

Table 3.3 (cont'd)

glycolipid	663	3'Neu5Gc-iGb5	Neu5Gca2-3Galb1-3GlcNAcb1-3Gala1-3Galb1-	0	-6	0	-12	0			-28	0	0	-17	0
Lewis	556	3'Neu5Gc-LeX-Gal - 04	Neu5Gca2-3Galb1-4(Fuca1-3)GlcNAcb1-3Galb-	0	-34	0	-94	0			-145	0	0	-80	-3
glycolipid	519	3'Neu5Gc-LNnT - 03	Neu5Gca2-3Galb1-4GlcNAcb1-3Galb-	0	-37	0	-90	2			-165	-3	3	-85	3
Lewis	207	3'-sulpho-LeA - 15	3-SO3-Galb1-3[Fuca1-4)GlcNAc-BSA	0	-14	5	-29	3			-37	0	3	-20	0
Lewis	205	3'-sulpho-LeX - 15	3-SO3-Galb1-4[Fuca1-3)GlcNAc-BSA	0	-17	3	-40	0			-54	0	2	-32	0
non-human	748	4-Me-GlcAa1-2Xylb	4-Me-GlcAa1-2Xylb1 -BSA	0	-26	0	-65	0			-63	-3	0	-46	0
non-human	805	4-Me-GlcAa1-2Xylb	4-Me-GlcAa1-2Xylb1 -BSA	0	-8	0	-30	0			-32	0	0	-16	0
carb-Sia	261	6'Neu5Ac-LacNAc-Sp - 05	Neu5Aca2-6Galb1-4GlcNAcb-Sp-BSA	0	-17	4	-42	0			-71	0	0	-40	5
Lewis	209	6'-sulpho-LeX - 08	6-SO3-Galb1-4[Fuca1-3)GlcNAc-BSA	0	-6	0	-22	0			-40	3	3	-11	0
N-linked	593	A2 (a2-6) - 01.5	Neu5Aca2-6Galb1-4GlcNAcb1-2Mana1-6(Neu5Aca2-6Galb1-4GlcNAcb1-2Mana1-3)Manb1-4GlcNAcb1-	0	0	0	-34	0			-49	0	3	-31	-3
peptide	413	Ac-APGSTAPPA-G-05	Ac-A-P-G-S-T-A-P-P-A-G-	0	-28	4	-71	17			-100	5	12	-56	8
peptide	416	Ac-APGSTAPPA-G-14	Ac-A-P-G-S-T-A-P-P-A-G-	0	-20	0	-49	5			-71	3	12	-48	0
peptide-Tn	415	Ac-APGS-Tn(Thr)-APPA-G-03	Ac-A-P-G-S-Tn(Thr)-A-P-P-A-G-	0	-38	0	-88	0			-144	0	3	-91	-3
peptide-Tn	414	Ac-APGS-Tn(Thr)-APPA-G-11	Ac-A-P-G-S-Tn(Thr)-A-P-P-A-G-	0	0	0	-6	0			-9	0	3	-6	0
peptide-Tn	147	Ac-A-Tn(Thr)-S-G - 05	Ac-Ala-(GalNAca)Thr-Ser-Gly-Hex-BSA (muc4)	0	-12	5	-28	0			-40	-3	6	-17	0
peptide-Tn	148	Ac-A-Tn(Thr)-S-G - 08	Ac-Ala-(GalNAca)Thr-Ser-Gly-Hex-BSA (muc4)	0	-14	22	-29	0			-42	0	23	-33	0
peptide-N-GlcNAc	380	Ac-F-N(GlcNAcb1)-S-G-Hex-12	AcPhe-(GlcNAcb1)Asn-Ser-Gly-Hex-12	0	-6	3	3	0			-37	0	0	-11	0
peptide-Fuc	387	Ac-G-S(Fuca)-S-G-Hex-15	Ac-G-S(Fuca)-S-G-Hex-BSA	0	-10	3	-20	0			-40	-3	0	-12	0
peptide-Xyl	388	Ac-G-S(Xylb)-G-G-Hex-04	Ac-Gly-Ser(Xylb)-Gly-Gly-Hex-BSA	0	-11	3	-31	0			-66	3	0	-29	3
peptide-Tn	390	Ac-G-S-T(Tna)A-P-G-Hex-06	Ac-G-S-T(GalNAca)A-P-G-Hex-BSA	0	-6	0	-23	0			-35	-3	0	-20	0
peptide-Tn	391	Ac-G-S-T(Tna)A-P-G-Hex-19	Ac-G-S-T(GalNAca)A-P-G-Hex-BSA	0	-9	4	-28	0			-47	0	0	-32	0
peptide	419	Ac-GSTAP-G-15	Ac-G-S-T-A-P-G-	0	-17	5	-34	5			-48	3	14	-26	5
peptide-Tn	184	Ac-G-V-Tn(Thr)-S-A-G - 04	Ac-Gly-Val-(GalNAca)Thr-Ser-Ala-Gly-Hex-BSA (muc1)	0	-14	5	-34	0			-43	0	6	-31	0
peptide-Tn	185	Ac-G-V-Tn(Thr)-S-A-G - 21	Ac-Gly-Val-(GalNAca)Thr-Ser-Ala-Gly-Hex-BSA (muc1)	0	-14	3	-45	0			-31	5	29	-20	0
peptide-Man	411	Ac-P-T(Mana)-A-G - 22	Ac-Pro-Thr$^{(Man\ a)}$-Ala-Gly-Hex-BSA	0	-28	0	-51	0			-94	-3	0	-68	-6
peptide-Tn	171	Ac-P-Tn(Thr)-T-G - 05	Ac-Pro-(GalNAca)Thr-Thr-Gly-Hex-BSA (muc2)	0	-22	14	-34	0			-37	0	17	-37	3
peptide-Tn	172	Ac-P-Tn(Thr)-T-G - 08	Ac-Pro-(GalNAca)Thr-Thr-Gly-Hex-BSA (muc2)	0	-15	63	-31	0			-35	4	43	-32	0
peptide-Core4	470	Ac-S-Core4(Thr)-S-G-03	Ac-Ser-Core4(Thr)-Ser-Gly-Hex-BSA	0	-20	43	-54	0			-94	0	0	-48	3
peptide-Core4	435	Ac-S-Core4(Thr)-S-G-10	Ac-Ser-Core4(Thr)-Ser-Gly-Hex-BSA	0	-13	5	-31	0			-68	0	0	-34	0
Peptide-core-5	384	Ac-Ser(core 5)-S-G-08	Ac-(GalNAca1-3GalNAca)Ser-Ser-Gly-Hex-BSA	0	-17	3	-32	0			-63	0	3	-23	-3
peptide-Man	625	Ac-S-S(Mana)-S-G - 06	Ac-S-S$^{(Man\ a)}$-S-G-Hex-OH	0	-17	0	-40	0			-60	2	0	-34	0
peptide-Man	409	Ac-S-S(Mana)-S-G - 20	Ac-S-S$^{(Man\ a)}$-S-G-Hex-OH	0	-20	13	-54	0			-92	0	0	-54	-3
Peptide-core-5	381	Ac-S-Ser(core 5)-S-G-04	Ac-Ser-(GalNAca1-3GalNAca)Ser-Ser-Gly-Hex-BSA	0	-13	2	-14	0			-60	0	6	-28	-3
Peptide-core-5	382	Ac-S-Ser(core 5)-S-G-18	Ac-Ser-(GalNAca1-3GalNAca)Ser-Ser-Gly-Hex-BSA	0	-17	0	-39	0			-73	0	6	-37	0
peptide	77	Ac-S-S-S-G - 24	Ac-Ser-Ser-Ser-Gly-Hex-BSA	0	-9	0	-34	0			-49	-5	3	-26	3
peptide-TF	103	Ac-S-TF(Ser)-S-G	AcSer-(Galβ1-3GalNAcα)Thr-Ser-Gly-Hex-HSA (S-TF-S)	0	-9	5	-37	0			-63	0	0	-37	-3
peptide-TF	109	Ac-S-TF(Ser)-S-G - 16	Ac-Ser-(Galb1-3GalNAca)Ser-Ser-Gly-Hex-BSA	0	-14	6	-37	0			-54	3	0	-34	0
peptide-TF	128	Ac-S-TF(Ser)-S-G - 28	Ac-Ser-(Galb1-3GalNAca)Ser-Ser-Gly-Hex-BSA	0	-9	0	-25	0			-48	-3	9	-31	0
peptide-TF	430	Ac-S-TFa(Ser)-TFa(Ser)-G-15	Ac-Ser-Ser(Galb1-3GalNAca-)-Ser(Galb1-3GalNAca-)-Gly-Hex	0	-17	0	-40	0			-68	-3	0	-46	-3
peptide-F1a	27	Ac-S-Thr(F1a)-S-G - 04	Ac-Ser-(Galb1-4GlcNAcb1-6GalNAca)Thr-Ser-Gly-Hex-BSA	0	-15	8	-40	0			-52	3	9	-31	-3

Table 3.3 (cont'd)

peptide	196	Ac-S-Thr-S-G - 18	Ac-Ser-Thr-Ser-Gly-Hex-BSA	0	-20	230	-50	0		-85	0	0	-63	0
peptide-Tn-Ser	429	Ac-S-Tn(Ser)-V-G-03	Ac-Ser-Ser(GalNAca)-V-G-	0	-12	0	-26	0		-49	3	0	-22	3
peptide-Tn-Ser	499	Ac-S-Tn(Ser)-V-G-13	Ac-Ser-Ser(GalNAca)-V-G-	0	-14	0	-25	0		-45	6	0	-26	3
peptide-Tn	142	Ac-S-Tn(Thr)-A-G - 08	Ac-Ser-(GalNAca)Thr-Ala-Gly-Hex-BSA (muc1)	0	-12	6	-37	0		-41	-3	15	-28	0
peptide-Tn	143	Ac-S-Tn(Thr)-A-G - 22	Ac-Ser-(GalNAca)Thr-Ala-Gly-Hex-BSA (muc1)	0	-20	34	-28	0		-34	0	40	-23	3
peptide-Tn	151	Ac-S-Tn(Thr)-G-G - 07	Ac-Ser-(GalNAca)Thr-Gly-Gly-Hex-BSA (muc4)	0	-12	5	-28	2		-48	3	6	-34	0
peptide-Tn	157	Ac-S-Tn(Thr)-S-G HSA-04	Ac-Ser-(GalNAca)Thr-Ser-Gly-Hex-HSA	0	-5	7	-31	0		-54	0	0	-25	0
peptide-Tn	156	Ac-S-Tn(Thr)-S-G HSA-23	Ac-Ser-(GalNAca)Thr-Ser-Gly-Hex-HSA	0	-12	0	-26	0		-34	0	3	-20	3
peptide-Tn	177	Ac-S-Tn(Thr)-Tn(Thr)-G - 05	Ac-Ser-(GalNAca)Thr-(GalNAca)Thr-Gly-Hex-BSA (muc2)	0	-15	4	-26	0		-37	0	-3	-29	0
peptide-Tn	178	Ac-S-Tn(Thr)-Tn(Thr)-G - 09	Ac-Ser-(GalNAca)Thr-(GalNAca)Thr-Gly-Hex-BSA (muc2)	0	-20	5	-42	0		-43	-3	6	-28	3
peptide-Tn	179	Ac-S-Tn(Thr)-Tn(Thr)-G - 22	Ac-Ser-(GalNAca)Thr-(GalNAca)Thr-Gly-Hex-BSA (muc2)	0	-6	3	-26	0		-22	-3	0	-7	0
peptide-Tn	182	Ac-S-Tn(Thr)-V-G - 04	Ac-Ser-(GalNAca)Thr-Val-Gly-Hex-BSA	0	-12	11	-32	0		-37	5	9	-29	0
peptide-Tn	183	Ac-S-Tn(Thr)-V-G - 22	Ac-Ser-(GalNAca)Thr-Val-Gly-Hex-BSA	0	-29	47	-31	0		-32	5	26	-45	3
peptide-TF	158	Ac-TF(Ser)-G - 04	Ac-(Galb1-3GalNAca)Ser-Gly-Hex-BSA	0	-9	3	-22	0		-34	3	6	-22	0
peptide-TF	159	Ac-TF(Ser)-G - 24	Ac-(Galb1-3GalNAca)Ser-Gly-Hex-BSA	0	-15	0	-32	0		-35	0	2	-26	0
peptide-Tn-Ser	121	Ac-Tn(Ser)Tn(Ser)Tn(Ser)-G - 03	Ac-(GalNAca)Ser-(GalNAca)Ser-(GalNAca)Ser-Gly-Hex-BSA	0	-17	5	-46	0		-74	5	0	-34	-3
peptide-Tn	174	Ac-Tn(Thr)-Tn(Thr)-Tn(Thr)-G - 05	Ac-(GalNAca)Thr-(GalNAca)Thr-(GalNAca)Thr-Gly-Hex-BSA (muc2)	0	-17	5	-26	0		-51	5	0	-35	3
peptide-Tn	175	Ac-Tn(Thr)-Tn(Thr)-Tn(Thr)-G - 08	Ac-(GalNAca)Thr-(GalNAca)Thr-(GalNAca)Thr-Gly-Hex-BSA (muc2)	0	-12	0	-34	0		-42	3	6	-37	-3
peptide-Tn	154	Ac-T-Tn(Thr)-P-G - 08	Ac-Thr-(GalNAca)Thr-Pro-Gly-Hex-BSA (muc2,6,7)	0	-11	5	-26	0		-31	3	3	-17	0
peptide-Tn	155	Ac-T-Tn(Thr)-P-G - 21	Ac-Thr-(GalNAca)Thr-Pro-Gly-Hex-BSA (muc2,6,7)	0	0	5	-11	0		-11	0	13	-12	3
peptide-Tn	162	Ac-V-Tn(Thr)-S-G - 04	Ac-Val-(GalNAca)Thr-Ser-Gly-Hex-BSA (muc1)	0	-12	5	-32	0		-23	3	3	-19	3
peptide-Tn	145	Ac-V-Tn(Thr)-S-G - 08	Ac-Val-(GalNAca)Thr-Ser-Gly-Hex-BSA (muc1)	0	-12	5	-32	0		-48	0	6	-28	0
peptide-Tn	146	Ac-V-Tn(Thr)-S-G - 19	Ac-Val-(GalNAca)Thr-Ser-Gly-Hex-BSA (muc1)	0	-3	8	-17	0		-14	0	6	-17	3
Blood Group A	115	Adi - 04	GalNAca1-3Galb-BSA	0	-14	5	-39	0		-59	3	3	-29	0
y-glycoprotein	352	AGE60	Advanced glycation endproducts day 60	0	-29	0	-57	0		-91	0	6	-51	-3
Blood Group A	213	A-LeB hexa - 06	GalNAca1-3(Fuca1-2)Galb1-3(Fuca1-4)GlcNAcb1-3Galb1-BSA	0	-9	5	-28	0		-48	0	3	-26	0
y-glycoprotein	591	alpha 1 acid glycopr	Asialo-alpha 1-Acid Glycoprotein, Asialo-Oroscomucoid, Human, from 75/54 treated with trifluoracetic acid	0	-6	0	-8	0		-14	-3	0	0	0
non-human-aGal	102	alphaGal- 08	Gala1-3Galb1-4GlcNAc-BSA	0	-5	0	-17	0		-40	0	9	-14	0
non-human-aGal	218	alphaGal-6-deoxy - 11	Gala1-3Galb1-4(6deoxy-GlcNAc)-HSA (alphaGal)-HSA	0	-3	3	-32	0		-48	3	5	-24	3
peptide	631	APF peptide		0	-3	0	-5	0		9	3	0	-3	3
non-human	741	Ara2 - 08	Araa1-5Ara-BSA	0	-22	0	-48	0		-74	-5	0	-48	0
non-human	756	Ara4 - 08	Araa1-5Araa1-5Araa1-5Ara-BSA	0	-14	0	-32	0		-97	0	0	-62	0
non-human	798	Arafa1-3(Arafa1-2)X	Arafa1-3(Arafa1-2)Xylb1 - BSA	0	-5	0	-3	0		-17	-3	0	-9	3
non-human	775	Arafa1-3(Arafa1-2)X	Arafa1-3(Arafa1-2)Xylb1-4Xylb -BSA	0	-8	0	-27	0		-23	0	0	-11	3
Peptide	724	ATPLPVTD-BSA	C-terminus MUC4- ATPLPVTD-BSA	0	-11	0	-28	0		-43	0	0	-33	0
non-human	509	AX2 - 04	Arafα1-2Xylβ1-4Xylβ-]; 2^3-α-L-Arabinofuranosyl-xylotriose	0	-9	0	-48	0		-20	0	0	-17	0
peptide-Tn	438	AzHex-D-Tn(Thr)-R-NH2-06	BSA--hexyl-D-T(GalNAc-a)-R-amide	0	-11	0	-26	0		-57	0	-3	-32	3
peptide-GalNAc Tyr	524	AzHex-G-Y(GalNAc-l	BSA-AzHex-G-Y(GalNAc-b)-A-amide	0	0	0	4	0		3	0	0	0	3
peptide	514	AzHex-G-Y-A-NH2 - 04	BSA-AzHex-G-Y-A-amide	0	49	0	9	0		11	0	0	10	6
peptide	515	AzHex-L-Y-W-NH2 -	BSA-AzHex-L-Y-W-amide	0	74	0	3	0		14	26	0	3	5
peptide	450	AzHex-P-D-T-R-P-NH2-07	BSA--hexyl-PDTRP-amide	0	-6	0	-12	0		-26	0	3	-18	3
peptide-Tn	442	AzHex-SAPD-Tn(Thr)-RPAP-NH2-07	BSA--hexyl-SAPD-T(GalNAc-a)-RPAP-amide	0	-14	0	-51	0		-91	0	5	-43	-3
peptide	451	AzHex-S-A-P-D-T-R-P-A-P-NH2-07	BSA--hexyl-SAPDTRPAP-amide	0	-9	3	-40	0		-74	5	0	-31	3
peptide-Tn-Ser	421	AzHex-S-Tn(Ser)-V-G-HexNH2-06	BSA-AzHex-S-Tn(Ser)-V-G-HexNH2	0	-29	3	-74	0		-122	0	0	-64	0
peptide-Tn-Ser	423	AzHex-S-Tn(Ser)-V-G-HexOH-06	BSA-AzHex-S-Tn(Ser)-V-G-HexOH	0	-19	0	-42	0		-69	0	0	-51	0

Table 3.3 (cont'd)

peptide-Tn	444	AzHex-VTSAPD-Tn(Thr)-RPAPGS-NH2-06	BSA--hexyl-VTSAPD-T(GalNAc-a)-RPAPGS-amide	0	-11	0	-28	0		-50	0	0	-14	0
Blood Group B	226	B tetra type 1-Sp - 16	Gala1-3[Fuca1-2]Galb1-3GlcNAcb-Sp-BSA	0	-6	3	-20	0		-34	3	0	-20	3
Blood Group B	235	B tetra type 2-Sp - 07	Gala1-3[Fuca1-2]Galb1-4GlcNAcb-Sp-BSA	0	-26	25	-26	0		-48	2	6	-25	0
non-human-aGal	223	Bdi-g - 06	Gala1-3Galb– BSA	0	-8	5	-31	0		-54	0	6	-28	0
Blood Group A	44	BG-A -19	GalNAca1-3(Fuca1-2)Galb -BSA	0	-11	5	-34	0		-45	0	6	-26	-3
Blood Group A	337	BG-A5-05	GalNAca1-3(Fuca1-2)Galb1-3Galb1-linker-BSA	0	-14	5	-37	0		-48	-1	-3	-26	-6
Blood Group A	343	BG-A6-04	GalNAca1-3(Fuca1-2)Galb1-4Glcb1-linker-BSA	0	-20	3	-34	0		-57	0	0	-28	-6
Blood Group A	344	BG-A6-23	GalNAca1-3(Fuca1-2)Galb1-4Glcb1-linker-BSA	0	-20	0	-57	0		-68	0	3	-29	0
Blood Group B	65	BG-B3-05	Gala1-3(Fuca1-2)Galb1-3GalNAcα1-linker-BSA	0	-23	68	-46	28		-85	-3	71	-57	0
Blood Group B	340	BG-B5-17	Gala1-3(Fuca1-2)Galb1-3Galb1-linker-BSA	0	-26	3	-31	0		-68	-3	0	-50	-6
Blood Group H	137	BG-H1- 06	Fuca1-2Galb1-3GlcNAcb1-linker-BSA	0	-9	4	-17	0		-17	0	3	-23	3
Blood Group H	138	BG-H2- 06	Fuca1-2Galb1-4GlcNAcb1-linker-BSA	0	-5	0	-29	0		-37	0	2	-14	3
Blood Group H	105	BG-H4- 15	Fuca1-2Galb1-3GalNAcb1-linker-BSA	0	-14	5	-40	0		-69	0	6	-45	0
Blood Group H	349	BG-H6-05	Fuca1-2Galb1-4Glcb1-linker-BSA	0	-28	5	-31	0		-43	0	3	-29	-3
y-glycoprotein	355	BSM	Bovine submaxillary mucin (Sigma M3895; STn, STF, S-GlcNAcb1-3, ~20% of Sia is acetylated at 7,8, or 9)	0	-6	0	-6	0		-9	0	3	-9	-3
y-glycoprotein	358	BSM (asialo)	Asialo-Bovine submaxillary mucin (aBSM, Tn, TF, GlcNAcb1-3GalNAc)	0	-3	0	0	0		6	0	6	-3	-3
non-human	709	cellotetraose - 17	Glcb1-4Glcb1-4Glcb1-4Glcb1-	0	-5	0	-23	0		-12	-1	0	-14	0
non-human	684	chitobiose - 03	GlcNAcb1-4GlcNAcb1-	0	-23	0	-57	0		-77	0	0	-43	
non-human	693	chitobiose - 12	GlcNAcb1-4GlcNAcb1-	0	-11	0	-23	0		-17	0		-17	
non-human	688	chitopentaose - 06	GlcNAcb1-4GlcNAcb1-4GlcNAcb1-4bGlcNAcb1-4GlcNAcb1-	0	-11	0	-37	0		-57	0	6	-25	3
non-human	697	chitotetraose - 11	GlcNAcb1-4GlcNAcb1-4GlcNAcb1-4bGlcNAcb1-	0	-6	0	-32	0		-40	0	3	-26	3
non-human	718	chitotriose - 16	GlcNAcb1-4GlcNAcb1-4GlcNAcb1-	0	-8	0	-37	0		-48	0	3	-28	0
Lewis	89	DFpLNH I, LeB - 09	Fuca1-2Galb1-3(Fuca1-4)GlcNAcb1-3Galb1-4GlcNAcb1-3Galb-BSA	0	-27	0	-77	0		-111	0	6	-79	8
y-protein	784	EGFR	EGFR Protein, Human, Recombinant (His Tag)	0	0	0	-6	0		-17	-3	0	-12	-3
y-glycoprotein	361	fetuin	fetuin from calf serum (Sigma #F2379; most abundant glycans are Neu5Ac2-3LacNAc, Neu5Ac2-6LacNAc, SiaLeC, STF)	0	-3	0	-14	0		-20	0	3	-20	0
y-glycoprotein	412	fetuin (human)	a2-HS-glycoprotein (aka human fetuin)	0	3	3	3	0		9	3	0	0	20
non-human	244	Forssman Tetra-BSA - 05	GalNAca1-3GalNAcb1-3Gala1-4Galb-BSA	0	-3	3	-17	0		-17	0	3	-3	0
Lewis+Sia	194	Fuc, 6'Neu5Ac-LNnH-APD-HSA - 12	Galb1-4[Fuca1-3]GlcNAcb1-6[Neu5Aca2-6Galb1-4GlcNAcb1-3]Galb1-APD-HSA	0	-9	3	-37	0		-51	3	3	-36	3
carb-Fuc	130	Fuc-a - 04	Fuc-a - BSA	0	-17	5	16	0		-74	5	6	-37	3
non-human	131	Fuc-b - 04	Fuc-b - BSA	0	-12	8	-37	0		-45	5	9	-20	3
glycolipid	262	Fuc-GM1a - 08	Fuca1-2Galb1-3GalNAcb1-4(Neu5Aca2-3)Galb1-4-BSA	0	-17	0	-51	0		-85	0	6	-43	-3
glycolipid-neutral	118	GA1 tri - 06	Galb1-3GalNAcb1-4Galb1-BSA (GA1tri or asialo-GM1)	0	-17	5	-51	0		-82	0	6	-46	-3
glycolipid-neutral	116	GA2di - 05	GalNAcb1-4Galb - BSA (aka: asialo-GM2)	0	-15	0	-32	0		-37	-3	6	-26	0
non-human-aGal	180	Gala3-type1 - 09	Gala1-3Galb1-3GlcNAc-BSA	0	-12	5	-28	0		-40	0	-6	-20	-5
carb-Gal	675	Galb1-3Galb1 - 07	Galb1-3Galb1-	0	-11	0	-34	0		-105	3	0	-40	0
carb-Gal	673	Gal-BSA-21	Gal-BSA-21 (dorothy)	0	-3	0	-14	0		-15	5	0	-6	6
non-human-aGal	596	Galili Hexa-05	Gala1-3(Galb1-4GlcNAcb1-3)$_2$Galb-	0	-23	0	-37	0		-85	0	0	-51	-3
non-human-aGal	608	Galili Hexa-13-HSA	Gala1-3(Galb1-4GlcNAcb1-3)$_2$Galb-	0	-11	0	-34	0		-40	0	0	-28	0
non-human-aGal	602	Galili Octa-05	Gala1-3(Galb1-4GlcNAcb1-3)$_3$Galb-	0	-26	3	-74	0		-113	0	0	-74	-3
non-human-aGal	610	Galili Octa-13	Gala1-3(Galb1-4GlcNAcb1-3)$_3$Galb-	0	-39	0	-74	0		-119	-3	0	-82	0
carb-GalNAc	113	GalNAc-a - 04	GalNAc-a - BSA	0	-17	3	-26	6		-46	0	6	-15	3
carb-GalNAc	114	GalNAca1-6Galb - 04	GalNAca1-6Galb-BSA	0	-11	4	-28	0		-40	0	6	-20	0
carb-GalNAc	717	GalNAca-phenyl amide- low	GalNAca-O-phenyl-amide linked	0	-28	0	-58	0		-94	0	0	-54	6
carb-GalNAc	729	GalNAca-phenyl Dz-high	GalNAca-O-phenyl-diazirine linker	0	-21	0	-17	0		-34	0	0	-20	0
carb-GalNAc	732	GalNAcb-phenyl amide- high	GalNAcb-O-phenyl-amide linked	0	-3	0	-12	0		-18	0	0	-9	0

Table 3.3 (cont'd)

carb-GalNAc	715	GalNAcb-phenyl Dz-low	GalNAcb-O-phenyl-diazirine linker	0	-6	0	-26	0		-32	0	3	-20	3
glycolipid-neutral	254	Gb4 tetra (P1 tetra)-Sp - 15	GalNAcb1-3Gala1-4Galb1-4GlcNAcb-Sp-BSA	0	-6	3	-20	0		-23	5	3	-6	-3
glycolipid-neutral	546	Gb4 tri - 07	GalNAcb1-3Gala1-4Galb-	0	-14	0	-37	0		-49	3	0	-34	-3
glycolipid related	603	Gb5 analogue type 1-14	Galb1-3GlcNAcb1-3Gala1-4Galb-	0	-9	0	-26	0		-29	3	0	-15	0
glycolipid related	607	Gb5 analogue type 2-12	Galb1-4GlcNAcb1-3Gala1-4Galb-	0	-11	0	-26	0		-29	-3	0	-20	0
glycolipid	658	GD1a (Ac, Ac)	Neu5Aca2-8Neu5Aca2-3(Galb1-3GlcNAcb1-4)Galb1-	0	-23	3	-68	0		-126	2	0	-68	6
glycolipid	655	GD1a (Kdn,Kdn)	Kdna2-8Kdna2-3(Galb1-3GlcNAcb1-4)Galb1-	0	-11	0	-23	0		-31	-3	0	-17	0
glycolipid	549	GD2 tetra (Ac/Ac) - 04	Neu5Aca2-8Neu5Aca2-3(GalNAcb1-4)Galb-	0	-20	0	-40	0		-68	3	-3	-45	-3
glycolipid	646	GD2 tetra (Ac-Gc)	Neu5Aca2-8Neu5Gca2-3(GlcNAcb1-4)Galb1-	0	-7	3	-29	0		-37	0	0	-17	3
glycolipid	521	GD2 tetra (Gc/Ac) - 04	Neu5Gca2-8Neu5Aca2-3(GalNAcb1-4)Galb-	0	-7	0	-20	0		-29	0	0	-23	0
glycolipid	505	GD2 tetra (Gc/Gc) - 04	Neu5Gca2-8Neu5Gca2-3(GalNAcb1-4)Galb-	0	-22	4	-62	0		-119	-3	0	-57	-3
glycolipid	566	GD2 Tetra-06	GalNAcb1-4(Neu5Aca2-8Neu5Aca2-3)Galb-	0	-17	0	-46	0		-57	0	0	-38	0
glycolipid	569	GD2 Tetra-12	GalNAcb1-4(Neu5Aca2-8Neu5Aca2-3)Galb-	0	-28	0	-66	0		-109	-5	0	-70	-3
glycolipid	453	GD_2-b-propyl-03	Neu5Aca2-8Neu5Aca2-3[GalNAcb1-4]Galb1-4Glcb-propyl-BSA	0	-17	3	-43	0		-60	5	0	-32	3
glycolipid	529	GD3 tri (Ac/Ac) - 04	Neu5Aca2-8Neu5Aca2-3Galb-	0	-38	0	-85	0		-161	-3	0	-85	-5
glycolipid	553	GD3 tri (Gc/Ac) - 04	Neu5Gca2-8Neu5Aca2-3Galb-	0	-25	0	-70	0		-114	0	0	-67	0
glycolipid	652	GD3 tri (Gc-Gc)	Neu5Gca2-8Neu5Gca2-3Galb1-	0	-6	0	-25	0		-40	-3	0	-21	3
glycolipid	543	GD3 tri (Kdn/Ac) - 05	Kdna2-8Neu5Aca2-3Galb-	0	-37	3	-80	0		-130	3	0	-91	0
carb-Glc	258	Glc-a - 05	Glc-a - BSA	0	-12	0	-37	0		-57	3	3	-23	0
Carb-Glc	759	Glca1-6Glca -05	Glca1-6Glca -BSA	0	-11	0	-28	0		-29	-1	0	-15	0
Carb-GlcA	448	GlcA-LNT-05	GlcAb1-3Galb1-3GlcNAcb1-3Galb-	0	-23	0	-65	0		-96	3	0	-54	3
Carb-GlcA	475	GlcA-LNT-16	GlcAb1-3Galb1-3GlcNAcb1-3Galb-	0	-28	0	-65	0		-108	-3	-3	-60	0
non-human	558	Glcb1-3Glcb- 06	Glcb1-3Glcb-	0	37	5	153	141		655	3	11	-26	6
non-human	781	Glcb1-3Glcb1-3Glcb	Glcb1-3Glcb1-3Glcb BSA	0	-11	3	-30	0		-31	0	6	-17	0
carb-Glc	720	Glcb1-4Glcb1-3Glc - 06	Glcb1-4Glcb1-3Glcb1-	0	-17	0	-60	0		-49	0	6	-48	6
carb-Glc	691	Glcb1-4Glcb1-3Glc - 17	Glcb1-4Glcb1-3Glcb1-	0	-9	5	-47	0		-10	3	11	-42	0
carb-Glc	708	Glcb1-4Glcb1-4Glc - 13	Glcb1-4Glcb1-4Glcb1-	0	-14	0	-40	0		-3	0	3	-37	3
Carb-Glc	735	Glcb1-4Manb1 - 05	Glcb1-4Manb1 - BSA	0	-23	3	-40	0		-51	0	0	-37	0
Carb-GlcNAc	745	GlcNAcb-ITC - 06	from Beat Ernst	0	-9	0	-20	0		-23	-3	3	-20	3
Blood Group B	106	Globo B - 05	Gala1-3(Fuca1-2)Galb1-3GalNAcb1-3Gala1-4Galb1-BSA	0	-17	12	-38	0		-48	0	9	-25	3
Blood Group H related	609	Globo H analogue type 1-04	Fuca1-2Galb1-3GlcNAcb1-3Gala1-4Galb-	0	-8	0	-23	0		-17	-4	0	-15	3
Blood Group H related	604	Globo H analogue type 1-10	Fuca1-2Galb1-3GlcNAcb1-3Gala1-4Galb-	0	-11	0	-17	0		-34	0	0	-22	0
Blood Group H related	599	Globo H analogue type 2-03	Fuca1-2Galb1-4GlcNAcb1-3Gala1-4Galb-	0	-9	2	-37	0		-47	0	0	-26	-3
glycolipid	554	GM1 (Ac) - 06	Galb1-3GalNAcb1-4(Neu5Aca2-3)Galb	0	-8	0	-26	0		-43	0	-3	-32	-2
glycolipid	645	GM1 (Gc)	Neu5Gca2-3(Galb1-3GlcNAcb1-4)Galb1-	0	-3	0	-20	0		-49	0	0	-11	2
glycolipid	648	GM1 (Kdn)	Kdna2-3(Galb1-3GlcNAcb1-4)Galb1-	0	-3	0	-12	0		-46	-3	0	-14	3
glycolipid	82	GM1a - 29	Galb1-3GalNAcb1-4(Neu5Aca2-3)Galb	0	-15	5	-48	0		-74	0	6	-42	0
glycolipid	649	GM2 tri (Kdn)	Kdna2-3(GlcNAcb1-4)Galb1-	0	-26	3	-65	0		-102	0	0	-49	3
glycolipid	336	GM2-Sp - 04	Neu5Aca2-3[GalNAcb1-4]Galb1-4Glcb-Sp-BSA	0	-25	5	-31	0		-37	3	0	-29	0
glycolipid	96	GM2-Sp - 14	Neu5Aca2-3[GalNAcb1-4]Galb1-4Glcb-Sp-BSA	0	-12	0	-17	0		-51	5	6	-31	0
glycolipid	282	GM3-Sp - 11	Neu5Aca2-3Galb1-4Glcb-Sp-BSA	0	-11	3	-15	0		-51	0	0	-17	0
carb-GlcNAc	252	GNLacNAc-Sp - 06	GlcNAcb1-3Galb1-4GlcNAcb-Sp-BSA	0	-20	110	-39	0		-71	3	3	-40	5
y-glycoprotein	370	gp120	gp120 from HIV; expressed in HEK293T cells;	0	-20	0	-22	0		-68	0	6	-31	0
y-protein	790	gp120 Clade B	gp120 from HIV BAL-120; expressed in HEK293T cells;	0	-6	0	-17	0		-40	-3	-3	-14	0
glycolipid	257	GT3-Sp - 03	Neu5Aca2-8Neu5Aca2-8Neu5Aca2-3Galb1-4Glcb-Sp-BSA	0	-14	3	-37	0		-57	-3	3	-31	0
peptide-TF	186	GTSSAS-TF(Thr)-GHATPLPVTD	BSA-PEG7-Gly-Thr-Ser-Ser-Ala-Ser-(Galb1-3GalNAca)Thr-Gly-His-Ala-Thr-Pro-Leu-Pro-Val-Thr-Asp	0	-9	5	-27	0		-41	-3	0	-17	3
peptide	190	GTSSASTGHATPLPVTD	BSA-PEG7-Gly-Thr-Ser-Ser-Ala-Ser-Thr-Gly-His-Ala-Thr-Pro-Leu-Pro-Val-Thr-Asp	0	-14	3	-34	0		-43	0	6	-23	0
peptide-TF	189	GTSSA-TF(Ser)-TF(Thr)-GHATPLPVTD	BSA-PEG7-Gly-Thr-Ser-Ser-Ala-(Galb1-3GalNAca)Ser-(Galb1-3GalNAca)Thr-Gly-His-Ala-Thr-Pro-Leu-Pro-Val-Thr-Asp	0	-11	3	-37	0		-37	0	0	-20	3
peptide-TF	187	GTSSA-TF(Ser)-TGHATPLPVTD	BSA-PEG7-Gly-Thr-Ser-Ser-Ala-(Galb1-3GalNAca)Ser-Thr-Gly-His-Ala-Thr-Pro-Leu-Pro-Val-Thr-Asp (MUC4)	0	-17	8	-28	0		-43	3	6	-25	0

Table 3.3 (cont'd)

GAG	203	Hep-5000 - 01	heparin polysaccharide (MW ~5000)	0	-8	5	-31	0		-37	3	6	-17	0
GAG	202	Hep-N-acetylated	fully N-acetylated heparin polysaccharide	0	-12	3	-34	0		-37	3	6	-23	0
GAG-Hep	571	Hep-NAc-Hepta-05	GlcAb1-4GlcNAca1-4GlcAb1-4GlcNAca1-4GlcAb1-4GlcNAca1-4GlcAb-Benzamide- (Heparosan)	0	-17	0	-34	0		-51	3	0	-34	0
GAG-Hep	568	Hep-NAc-Octa-03	GlcNAca1-4GlcAb1-4GlcNAca1-4GlcAb1-4GlcNAca1-4GlcAb1-4GlcNAca1-4GlcAb-Benzamide- (Heparosan)	0	-6	0	-26	0		-43	-3	0	-29	0
GAG-Hep	542	Hep-NAc-Penta-04	GlcAb1-4GlcNAca1-4GlcAb1-4GlcNAca1-4GlcAb-Benzamide- (Heparosan)	0	-17	0	-46	0		-79	-5	-3	-48	-3
GAG-Hep	511	Hep-NAc-Tetra-06	GlcNAca1-4GlcAb1-4GlcNAca1-4GlcAb-Benzamide- (Heparosan)	0	-14	5	-34	0		-60	0	0	-20	-3
GAG-Hep	575	Hep-Nona-GT13-02	GlcAb1-4GlcNSa1-4GlcAb1-4GlcNSa1-4GlcAb1-4GlcNSa1-4GlcAb1-4Glc(6S, NS)a1-4GlcAb-Benzamide-	0	-20	0	-38	0		-54	0	0	-34	3
GAG-Hep	567	Hep-NS-Octa-03	GlcNSa1-4GlcAb1-4GlcNSa1-4GlcAb1-4GlcNSa1-4GlcAb1-4GlcNSa1-4GlcAb-Benzamide-	0	-9	0	-26	0		-40	0	3	-20	0
GAG-Hep	534	Hep-NS-Tetra-05	GlcNSa1-4GlcAb1-4GlcNSa1-4GlcAb-Benzamide-	0	-11	3	-31	0		-60	3	3	-31	0
GAG-Hep	738	Hep-Octa-GT24-C5-03	Glc(6S, Nac)a1-4GlcAb1-4Glc(6S, 3S, NS)a1-4IdoA(2S)a1-4Glc(6S, NS)a1-4IdoA(2S)a1-4Glc(6S, NS)a1-4GlcAb-Benzamide-	0	3	4	-6	0		-20	3	0	11	3
y-protein	787	Her2	Her2 / ERBB2 Protein, Human, Recombinant (His Tag)	0	0	0	-15	0		-17	-3	0	-11	3
GAG-Hya	576	Hya7-03	GlcAb1-3(GlcNAcb1-4GlcAb1-3)$_3$-	0	-8	0	-31	0		-37	0	0	-32	0
GAG-Hya	206	Hya9 - 03	(GlcAb1-3GlcNAcb1-4)$_4$b1-3GlcAb1-BSA	0	-6	5	-28	0		-51	5	6	-20	2
glycolipid-neutral	432	iFs-05	GalNAca1-3GalNAcb1-3Gala1-3Galb- (iso-Forssman)	0	3	5	-17	0		-77	5	3	-37	3
glycolipid-neutral	436	iFs-11	GalNAca1-3GalNAcb1-3Gala1-3Galb- (iso-Forssman)	0	-38	0	-96	0		-156	3	0	-93	3
glycolipid-neutral	487	iGb4-19	GalNAcb1-3Gala1-3Galb-	0	-20	2	-57	0		-97	0	3	-51	-3
glycolipid-neutral	544	iGb5 tetra - 09	Galb1-3GalNAcb1-3Gala1-3Galb-	0	-11	0	-51	0		-82	0	0	-42	0
glycolipid-neutral	490	iGb5-15	Galb1-3GalNAcb1-3Gala1-3Galb-	0	-23	0	-77	0		-121	0	0	-66	3
carb-type1	216	iLNO - 06	Galb1-3GlcNAcb1-3Galb1-4GlcNAcb1-6 (Galb1-3GlcNAcb1-3)Galb1-BSA	0	-6	5	-34	0		-29	0	3	-23	0
carb-Glc	30	Isomaltose - 13	Glca1-6Glcb-BSA	0	-15	5	-39	3		-51	6	3	-28	0
non-human	550	KDOa2-8KDOa - 09	KDOa2-8KDOa-APTE-BSA	0	-17	3	-32	0		-54	0	3	-26	0
non-human	541	KDOa2-8KDOa2-4KI	KDOa2-8KDOa2-4KDOa-APTE-BSA	0	-13	0	-43	0		-82	-1	0	-40	0
y-glycoprotein	369	KLH	Keyhole limpet hemocyanin (Sigma H7017)	0	3	0	0	0		16	0	-3	9	0
glycolipid-neutral	224	Lac-C5 - 14	Galb1-4Glcb – BSA	0	-8	5	-26	0		-29	0	6	-17	5
carb-type 2	107	LacNAc (trimeric) - 08	Galb1-4GlcNAcb1-3Galb1-4GlcNAcb1-3Galb1-4GlcNAcb-APE-HSA	0	-12	0	-37	0		-74	-5	6	-37	0
N-linked	198	LacNAc-Man5 - 02	Mana1-6(Mana1-3)Mana1-6(Galb1-4GlcNAcb1-2Mana1-3)Manb1-4GlcNAcb-BSA	0	-6	5	-23	0		-23	0	3	-17	0
non-human	690	laminaritriose - 06	Glcb1-3Glcb1-3Glcb1-	0	-5	3	-26	0		-20	0		-12	
glycolipid-neutral	525	Lc3 di - 11	GlcNAcb1-3Galb-	0	-17	0	-32	0		-77	0	0	-37	2
Lewis	700	LeA tri	Galb1-3[Fuca1-4)GlcNAcb1; LeA trisacch from De	0	-6	0	-17	0		-11	0	0	-9	2
Lewis	38	LeB-Lac - 09 (LNDFH I)	Fuca1-2Galb1-3(Fuca1-4)GlcNAcb1-3Galb1-4Glcb-BSA	0	-6	0	-34	3		-54	-3	6	-25	0
Lewis	221	LeC (dimeric)-Sp - 16	Galb1-3GlcNAcb1-3Galb1-3GlcNAcb-Sp-BSA	0	-12	4	-34	0		-54	5	6	-26	0
lewis	111	LeC-Sp - 06	Galb1-3GlcNAcb-Sp-BSA	0	-16	-1	-37	0		-68	0	3	-39	0
Lewis	259	LeC-Sp - 15	Galb1-3GlcNAcb-Sp-BSA	0	-10	3	-28	0		-54	0	3	-20	0
Lewis	730	LeX trisaccharide	Galb1-4[Fuca1-3)GlcNAc-; SSEA-1; CD-15; Dextra	0	-18	0	-17	0		-34	-1	0	-26	-6
Lewis	39	LeY -08	Fuca1-2Galb1-4[Fuca1-3)GlcNAc –HSA	0	-11	37	-34	0		-69	0	3	-20	0
Lewis	666	LeY tetra-HSA -05	Fuca1-2Galb1-4[Fuca1-3)GlcNAcb1-	0	-12	0	-22	0		-51	-3	0	-20	0
Lewis	667	LeY tetra-HSA -10	Fuca1-2Galb1-4[Fuca1-3)GlcNAcb1-	0	-6	0	-23	0		-43	0	0	-32	0
carb-type 1+2	133	LNH - 13	Galb1-4GlcNAcb1-6(Galb1-3GlcNAcb1-3)Galb1-BSA	0	-23	11	-63	0		-88	-3	0	-51	0
carb-type 1+2	640	LNH - 13-HSA	Galb1-4GlcNAcb1-6(Galb1-3GlcNAcb1-3)Galb1-	0	-5	0	-14	0		-32	0	3	-14	-3
carb-type 2	134	LNnH - 11	Galb1-4GlcNAcb1-6(Galb1-4GlcNAcb1-3)Galb1-BSA	0	-15	5	-20	0		-31	-3	0	-17	6
carb-type 2	642	LNnH - 12-HSA	Galb1-4GlcNAcb1-6(Galb1-4GlcNAcb1-3)Galb1-	0	-11	0	-17	0		-20	-4	0	-17	3
carb-type 2	595	LNnO-05	Galb1-4GlcNAcb1-3Galb1-4GlcNAcb1-3Galb1-4GlcNAcb1-3Galb-	0	-23	0	-57	0		-85	0	0	-51	0
carb-type 2	601	LNnO-16	Galb1-4GlcNAcb1-3Galb1-4GlcNAcb1-3Galb1-4GlcNAcb1-3Galb-	0	-17	0	-31	0		-60	0	3	-34	0
glycolipid-neutral	135	LNnT - 04	Galb1-4GlcNAcb1-3Galb1-BSA	0	-11	3	-17	0		-71	3	-3	-28	0
glycolipid-neutral	580	LNnT - 04	Galb1-4GlcNAcb1-3Galb-	0	-28	0	-71	0		-122	0	0	-65	3
glycolipid-neutral	622	LNnT - 13-HSA	Galβ1-4GlcNAcβ1-3Galβ1-HSA (LNnT)	0	-17	0	-32	0		-40	0	3	-22	0
glycolipid-neutral	85	LNnT - 14	Galb1-4GlcNAcb1-3Galb1-BSA	0	-17	5	-42	0		-59	3	6	-40	0
glycolipid-neutral	117	LNT - 05	Galb1-3GlcNAcb1-3Galb-BSA	0	-14	5	-37	0		-68	0	0	-34	0
glycolipid-neutral	53	LNT - 21	Galb1-3GlcNAcb1-3Galb-BSA	0	-26	5	-77	0		-121	0	9	-71	3
glycolipid	56	LSTc - 07	Neu5Aca2-6Galb1-3GlcNAcb1-3Galb1-BSA	0	-17	0	-46	3		-51	0	6	-34	3
glycolipid	483	LSTd-03	Siaa2-3Galb1-4GalNAcb1-3Galb-	0	-15	0	-26	0		-52	3	3	-20	3

Table 3.3 (cont'd)

glycolipid	483	LSTd-03	Siaa2-3Galb1-4GalNAcb1-3Galb-	0	-15	0	-26	0		-52	3	3	-20	3
carb-Man	489	Ma2Ma2Ma2-04	aMan(1-2)aMan(1-2)aMan(1-2)	0	-32	0	-74	0		-110	-3	-6	-51	0
carb-Man	486	Ma2Ma2Ma3(Ma3M	aMan(1-2)aMan(1-2)aMan(1-3)[aMan(1-3)aMan(1-6)]	0	-26	0	-71	0		-127	-3	-3	-74	6
carb-Man	473	Ma2Ma2Ma3(Ma6)-	aMan(1-2)aMan(1-2)aMan(1-3)[aMan(1-6)]	0	-23	0	-68	0		-94	0	3	-51	-3
carb-Man	424	Ma2Ma2Ma3-04	aMan(1-2)aMan(1-2)aMan(1-3)	0	-12	0	-51	0		-108	3	3	-60	-2
carb-Man	477	Ma2Ma2Ma3-12	aMan(1-2)aMan(1-2)aMan(1-3)	0	-28	0	-80	0		-131	3	0	-76	0
carb-Man	456	Ma2Ma3(Ma6)Ma6-	aMan(1-2)aMan(1-3)[aMan(1-6)]aMan(1-6)	0	-37	0	-85	0		-145	-3	-6	-82	3
carb-Man	466	Ma2Ma3Ma6(Ma3)-	aMan(1-2)aMan(1-3)aMan(1-6)[aMan(1-3)]	0	-23	0	-45	0		-77	0	0	-43	-1
carb-Man	479	Ma2Ma3Ma6-15	aMan(1-2)aMan(1-3)aMan(1-6)	0	-23	0	-63	0		-99	-4	2	-53	-3
carb-Man	422	Ma2Ma6(Ma2Ma3)-	aMan(1-2)aMan(1-6)[aMan(1-2)aMan(1-3)]	0	-17	5	-43	0		-85	3	9	-37	5
carb-Man	498	Ma2Ma6(Ma2Ma3)-	aMan(1-2)aMan(1-6)[aMan(1-2)aMan(1-3)]	0	-17	0	-40	0		-117	0	-2	-49	0
carb-Man	501	Ma2Ma6(Ma3)-03	aMan(1-2)aMan(1-6)[aMan(1-3)]	0	-25	0	-48	0		-147	3	6	-55	3
carb-Man	447	Ma2Ma6(Ma3)-07	aMan(1-2)aMan(1-6)[aMan(1-3)]	0	-17	0	-37	0		-54	0	0	-40	3
carb-Man	474	Ma3(Ma6)Ma6(Ma2	aMan(1-3)[aMan(1-6)]aMan(1-6)[aMan(1-2)aMan(1-3)]	0	-17	7	-43	0		-94	0	0	-45	0
carb-Man	480	Ma3Ma6(Ma2Ma3)-	aMan(1-3)aMan(1-6)[aMan(1-2)aMan(1-3)]	0	-9	0	-32	0		-63	5	0	-29	3
carb-Man	485	Ma3Ma6(Ma2Ma3)-	aMan(1-3)aMan(1-6)[aMan(1-2)aMan(1-3)]	0	-19	0	-51	0		-74	0	3	-48	-2
carb-Man	445	Ma3Ma6-05	aMan(1-3)aMan(1-6)	0	-25	0	-65	0		-100	0	-6	-60	-3
carb-Man	471	Ma3Ma6-13	aMan(1-3)aMan(1-6)	0	-8	0	-20	0		-44	0	-3	-29	0
carb-Man	465	Ma4(Ma6)-07	aMan(1-4)[aMan(1-6)]	0	-12	0	-28	0		-60	0	6	-36	0
carb-Man	468	Ma6Ma4(Ma6Ma6)-	aMan(1-6)aMan(1-4)[aMan(1-6)aMan(1-6)]	0	-20	0	-51	0		-91	0	0	-49	3
carb-Man	462	Ma6Ma6(Ma2Ma3)-	aMan(1-6)aMan(1-6)[aMan(1-2)aMan(1-3)]	0	-15	3	-49	0		-108	0	3	-54	0
carb-Man	482	Ma6Ma6-05	aMan(1-6)aMan(1-6)	0	-9	0	-26	0		-28	0	0	-17	-3
carb-Man	488	Ma6Ma6-09	aMan(1-6)aMan(1-6)	0	-14	0	-48	0		-66	0	3	-46	0
carb-Glc	705	maltoheptaose - 04	Glca1-4Glca1-4Glca1-4Glca1-4Glca1-4Glca1-4Glca1-	0	-8	0	-23	0		-34	-3	0	-9	0
carb-Glc	721	maltononaose - 04	Glca1-4Glca1-4Glca1-4Glca1-4Glca1-4Glca1-4Glca1-4Glca1-4Glca1-	0	3	0	-26	0		-45	0	6	-22	3
carb-Glc	678	maltononaose - 14	Glca1-4Glca1-4Glca1-4Glca1-4Glca1-4Glca1-4Glca1-4Glca1-4Glca1-	0	-8	0	-17	0		-32	0	0	-17	2
carb-Glc	712	maltooctaose - 04	Glca1-4Glca1-4Glca1-4Glca1-4Glca1-4Glca1-4Glca1-4Glca1-	0	-20	2	-42	0		-74	3	0	-39	3
carb-Glc	696	maltooctaose - 20	Glca1-4Glca1-4Glca1-4Glca1-4Glca1-4Glca1-4Glca1-4Glca1-	0	-6	0	-20	0		-26	3		-20	
carb-Glc	706	maltopentaose - 06	Glca1-4Glca1-4Glca1-4Glca1-4Glca1-	0	-11	0	-20	0		-28	5	0	-15	0
carb-Glc	703	maltose - 05	Glca1-4Glca1-	0	-6	0	-31	0		-43	0	0	-23	-3
carb-Glc	679	maltose - 20	Glca1-4Glca1-	0	-17	0	-29	0		-36	3	0	-20	6
N-linked	264	Man1 - 04	Manβ1-4GlcNAcβ1-4GlcNAcβ1-BSA	0	-17	0	-40	0		-48	0	3	-28	0
N-linked	204	Man6 - I - 04	Mana1-6(Mana1-3)Mana1-6(Mana1-2Mana1-3)Manb1-BSA	0	-14	5	-37	0		-51	0	3	-23	3
N-linked	613	Man6 I - 03	Mana1-6(Mana1-3)Mana1-6(Mana1-2Mana1-3)Manb-	0	-22	3	-59	0		-102	5	0	-54	3
N-linked	394	Man8D1D3 #2	Mana1-2Mana1-6(Mana1-3)Mana1-6(Mana1-2Mana1-2Mana1-3)Manb1-4GlcNAc-BSA	0	-11	0	-30	0		-51	0	6	-32	3
N-linked	91	Man9 - 05 #2	Mana1-2Mana1-6(Mana1-2Mana1-3)Mana1-6(Mana1-2Mana1-2Mana1-3)Manb1-4GlcNAc-BSA	0	-10	8	-46	0		-85	3	3	-37	0
N-linked	503	Man9 - 08	Mana1-2Mana1-6(Mana1-2Mana1-3)Mana1-6(Mana1-2Mana1-2Mana1-3)Manb1-4GlcNAcb-	0	-29	0	-54	0		-75	-3	6	-61	0
carb-Man	504	Man-a - 20	Man-a - BSA	0	-3	0	-20	0		-33	0	3	-12	0
Carb-Man	681	Mana1-2Man	Mana1-2Man-BSA	0	-9	0	-23	0		-28	0	0	-17	5
Carb-Man	694	Mana1-3Man	Mana1-3Man-BSA	0	-9	0	-14	0		-23	2	0	-17	2
carb-Man	225	Mana1-6Man-a - 04	Mana1-6Man-a - BSA	0	-12	0	-39	2		-46	0	3	-26	0
non-human	747	Manb2 - 04	Manb1-4Manb1-BSA	0		21		0		-63	3	0		0
non-human	753	Manb3 - 04	Manb1-4Manb1-4Manb1-BSA	0	-14	0	-43	0		-85	0	0	-48	3
non-human	804	Manb3 - 10	Manb1-4Manb1-4Man	0	3	8	-11	0		1	0	0	-8	0
non-human	733	Manb3 - 16	Manb1-4Manb1-4Manb1-BSA	0	13	20	-60	0		128	0	2	-43	-6
carb-Man	32	ManT -26	Mana1-6[Mana1-3]Manb□-BSA	0	-9	5	-48	3		-62	0	3	-37	0
Blood Group H	217	MFLNH I - 11	Galb1-4GlcNAcb1-6 (Fuca1-2Galb1-3GlcNAcb1-3)Galb1-BSA	0	-12	0	-32	0		-50	3	0	-23	0
Lewis	219	MFLNH III - 14	Galb1-4(Fuca1-3)GlcNAcb1-6 (Galb1-3GlcNAcb1-3)Galb1-BSA	0	-16	5	-43	0		-33	0	6	-29	0
Blood Group H	212	MSMFLNH I - 11	Neu5Aca2-6Galb1-4GlcNAcb1-6 (Fuca1-2Galb1-3GlcNAcb1-3)Galb1-BSA	0	-8	0	-45	0		-57	3	3	-29	0
Lewis	215	MSMFLnNH - 09	Galb1-4(Fuca1-3)GlcNAcb1-6 (Neu5Aca2-6Galb1-4GlcNAcb1-3)Galb1-BSA	0	-8	3	-32	0		-34	0	0	-29	0
peptide	395	Muc1	BSA--hexyl-G-V-T-S-A-P-D-T-R-P-A-P-G-S-T-A-P-P-A-amide	0	-3	0	-20	0		-23	3	3	-11	0
peptide-Tn	397	Muc1-Tn15	BSA--hexyl-G-V-T-S-A-P-D-T-R-P-A-P-G-S-T(GalNAc-a)-A-P-P-A-amide	0	-11	2	-31	0		-40	3	3	-20	0
N-linked	153	NA2 - 08	Galb1-4GlcNAcb1-2Mana1-6[Galb1-4GlcNAcb1-2Mana1-3]Manb1-4GlcNAc -BSA	0	-9	3	-31	0		-54	0	3	-25	-3
N-linked	150	NA3 - 05	Galb1-4GlcNAcb1-2Mana1-6[Galb1-4GlcNAcb1-2(Galb1-4GlcNAcb1-4)Mana1-3]Manb1-4GlcNAc -BSA	0	-23	5	-48	0		-60	-4	5	-48	3
N-linked	144	NGA2 - 07	GlcNAcb1-2Mana1-6(GlcNAcb1-2Mana1-3)Manb1-4GlcNAc -BSA	0	-15	3	-40	0		-69	-5	-6	-34	-3
N-linked	141	NGA2B - 05	GlcNAcb1-2Mana1-6(GlcNAcb1-2Mana1-3)(GlcNAcb1-4)Manb1-4GlcNAc -BSA	0	-17	0	-35	0		-63	0	0	-31	0
N-linked	165	NGA3B - 06	GlcNAcb1-2Mana1-6[GlcNAcb1-2(GlcNAcb1-4)Mana1-3](GlcNAcb1-4)Manb1-4GlcNAc -BSA	0	-15	3	-37	0		-54	-3	3	-26	0
y-glycoprotein	385	OSM	Ovine submaxillary mucin (94% STn, 4% TF, 2% Fuca1-2Galb1-3GalNAc)	0	11	2	-37	0		-71	0	3	203	0
y-glycoprotein	372	OSM (asialo)	asialo-Ovine submaxillary mucin	0	6	0	3	0		3	3	3	8	0
y-protein	793	PD-L1	Human PD-L1/B7-H1 Protein, His Tag	0	12	0	8	0		17	3	3	11	0
carb-type 1	136	pLNH - 07	Galb1-3GlcNAcb1-3Galb1-4GlcNAcb1-3Galb1-BSA	0	-17	5	-43	0		-40	2	3	-46	0

Table 3.3 (cont'd)

carb-type 1	83	pLNH - 21	Galb1-3GlcNAcb1-3Galb1-4GlcNAcb1-3Galb1-BSA	0	-23	5	-69	0		-116	-3	0	-68	6
non-human PNAG	739	PNAG 10 (01010)	GlcNb1-6GlcNAcb1-6GlcNb1-6GlcNAcb1-6GlcNb1-	0	-14	0	-22	0		-29	0	-2	-14	0
non-human PNAG	742	PNAG 11 (01011)	GlcNb1-6GlcNAcb1-6GlcNb1-6GlcNAcb1-6GlcNAcb1-	0	-11	0	-17	0		-32	0	0	-17	3
non-human PNAG	751	PNAG 12 (01100)	GlcNb1-6GlcNAcb1-6GlcNAcb1-6GlcNb1-6GlcNb1-	0	3	0	-14	0		-28	5	0	-17	0
non-human PNAG	757	PNAG 13 (01101)	GlcNb1-6GlcNAcb1-6GlcNAcb1-6GlcNb1-6GlcNAcb1-	0	-6	5		0		-34	5	3	-34	0
non-human PNAG	771	PNAG 15 (01111)	GlcNb1-6GlcNAcb1-6GlcNAcb1-6GlcNAcb1-6GlcNAcb1-	0	-3	0	-8	0		-31	-1	3	-14	3
non-human PNAG	762	PNAG 2 (00010)	GlcNb1-6GlcNb1-6GlcNb1-6GlcNAcb1-6GlcNb1-	0	-8	0	-21	0		-16	0	0	-3	3
non-human PNAG	777	PNAG 21 (10101)	GlcNAcb1-6GlcNb1-6GlcNAcb1-6GlcNb1-6GlcNAcb1-	0	-6	0	-6	0		-8	0	0	-3	3
non-human PNAG	780	PNAG 23 (10111)	GlcNAcb1-6GlcNb1-6GlcNAcb1-6GlcNAcb1-6GlcNAcb1-	0	-20	0	-43	0		-148	0	3	-57	-6
non-human PNAG	783	PNAG 24 (11000)	GlcNAcb1-6GlcNAcb1-6GlcNb1-6GlcNb1-6GlcNb1-	0	-17	0	-40	0		-119	0	0	-43	0
non-human PNAG	765	PNAG 26 (11010)	GlcNAcb1-6GlcNAcb1-6GlcNb1-6GlcNAcb1-6GlcNb1-	0	-15	0	-12	0		-26	-3	0	-20	0
non-human PNAG	786	PNAG 28 (11100)	GlcNAcb1-6GlcNAcb1-6GlcNAcb1-6GlcNb1-6GlcNb1-	0	0	0	-1	0		-28	0	2	-12	0
non-human PNAG	768	PNAG 29 (11101)	GlcNAcb1-6GlcNAcb1-6GlcNAcb1-6GlcNb1-6GlcNAcb1-	0	-6	0	-11	0		-37	5	0	-15	0
non-human PNAG	789	PNAG 30 (11110)	GlcNAcb1-6GlcNAcb1-6GlcNAcb1-6GlcNAcb1-6GlcNb1-	0	-6	0	-9	0		-25	0	3	-6	0
non-human PNAG	774	PNAG 6 (00110)	GlcNb1-6GlcNb1-6GlcNAcb1-6GlcNAcb1-6GlcNb1-	0	-3	0	-6	0		-25	-3	0	-9	3
non-human PNAG	754	PNAG 9 (01001)	GlcNb1-6GlcNAcb1-6GlcNb1-6GlcNb1-6GlcNAcb1-	0	-3	0	-20	0		-25	3	-2	-11	0
non-human	426	Rha-a - 05	Rha-a – BSA	0	-17	0	-48	0		-90	-3	6	-40	0
non-human	428	Rha-b - 05	Rha-b - BSA	0	23	8	-28	0		-46	5	3	-29	2
Blood Group H	220	TFiLNO(1-2,1-2,1-3) - 04	Fuca1-2Galb1-3GlcNAcb1-3Galb1-4(Fuca1-3)GlcNAcb1-6(Fuca1-2Galb1-3GlcNAcb1-3)Galb-BSA (mixed with other stuff by MS)	0	-6	4	-25	0		-26	0	0	-8	0
peptide-TF	723	TSSA(S-TF)-TGH-BSA	TF-S5-N-terminus Muc4- TSSA(S-TF)-TGH-BSA	0	-15	0	-37	0		-63	0	0	-43	0
peptide-TF	632	TSSA-(TF)S-TGHATP	BSA-Mal-PEG6-TSSA(Galb1-3GalNAca)STGHATPLPVTD	0	-19	0	-43	0		-66	-1	0	-54	0
peptide-TF	727	TSSASTGHA(T-TF)PLPVTD-BSA	TF-10-MUC4- TSSASTGHA(T-TF)PLPVTD-BSA	0	-17	0	-20	0		-48	0	0	-30	0
peptide	629	TSSASTGHATPLPVTI	BSA-Mal-PEG6-TSSASTGHATPLPVTD (MUC4 TR)	0	-23	0	-26	0		-67	0	3	-40	0
Blood Group H	36	BG-H1-Lac- 20 (LNF I)	Fuca1-2Galb1-3GlcNAcb1-3Galb1-4Glcb–APD-HSA	-2	-34	4	-48	0		-110	0	0	-79	3
non-human	702	chitotetraose - 03	GlcNAcb1-4GlcNAcb1-4GlcNAcb1-4bGlcNAcb1-	-2	-12	5	-34	0		-57	3	3	-22	6
glycolipid	664	GD1a (Gc, Ac)	Neu5Gca2-8Neu5Aca2-3(Galb1-3GlcNAcb1-4)Galb1-	-2	-14	11	-48	0		-88	-1	0	-46	6
Blood Group A	248	A tetra type 2-Sp - 17	GalNAca1-3[Fuca1-2]Galb1-4GlcNAcb-Sp-BSA	-3	-26	3	-34	0		-45	0	0	-29	-3
Blood Group A	35	2'F-A type 2-Sp - 13	GalNAca1-3[Fuca1-2]Galb1-4[Fuca1-3]GlcNAcb-Sp-BSA	-3	-12	2	-25	0		-26	3	6	-20	3
carb-Sia	548	3'Neu5Ac-Galb- 07	Neu5Aca2-3Galb-	-3	-42	5	-116	0		-158	-3	0	-110	0
non-human	763	4-Me-GlcAa1-2Xylb	4-Me-GlcAa1-2Xylb1-4Xylb- BSA	-3	-17	0	-23	0		-50	0	0	-26	0
carb-Sia	230	6'Neu5Gc-LacNAc-Sp - 05	Neu5Gca2-6Galb1-4GlcNAcb-Sp-BSA	-3	-20	3	-26	0		-48	0	6	-32	0
Blood Group A	68	BG-A1-12	GalNAca1-3(Fuca1-2)Galb1-3GlcNAcb1-linker-BSA	-3	-15	3	-37	0		-66	0	0	-37	0
y-protein	682	CRM197	ecoCRM197 from _____	-3	-6	0	6	0		13	3	0	3	3
glycolipid	661	GD1a (Kdn,Gc)	Kdna2-8Neu5Gca2-3(Galb1-3GlcNAcb1-4)Galb1-	-3	-22	0	-54	0		-119	-3	0	-66	0
GAG-Hep	572	Hep-Nona-GT16-03	GlcAb1-4Glc(6S, NS)a1-4GlcAb1-4Glc(6S, NS)a1-4GlcAb1-4Glc(6S, NS)a1-4GlcAb1-4Glc(6S, NS)a1-4GlcAb-Benzamide-	-3	-12	0	-37	0		-48	0		-23	0
glycolipid-neutral	418	iGb4-07	GalNAcb1-3Gala1-3Galb-	-3	-57	6	-128	0		-213	-3	3	-128	-3
Lewis	200	LeA-LeX - 21	Galb1-3(Fuca1-4)GlcNAcb1-3Galb1-4(Fuca1-3)GlcNAcb1-3Galb1-APD-HSA	-3	-20	3	-31	0		-50	0	3	-34	-5
Lewis	592	LeY-LeX	Fuca1-2Galb1-4(Fuca1-3)GlcNAcb1-3Galb1-4(Fuca1-3)GlcNAcb1-O-APE-HSA; Tri-fucosyl-Lewis y-heptasaccharide	-3	-17	0	-40	0		-55	0	0	-32	0
glycolipid	55	LSTb - 11	Galb1-3(Neu5Aca2-6)GlcNAcb1-3Galb1-BSA	-3	-31	5	-65	3		-114	-3	0	-68	0
carb-Man	476	Ma2Ma3-11	aMan(1-2)aMan(1-3)	-3	-17	0	-68	0		-110	0	5	-54	-3

Table 3.3 (cont'd)

carb-Man	437	Ma3(Ma6Ma6Ma3)-	aMan(1-3)[aMan(1-6)]aMan(1-6)[aMan(1-3)]	-3	-34	8	-91	3		-139	3	6	-85	6
carb-Man	458	Ma6(Ma3)Ma6-10	aMan(1-6)[aMan(1-3)]aMan(1-6)	-3	-17	0	-40	0		-59	0	0	-26	3
carb-Glc	711	maltotetraose - 18	Glca1-4Glca1-4Glca1-4Glca1-	-3	-14	0	-28	0		-37	0	3	-26	0
carb-Glc	714	maltotriose - 05	Glca1-4Glca1-4Glca1-	-3	-40	0	-83	0		-105	0	6	-49	0
Carb-Man	699	Mana1-4Man	Mana1-4Man-BSA	-3	-11	0	-23	0		-26	0		-12	
non-human	799	Manb1-4Glcb1 - 14	Manb1-4Glcb1 -BSA	-3	-20	0	-54	0		31	0	0	-43	-3
non-human	778	Manb5 - 04	Manb1-4Manb1-4Manb1-4Manb1-4Man	-3	-3	0	-8	0		-15	-5	0	-9	-6
non-human PNAG	760	PNAG 17 (10001)	GlcNAcb1-6GlcNb1-6GlcNb1-6GlcNb1-6GlcNAcb1-	-3	-6	0	-14	0		-29	1	0	-14	0
non-human PNAG	772	PNAG 8 (01000)	GlcNb1-6GlcNAcb1-6GlcNb1-6GlcNb1-6GlcNb1-	-3	-3	0	-8	0		-13	0	3	-3	0
peptide-TF	726	TSSAS(T-TF)GHA(T-TF)PLPVTD-BSA	TF-6,10-MUC4- TSSAS(T-TF)GHA(T-TF)PLPVTD-BSA	-3	-11	0	-23	0		-31	-1	0	-23	5
non-human	796	Xylb2 - 13	Xylb1-4Xylb1-BSA	-3	-6	0	-12	0		812	0	3	-11	0
z-control	1	Alexa Fluoro 647	Alexa Fluoro 647-BSA (25 ug/ml +100ug/mL BSA, 125 ug/ml total)	71	79	133	29	120		-15	54	151	23	79
z-control	808	Alexa Fluoro 647 end	Alexa Fluoro 647-BSA (25 ug/ml +100ug/mL BSA, 125 ug/ml total)	11	-3	10	-14	11		-28	12	9	-22	14
z-control	634	Biotin-BSA	Biotin-BSA	0	-8	0	-22	0		-29	0	0	-15	3
z-control	2	BSA	Bovine serum albumin	6	-11	8	-32	8		-43	5	6	-26	0
z-control	245	BSA - C5 (Alkyne) - 10	DF-168B-175-1 C5-alkyne-BSA	3	3	3	-8	0		-17	3	3	-6	0
z-control	332	BSA - C5 (Alkyne) - 23	DF-168C-16-B5 C5-alkyne-BSA	6	6	7	-5	0		-23	2	3	-3	6
z-control	670	BSA (ozonyzed)	bovine serum albumin treated with ozone	0	-11	3	-17	0		-40	-3	3	-12	3
z-control	813	Cy3	Cy3-BSA undoped											
z-control	815	Cy3	Cy3-BSA undoped											
z-control	4	Cy3	Cy3-BSA undoped	950										
z-control	814	Cy3	Cy3-BSA undoped											
z-control	29	HSA	Human serum albumin (isolated from serum)	3	0	11	-40	8		-51	2	9	-31	0
z-control	689	HSA (ozonyzed)	human serum albumin treated with ozone	444	-6	33	-28	0		-32	15	0	-22	-3
z-control	93	HSA (recomb)	human serum albumin (recombinant)	6	-17	3	-37	0		-60	5	6	-29	0
z-control	399	human IgA	use 50ug/mL + 75ug/mL BSA	3	-8	5	-12	0		-74	0	0	-23	3
z-control	400	human IgG	use 50ug/mL + 75ug/mL BSA	130	15	145	9	215		3	119	125	20	215
z-control	624	Human IgG1	used 50ug/mL + 75 ug/mL BSA; next time up to 100ug/mL + 25 BSA	17	-3	112	-20	293		-34	12	48	-3	43
z-control	630	Human IgG2	used 50ug/mL + 75 ug/mL BSA; next time up to 100ug/mL + 25 BSA	224	17	108	12	551		5	246	94	17	326
z-control	633	Human IgG3	used 50ug/mL + 75 ug/mL BSA; next time up to 100ug/mL + 25 BSA	576	22	124	30	425		-9	432	62	3	381
z-control	627	Human IgG4	use 50ug/mL + 75 ug/mL BSA	128	80	474	119	569		374	131	227	125	257
z-control	398	human IgM	use 50ug/mL + 75ug/mL BSA;	14	-6	8	-11	5		-29	15	8	-6	8
z-control	404	mouse IgG	use 50ug/mL + 75ug/mL BSA											
z-control	403	mouse IgM	use 50ug/mL + 75ug/mL BSA; monoclonal IgM purified from hybridoma	12	-33	3	-74	0		-150	5	6	-74	14
z-control	405	No Data (BSA for carry over)	Bovine serum albumin	3	-3	3	-17	0		-60	0	-3	-20	0
z-control	636	No Data (BSA for carry over)		29	-9	12	-20	0		-74	22	11	-29	34
z-control	407	No Data (BSA for carry over)		31	3	66	-1	82		-6	26	46	0	57
z-control	7	No Data (BSA for carry over)	BSA	14	-12	34	-34	20		-40	12	20	-23	11
z-control	373	No Data (BSA for carry over)		0	-11	0	-28	0		-74	0	3	-29	-3
z-control	406	No Data (BSA for carry over)		3	-20	3	-57	0		-127	0	0	-57	-3
z-control	637	No Data (BSA for carry over)		0	-5	0	-17	0		-23	-1	0	-11	0
z-control	685	No Data (BSA for carry over)		0	-6	0	-25	0		-37	0	0	-22	0
z-control	811	No Data (BSA for carry over)	BSA	-3	-3	0	-13	0		-10	0	-3	-11	0
z-control	191	PEG-linker - 06	OH-(CH2)2-NH-Gly-CO-PEG7-NH-(CO)Hept-SH-Mal-Cychex-CO-BSA	0	-6	0	-30	0		-15	0	6	-15	3
z-control	402	rabbit IgG	use 50ug/mL + 75ug/mL BSA	94	37	93	28	349		44	78	94	46	85
z-control	260	Triazole linker from Xuefei - 43	BSA-linker-triazole from Xuefei	8	-3	5	-9	0		-8	5	3	-3	8
z-control	776	XH Cys linker	Cys-S-CH2CONHCH2CH2CONH-BSA	14	-5	5	-11	0		-20	0	0	-9	3
	816			6	3	21	0	26		-1	6	14	5	11

REFERENCES

REFERENCES

[1] Y. Puckett, K. Garfield, Pancreatic Cancer, in: StatPearls, StatPearls PublishingCopyright © 2021, StatPearls Publishing LLC., Treasure Island (FL), 2021.

[2] P. Sarantis, E. Koustas, A. Papadimitropoulou, A.G. Papavassiliou, M. V Karamouzis, Pancreatic ductal adenocarcinoma: Treatment hurdles, tumor microenvironment and immunotherapy, World J Gastrointest Oncol. 12 (2020) 173–181. https://doi.org/10.4251/wjgo.v12.i2.173.

[3] G.A. Arias-Pinilla, H. Modjtahedi, Therapeutic Application of Monoclonal Antibodies in Pancreatic Cancer: Advances, Challenges and Future Opportunities, Cancers (Basel). 13 (2021) 1781. https://www.mdpi.com/2072-6694/13/8/1781.

[4] S. Kato, K. Honda, Use of Biomarkers and Imaging for Early Detection of Pancreatic Cancer, Cancers (Basel). 12 (2020) 1965. https://www.mdpi.com/2072-6694/12/7/1965.

[5] S. Kato, K. Honda, CA19-9 as a therapeutic target in pancreatitis., Ann. Transl. Med. 7 (2019) S318. https://doi.org/10.21037/atm.2019.09.161.

[6] D.D. Engle, H. Tiriac, K.D. Rivera, A. Pommier, S. Whalen, T.E. Oni, B. Alagesan, E.J. Lee, M.A. Yao, M.S. Lucito, B. Spielman, B. Da Silva, C. Schoepfer, K. Wright, B. Creighton, L. Afinowicz, K.H. Yu, R. Grützmann, D. Aust, P.A. Gimotty, K.S. Pollard, R.H. Hruban, M.G. Goggins, C. Pilarsky, Y. Park, D.J. Pappin, M.A. Hollingsworth, D.A. Tuveson, The glycan CA19-9 promotes pancreatitis and pancreatic cancer in mice, Science (80-.). 364 (2019) 1156–1162. https://doi.org/10.1126/science.aaw3145.

[7] G. Luo, K. Jin, S. Deng, H. Cheng, Z. Fan, Y. Gong, Y. Qian, Q. Huang, Q. Ni, C. Liu, X. Yu, Roles of CA19-9 in pancreatic cancer: Biomarker, predictor and promoter, Biochim. Biophys. Acta - Rev. Cancer. 1875 (2021) 188409. https://doi.org/10.1016/j.bbcan.2020.188409.

[8] R. Kannagi, Carbohydrate antigen sialyl Lewis a--its pathophysiological significance and induction mechanism in cancer progression., Chang Gung Med. J. 30 (2007) 189–209.

[9] U.K. Ballehaninna, R.S. Chamberlain, The clinical utility of serum CA 19-9 in the diagnosis, prognosis and management of pancreatic adenocarcinoma: An evidence based appraisal, J. Gastrointest. Oncol. 3 (2012) 105–119. https://doi.org/10.3978/j.issn.2078-6891.2011.021.

[10] R. Passerini, M.C. Cassatella, S. Boveri, M. Salvatici, D. Radice, L. Zorzino, C. Galli, M.T. Sandri, The Pitfalls of CA19-9: Routine Testing and Comparison of Two Automated Immunoassays in a Reference Oncology Center, Am. J. Clin. Pathol. 138 (2012) 281–287. https://doi.org/10.1309/AJCPOPNPLLCYR07H.

[11] J.L. Houghton, D. Abdel-Atti, W.W. Scholz, J.S. Lewis, Preloading with Unlabeled CA19.9 Targeted Human Monoclonal Antibody Leads to Improved PET Imaging with 89Zr-5B1,

Mol. Pharm. 14 (2017) 908–915. https://doi.org/10.1021/acs.molpharmaceut.6b01130.

[12] A. Takada, K. Ohmori, N. Takahashi, K. Tsuyuoka, A. Yago, K. Zenita, A. Hasegawa, R. Kannagi, Adhesion of human cancer cells to vascular endothelium mediated by a carbohydrate antigen, sialyl Lewis A, Biochem. Biophys. Res. Commun. 179 (1991) 713–719. https://doi.org/10.1016/0006-291X(91)91875-D.

[13] T. Matsui, H. Kojima, H. Suzuki, H. Hamajima, H. Nakazato, K. Ito, A. Nakao, J. Sakamoto, Sialyl Lewisa expression as a predictor of the prognosis of colon carcinoma patients in a prospective randomized clinical trial, Jpn. J. Clin. Oncol. 34 (2004) 588–593. https://doi.org/10.1093/jjco/hyh110.

[14] K. Miyazaki, K. Ohmori, M. Izawa, T. Koike, K. Kumamoto, K. Furukawa, T. Ando, M. Kiso, T. Yamaji, Y. Hashimoto, A. Suzuki, A. Yoshida, M. Takeuchi, R. Kannagi, Loss of disialyl Lewisa, the ligand for lymphocyte inhibitory receptor sialic acid-binding immunoglobulin-like lectin-7 (Siglec-7) associated with increased sialyl Lewisa expression on human colon cancers, Cancer Res. 64 (2004) 4498–4505. https://doi.org/10.1158/0008-5472.CAN-03-3614.

[15] F. Dall'Olio, N. Malagolini, M. Trinchera, M. Chiricolo, Mechanisms of cancer-associated glycosylation changes, Front. Biosci. 17 (2012) 670–699. https://doi.org/10.2741/3951.

[16] T. Dohi, M. Hashiguchi, S. Yamamoto, H. Morita, M. Oshima, Fucosyltransferase□ producing sialyl Lea and sialyl Lex carbohydrate antigen in benign and malignant gastrointestinal mucosa, Cancer. 73 (1994) 1552–1561. https://doi.org/10.1002/1097-0142(19940315)73:6<1552::AID-CNCR2820730605>3.0.CO;2-6.

[17] G.C. Hansson, D. Zopf, Biosynthesis of the cancer-associated sialyl-Le(a) antigen, J. Biol. Chem. 260 (1985) 9388–9392. https://doi.org/10.1016/s0021-9258(17)39378-x.

[18] R. Indellicato, A. Zulueta, A. Caretti, M. Trinchera, Complementary use of carbohydrate antigens lewis a, lewis b, and sialyl-lewis a (Ca19.9 epitope) in gastrointestinal cancers: Biological rationale towards a personalized clinical application, Cancers (Basel). 12 (2020) 1–14. https://doi.org/10.3390/cancers12061509.

[19] S.S. Pinho, A.J. Matos, C. Lopes, N.T. Marcos, J. Carvalheira, C.A. Reis, F. Gärtner, Sialyl Lewis x expression in canine malignant mammary tumours: Correlation with clinicopathological features and E-Cadherin expression, BMC Cancer. 7 (2007). https://doi.org/10.1186/1471-2407-7-124.

[20] Z. Yin, X. Huang, Recent development in carbohydrate based anticancer vaccines, J. Carbohydr. Chem. 31 (2012) 143–186. https://doi.org/10.1080/07328303.2012.659364.

[21] M.M. Wei, Y.S. Wang, X.S. Ye, Carbohydrate-based vaccines for oncotherapy, Med. Res. Rev. 38 (2018) 1003–1026. https://doi.org/10.1002/med.21493.

[22] S. Sait, S. Modak, Anti-GD2 immunotherapy for neuroblastoma, Expert Rev. Anticancer Ther. 17 (2017) 889–904. https://doi.org/10.1080/14737140.2017.1364995.

[23] D. Feng, A.S. Shaikh, F. Wang, Recent advance in tumor-associated carbohydrate antigens (TACAs)-based antitumor vaccines, ACS Chem. Biol. 11 (2016) 850–863. https://doi.org/10.1021/acschembio.6b00084.

[24] C.J. Dimitroff, I-branched carbohydrates as emerging effectors of malignant progression, Proc. Natl. Acad. Sci. U. S. A. 116 (2019) 13729–13737. https://doi.org/10.1073/pnas.1900268116.

[25] T. Dingjan, I. Spendlove, L.G. Durrant, A.M. Scott, E. Yuriev, P.A. Ramsland, Structural biology of antibody recognition of carbohydrate epitopes and potential uses for targeted cancer immunotherapies, Mol. Immunol. 67 (2015) 75–88. https://doi.org/https://doi.org/10.1016/j.molimm.2015.02.028.

[26] G. Ragupathi, P. Damani, G. Srivastava, O. Srivastava, S.J. Sucheck, Y. Ichikawa, P.O. Livingston, Synthesis of sialyl Lewisa (sLea, CA19-9) and construction of an immunogenic sLea vaccine, Cancer Immunol. Immunother. 58 (2009) 1397–1405. https://doi.org/10.1007/s00262-008-0654-7.

[27] R. Sawada, S.M. Sun, X. Wu, F. Hong, G. Ragupathi, P.O. Livingston, W.W. Scholz, Human monoclonal antibodies to sialyl-Lewisa (CA19.9) with potent CDC, ADCC, and antitumor activity, Clin. Cancer Res. 17 (2011) 1024–1032. https://doi.org/10.1158/1078-0432.CCR-10-2640.

[28] N.T. Viola-Villegas, S.L. Rice, S. Carlin, X. Wu, M.J. Evans, K.K. Sevak, M. Drobjnak, G. Ragupathi, R. Sawada, W.W. Scholz, P.O. Livingston, J.S. Lewis, Applying PET to Broaden the Diagnostic Utility of the Clinically Validated CA19.9 Serum Biomarker for Oncology, J. Nucl. Med. 54 (2013) 1876 LP – 1882. https://doi.org/10.2967/jnumed.113.119867.

[29] X. Wu, Z. Yin, C. McKay, C. Pett, J. Yu, M. Schorlemer, T. Gohl, S. Sungsuwan, S. Ramadan, C. Baniel, A. Allmon, R. Das, U. Westerlind, M.G. Finn, X. Huang, Protective Epitope Discovery and Design of MUC1-based Vaccine for Effective Tumor Protections in Immunotolerant Mice, J. Am. Chem. Soc. 140 (2018) 16596–16609. https://doi.org/10.1021/jacs.8b08473.

[30] X. Wu, J. Ye, A.T. DeLaitsch, Z. Rashidijahanabad, S. Lang, T. Kakeshpour, Y. Zhao, S. Ramadan, P.V. Saavedra, V. Yuzbasiyan-Gurkan, H. Kavunja, H. Cao, J.C. Gildersleeve, X. Huang, Chemoenzymatic Synthesis of 9NHAc-GD2 Antigen to Overcome the Hydrolytic Instability of O-Acetylated-GD2 for Anticancer Conjugate Vaccine Development, Angew. Chemie Int. Ed. n/a (2021). https://doi.org/https://doi.org/10.1002/anie.202108610.

[31] P. Weitzenfeld, S. Bournazos, J. V Ravetch, Antibodies targeting sialyl Lewis A mediate tumor clearance through distinct effector pathways, J. Clin. Invest. 129 (2019) 3952–3962. https://doi.org/10.1172/JCI128437.

[32] J.L. Houghton, B.M. Zeglis, D. Abdel-Atti, R. Aggeler, R. Sawada, B.J. Agnew, W.W. Scholz, J.S. Lewis, Site-specifically labeled CA19.9-targeted immunoconjugates for the PET, NIRF, and multimodal PET/NIRF imaging of pancreatic cancer, Proc. Natl. Acad. Sci. U. S. A. 112 (2015) 15850–15855. https://doi.org/10.1073/pnas.1506542112.